Assessing the palaeoceanographic and glaciological changes from the LGM to present in the Baltic Sea Basin and Baffin Bay, a multi-geochemical approach

OWNSWORTH, EMMA,MARIA

Assessing the palaeoceanographic and glaciological changes from the LGM to present in the Baltic Sea Basin and Baffin Bay, a multi-geochemical approach

Emma Ownsworth

Durham University

This thesis is submitted in partial fulfilment of the requirements for the degree of Doctor of Philosophy at Durham University

Department of Earth Sciences

September 2021

Abstract

The application of multiple geochemical techniques provides a robust tool for analysis, especially in regard to the study of sediment cores affected by complicated provenance, oceanographic and glaciological dynamics over time.

A multi-geochemical approach utilising proxies such as osmium isotopes ($^{187}Os/^{188}Os$), biomarker, XRF, qXRD, REE, radiocarbon dating and sedimentological details was applied to sediment cores from Baffin Bay, the Baltic Sea and the Skagerrak. This approach was applied with the goal of further understanding the complicated ice sheet dynamics and palaeoceanographic changes since the Last Glacial Maximum around the core localities, and how these may have been influenced by changes in climate (e.g., the Younger Dryas), which has the potential to help provide context for future glaciological and oceanographical changes in response to climate shifts. The use of the $^{187}Os/^{188}Os$ system as a proxy for glaciological and changes in basin inflow/drainage was also further tested, being applied to cores in the Skagerrak and Baltic Sea for the first time.

Through using combinations of the geochemical techniques listed above, large scale changes in the Baltic Sea Basin's history can be identified through the tracking of inflow and drainage events both inside and outside the basin. The first evidence in the central Skagerrak for the final drainage of the Baltic Ice Lake through south-central Sweden is found, and the transition of the freshwater Ancylus Lake into the brackish Littorina Sea stage are clearly depicted in the data from the central Baltic Sea. These techniques, however, are unable to differentiate the weak, short-lived marine incursions into the Baltic Basin during the Yoldia Sea stage from the varying influxes of freshwater due to melt of the Fennoscandian Ice Sheet. Further, in Baffin Bay, a radiogenic, felsic sediment source is recorded during the Baffin Bay Detrital Carbonate layers. The potential provenance of this is likely material transported by the Greenland Ice Sheet, although a Laurentide Ice Sheet source is not ruled out completely due to similar geologies between west Greenland and Baffin Island. Further, synchronous behaviour of ice sheets is recorded over BBDC1 coincident with the Bølling-Allerød and Older Dryas, and asynchronous behaviour is recorded over BBDC0 coincident with the Younger Dryas showing a dynamic response from the ice sheets over both warmer and cooler climate periods.

Declaration

I declare that this thesis, which I submit for the degree of Doctor of Philosophy at Durham University, is not substantially the same as any which has previously been submitted at this or any other university, and is my own work, except where reference is made to previously published or unpublished work.

Emma Ownsworth
September 2021

Acknowledgements

First and foremost, I'd like to thank my amazing supervisor Dave Selby for being literally the best supervisor anyone could ask for. Always there to help and offer advice and the speediest of writing readers. Thank you to my other supervisors Jerry Lloyd and Matthias Moros for their help and support throughout my PhD too. I also want to say thanks to Antonia Hoffman, for all her help and for great company and being a great music DJ in the lab in the first few years of my PhD.

I have absolutely loved my time here and I'd like to thank many great friends I've made in the department, past and present, for our regular 10.30 and 2.30 tea breaks, for all the laughs and banter. Special thanks to Madeleine Stow for always being there for a good old lab rant when things don't quite work out (and still being here through covid!). Thanks to Katharine Groves, Eloïse Bretagne, Tim Armitage, Olly Sanford, Katy Burrows, Miles Wilson, Sarah Clancy, Jack Lee, Bob Elliott, and many others. My time here would not have been the same without you all both in and outside the department!

Thanks to my parents also, for putting up with me still being a student for so long, and for putting up with my whinging 'I caaaaaan't do ittttt,' 'I'm soooooooo rubbish,' 'what's for teaaaaaaaaa?' and for still thinking I look at seaweed even though I don't. To the rest of my family also, and the constant 'oh so you'll be a doctor at the end then?' 'Yes, I will.' 'Oh, great so you'll be able to tell me what is wrong with my 'insert random body part' here then?'… Special shout out to my cat, Leo, for constantly being there for cuddles (albeit frequently resisted).

I would however, definitely not like to thank coronavirus. Thanks A LOT for meaning we had to miss out on over a year of tea breaks and lunches, on away weekends and birthday celebrations… oh and the closing of the lab and not being able to do as much work thing too obviously… But attached to this I would like to thank all the University staff including Chris Ottley, Geoff Nowell, James Dyson, Andy Aplin, and countless others who worked and worked for us to be able to get back into the labs and department safely and have kept things running as smoothly and safely as possible during these strange times.

Finally, I'd like to thank cake, chocolate, biscuits, and basically just sugar in general and well, pretty much anything edible really for being there, alongside a giant cup of tea,

whenever I needed them. And to the entire chocolate cake and gallon of tea I'm about to immediately stress consume as soon as I submit this large document!!!!

P.S. I guess I should probably mention Chris Ward in here somewhere too. No matter how annoying, stressful, and frustrating my PhD lab work and writing could be, you were always there to be ***even more*** annoying, stressful, and frustrating! ;)

Contents

Chapter 1: Introduction

The Holocene and late Pleistocene (~last 40,000 years) was a time of significant climatic change in the Northern Hemisphere (Clark et al., 1999; Shakun & Carlson, 2010). The climate switched from a glacial period with the hemisphere covered by large ice sheets, into its present-day interglacial state with limited ice coverage (Fig. 1.1; Clark et al., 1999, 2009). Glacial conditions peaked during the Last Glacial Maximum (LGM - ~33 – 19 cal ka BP), when ice sheets were at their maximum extents and eustatic sea levels were low (Clark et al., 2009; Ó Cofaigh et al., 2019). Since the LGM the Northern Hemisphere climate has fluctuated between warmer and cooler periods. Warmer phases include the Bølling-Allerød interstadial (~14.7 – 12.9 cal ka BP; Rasmussen et al., 2006). This interstadial was punctuated by the Older Dryas and ended with the Younger Dryas cold event (~ 14 cal ka BP and 12.8 – 11.7 cal ka BP, respectively) which were cooler, glacial like climates that caused ice margin retreat to slow, pause or even re-advance in places (Rasmussen et al., 2006).

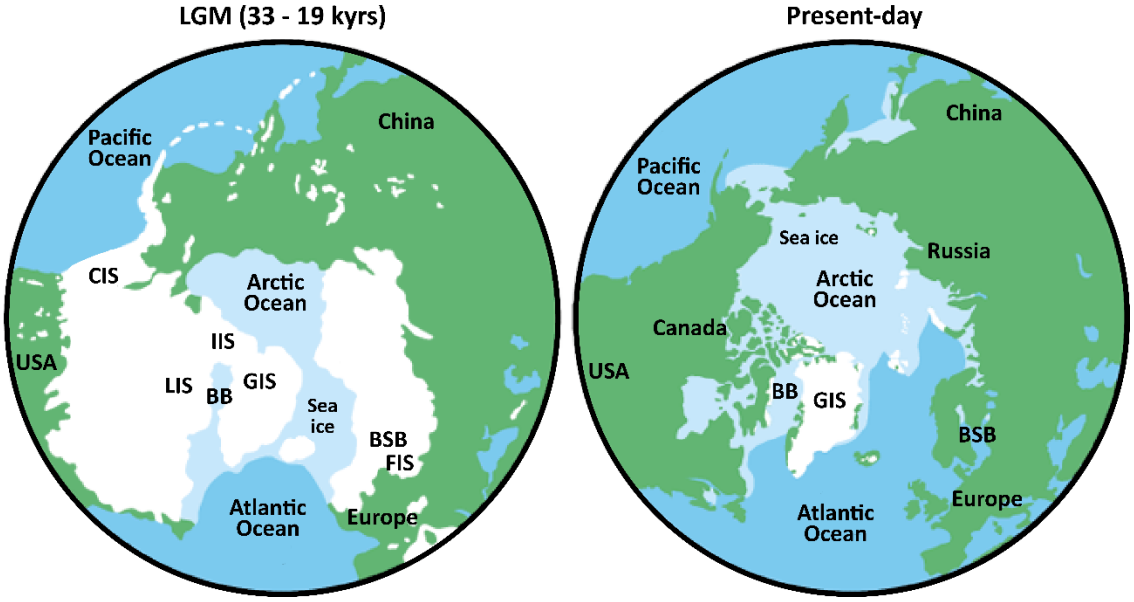

Figure 1.1: Ice sheet coverage at the LGM compared to the present day. FIS = Fennoscandian Ice Sheet, GIS = Greenland Ice Sheet, IIS = Innuitian Ice Sheet, LIS = Laurentide Ice Sheet, CIS = Cordilleran Ice Sheet. BSB = Baltic Sea Basin, BB = Baffin Bay. Adapted from CDM (2021). See text for discussion.

These different climatic changes are evident and recorded in several different ways including in sediment deposits both on land and sea, in ice cores, using foraminifera and in speleothems (e.g., Baldini et al., 2015; Clark et al., 2009; Jennings et al., 2014, 2018; Rasmussen et al., 2006; Rosentau et al., 2017; and references therein). Regions to study these changes are in areas that were most greatly impacted by climatic variability, for example areas that are surrounded by, or influenced by ice sheets, which are highly

susceptible to changes in climatic factors such as temperature, sea surface temperature and sea levels (e.g., Björck, 1995; Jennings et al., 2014, 2017; Marshall & Koutnik, 2006; Rasmussen et al., 2014; Rosentau et al., 2017). Basins that are restricted and therefore have limited further external influences are also potential study regions. This includes regions such as the Baltic Sea Basin, which was covered by the Fennoscandian Ice Sheet (FIS) during the last glacial cycle and is a restricted basin with limited connections to the North Sea. It also includes Baffin Bay, which was almost completely surrounded by three different ice sheets; the Greenland, Laurentide and Innuitian Ice Sheets (GIS, LIS, IIS) and is more restricted than an open ocean environment (Andrén et al., 2011; Björck, 1995; Dyke et al., 2002; England et al., 2006; Jackson et al., 2017; Rosentau et al., 2017; Simon et al., 2012, 2014). Sediment cores from these localities provide unique, high-resolution archives to understand ice sheet responses to changes in climate. Understanding this gives key insights into further potential changes we may witness if climate change continues as it is now (Marshall & Koutnik, 2006; Sheldon et al., 2016; Simon et al., 2014).

Although Baffin Bay and the Baltic Sea may seem vastly different localities, they both have similarities giving them the potential to be valuable study sites for assessing palaeoclimate, oceanography and glaciological changes (Fig. 1.1). Firstly, both sites were surrounded by ice sheet(s) that overlay chemically distinct Precambrian geologies, which have different chemical signatures to other geologies in the area and differ to the chemical signature of a typical open marine setting (Andrews, 1987; Andrews et al., 1998; Andrews & Eberl, 2011; Björck, 1995; Hiscott et al., 1989; MacLean et al., 1990; Peucker-Ehrenbrink & Ravizza, 1996; Rosentau et al., 2017; Simon et al., 2012, 2014; Solheim & Grønlie, 1983; Tuuling et al., 2011). This creates more distinctive changes in the chemistry recorded in sediment cores as the ice sheet(s) advance and retreat. The regions are both also partially restricted in some way to the general open ocean signature, meaning that marine influxes into the area potentially can also be identified. Finally, as they are both located in the Northern Hemisphere, they have been subjected to similar climatic changes over time (e.g., LGM, Younger Dryas) and so these changes can be explored in both localities relating to the subsequent ice sheet and basin dynamics.

1.1 Baffin Bay study site

Baffin Bay is a narrow ocean basin situated between Greenland to the east, Baffin Island to the west, the Canadian Arctic Archipelago to the north and the Labrador Sea to the south (Fig. 1.2; Aksu & Piper, 1979; Andrews et al., 1998; MacLean et al., 1990; Simon et al., 2012, 2014). The central abyssal plain of Baffin Bay is ca. 2 km deep, shallowing

towards the north and south and with steep slopes leading up to the continental shelves which are generally 200 to 600 m deep (Aksu & Piper, 1979; Li et al., 2011). The bay is asymmetric in bathymetry, with a relatively wide west Greenland shelf on the eastern side of Baffin Bay (135 - 200 km; Jakobsson et al., 2012; Li et al., 2011; MacLean et al., 1990), and a narrower Baffin Island shelf on the western side of the bay (25 - 50 km; Andrews et al., 2014; Jakobsson et al., 2012; Li et al., 2011; MacLean et al., 1990).

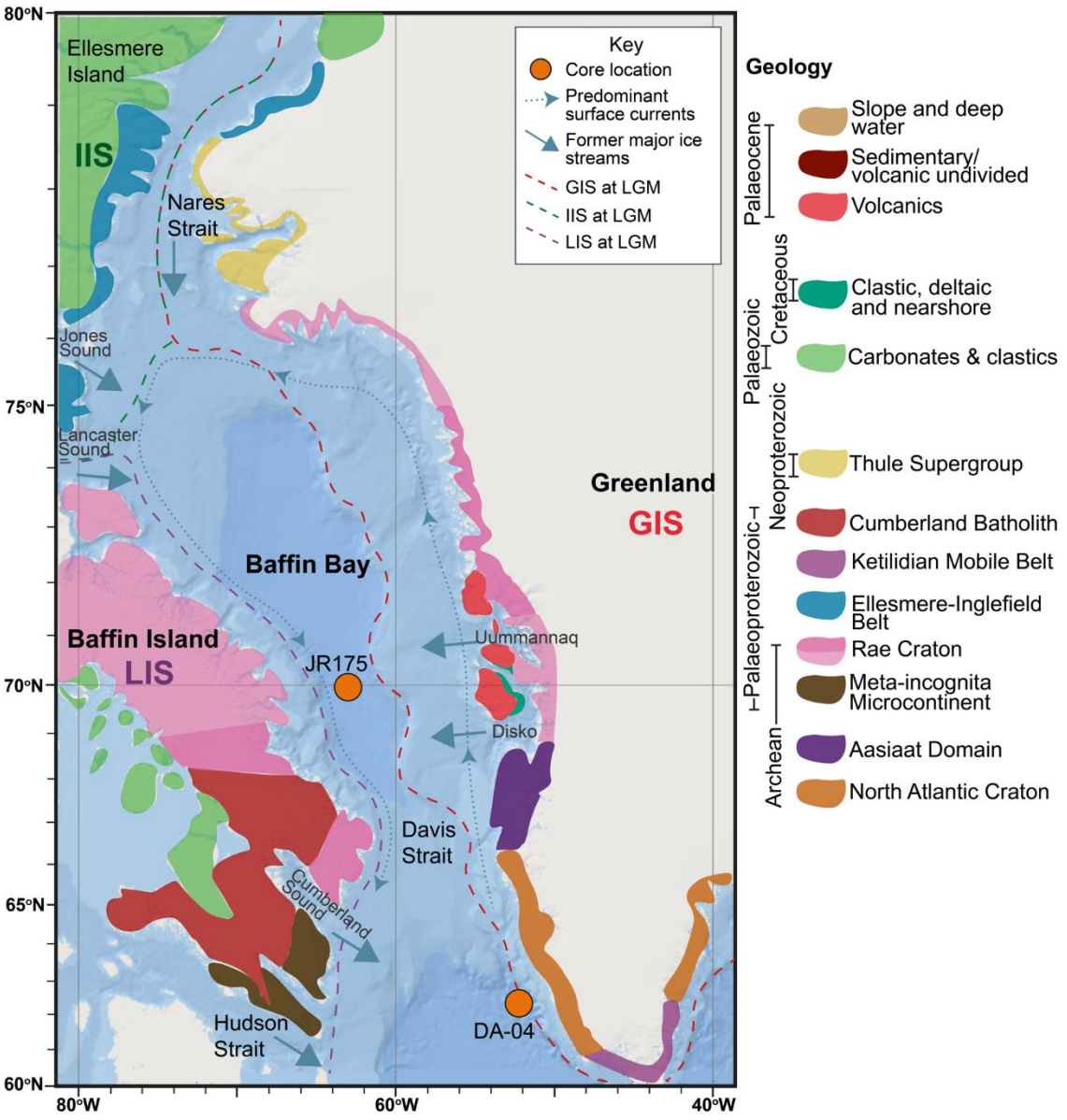

Figure 1.2: Map of Baffin Bay and its surrounding ice sheets at the Last Glacial Maximum (LGM) and the simplified surrounding geology. Base map from ArcGIS. Geology, circulation patterns and ice sheet extents extracted from Harrison et al., (2011), Simon et al., (2014) and references therein (England et al., 2006; Ó Cofaigh et al., 2013; Tang et al., 2004). GIS = Greenland Ice Sheet, IIS = Innuitian Ice Sheet, LIS = Laurentide Ice Sheet. Light and darker pink shades of the Rae Craton represent slightly different ages. Light pink = slightly older Archean to Mid-Palaeoproterozoic. Dark pink = Palaeoproterozoic age, on Baffin Island side this is the Foxe Fold and Pilling Group, on the Greenland side this is the Rinikian Fold Belt (Karrat and Anap Nua Groups).

At the Last Glacial Maximum Baffin Bay was surrounded by an almost continuous ring consisting of three Quaternary Ice Sheets: The Laurentide Ice Sheet (LIS) to the west, the Innuitian Ice Sheet (IIS) to the north, and the Greenland Ice Sheet (GIS) to the east (Dyke

et al., 2002; England et al., 2006; Jackson et al., 2017; Simon et al., 2012, 2014). The geology surrounding Baffin Bay is variable and this is described in more detail in Chapter 2. Briefly, the geologies of western Greenland and Baffin Island are fairly similar as prior to rifting in the Cretaceous-Palaeocene, these two landmasses were connected (Andrews et al., 2018; Harrison et al., 2011; MacLean et al., 1990; St-Onge et al., 2009). Precambrian crystalline basement is the main constituent with metamorphosed clastics, granites and volcanics mainly of Paleoproterozoic age on Baffin Island, and Archean gneisses on western Greenland, alongside some Palaeocene basalts on the shelf and islands around Disko Island (Hiscott et al., 1989; MacLean et al., 1990; Simon et al., 2012, 2014). In the north and north-west of Baffin Bay however, the predominant geology is Palaeozoic carbonate rocks of limestone and dolostone (Andrews et al., 1998; Hiscott et al., 1989; Jackson et al., 2017). Erosion and discharge events from the north are therefore distinct and are recorded as layers rich in detrital carbonate in Baffin Bay cores, so called Baffin Bay detrital carbonate layers (BBDC; Andrews, 1987; Andrews et al., 1998; Andrews & Eberl, 2011; Hiscott et al., 1989; Simon et al., 2014).

The Innuitian Ice Sheet lied mainly over these Palaeozoic carbonate outcrops, and the Laurentide and Greenland Ice Sheet lied mainly over the Precambrian crystalline basement and so changes in ice stream dynamics and discharges should show records of differing sediments depending on which ice sheet is active (Hiscott et al., 1989; MacLean et al., 1990; Simon et al., 2012, 2014). However, due to the range of geologies and complicated ice dynamics from a number of ice sheets, tracking the provenance of the sediments and understanding the past movements and ice streaming activities can be complicated, and the exact timings of advance and retreat of the different ice sheets are still uncertain (Andrews et al., 2018; Ó Cofaigh et al., 2013).

A key objective of this study therefore aims to look at whether changes in ice dynamics of the northern Innuitian Ice Sheet leading to BBDC events was also contemporaneous with surging or break up with the other surrounding ice sheets, and to chronologically constrain the events. However, distinguishing between sediments from the Greenland Ice Sheet and Laurentide Ice Sheet is challenging as Greenland and Baffin Island were once connected, and so share very similar geologies meaning similar isotope compositions and mineral/ element contributions (Aksu & Piper, 1979; Andrews et al., 2014, 2018; Harrison et al., 2011; Hiscott et al., 1989; Jennings et al., 2018; MacLean et al., 1990; Simon et al., 2014; St-Onge et al., 2009). In previous studies, layers containing low detrital carbonate and fine grained titanium-rich sediments were attributed to a ‘lateral’

mode of sediment delivery from western Greenland and eastern Baffin Island, but the layers have not been distinguished between the two sources, and other studies have also had similar problems (e.g., Aksu & Piper, 1979; Andrews et al., 2014; Harrison et al., 2011; Hiscott et al., 1989; Jennings et al., 2018; MacLean et al., 1990; Simon et al., 2014). Simon et al. (2014) were able to identify distinct sources by removing the detrital carbonate signatures and using detailed qXRD and a SedUnMix program showing differences between sediments from eastern Baffin Island and Uummannaq (off the west coast of Greenland) from a core in Baffin Bay over the last 120 kyrs. From this they were able to infer different ice streaming activities from each side of Baffin Bay. However, due to such a long timescale, there is less detail relating specifically to changes since the LGM, and contributions from West Greenland other than Uummannaq were not distinguished. Therefore, it is intended that this study, which combines several geochemical techniques and proxies including quantitative x-ray diffraction (qXRD), x-ray fluorescence (XRF), osmium isotopic analysis ($^{187}Os/^{188}Os$), rare earth elements (REEs), major oxides and trace elements as well as sedimentological analyses such as foraminifera, grain size analysis, carbon content, alongside an understanding of circulation and oceanography of Baffin Bay, will help differentiate between the different ice sheet activities. This is complemented by a robust chronology of radiocarbon dates from foraminifera and the development an age model. Timings of ice sheet dynamics in Baffin Bay are complex and still not fully understood (Simon et al., 2014). This is, in part, due to slow sedimentation rates and poor preservation of biogenic carbonate in the Holocene, especially in deeper sediments, and limited research on the LGM which means that well-dated sedimentary records from within Baffin Bay are lacking (Andrews et al., 1998; Jackson et al., 2017; Jennings et al., 2018; Simon et al., 2012).

To help understand past ice sheet activities and their timings, knowing ice sheet behaviour in response to different climate forcing is becoming increasingly more essential in the modern world. It is important to understand the changes in ice sheet advance, retreat, and standstill over time, especially how their margins and ice streams change in response to different climate and ocean forcing scenarios. This allows changes to be put into a much longer time scale, providing context to help understand what is happening to current ice sheets today, and to help model their response to future climate change predictions (Jackson et al., 2017; Jennings et al., 2014; Sheldon et al., 2016; Simon et al., 2014). This is especially relevant for the present-day Greenland Ice Sheet due to the potential it poses to raise sea levels and alter ocean circulation as it loses mass through ice discharge and surface melting (e.g. Bamber et al., 2012; Enderlin et al., 2014; Jennings et al., 2017).

These modern-day observations of GIS behaviour are very important. However, due to the short timescale over which these observations exist, it makes it much harder to model the response to current and future climate changes, hence detailed understanding of past activities are also needed to solidify these climate models and predictions for the future (Jennings et al., 2014, 2017; Sheldon et al., 2016; Simon et al., 2014). Therefore, another key objective of this study is to consider changes in ice sheet dynamics against known climate fluctuations over the Holocene and late Pleistocene including the Bølling-Allerød interstadial and Younger and Older Dryas cold events.

To help achieve these goals, a core site was chosen in a central location within Baffin Bay, core JR175-GC01 (henceforth labelled JR175; Fig. 1.2). The core was recovered from the RRS James Clark Ross expedition (August-September 2009) and is stored by the Department of Geography at Durham University. Its central position, not on a continental shelf, has the potential to record inputs from all three of the surrounding ice sheets, not just one large influence, as well as a more open marine signal, therefore providing a valuable place to study the surrounding ice sheet dynamics as well as sedimentary provenance. The core and locality are described in detail in Chapter 2.

A second core DA04-31P (henceforth named DA04), off the south-west of Greenland, was chosen at it is sufficiently south of Baffin Bay as to have limited input of detrital carbonate from northern Baffin Bay, therefore potentially recording only a $^{187}Os/^{188}Os$ signature of more open marine waters through time (Fig. 1.2). The core was collected during a cruise of the R/V Dana in 2004 (Knutz et al., 2011). Due to its more southerly position, any influence of marine waters entering Baffin Bay during the Holocene as ice sheets melted would be recorded earlier in DA04 and could provide a comparison to tracking this influence into the central Baffin Bay core.

Further, carbonate rock samples were obtained from Devon Island and Somerset Island, located to the north-west of Baffin Bay (through Lancaster Sound; Fig. 1.2). Osmium isotope analysis, REE and major oxide analysis was also undertaken on these carbonate rocks with the objective of defining the chemical signature of these rocks responsible for Baffin Bay detrital carbonate layers and ruling them out as being the sole source into Baffin Bay over these detrital periods.

1.2 Baltic Sea Basin and Skagerrak study sites

The Baltic Sea Basin is one of the world's largest intracontinental basins and the largest brackish water body (~373,000 km^2; Andrén et al., 2015; Björck, 1995; Rosentau et al., 2017). The Baltic Sea is split into a number of sub-basins and arms including the Gotland Basin, Bornholm Basin and the Gulfs of Bothnia and Finland, with narrow and shallow connections to the North Sea through the Straits of Öresund and the Great Belt between Sweden and Denmark (Fig. 1.3; Björck, 1995; Rosentau et al., 2017). Between the North Sea and the Baltic Sea Basin there are the connected waterways of Kattegat Bay and the Skagerrak Strait, together acting as a large estuary, so any exchange between the two must first pass through these areas (Nordberg, 1991). Precambrian crystalline basement dominates the geology of the north, north-east and north-west of the Baltic Sea Basin (Peucker-Ehrenbrink & Ravizza, 1996; Rosentau et al., 2017). This is in contrast to the Phanerozoic European Sedimentary Platform in the south and south east, and the Palaeozoic Western European Sedimentary Platform in the south west of the Baltic Sea Basin and also through the majority of the Skagerrak area (Björck, 1995; Peucker-Ehrenbrink & Ravizza, 1996; Rosentau et al., 2017; Solheim & Grønlie, 1983; Tuuling et al., 2011). More detailed descriptions of the Baltic Sea Basin and the Skagerrak are presented in Chapters 3 and 4.

Throughout the Holocene and Late Pleistocene the Baltic Sea Basin has been influenced by the continually changing Fennoscandian Ice Sheet (FIS; Andrén et al., 2015; Björck, 1995). Eustatic sea level rise along with isostatic changes, glacial advance and retreat have combined to create several different sea stages in the Baltic Basin since the Last Glacial Maximum. This includes the freshwater Baltic Ice Lake (~16 – 11.7 cal ka BP) which catastrophically drained through a channel in south-central Sweden (~13 – 11.7 cal ka BP), leading into the Yoldia Sea Stage (~11.7 – 10.7 cal ka BP) characterised by short bursts of marine influence into the basin, before another freshwater lake stage termed the Ancylus Lake (10.7 – 9.7 cal ka BP). Finally, into the Littorina Sea stage lasting up to the present-day where the final remnants of the FIS melted and marine waters were able to flow into the Baltic Basin through channels in the Danish Straits (Andrén et al., 2008, 2011; Berglund et al., 2005; Björck, 1995; Jakobsson et al., 2007; Lemke et al., 2001; Rosentau et al., 2017)

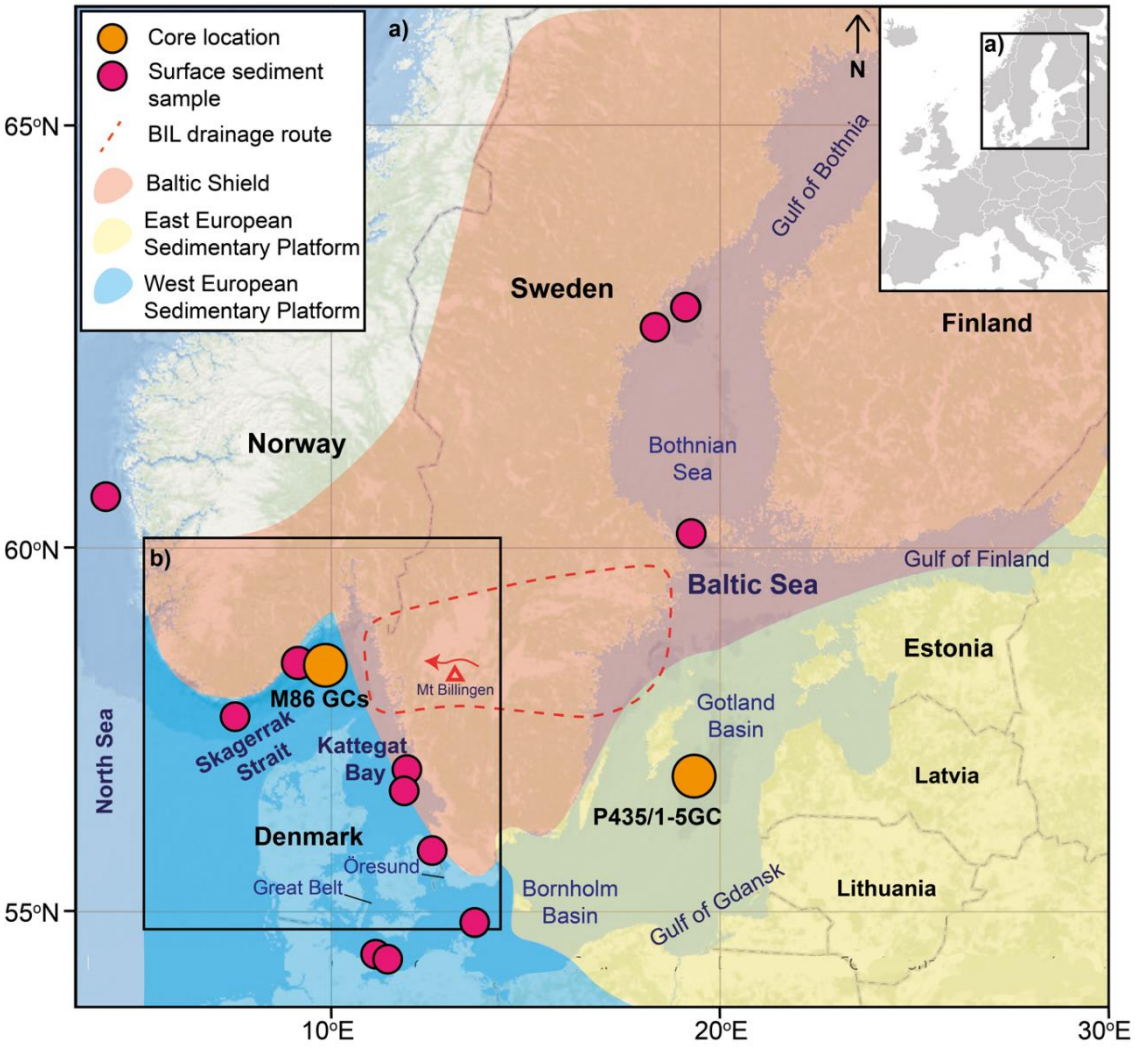

Figure 1.3: Map of the Baltic Sea, Kattegat and Skagerrak showing locations of surface sample sites and gravity cores including three from the Skagerrak and one from the Baltic Sea, dominant geology types and the area in south central Sweden around Mt. Billingen through which drainage of the Baltic Ice occurred. Grey and white Europe map from Wikipedia (https://en.wikipedia.org/wiki/File:Europe_blank_map.png), colour map from ArcGIS, current and subsurface currents adapted from Gyllencreutz (2005), geological data from Peucker-Ehrenbrink & Ravizza (1996) and Rosentau et al. (2017).

However, the exact timings of some of these transitions and the interaction with the north sea still remain uncertain (Berglund et al., 2005; Björck, 1995). For example, although the Baltic Ice Lake drained catastrophically through south-central Sweden, little to no evidence of this drainage has thus far been found in the Skagerrak (Bodén et al., 1997; Dickens, 2013; Erbs-Hansen et al., 2011; Gyllencreutz, 2005; Jiang et al., 1997; Knudsen et al., 1996). In deeper basins especially, cores record little to no organic material and microfossils for dating, and hence a robust chronology is not possible (Hyttinen et al., 2014; Kögler & Larsen, 1979; Kortekaas, 2007). Common stratigraphic markers depicting the different Baltic Sea stages in shallower cores are also not often found in deeper basin cores (e.g., Moros et al., 2002), and hence it is often difficult to identify pre-Littorina stages (Andrén et al., 2008; Berglund et al., 2005; Björck, 1995; Westman et al., 1999).

The Baltic Sea Basin generally experiences high sedimentation rates (~100-500 cm/1000 years; Andrén et al., 2015). Therefore, it has the potential to provide unique, high-resolution records. This makes it an excellent site for reconstructing longer and shorter timescale climatic oscillations and palaeoenvironments, both within the Baltic Sea itself, and also for its extensive drainage area (Andrén et al., 2015). The key objectives of this study are to further understand the palaeoceanography and evolution of the Baltic Sea Basin stages and interactions with the North Sea and connecting waterways such as the Skagerrak. This will be achieved by developing a high-resolution multi-proxy geochemical record including XRF, sand content, osmium isotope analysis, x-radiograph imagery, biomarker indices, radiocarbon dating and sedimentology on core and surface sediment samples from within, and external to, the Baltic Sea Basin.

The cores to be studied (Fig. 1.3) were chosen based primarily on localities considered to have a good chance of recording as many of the Baltic Sea Stages in as greater detail as possible. Cores were chosen that were proximal or within the pathway of the drainage channel through south-central Sweden through which the Baltic Ice Lake drained and influxes of marine waters during the Yoldia Sea were first recorded, whilst still being close to the modern day Danish Straits through which exchanges presently occur (Andrén et al., 2008, 2011; Björck, 1995; Jakobsson et al., 2007; Rosentau et al., 2017). The first core, P435/1-5 GC was collected during the RV 'Poseidon' cruise in 2012 and was chosen as it is located centrally in the Baltic Basin and to the east of the old drainage channel through south-central Sweden. It is also far enough south through the Basin that it would have been de-glaciated before the end of the Baltic Ice Lake (Rosentau et al., 2017) so may still record this earlier sea stage. Further cores were chosen from within the Skagerrak, proximal and to the west of the drainage channel through south-central Sweden, with the goal of recording the first evidence of the Baltic Ice Lake drainage in the central Skagerrak. Cores M86-1-07-1 GC, M86-1-05-1 GC, and M86-1-06-1 GC were collected in 2011 by the R/V 'Meteor' cruise.

Numerous surface samples were also analysed from around the inside of the Baltic Sea, through the Danish Straits and the Kattegat, Skagerrak, and North Sea to encompass a large geographical coverage. Sites were selected based on the undisturbed, core top and surface samples that were available and from localities avoiding strong currents or extremely shallow sections to limit re-working of the sediments to get the best possible representation of current conditions. The surface samples were analysed for their osmium

isotope ratios with the objective of understanding of the current conditions in the Baltic Sea to compare with older sediments from differing Sea Stages.

1.3 The rhenium - osmium isotope system

Rhenium and osmium are only found at ultra-trace levels within the Earth's crust. Rhenium has an average crustal abundance of 350 ppt, and osmium 50 ppt (Cohen, 2004; Esser & Turekian, 1993). However, concentrations of these elements in organic rich rocks can reach up to ~500 ppb Re and 4 ppb Os (Cohen, 2004; Esser & Turekian, 1993; Ravizza & Turekian, 1989).

The rhenium-osmium (Re-Os) isotope system has been used for many years for several different applications. For example, a geochronometer in the dating of rocks and oil, identifying OAEs, identification of extra-terrestrial impacts, flood basalt volcanism, anthropogenic pollution from platinum group element (PGE) ores, changes in warming and cooling of climate and palaeoceanographic changes (e.g., Chen et al., 2009; Kuroda et al., 2016; Liu et al., 2020; Paquay & Ravizza, 2012; Peucker-Ehrenbrink & Ravizza, 2000, 2012; Poirier & Hillaire-Marcel, 2011; Rooney et al., 2016; Sproson et al., 2018). The usefulness of the Re-Os proxy is due to the radioactive parent-daughter relationship between the two elements where ^{197}Re decays by beta-emission to ^{187}Os (half-life c. 44 Ga; Cohen, 2004), and also that Re behaves moderately incompatibly and partitions into the melt, whereas Os behaves as a compatible element and so remains in mantle, hence Re and Os are fractionated (e.g., Burton et al., 2002; Dickin, 2018; Gannoun & Burton, 2014; Sproson et al., 2018). These two factors create differences in the natural variation in osmium isotopes which are recorded as the ^{187}Os/^{188}Os ratio. Crustal rock has a higher ^{187}Re content and hence the Re/Os ratio is much higher than that of the mantle. Radioactive decay then takes place over time meaning that these crustal rocks, especially old crustal rocks, evolve to have a more radiogenic composition with higher amounts of ^{187}Os and hence a high ^{187}Os/^{188}Os ratio (e.g., Burton et al., 2002; Cohen, 2004; Dickin, 2018; Gannoun & Burton, 2014; Sproson et al., 2018). The mantle, which contains less ^{187}Re (hence less radiogenic ^{187}Os) and more ^{188}Os, therefore, has an unradiogenic, or low, ^{187}Os/^{188}Os value (Cohen, 2004; Dickin, 2018; Esser & Turekian, 1993). In some lithologies, these properties allow the differentiation between crustal and mantle sources, and inferences to be made on the age of the crustal contribution i.e., depending on how radiogenic it is (Cohen, 2004). Older, continental sourced material generally has a higher, more radiogenic, ratio (~2.4 average but can be much higher; Peucker-Ehrenbrink & Jahn, 2001), whereas younger mantle sourced and extra-terrestrial materials generally have a much lower, unradiogenic ratio (~0.13; Peucker-Ehrenbrink & Ravizza, 2000). The open

marine ocean therefore records a mix of the different sources, recording a present-day $^{187}Os/^{188}Os$ value of ~1.06 (Burton et al., 1999; Cohen, 2004; Levasseur, 1998; Peucker-Ehrenbrink & Ravizza, 2000; Rooney et al., 2016; Sharma et al., 1997). In some coastal regions, anthropogenically released osmium has also been detected. This usually tends to have an unradiogenic mantle like $^{187}Os/^{188}Os$ composition, as many of the platinum group elements used are extracted from mantle derived deposits. Anthropogenic osmium can be found in catalytic converters, sewage sludge and from biomedical research (Chen et al., 2009; Peucker-Ehrenbrink & Ravizza, 2000; Sproson et al., 2020).

Achieving the measured value of 1.06 for average seawater has been accomplished through directly analysing the seawater using ultralow blank techniques (Chen et al., 2009; Gannoun & Burton, 2014; Levasseur, 1998). However, this can be a very challenging process due to the extremely low osmium concentrations (ultra-trace element) and its multiple oxidation states (Dickin, 2018; Peucker-Ehrenbrink & Ravizza, 2000, 2012). The predominant source of Os into seawater is through erosion and weathering of continental crust, with a smaller proportion also from cosmic dust and hydrothermal inputs, transported into the oceans directly or via rivers (e.g., McDaniel et al., 2004; Peucker-Ehrenbrink & Ravizza, 1996, 2000, 2020; Sharma et al., 2000). Oceanic concentrations of rhenium and osmium are extremely low, ~8.2 ppt and 10 ppq, respectively (Peucker-Ehrenbrink & Ravizza, 2000, 2012; Sproson et al., 2018). However, Re and Os are organophilic, this means they can be concentrated into organic-rich sediments during deposition from seawater, making analysis of the sediments much easier (Cohen et al., 1999; Cohen, 2004; Ravizza & Turekian, 1989; Selby et al., 2013; Selby & Creaser, 2003). In organic rich rocks, rhenium and osmium taken up is hydrogenous (sequestered from seawater) and hence is a measure of the hydrological conditions at the time rather than a detrital component (Selby & Creaser, 2003). This means that the $^{187}Os/^{188}Os$ values recorded in the sediments reflect the composition found in the contemporaneous seawater, and so environmental conditions at the time can also be inferred (Cohen et al., 1999; Cohen, 2004; Ravizza & Turekian, 1989; Selby & Creaser, 2003). The average $^{187}Os/^{188}Os$ composition of seawater has fluctuated through history (~0.2 to 2.2 over the last 80 Ma) but not significantly so over the last ~40 kyr timescale of the cores studied in Chapters 2 to 4 (staying at ~1), and hence can be considered constant (Fig. 1.4; Peucker-Ehrenbrink & Ravizza, 2020). Present-day global seawater $^{187}Os/^{188}Os$ is considered to be very similar and constant at ~1.06 (Burton et al., 1999; Cohen, 2004; Levasseur, 1998; Peucker-Ehrenbrink & Ravizza, 2000; Rooney et al., 2016; Sharma et al., 1997). Although globally constant, at a local scale the $^{187}Os/^{188}Os$ can vary considerably where other inputs dominate over that of the open ocean, especially

in areas that are restricted. For example, in Baffin Bay a study by Rooney et al. (2016) showed that a core (MSM-520) just outside of Uummannaq Fjord recorded a $^{187}Os/^{188}Os$ of 0.8 closest to the surface (4 – 14 cm depth), likely influenced by the surrounding Palaeocene lavas, whereas a temporally correlated core (DA00-06) interval in Disko Bugt recorded a $^{187}Os/^{188}Os$ of 1.55 closest to the surface (8 – 16 cm depth), this time likely influenced by the old Archean and Palaeoproterozoic crystalline basement of west Greenland. Further, a core was also analysed from just south of the Davis Strait off of south-west Greenland, here the surface (0 – 2 cm depth) $^{187}Os/^{188}Os$ values are ~1, reflecting the open ocean values with less continental input (Rooney et al., 2016). In regards to the Baltic Sea and the Skagerrak, present day $^{187}Os/^{188}Os$ seawater values to date consist of measurements of Mn nodules and crusts from Bothnian Bay, the Bothnian Sea, Gulf of Finland and Mecklenburg Bight in the Baltic Sea, with $^{187}Os/^{188}Os$ of 2.56, 2.50, 2.40 and 1.49, respectively, representing a restricted influence of the open ocean and more input from the radiogenic continental shield (Peucker-Ehrenbrink & Ravizza, 1996).

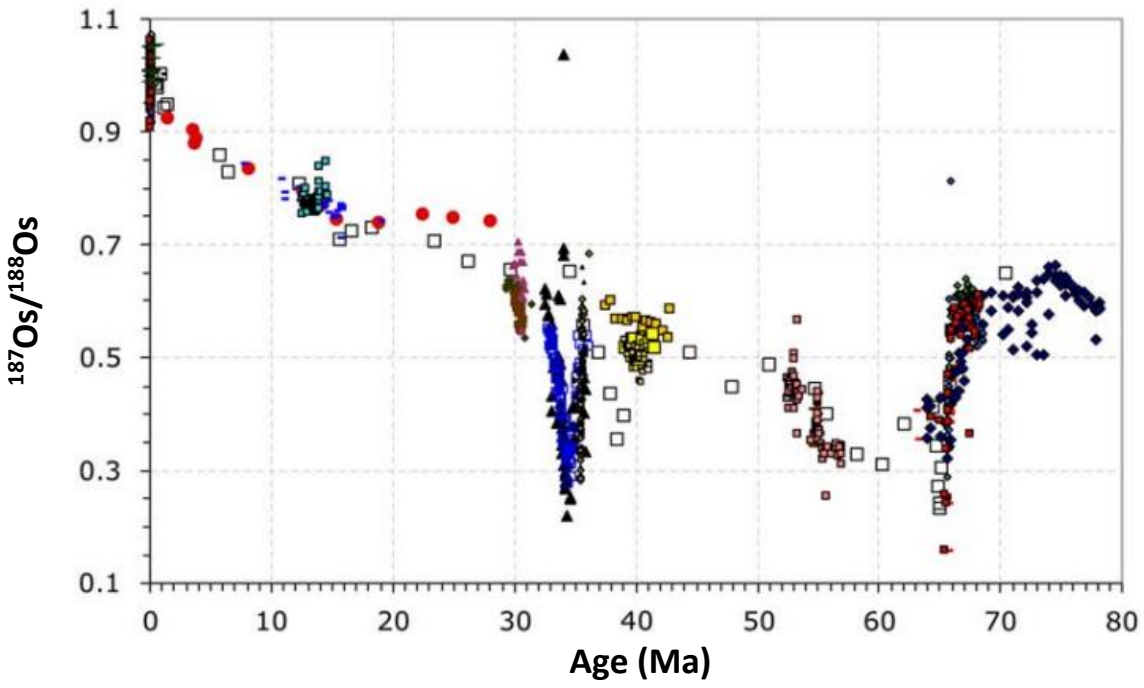

Figure 1.4: The variability of the $^{187}Os/^{188}Os$ ratio of seawater over the last 80 million years. Graph copied from Peucker-Ehrenbrink & Ravizza (2020). The authors utilised numerous studies, the references to which can all be found in Peucker-Ehrenbrink & Ravizza (2020).

Due to the short residence time of osmium in the oceans of 1 to 50 kyrs, with many studies now estimating this as < 10 kyrs, the $^{187}Os/^{188}Os$ proxy allows the differentiation between long- and short-term changes in the environment such as tectonic forcing and climate fluctuations (Levasseur et al., 1999; Oxburgh, 1998, 2001; Peucker-Ehrenbrink & Ravizza, 2012; Rooney et al., 2016; Sharma et al., 1997).

The $^{187}Os/^{188}Os$ analysis was undertaken on all central Baltic, Skagerrak, and Greenland cores, as well as on the Baltic Sea surface sediment samples, and the carbonate rocks collected from Devon and Somerset Islands (NW Baffin Bay). Further, the nature of the osmium isotope system means that the $^{187}Os/^{188}Os$ changes depending on the source. Greenland and the Baltic Sea therefore are key localities for the use of osmium isotopes as they both have surrounding older, continental geologies with a continuous to intermittent input of an open marine source. Indeed, work by Peucker-Ehrenbrink & Ravizza (1996) in the Baltic Sea Basin showed differences in runoff from Precambrian Baltic Shield ($^{187}Os/^{188}Os$ = 3.75 – 7.87) and the European Sedimentary Platform ($^{187}Os/^{188}Os$ = 1.03 – 1.32), with the Baltic Sea recording a mixing of these sources with the North Sea inputs ($^{187}Os/^{188}Os$ = 1.49 – 2.55). The isotope system has also successfully been used by Rooney et al. (2016) as an indicator of glacial advance ($^{187}Os/^{188}Os$ = 2.0 to 2.4) and retreat ($^{187}Os/^{188}Os$ = 1.3 to 1.6) of the Jakobshavn Isbræ ice margin closer and further away from the core site located in Disko Bugt over the Holocene, and has also been applied to detecting glaciations in deeper time (e.g., Finlay et al., 2010; Ravizza & Peucker-Ehrenbrink, 2003). The use of $^{187}Os/^{188}Os$ has also been successful in the Mediterranean in detecting the Messinian Salinity Crisis and limited connection to the Atlantic Ocean, shown by more unradiogenic values linked to restricted marine input and the surrounding ultramafic ophiolites (Kuroda et al., 2016).

1.4 Rationale of other geochemical techniques used

Multiple geochemical techniques have been utilised in order produce a robust data set possible to be able to draw solid conclusions from the information acquired. Justifications for the main techniques used throughout chapters 2, 3 and 4 are discussed below.

1.4.1 XRF, XRD and REE analysis

X-Ray Fluorescence (XRF) analysis was undertaken on all cores from the Baltic Sea and Skagerrak, and from the central Baffin Bay core. XRF provides high resolution data sets of elements and how they change through the core. In Greenland, the element of particular interest was calcium (Ca) as this provides an indication of the carbonate content of the core and hence can be used to record the Baffin Bay detrital carbonate layers. In the Baltic Sea and Skagerrak studies of combinations of elemental ratios can be very useful proxies. The Ti/Ca and K/Ti proxies are used to help understand biogenic vs. terrestrial inputs, ice rafting events, carbonate weathering and clay mineral abundance (Demina et al., 2019;

Diekmann et al., 2008; Hepp et al., 2006; Kylander et al., 2011; Rothwell & Croudace, 2015).

Quantitative X-Ray Diffraction (qXRD) was utilised to identify the mineralogy of compounds. qXRD analysis was undertaken on the central Baffin Island core to aid in identifying specific key minerals or signatures which may differentiate between a Baffin Island and western Greenland sediment source.

Rare Earth Elemental (REE) analysis looks specifically at the abundance of rare earth elements. The elemental abundance normalised to upper crust yields patterns that can be useful in identifying specific sediment provenances by comparing negative and positive anomalies, and the amount of light REE (LREE) enrichment to heavy REE (HREE) enrichment and comparing these against REE patterns from the differing source areas. The REE analysis was undertaken on several samples from the central Baffin Bay core, as well as from the Somerset and Devon Island carbonate samples, to help understand the ice sheet dynamics in the area.

1.4.2 Biomarkers

Biomarkers can show where there is a change in conditions such as salinity, freshwater input, continental input as well as past temperature and rainfall amount which in turn has caused changes in the chemical/ biological components of the organic molecules left by organisms that were living at the time (e.g., Moros et al., 2016; Peters et al., 2004; Warden et al., 2018; and references therein). For a specific core interval in M86-1-06-1 GC in the Skagerrak, $\%C_{37:4}$ biomarker analysis is used. This has previously been used to record freshwater influences as it has been shown to be an indicator of lower surface salinities (Bendle et al., 2005; Moros et al., 2016; Rosell-Melé, 1998; Rosell-Melé et al., 2002; Sicre et al., 2002). It therefore should be a perfect indicator for recording any potential drainage of the Baltic Ice Lake out into the Skagerrak, and has actually been used before to show changes in Baltic Sea outflow into the Kattegat (Krossa et al., 2015). For the central Baltic Core (P435/1-5 GC) the BIT index (Branched and Isoprenoid Tetraether) has been used which is a terrestrial biomarker proxy varying between 0 and 1 which is pure marine and pure terrestrial organic matter, respectively (Kim et al., 2006; Wang et al., 2013; Warden et al., 2018). Again, in the Central Baltic Basin this has the potential to show marine incursions vs. times of greater terrestrial input to help differentiate between the different sea stages in the Baltic Basin since the LGM.

1.4.3 Radiocarbon

To place any of the previously described techniques on a timescale and to be able to compare to known climatic events, a robust chronology is needed. As the cores are relatively young (< 50 kyrs), radiocarbon dating is a good way to achieve this. In the Skagerrak and Greenland cores, foraminifera are present in the sediments and so several intervals were able to be dated. Unfortunately, the core from the central Baltic does not contain sufficient foraminifera to be dated, thus no age model could be established.

1.4.4 Mixing model

In Chapter 2 a simplified mixing model is used to help determine whether the radiogenic $^{187}Os/^{188}Os$ values recorded in a central Baffin Bay core are sourced from Palaeozoic carbonate materials originating in the north/ north-west of the bay which are prevalent during the $^{187}Os/^{188}Os$ peaks. The two-component mixing model follows that of van der Ploeg et al. (2018) who used it to understand how Os derived from the input of mantle-derived basalts affects the flux of mantle signature $^{187}Os/^{188}Os$ in seawater, and developed the model from that of strontium isotopes by Faure (1986). Instead of using the mixing model with the two components of seawater and basalts (van der Ploeg et al., 2018), in Chapter 2 the two end members are seawater and carbonate rock. The model requires input of both the $^{187}Os/^{188}Os$ value and Os concentration in each component. Using equations 2 to 11 listed in van der Ploeg et al. (2018; page 7), the model is able to calculate what percentage of osmium flux into Baffin Bay would need to be that of carbonate rock to increase the seawater $^{187}Os/^{188}Os$ and total Os values to those recorded in the core sediments during the $^{187}Os/^{188}Os$ peaks.

1.4.5 Carbonate correction

In Chapter 2 some of the major element, oxide and REE data is carbonate corrected over the detrital carbonate layers recorded in the Baffin Bay core. This was done to remove the effect of carbonate dilution on the data sets in order to see any trends in the data not caused by a large influx of carbonate material. In order to do this, the percentage carbonate of each peak and the background carbonate percent must be known, as well as the average element/oxide/REE concentration/% in the carbonate rocks and the core sediments. The effect of the carbonate dilution is then removed using the equation:

$$\left(\frac{(100 - A) \times \big((B \times 100) - (C \times D)\big)}{(100 - C) + (A \times D)}\right) \div 100$$

Where: A = the background carbonate %; B = chosen element value (ppm/%) at a chosen core depth (to be corrected); C = % carbonate at chosen core depth; D = the average chosen element value (ppm/%) of the carbonate rock.

1.5 Synopsis of research – Chapter 2: *Ice sheet dynamics and glacial palaeoceanography of Baffin Bay for the last 40 kyrs: new insights from a multi-geochemical approach*

Chapter 2 presents XRF, qXRD, REE, major oxides, $^{187}Os/^{188}Os$, foraminifera, sedimentology, and a robust radiocarbon age model study from a core in central Baffin Bay, and $^{187}Os/^{188}Os$, and radiocarbon ages for a second core south of Baffin Bay. The key objective is to enhance our understanding of the palaeoceanography and ice stream dynamics in this area from the LGM through the Holocene. The data also show the successful use of $^{187}Os/^{188}Os$ isotopes in a glacial setting. The study further constrains the timings of BBDC layers and finds that BBDC1 and BBDC0 are coincident with the Bølling-Allerød and Older Dryas and the Younger Dryas, respectively, indicating ice sheet response to both warmer and cooler climates. A radiogenic and felsic source provenance is also found over the BBDC layers, synonymous with granites, granodiorites, gneisses and gabbros, suggesting that the GIS was a large contributor. However, an LIS source cannot be ruled out due to similar geologies over west Greenland and Baffin Island. Finally, the GIS, LIS and IIS did not always react synchronously, with asynchronous behaviour between the IIS and GIS/LIS noted over BBDC0. A version of this chapter will be submitted to Quaternary Science Reviews (QSR) co-authored by David Selby (Earth Sciences, Durham University), Jeremy Lloyd, Colm O'Cofaigh and Peter Codling (Geography, Durham University), Paul Knutz (GEUS) and Sönke Szidat (University of Bern). I completed all Re-Os laboratory analysis, picking and sending of samples for external major, trace and REE analysis, foraminifera picking for radiocarbon dating on JR175, data synthesis, literature reviews and formulisation of the manuscript. Co-authors Selby, Lloyd and O'Cofaigh contributed through supervisor discussions and editorial comments on the manuscript. Peter Codling kindly allowed the use of data collected during his MSc at Durham University including foraminifera counts, grain size analysis, XRF data and magnetic susceptibility. Paul Knutz provided core samples and supporting radiocarbon data from core DA-04 as well as editorial manuscript comments. Sönke Szidat preformed the MICDAS radiocarbon analysis on 5 foraminifera samples from core JR175.

1.6 Synopsis of research – Chapter 3: *Postglacial palaeoceanography of the Baltic Sea Basin*

Chapter 3 presents $^{187}Os/^{188}Os$, BIT index biomarker, XRF, x-radiograph imagery, and sedimentological data for a core in the central Baltic Sea as well as $^{187}Os/^{188}Os$ data for several sediment surface samples from within and outside of the Basin. The goal is to further constrain the different sea stages the Baltic Basin has undergone since the LGM and through the Holocene and to show the key changes in chemistry associated with these changes, using the first application of $^{187}Os/^{188}Os$ to cores in the Baltic Basin. Due to low organic matter and microfossils for dating in deeper basins, pre-Littorina Baltic Sea stages are difficult to identify. The $^{187}Os/^{188}Os$ analysis of surface sediments shows a strong correlation between $^{187}Os/^{188}Os$ and salinity, and a clear difference between the $^{187}Os/^{188}Os$ of more open marine waters and more freshwater waters, hence indicating that $^{187}Os/^{188}Os$ values should be able to track marine vs. freshwater outflows and influxes. This study finds that $^{187}Os/^{188}Os$ combined with BIT index, XRF and sedimentology is successful in recording large changes in environment and clearly shows the change from the freshwater Ancylus Lake stage into the brackish Littorina Sea stage. These proxies, however, are not able to detect the smaller marine incursions during the Yoldia Sea stage. Although this may also be due to dilution of the signal by freshwater influx released the receding FIS. A version of this chapter will be submitted to Boreas co-authored by David Selby (Earth Sciences, Durham University), Jeremy Lloyd (Geography, Durham University), Matthias Moros (Leibniz Institute for Baltic Sea Research), Jaap Damste (Utrecht University) and Slawomir Dobosz (Szczecin University). I completed all Re-Os laboratory analysis, data synthesis, literature reviews and formulisation of the manuscript. Co-authors Selby and Lloyd contributed through supervisor discussions and editorial comments on the manuscript. Moros provided access to all core samples and XRF, TIC data, x-ray, and core images as well as through supervisor discussions and editorial comments. Damste provided the BIT index data and Dobosz the diatom data.

1.7 Synopsis of research – Chapter 4: *First evidence from the open Skagerrak of the absolute timing for the onset of Baltic Ice Lake drainage and evolution to the Baltic Sea since the LGM: Insights from radiocarbon ages, trace element and osmium geochemistry*

Chapter 4 presents XRF, TIC, sand content, $^{187}Os/^{188}Os$, and $\%C_{37:4}$ biomarker data alongside a robust radiocarbon geochronology for three cores located in the Skagerrak. This is with the aim of showing the first record of the Baltic Ice Lake drainage in the

Skagerrak through south-central Sweden and the further transitions into the Baltic Sea from the LGM and through the Holocene. The data suggest a high energy, short-lived freshwater influx entering the Skagerrak at ~11.7 cal ka BP. This is coincident with the final drainage of the Baltic Ice Lake and hence is the first record in the open Skagerrak of this event. The data also suggest that the initial first drainage of the Baltic Ice Lake dated to ~13 cal ka BP was not large enough to produce a detrital signature in the Skagerrak, but may still be recorded in biomarker data and hydrogenous $^{187}Os/^{188}Os$. A version of this chapter will be submitted to Boreas co-authored by David Selby (Earth Sciences, Durham University), Jeremy Lloyd (Geography, Durham University), Matthias Moros (Leibniz Institute for Baltic Sea Research), Ole Bennike and Jørn Bo Jensen (GEUS), and Thomas Blanz and Ralph R. Schneider (Geology, Kiel University). I completed all Re-Os laboratory analysis, data synthesis, literature reviews and formulisation of the manuscript. Co-authors Selby and Lloyd contributed through supervisor discussions and editorial comments on the manuscript. Moros provided access to all core samples and XRF, sand content and TIC data, as well as supervisor discussions and editorial comments. Bennike and Bo Jensen contributed radiocarbon dating and scientific background. Blanz and Schneider conducted the $\%C_{37:4}$ biomarker analysis.

1.8 Synopsis of research – Chapter 5: *Conclusions and further work*

Chapter 5 gives a summary of the major conclusions from the previous chapters and any further work recommendations to be undertaken.

Chapter 2: Ice sheet dynamics and glacial palaeoceanography of Baffin Bay for the last 40 kyrs: new insights from a multi-geochemical approach

*A version of this chapter will be submitted for publication to Quaternary Science Reviews (QSR) co-authored by David Selby of the Department of Earth Sciences, Durham University, Jeremy Lloyd, Colm O'Cofaigh and Peter Codling of the Department of Geography, Durham University, Paul Knutz of GEUS, and Sönke Szidat of the Department of Chemistry and Biochemistry & Oeschger Centre for Climate Change Research, University of Bern.

I completed all Re-Os laboratory analysis, picking and sending of samples for external major, trace and REE analysis, foraminifera picking for radiocarbon dating on JR175, data synthesis, literature reviews and formulisation of the manuscript. Co-authors Selby, Lloyd and O'Cofaigh contributed through supervisor discussions and editorial comments on the manuscript. Peter Codling kindly allowed the use of data collected during his MSc at Durham University including foraminifera counts, grain size analysis, XRF data and magnetic susceptibility. Paul Knutz provided core samples and supporting radiocarbon data from core DA-04 as well as editorial manuscript comments. Sönke Szidat preformed the MICDAS radiocarbon analysis on 5 foraminifera samples from core JR175.

2.1 Introduction

Baffin Bay provides a rich archive preserving a record of Quaternary glacial history of the surrounding regions with a particularly detailed record covering the last 40 kyrs. At the Last Glacial Maximum, Baffin Bay was surrounded by three major ice sheets. These were the Greenland Ice Sheet (GIS) to the east, the Innuitian Ice Sheet (IIS) to the north, and the Laurentide Ice Sheet (LIS) to the west, forming an almost continuous ring around the Bay (Fig. 2.1; Dyke et al., 2002; England et al., 2006; Jackson et al., 2017; Simon et al., 2012, 2014).

The exact timings of ice sheet advance and retreat from the continental shelves since the Last Glacial Maximum (LGM) remains uncertain (Andrews et al., 2018; Briner et al., 2006; Miller et al., 2002; Ó Cofaigh et al., 2013). This is, in part, due to slow sedimentation rates and poor preservation of biogenic carbonate during deglaciation into the Holocene, especially in deeper sedimentary records, as well as limited research on the

LGM, which means that well-dated sedimentary records from within Baffin Bay are lacking (Andrews et al., 1998; Jackson et al., 2017; Jennings et al., 2018; Simon et al., 2012). Further, modern-day observations of the Greenland Ice Sheet behaviour are becoming increasingly important due to the potential of the GIS to raise sea levels and alter ocean circulation as it loses mass through ice discharge and surface melting (e.g. Bamber et al., 2012; Enderlin et al., 2014; Jennings et al., 2017). However, this is challenging given the short timescale of these observations. An important aim of this study, therefore, is to gain a better understanding of the potential vulnerability of the GIS to future climate change. This is addressed by providing additional information on how the GIS, and the other ice sheets that surrounded Baffin Bay (IIS and LIS), have responded to changes in the past, particularly how their margins and ice streams change in response to different climate and ocean forcing scenarios, to provide context for modern changes and climate models (Jennings et al., 2014, 2017; Sheldon et al., 2016; Simon et al., 2014).

Past research has identified a sedimentary signature of major ice sheet dynamics within Baffin Bay. These are so called Baffin Bay Detrital Carbonate (BBDC) layers, which thin out southwards latitudinally across the bay. The layers are associated with a dynamical response of the Innuitian Ice Sheet to the north of Baffin Bay and the NE Laurentide Ice Sheet to the west that covered areas of Palaeozoic age carbonate-rich rocks including the landmass and smaller islands as well as on the floor of the Canadian Arctic Channels (Fig. 2.1; Andrews, 1987; Andrews et al., 1998; Andrews & Eberl, 2011; Hiscott et al., 1989; Simon et al., 2014). Input from the LIS in the west and GIS in the east of Baffin Bay may also contribute to these layers (Aksu & Piper, 1987; Hiscott et al., 1989; Simon et al., 2014). The GIS and LIS covered areas of mainly Archean to Paleoproterozoic granites, gneisses, and metasedimentary units (Hiscott et al., 1989; MacLean et al., 1990; Simon et al., 2012, 2014). The geological similarities either side of Baffin Bay make understanding the sediment provenance and the ice dynamics of the past ice sheets difficult (Aksu & Piper, 1979; Andrews et al., 2014; Harrison et al., 2011; Hiscott et al., 1989; Jennings et al., 2018; MacLean et al., 1990; Simon et al., 2014).

This study utilises a range of geochemical, radiogenic isotope and microfossil proxies on a sediment core from central Baffin Bay to unravel the potential contributions of the three major ice sheets surrounding Baffin Bay to the recorded BBDC layers to improve our understanding of the dynamical response of the ice sheets to climate changes since the LGM. The multi-geochemical approach of this study to tackling the complicated

glaciological and oceanographical history of Baffin Bay provides a new radiocarbon age model to further constrain the timings of the BBDC layers and reveals both synchronous and asynchronous behaviour of the three surrounding ice sheets. The defined ages of the carbonate layers BBDC1 and BBDC0 are coincident with the Bølling-Allerød and Older Dryas (BBDC1) and the Younger Dryas (BBDC0), indicating a dynamic and extensive response of the ice sheets to both warmer and cooler climate phases. The geochemical data point to a radiogenic, felsic source provenance synonymous with gabbros, granites, granodiorites, and gneisses as well as a carbonate source during the BBDC layers. The evidence available suggests a large contribution from a west Greenland GIS source, although a Baffin Island LIS source cannot be ruled out due to their similar geologies.

2.2 Oceanography and Geology of Baffin Bay

Baffin Bay is a narrow (max width = 650 km) ocean basin situated between Greenland, Baffin Island and the Canadian Arctic Archipelago (Fig. 2.1a) that is a product of extension of the Cretaceous-Palaeocene North Atlantic-Labrador Shelf Sea rift system (MacLean et al., 1990; Simon et al., 2012, 2014). Baffin Bay is connected to both the Arctic Ocean through the Nares Strait, and the Atlantic Ocean through the Davis Strait and Labrador Sea (Aksu & Piper, 1979; Andrews et al., 1998; Simon et al., 2012). The central abyssal plain of Baffin Bay is ca. 2 km deep, shallowing towards the north and south, and bordered by steep continental slopes. The water depth on the continental shelves ranges between 200 – 600 m (Aksu & Piper, 1979; Li et al., 2011). The west Greenland continental shelf is relatively wide (135 – 200 km) and is bisected by a number of troughs leading to large trough mouth fans (Jakobsson et al., 2012; Li et al., 2011; MacLean et al., 1990). On the western side of the bay, the Baffin Island shelf is narrower (25 – 50 km) with little evidence of trough mouth fans, creating an asymmetric shape to the bathymetry (Fig. 2.1b; Andrews et al., 2014; Jakobsson et al., 2012; Li et al., 2011; MacLean et al., 1990).

Figure 2.1: (Page 30) a) Map of Baffin Bay and its surrounding ice sheets at the last glacial maximum (LGM) and the simplified surrounding geology. Core 12PC is core HU2008029-12PC (Jennings et al., 2018). Base map from ArcGIS. Geology, circulation patterns and ice sheet extents extracted from Harrison et al., (2011), Simon et al., (2014) and references therein (England et al., 2006; Ó Cofaigh et al., 2013; Tang et al., 2004). GIS = Greenland Ice Sheet, IIS = Innuitian Ice Sheet, LIS = Laurentide Ice Sheet. Light and darker pink shades of the Rae Craton represent slightly different ages. Light pink = slightly older Archean to Mid-Palaeoproterozoic. Dark pink = Palaeoproterozoic age, on Baffin Island side this is the Foxe Fold and Pilling Group, on the Greenland side this is the Rinikian Fold Belt (Karrat and Anap Nua Groups). b) Cross sections and simplified geology across Baffin Bay from Baffin Island to the west coast of Greenland. Lines of the cross section are shown in part a). Cross section profiles obtained from GoogleEarthPro. Geology added using Harrison et al., (2011).

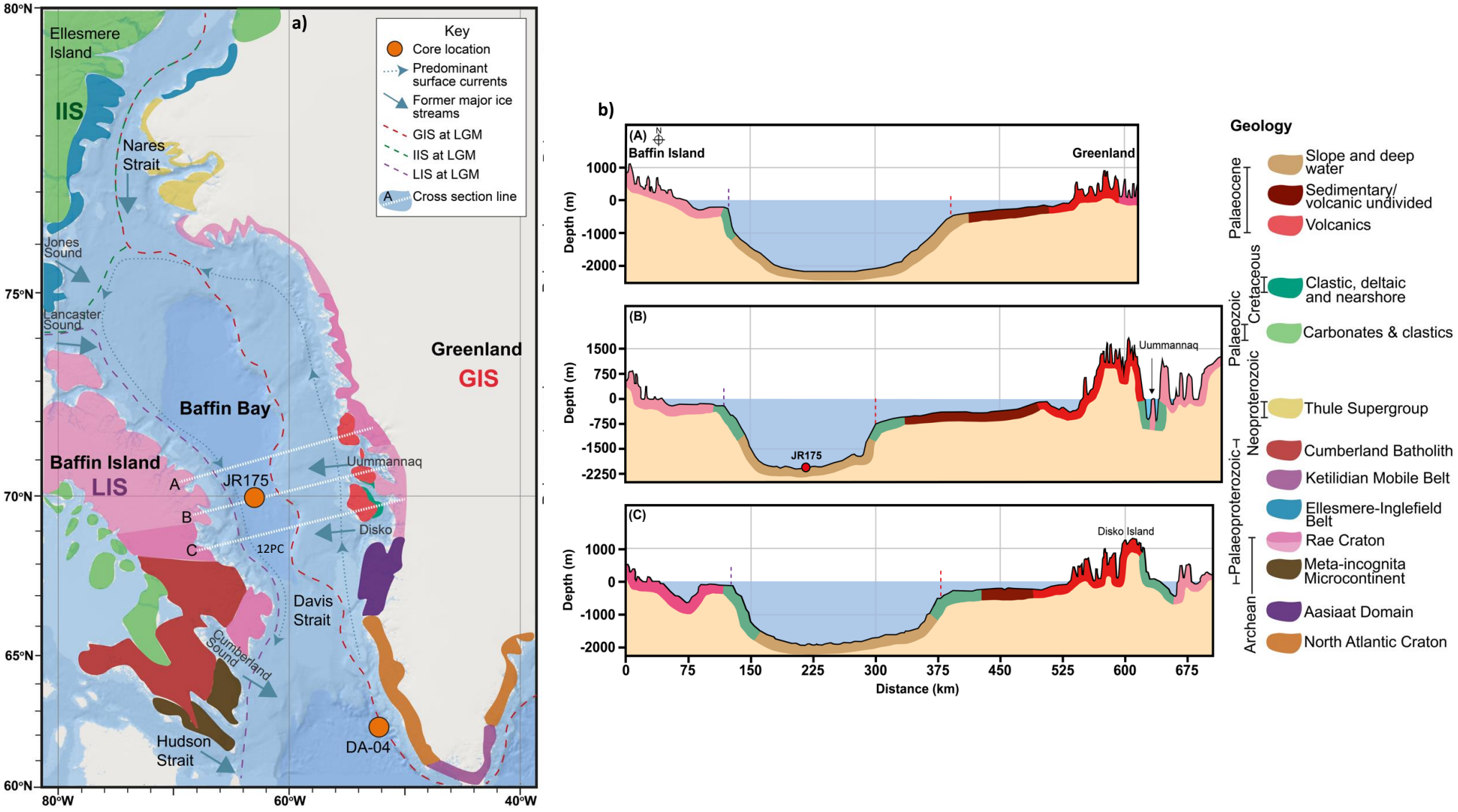
a)
Key
Core location
Predominant surface currents
Former major ice streams
GIS at LGM
IIS at LGM
LIS at LGM
Cross section line
Ellesmere Island
IIS
Nares Strait
Jones Sound
Lancaster Sound
Greenland
GIS
Baffin Bay
Baffin Island
LIS
A
B
C
JR175
12PC
Uummannaq
Disko
Davis Strait
Cumberland Sound
Hudson Strait
DA-04
80°N
75°N
70°N
65°N
60°N
80°W
60°W
40°W
b)
(A)
Baffin Island
Greenland
(B)
Uummannaq
JR175
(C)
Disko Island
Depth (m)
Distance (km)
Geology
Palaeocene
Slope and deep water
Sedimentary/ volcanic undivided
Volcanics
Palaeozoic
Cretaceous
Clastic, deltaic and nearshore
Carbonates & clastics
Neoproterozoic
Thule Supergroup
Palaeoproterozoic
Cumberland Batholith
Ketilidian Mobile Belt
Ellesmere-Inglefield Belt
Rae Craton
Meta-incognita Microcontinent
Archean
Aasiaat Domain
North Atlantic Craton

Maximum sea ice cover in Baffin Bay reaches approximately 60 ^{o}N latitude in February/ March covering much of the bay, then retreats to a minimum along the northern margins of the bay in September each year (~75 ^{o}N; Tang et al., 2004). The present-day anti-clockwise circulation is dominated by a number of currents (Fig. 2.1a; Andrews, 1987; Tang et al., 2004). The West Greenland Current flows north through the Davis Strait into Baffin Bay and along the west coast of Greenland and is formed from a combination of the East Greenland Current (cooler) and Irminger Current (warmer; Aksu & Piper, 1979; Jackson et al., 2017; Sheldon et al., 2016; Tang et al., 2004). Once the West Greenland Current reaches the northern most regions of the bay, it mixes with colder Arctic waters from the Nares Strait and through the Canadian Arctic Archipelago and heads south along the margins of Baffin Island, becoming the Baffin Island Current. Most of the Baffin Island Current eventually flows back out of the Davis Strait, although some is recirculated east, back towards Greenland (Aksu & Piper, 1979; Jackson et al., 2017). The deepest parts of Baffin Bay are occupied by the 'Baffin Bay Deep Water' and 'Baffin Bay Bottom Water' which are relatively cold (~ –0.5 ^{o}C) and saline water masses (Tang et al., 2004). These surface and subsurface waters also flow into the deep cross shelf troughs and fjords that surround the bay, allowing them to reach the current ice margins (Sheldon et al., 2016; Tang et al., 2004). However, circulation patterns in Baffin Bay likely haven't remained constant over time. At the Last Glacial Maximum (~33 – 19 Ka; Clark et al., 2009; Ó Cofaigh et al., 2019) for example, grounded and continuous ice sheets in the north of the bay would have blocked any channels and prevented Arctic waters from flowing southwards into Baffin Bay until the early Holocene (England, 1999; Jennings et al., 2011, 2018).

Prior to rifting and the formation of Baffin Bay during the Cretaceous-Palaeocene, Greenland and Baffin Island were joined and as a result share very similar geology (Fig. 2.1; Andrews et al., 2018; Harrison et al., 2011; MacLean et al., 1990; St-Onge et al., 2009). The geology of the eastern and western margins of Baffin Bay predominantly comprises Archean and Paleoproterozoic age crystalline units. On Baffin Island this includes metamorphosed clastics, granites, gneisses and volcanics of the Rae Craton, Foxe Fold Belt, and the Cumberland Batholith. On the west coast of Greenland this includes Archean gneisses and granites of the North Atlantic Craton and Aasiaat Domain, as well as Archean to Palaeoproterozoic aged metasediments, gneisses and granites of the Karrat Group and Rae Craton (Hiscott et al., 1989; MacLean et al., 1990; Simon et al., 2012, 2014). Palaeocene age basalts occur near Disko Island and Uummannaq Fjord as well as east of Baffin Island around Cape Dyer (Harrison et al., 2011; MacLean et al.,

1990; Simon et al., 2014). In the northern and north-eastern regions of Baffin Bay, the crystalline basement is overlain by a Palaeozoic marine carbonate and marine clastic dominated stratigraphic succession (Fig. 2.1a; Harrison et al., 2011; Hiscott et al., 1989; Simon et al., 2014).

More extensively on the Greenland Shelf but also on the inner Baffin Island Shelf, the offshore geology is consistent with the predominant onshore geology (Fig. 2.1b; MacLean et al., 1990). Precambrian rocks also occur further out on the shelf margin exposed by fault related structures (MacLean et al., 1990). Cretaceous and Tertiary aged sedimentary units then overlie the majority of the Baffin Island Shelf and Greenland Shelf, with only minor Palaeozoic carbonate exposures present in the south-east of the bay (Andrews et al., 1991; MacLean et al., 1990). The continental shelf surrounding Disko Island and Svartenhuk in the east, and Cape Dyer in the west, is made up of extensive Tertiary volcanic rocks (MacLean et al., 1990). It is then thought that Neogene age sediments, fan-delta sandstones and interbedded mudstones overlie much of the seafloor across Baffin Bay (MacLean et al., 1990).

The present-day sediments found within Baffin Bay originate from the surrounding bedrock as described above, arriving in the form of debris flows, meltwater plumes and turbidites sourced from the continental shelf and ice streams, as well as being released from icebergs (Aksu & Piper, 1979; Andrews & Eberl, 2011). On the Greenland Shelf, the main sediment contribution comes from ice rafting and meltwater from the Greenland Ice Sheet (Andrews et al., 2018; Chauché et al., 2014; Hudson et al., 2014). On the Baffin Island shelf, transport of sediments is mainly through fluvial and meltwater inputs (Andrews et al., 2018; Andrews & Syvitski, 1994). Sediment thickness in Baffin Bay increases further north, with ~2 km thickness around Davis Strait, and up to 14 km thickness in the north (MacLean et al., 1990). Carbonate-rich sediments (predominantly dolomite) are mainly found in the north, north-west and down the central portion of Baffin Bay, with contributions thinning southwards along the bay (Andrews et al., 1998, 2018; Andrews & Eberl, 2011). Sediments enriched in basaltic rock detritus are localised on the Greenland Shelf near Disko Island (Andrews et al., 2018; Andrews & Eberl, 2011). A west Greenland provenance is found largely for sedimentary units on the Greenland continental shelf (Andrews et al., 2015). This west Greenland provenance is also apparent in some areas along the Baffin Island continental shelf (Andrews et al., 2018).

2.3 Materials and methodological approach

2.3.1 Core details

This study focuses on the sedimentology of core JR175-GC01 (1.68 m gravity core; henceforth JR175) and BC06 (0.48 m box core) that were collected during the RRS *James Clark Ross* expedition (August-September 2009) at a latitude of 69º56.01 N and longitude of 63º03.4 W, at a water depth of 2034 m (Fig. 2.1; Table 2.1). The cores central position, not on one continental shelf, provides an ideal study site for understanding the dynamic glacial contributions and movements of all three ice sheets that surrounded Baffin Bay over the last 40 kyrs.

The sedimentology of a second 8.78 m long piston core DA04-31P was also investigated (henceforth DA04; Fig. 2.1; Table 2.1). Core DA04 has previously been studied in detail by Knutz et al. (2011). In this study the osmium isotope composition ($^{187}Os/^{188}Os$) of DA04 is investigated to understand the composition of a more open ocean signature through time to potentially track any marine inputs through the Davis Strait and into the Baffin Bay core site. The core was collected from a water depth of 2525 m at a latitude of 62º33.78 N and longitude of 54.22 W during a cruise of the R/V Dana in 2004 (Knutz et al., 2011). The chronology is based on 12 AMS radiocarbon dates that indicate c. 31 kyrs of sedimentation (Knutz et al., 2011). The core records distinct pale coloured carbonate horizons (15 – 20 wt.% $CaCO_3$) relating to Hudson Strait Heinrich events (Andrews & Voelker, 2018) HE1, HE2 and HE3 at ~2 m (~16 cal ka BP), 6 m (~24 – 23 cal ka BP) and 7.5 m (~29.8 cal ka BP), respectively (Knutz et al., 2011). BBDC layers are not recorded in the DA04 core, although ice rafted debris is present throughout. Between these horizons the lithofacies consist of laminated silty mud with some organic matter and also bioturbation above HE1 and in the Holocene at ~35 to 55 cm depth (Knutz et al., 2011, 2013). The sediments represent an open ocean setting which is away (~90 km) from the continental shelf and any immediate influence from grounded ice. Between 11 and 9 ka cal BP the core also records a decreased influence of Greenland Ice Sheet sourced meltwater and from then a stronger influence from the West Greenland Current flowing across the Davis Strait towards the south of Baffin Island (Knutz et al., 2011).

To provide clearer detail on the potential source of the $^{187}Os/^{188}Os$ signature in the sediment cores, a series of representative carbonate rock samples of the Palaeozoic (Cambrian to Silurian) succession were also sampled and analysed for their $^{187}Os/^{188}Os$ signature. These rocks originate from north-west of Baffin Bay through Lancaster Sound on Somerset Island and Devon Island (Table 2.1). This sample suite represents the

formations of Turner Cliffs, Ship Point, Bay Fiord, Irene Bay, Cape Phillips, and Allen Bay.

2.3.2 Radiocarbon dates and age modelling

A series of twelve radiocarbon dates were collected from the core (Table 2.2). The position of radiocarbon dates was partly based on presence of calcareous foraminifera as well as targeting specific sections of the core showing clear changes in proxies measured. Due to the low abundance of foraminifera in some sections of the core, dated samples were determined from a mix of benthic foraminifera species (though *Cassidulina neoteretis* was the dominant benthic species used for radiocarbon dates). Planktonic foraminifera (*Neogloboquadrina pachyderma*) were also utilised due to a scarcity of benthic species within some lower core intervals (see SM 2.1; section 2.4.3 for details).

Where foraminifera were more abundant accelerator mass spectroscopy (AMS) radiocarbon analysis on graphite was undertaken by BETA Analytic using between 4 and 10 mg of foraminifera, after pre-treatment with sonication in de-ionised water. Radiocarbon analysis where foraminifera were less abundant was undertaken at the Laboratory for the Analysis of Radiocarbon, Bern, using between 0.4 and 1.5 mg of sample utilising the MIni CArbon DAting System (MICADAS) AMS which allows analysis in gas form (CO_2), without the need for graphitisation, and hence allows for much smaller sample sizes whilst still being accurate and reproducible (Gottschalk et al., 2018; Missiaen et al., 2020; Szidat et al., 2014).

A Delta R (ΔR) value of 140 ± 30 years was applied to all radiocarbon dates to correct for isotopic fractionation effects and the marine carbon reservoir effects based on previous works and consistency with other studies (Jackson et al., 2017; Jennings et al., 2014, 2018). However, it is noted that the marine reservoir effects could be quite variable over the time interval of core JR175. Corrected radiocarbon ages shown in Table 2.2 are obtained using the Calib 8.2 software using the MARINE20 calibration curve. Utilising the raw radiocarbon dates an age-depth model was developed using the BACON age modelling package in R, which also follows the MARINE20 database (SM 2.2; Blaauw & Christen, 2011; Reimer et al., 2013; Stuiver et al., 2020). In the BACON model a boundary was placed at 22 cm and 122 cm creating three 'sections' to distinguish between averaged sedimentation rates of 500, 60 and 580 years per cm at 0 – 22 cm, 22 – 122 cm and 122 – 154 cm, respectively.

2.3.3 Particle size analysis, magnetic susceptibility, X-rays, ice rafted debris (IRD), TIC/TOC

To attain the basic physical properties of the core, sedimentological data such as grain size and IRD counts and properties such as magnetic susceptibility and X-ray imagine was undertaken. Particle size analysis (PSA) was undertaken using ~0.5 g of core material at 4 cm intervals down core JR175. To break down all organic matter, 20 ml of hydrogen peroxide (H_2O_2; 6%) was added to each sample and then left for 24 h in a boiling water bath. Hydrochloric acid (HCl; 10%) was then added to dissolve the very high amounts of calcareous foraminifera present in some intervals to give a better representation of particle size. Samples were centrifuged for 4 minutes and the liquid removed then refilled with distilled water, which was repeated twice to remove all the H_2O_2 and HCl. Next, 20 ml of sodium hexametaphosphate solution is added and samples are stirred to aid deflocculation before analysis on a Coulter LS 13 320 laser diffraction particle size analyser equipped with laser granulometer and Polarisation Intensity Differential Scattering (PIDS). PSA measurement range is 0.04 to 2000 μm. The data was then analysed using GRADISTAT (Blott & Pye, 2001). Magnetic susceptibility (MSCL) data was obtained using a Geotek multi-core scanner and Geotek Vertical X-Ray CT system at the Department of Geography at Durham University. The system enables a downcore spatial resolution of ≤ 100 μm and produces a detailed 2D x-ray image that was utilised to identify clasts and sedimentary structures. The core was analysed using the ImageJ software package. IRD was counted as sediment that was over 2 mm in size and was counted with the aid of the x-ray images produced in ImageJ.

Total carbon (TC), total organic carbon (TOC) and total inorganic carbon (TIC) was measured using an Analytik Jena Multi Elemental Analyser 4000 at the Department of Geography at Durham University. Approximately 20 g of sediment was freeze-dried, and ball milled. A 20 to 30 mg aliquot of this was used for the TC run and then 40 to 50 mg was used for the TIC run which was further treated with 40% Orthophsphoric acid (to remove any organic component). Both were then combusted at 1000 to 1500 ^{o}C in the presence of O_2 and no catalyst and the resulting gas was analysed by a Non-Dispersive Infrared (NDIR) detector. TOC is calculated as TOC = TC – TIC.

2.3.4 Foraminifera abundance

Foraminiferal data was collected as it is necessary for radiocarbon dating but also numbers can be linked to changes in productivity and nutrient flux which can be associated with shifts in sea ice (Jennings et al., 2017, 2018; Lloyd, 2006; Nørgaard-

Pedersen et al., 2003; Wollenburg et al., 2004). A record of foraminifera (benthic and planktonic) was developed for JR175 at a resolution ranging from 1 to 2 cm. For each sample 1 cm^3 of sediment was soaked in distilled water overnight to disaggregate the sediment before washing through a 500 and 63 μm mesh (Scott et al., 2001). Specimens were identified and counted under suspension in distilled water using a Leica light microscope. The target foraminiferal count was 300 specimens per sample, however, for many samples this was not possible, with many samples having less than 100 specimens and some being barren. Species identification was undertaken following the criteria of Feyling-Hanssen (1964) and Lloyd, (2006).

2.3.5 XRF and qXRD

High resolution X-ray fluorescence (XRF) data was obtained for the whole length of core JR175 as well as several samples for quantitative X-ray diffraction (qXRD) analysis. Although a large suite of elemental data was produced by XRF this study focusses specifically on the relative abundance of calcium (Ca) as a proxy for carbonate recorded in JR175. qXRD analysis combined with the use of the SedUnMixMC program described below allows the identification of potential source areas into Baffin Bay to aid with the understanding of the ice sheet dynamics at that time.

Prior to sampling core JR175, XRF data was obtained using a Geotek multi-core scanner and Geotek Vertical X-Ray CT system at the Department of Geography at Durham University. The system enables a downcore spatial resolution of ≤ 100 μm. The XRF data from the core surface was obtained by the bombardment of high energy x-rays (15W/50kV) generated in a rhodium x-ray tube, with x-ray detection using a Canberra Silicon Drift Detector. To improve the sensitivity of light element determinations (e.g., calcium, magnesium, aluminium, and silicon), the measurement cell was flushed with helium.

qXRD analysis was performed using established protocols (Andrews et al., 2018; Andrews & Eberl, 2011; Eberl, 2003). In brief, qXRD was determined on the < 2 mm sediment fraction of 25 samples over the length of JR175 with an interval spacing between 4 and 9 cm. The samples were measured on a Siemens D5000 XRD unit between 5 and 65 2-theta at a 0.02 2-theta step with a 2 s count, resulting in 3000 data points. The XRD data was imported into the Excel macro-program Rockjock v6 to quantify the wt. % of thirty-three nonclay and clay minerals including alkali-feldspars, plagioclase, dolomite and illite minerals, which were then normalised to sum to 100%. This method

is ranked 3rd in the international Reynold Cup, whereby the results are tested against artificial known mineral mixtures (McCarty, 2002). The average bias on a mixture of 11 common minerals (bias = abs [Measured wt. % – Estimated qXRD wt. %]) was ±1 wt. %. To further understand the sediment composition the program SedUnMixMC (Andrews et al., 2018; Andrews & Eberl, 2011; Eberl, 2003) which uses a Monte Carlo approach to randomly sample (n = 100) the available source samples (including a mixture of bedrock samples and large IRD clasts found in Baffin Bay cores) and calculate a standard deviation on the estimates was used. The analysis allows the determination of geochemical assemblages and identification of samples with similar mineral compositions to allow simplified changes in provenance of the core sediments to be seen (Andrews et al., 2018 and references therein). The simplified provenance sources used in this study are: detrital carbonate; west Greenland granites and granite-gneisses; south-west Greenland bedrock; weathered Tertiary and Cretaceous bedrock; Foxe Fold Belt rocks; and Baffin granitoids (igneous and metamorphic bedrock of Baffin Island; based on methodology and sources described by Andrews et al. 2018).

2.3.6 Lithogeochemistry

A representative suite (N = 23) of samples from JR175, each recording a 1 cm stratigraphic interval, were analysed for major, trace and rare earth elements (REEs) to provide further information that can be related to specific source areas to help understand the provenance of the core sediments. These were analysed using a combination of fusion inductively coupled plasma mass spectrometry (ICP-MS) and total digestion (TD) ICP-MS by Activation Laboratories following standard analytical protocols (4Lithores – research). The same set of analysis was also undertaken for 10 carbonate rock samples from Somerset and Devon Islands to understand the chemical composition of this potential source of Baffin Bay sediments. Samples were dried at 60˚C overnight and then powdered in agate prior to analysis. Powdered samples for ICP-MS analysis are mixed with lithium metaborate-tetraborate and fused to ensure complex sample digestion of all phases. Detection limits for the 4Lithores research analysis are low ppm / ppb for most trace elements. Standards and duplicates analyses are within a few ppm for the majority of the elements.

2.3.7 Rhenium-osmium (Re-Os) isotope analysis

Ninety-nine samples were selected for Re-Os analysis from the cores of JR175 (N = 77), BC06 (N = 1) and DA04 (N = 21). Each sampled interval records ~1 cm of stratigraphy. The collected samples were dried at 60˚C overnight, and then sieved to remove any large

clasts (> 2 mm), and then powdered using an agate pestle and mortar. The Re-Os analysis is based on established procedures (Selby & Creaser, 2003) and was conducted at Durham University in the Durham Geochemistry Centre in the Department of Earth Sciences. In brief, approximately 1 g of powdered sample is sealed into a Carius tube with 8 mL CrO_3 4N H_2SO_4 and a pre-determined known amount of mixed tracer solution (^{185}Re + ^{190}Os) and heated at 220 ^{o}C for 48 h in an oven. The Carius tubes are opened and a solvent extraction is undertaken using 9 mL chloroform ($CHCl_3$) to separate the Os into a glass vial that is then back extracted into 3 mL HBr. The Os fraction is further purified by H_2SO_4-CrO_3-HBr microdistillation. A pure Re fraction is obtained from 1 mL of the Os extracted CrO_3-H_2SO_4 solution using a NaOH (5 N) -acetone extraction. The Re-bearing acetone fraction is further purified using HCl-HNO_3 anion bead chromatography. The Re and Os fractions are loaded onto Ni and Pt filaments, respectively and analysed using a ThermoScientific TRITON mass spectrometer using negative thermal ionisation mass spectrometry (NTIMS). The isotope composition of Re and Os is determined using Faraday collectors in static mode and an electron multiplier in dynamic mode, respectively.

The main application of Re-Os analysis in this study is the use of the hydrogenous osmium isotopic composition ($^{187}Os/^{188}Os$). The $^{187}Os/^{188}Os$ of organic-rich sediment units is used to establish a high-resolution $^{187}Os/^{188}Os$ composition record of the water column at the time of deposition and thus can be used to aid in reconstructing Pleistocene ice sheet fluctuations (Peucker-Ehrenbrink & Ravizza, 1996; Rooney et al., 2016). The $^{187}Os/^{188}Os$ composition of the water column responds rapidly (residence time = 1 – 50 ka, many studies < 10 ka), and the inferred $^{187}Os/^{188}Os$ of the water column can identify shifts in the flux of radiogenic glacially eroded material that can be used to track ice sheet advance and retreat patterns (Levasseur et al., 1999; Oxburgh, 1998, 2001; Peucker-Ehrenbrink & Ravizza, 2012; Rooney et al., 2016; Sharma et al., 1997)

Further, seven of the carbonate rock samples obtained from Somerset and Devon Island and five larger clasts found within core JR175 (both carbonates and granites/gneisses), were also analysed. This was in order to ascertain the $^{187}Os/^{188}Os$ composition of the potential carbonate source and of the IRD clasts found in core JR175 which provides an idea of the source materials at the time of their deposition. This followed the same method as described above except digestion is undertaken using inverse aqua regia (3 mL 11 N H_2SO_4, 6 mL 15.5 N HNO_3), and samples were left in the oven at 220^{o} C for longer (~72 h) to ensure full digestion.

The H_2SO_4-CrO_3 solution is manufactured from the same stock of H_2SO_4 and CrO_3 materials and as a result the total analytical protocol blanks are similar throughout the study (Re = 15.97 ± 6.26 ppt, Os = 0.10 ± 0.07 ppt, with a $^{187}Os/^{188}Os$ of 0.23 ± 0.22; 1 S.D., N = 8). To monitor the long-term reproducibility of the Re-Os isotope composition determinations, Re and Os solution standards were routinely analysed. A 50 pg osmium standard solution (DROsS - Durham Romil Osmium Standard) gives $^{187}Os/^{188}Os$ values of 0.16074 ± 0.00026 (1 S.D., N = 26), which is in agreement with proposed values for the solution and the laboratory running average (0.16082 ± 0.00063 1 S.D; N = 816; Luguet et al., 2008; Nowell et al., 2008). The 125 pg rhenium standard solution (Restd) yields $^{185}Re/^{187}Re$ values of 0.59855 ± 0.00096 (1 S.D., N = 26), which is in agreement the laboratory running average (0.59861 ± 0.0015 1 S.D; N = 720).

2.4 Results

2.4.1 Radiocarbon dates and age modelling

Radiocarbon dates were established for twelve foraminifera samples and the calibrated ages are presented in Table 2.2 and Figure 2.2. The length of JR175 represents ~40 kyrs of sedimentation. The two dates obtained from the depth of 106 cm record calibrated ages with only 35 years difference at the 2σ middle value using both the AMS and MICADAS AMS methods at 16,002 and 15,967 cal BP, respectively, showing both techniques produce concordant results.

Using the BACON age modelling software (with the MARINE20 calibration and a Delta-R value of 140 ± 30 years), an age-depth model for JR175 is presented (Fig. 2.2; SM 2.2). This age model constrains the chronology of the core from the late Quaternary through to the Holocene with the oldest radiocarbon date of 39,900 cal years BP at 154 cm. The date of 34.5 cal ka BP at 168 cm is rejected by the BACON software. As this sample was taken from the very base of the core it may have experienced re-working or contamination during core extraction. This period of time covers a number of significant events in Baffin Bay including: the LGM (~33 – 19 Ka; Clark et al., 2009; Ó Cofaigh et al., 2019); Baffin Bay detrital carbonate layers BBDC0 (~12.7 – 11 cal ka BP), BBDC1 (~14.2 – 13.7 cal ka BP), BBDC2 (~25 – 24.7 cal ka BP), BBDC3 (~27.7 – 26.4 cal ka BP) and BBDC4 (~37 – 31.9 cal ka BP; Jackson et al., 2017; Simon et al., 2014), the Bølling-Allerød period (~14.7 – 12.9 cal ka BP; Rasmussen et al., 2006), and the Younger Dryas (12.9 – 11.7 cal ka BP; Rasmussen et al., 2006).

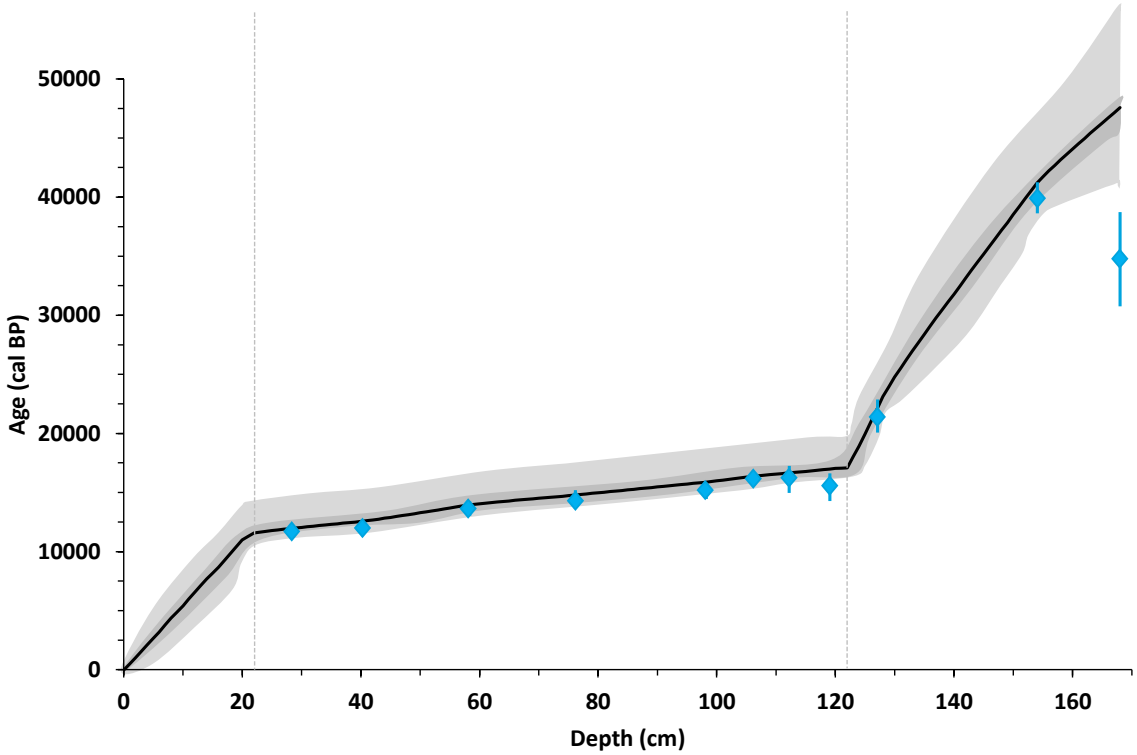

Figure 2.2: Age model developed for core JR175 calibrated using the MARINE20 curve and the Bayesian modelling of radiocarbon dates using the BACON software. Blue lines show the calibration range of the raw input ^{14}C ages. The grey area shows 95% confidence limits with darker grey indicating the more likely calendar ages (Blaauw & Christen, 2011).

2.4.2 Physical properties and lithofacies

Utilising the physical sediment properties of core JR175 (Fig. 2.3) eight lithofacies are identified and described below against depth in terms of their sedimentology, x-rays, grain size, IRD, magnetic susceptibility and TOC. In general, the sediments in JR175 vary between laminated sandy beds, silty organic matter-bearing clays, and diamicton units. The top 100 cm of the core is more clay-rich, and below the units become more sand-rich (SM 2.3a). The magnetic susceptibility of JR175 is highest within the sandy units (~202 - 850 SI x10^{-5}), decreasing abruptly in more clay and silt-rich units (~0 - 200 SI x10^{-5}; Fig. 2.3; SM 2.3b). TOC is stable at < 1% for most of the core except for two peaks to 2.8 and 3.8% between 78 and 58 cm and 42 and 20 cm, respectively (Fig. 2.3; SM 2.3c). Larger (> 2 mm) ice rafted debris (IRD) clasts are found throughout the core (Fig. 2.3; SM 2.3d). Clast lithology is both granitic and carbonate in composition. Larger lithic clasts within the core were identified visually using a light microscope.

2.4.2.1 Lithofacies 1

Core imagery (168 to ~122 cm) shows dark, homogeneous sediments with exception to the deepest ~10 cm which is slightly lighter and between 140 and 135 cm where a lighter banded layer is found corresponding to a higher silt content. This lithofacies (Lithofacies

1) consists of mid- to dark brown massive sandy silt and represents the more sand-rich sediment of the core. Although the sand content varies greatly (0 and 80%; Fig. 2.3). This section possesses TOC values of < 0.5%. The interval is largely devoid of IRD except for 5 clasts between 122 and 129 cm. Characteristic of Lithofacies 1 is the highest and most variable magnetic susceptibility values, varying between 3.9 and 855 SI $x10^5$, the largest peak occurring at 126 cm. The top of this lithofacies is placed at 122 cm in the Bacon age model (Fig. 2.2) as discussed in the methods, due to a change in sedimentation rates shown by the larger change in ages over a shorter depth (~20 kyrs over 50 cm compared to e.g., ~5 kyrs between 122 and 72 cm; Fig. 2.3). Based on the age model produced (SM 2.2), this facies records sedimentation between 47.6 and 17.1 cal ka BP.

2.4.2.2 Lithofacies 2

In the interval between ~122 and 108 cm, lithofacies 2 is characterised by light-brown massive clayey-silt sediments (Fig. 2.3). Silt is the predominant grain-size throughout this interval with the proportion of clay increasing upcore. The sand content is relatively constant. TOC remains low at < 0.5% and by the start of this lithofacies the magnetic susceptibility has decreased to 110 SI $x10^5$ and remains constant except for one peak to 280 SI $x10^5$ at 117 cm. No IRD is recorded in this section. Based on the age model produced (SM 2.2), this facies records sedimentation between 17.1 and 16.5 cal ka BP.

2.4.2.3 Lithofacies 3

The change between lithofacies 2 and 3 is a fairly sharp and curved contact as sediments return to a darker x-ray shading, indicating more dense sediments from 108 cm until 86 cm, and a return to mid- to dark brown sandy and silty sediments (Fig. 2.3). Lithofacies 3 is associated with numerous IRD clasts, stable clay (~20%), increasing silt (up to ~70%) and decreasing sand contents (to ~15%). TOC is < 0.5% and magnetic susceptibility peaks at 204 SI $x10^5$ between 100 and 94 cm. Based on the age model produced (SM 2.2), this facies records sedimentation between 16.5 and 15.3 cal ka BP.

2.4.2.4 Lithofacies 4

Lithofacies 4 records light brown massive clayey and silty sediments. Between 86 and 76 cm the sediments and x-ray images return to a paler colour and IRD clasts disappear completely within this interval (Fig. 2.3). TOC and magnetic susceptibility are both low at the bottom of lithofacies 4 (< 0.5% and 90 SI $x10^5$, respectively) but both increase to the top of the lithofacies to ~1% and 130 SI $x10^5$, respectively. Based on the age model produced (SM 2.2), this facies records sedimentation between 15.3 and 14.8 cal ka BP.

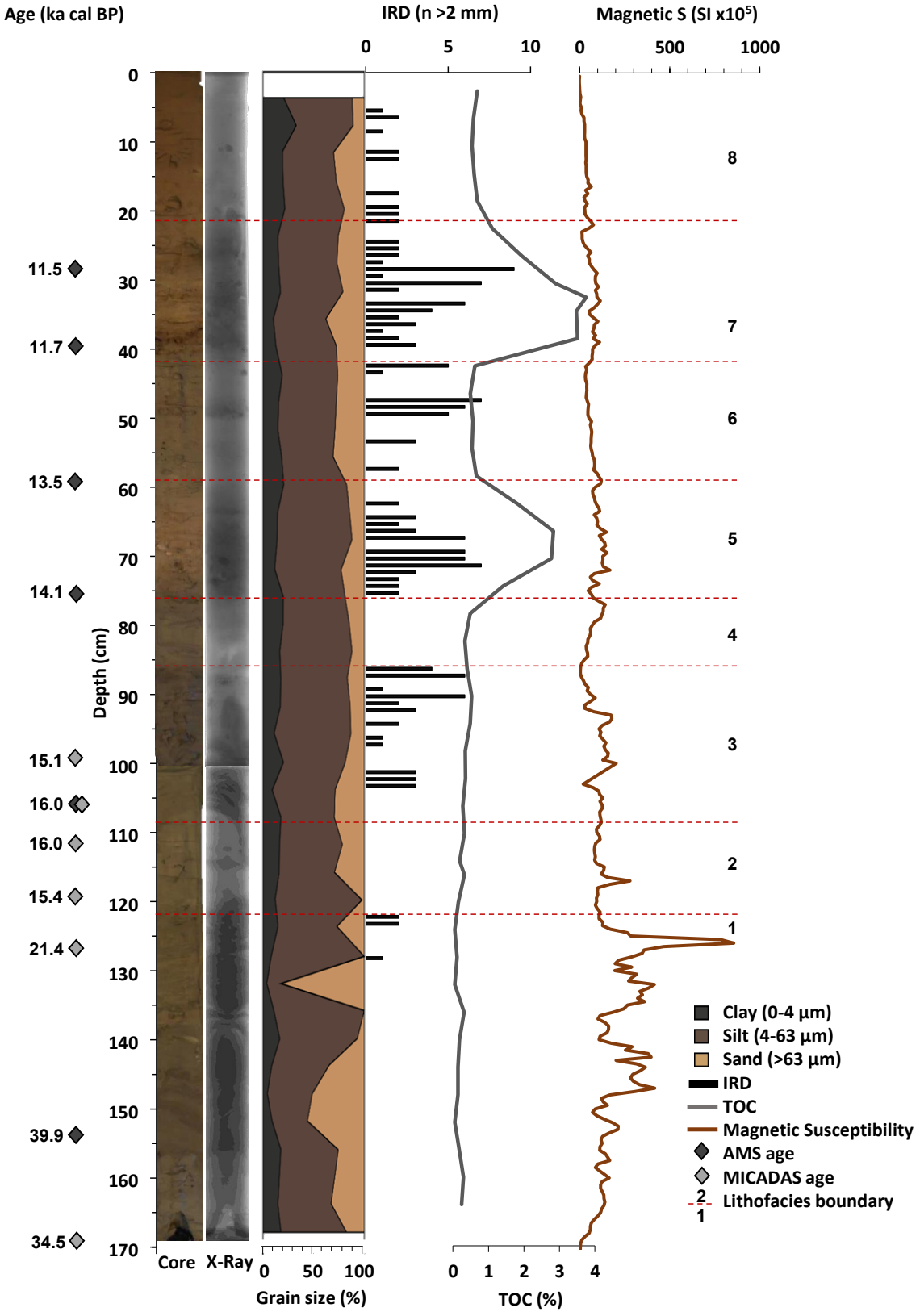

Figure 2.3: Radiocarbon data (cal ka BP), core and X-ray photos, grain size (%), IRD (n > 2 mm), TOC (%), and magnetic susceptibility (SI x10^5) against depth (cm). Dark coloured diamonds next to the radiocarbon age indicate calibrated ^{14}C AMS ages and light-coloured diamonds indicates calibrated ^{14}C MICADAS AMS ages. Dashed red lines denote the different lithofacies boundaries

2.4.2.5 Lithofacies 5

From 76 to ~59 cm lithofacies 5 is comprised of a light brown to cream coloured massive diamicton, with a darker coloured x-ray (Fig. 2.3). As well as the noticeable colour change in the sediments, this lithofacies represents the first of two peaks in TOC levels, in this case up to 2.8%. IRD clasts are abundant between 76 and 62 cm, and clay, silt and sand levels are relatively stable. Magnetic susceptibility also records a small peak (170 SI $x10^5$) with more fluctuating values (65 – 170 SI $x10^5$). Based on the age model produced (SM 2.2), this facies records sedimentation between 14.8 and 14.0 cal ka BP.

2.4.2.6 Lithofacies 6

Between the depths of ~59 cm to 42 cm, the sediments of lithofacies 6 are grey to mid-brown coloured, lightly laminated sandy to clayey silts and the x-ray image returns to a lighter colour (Fig. 2.3). Less abundant IRD clasts are found in this section except for ~47 to 50 cm depth which corresponds with a darker band in both the x-ray and core images. The sand content also increases just before this peak in IRD to ~25%. This lithofacies is also marked by TOC levels dropping to between 0.4 and 0.7% and the magnetic susceptibility smoothly and gradually decreasing from ~120 to 40 SI $x10^5$. Based on the age model produced (SM 2.2), this facies records sedimentation between 14.0 and 12.7 cal ka BP.

2.4.2.7 Lithofacies 7

Lithofacies 7 shares very similar characteristics with lithofacies 5. The sediments are light brown to cream coloured diamictons between 42 and 22 cm and have a darker x-ray colour (Fig. 2.3). Like with lithofacies 5, further defining aspects of lithofacies 7 are abundant IRD clasts and a peak in TOC, this time to 3.8% but with a more asymmetrical peak shape. Magnetic susceptibility also again records a fluctuating and shallow peak between 42 and 22 cm from 40 to 115 SI $x10^5$. Sand, silt, and clay contents are stable except a decrease in clay content (to ~10%) and increase in sand content (to ~35%) at 30 cm. The end of this lithofacies (22 cm) is also the positioning of another boundary in the Bacon age model (Fig. 2.2). This boundary was chosen due to a perceived change in sedimentation rates between the top portion of the core recording ~11 kyrs in ~20 to 25 cm of sediment, compared to lithofacies 7 recording < 1 kyrs also in 20 to 25 cm of sediment. The boundary is placed at 22 cm to coincide with the juxtaposition between lithofacies 7 and 8 as it seems more logical a change in sedimentation rates would occur between two sediment types rather than in the middle. Based on the age model produced (SM 2.2), this facies records sedimentation between 12.7 and 11.6 cal ka BP.

2.4.2.8 Lithofacies 8

The final lithofacies represents the depth from 22 cm to the core top (0 cm). Sediments here begin as lightly laminated sandy silts of mid-brown colour moving to a darker brown, lightly laminated, more clay rich unit at the core top, with some larger clasts throughout, and the x-ray image returns to a light colour picking out some of the larger clasts (Fig. 2.3). TOC levels are between 0.5 and 0.7%, and magnetic susceptibility decreases to almost zero by the core top. Based on the age model produced (SM 2.2), this facies records sedimentation between 11.6 cal ka BP and the present day.

2.4.3 Foraminifera species and abundance

The benthic foraminiferal fauna shows a relatively low diversity with a total of 19 benthic species identified. The benthic foraminiferal assemblages were overwhelmingly dominated by *Cassidulina neoteretis,* with *Trioculina spp* also common. The remaining species were only present in low abundances (1 to 5 foraminifera per sample). The planktonic foraminifera species *Neogloboquadrina pachyderma* was also identified (SM 2.1). Due to the very low diversity, the full assemblage details are not presented here, only the absolute abundance of benthic and planktic specimens. Between 40 to 17 cal ka BP and 11 to 0 cal ka BP only infrequent, very small numbers of foraminifera can be found in core JR175 (Fig. 2.3). Greater foraminifera abundances are found between 17 and 15.5 cal ka BP (> 2000 individuals per 4 ml; lithofacies 2 and 3), 15 and 13.5 cal ka BP (up to ~560 individuals per 4 ml; lithofacies 5 and 6), and in lithofacies 7 between 12.7 and 11.6 cal ka BP (up to ~680 individuals per 4 ml). The greater abundances in lithofacies 7 are dominated by benthic foraminifera, whereas the older foraminifera rich intervals (lithofacies 2 to 3 and 5 to 6) are dominated by planktic foraminifera.

2.4.4 Lithogeochemistry – XRF, ICP-MS, and qXRD data

2.4.4.1 XRF

Whilst XRF scanning measured a wide range of elements, only the calcium (Ca) data is presented here in detail, for use as a proxy for carbonate content to identify the BBDC layers. For the entire core the Ca cps varies between 1,500 and 25,000 cps (Fig. 2.4; SM 2.4). In lithofacies 1 between ~39.9 and 17.1 cal ka BP Ca counts vary between 3000 and 13,000 cps as the profile is interrupted by several peaks. The most significant of these peaks in Ca cps occurs between ~36 and 29 cal ka BP (13,000 cps), ~28 and 23 cal ka BP (10,000 cps), and ~21 and 17 cal ka BP (9400 cps). Peaks in Ca also occur in lithofacies 2 (~17 – 16 cal ka BP; 6615 cps), and lithofacies 3 (~16 – 15 cal ka BP; 7548 cps). In

lithofacies 4, Ca content begins to increase to 15,400 cps forming the start of a peak to the highest counts of Ca over the core recorded in lithofacies 5. This is a peak to 25,000 cps between ~15.0 and 14.0 cal ka BP. Calcium counts then decline to an average of ~6000 cps in lithofacies 6, except for a peak to 12,000 cps at 12.8 cal ka BP. The second largest peak in Ca occurs in lithofacies 7 between ~12.7 and 11.6 cal ka BP. From ~11.6 to 0 cal ka BP, Ca cps gradually decrease from 7300 – 1900 cps. The age constraints for the two large Ca peaks in lithofacies 5 and 7 coincide with the timings suggested for BBDC1 (~14.2 – 13.7 cal ka BP) and BBDC0 (~12.7 – 11 cal ka BP; Jackson et al., 2017; Simon et al., 2014).

2.4.4.2 qXRD

The mineral compositions of sediment samples determined by qXRD in JR175 including calcite, dolomite, smectite, kaolinite, illites, biotite, FeO, plagioclase, amphibole, quartz, pyroxene, SiO_2, and alkali feldspar (Table 2.3) are fed into the SedUnMix model. These are compared to rock samples that are representative of simplified source areas into Baffin Bay including: detrital carbonate; west Greenland; south-west Greenland; weathered Tertiary and Cretaceous bedrock; the Foxe Fold Belt; and Baffin granitoids. This then provides an idea of sediment provenance from the sediments analysed in JR175 (Fig. 2.5; SM 2.5).

In lithofacies 1 the predominant sources to the sediments found in JR175 are from south-west Greenland, west Greenland, and Baffin Island, with lesser input from a detrital carbonate source and minimal input from the Foxe Fold Belt and weathered Tertiary and Cretaceous rocks (Fig. 2.5). In lithofacies 2, a west Greenland and Baffin Island source is dominant as input from SW Greenland decreases. Lithofacies 3 sees an increase in detrital carbonate sourced material as well as from the Foxe Fold Belt, and a further peak in material from SW Greenland as contributions from west Greenland and Baffin Island decrease. This trend continues into lithofacies 4 apart from the detrital carbonate source which decreases to almost zero. Lithofacies 5 sees the detrital carbonate component dominate almost completely, with all other source contributions except the weathered Tertiary and Cretaceous component dropping to zero. The contribution of detrital carbonate drops to about half during lithofacies 6, with the remaining contribution coming from the Foxe Fold Belt, SW and W Greenland, and Baffin Island. Lithofacies 7 is very similar to lithofacies 5, with detrital carbonate making up almost the whole contribution whilst inputs from the other 5 sources decrease to almost zero. Finally, through lithofacies 8 the contribution of detrital carbonate declines to ~25%, the W and SW Greenland

contributions decrease to almost zero, the Baffin Island input increases slightly, but the largest contributions combining to make up 75% of the total input into the sediments from JR175 are that from the Foxe Fold Belt and the weathered Tertiary and Cretaceous rocks (Fig. 2.5).

2.4.4.1 Major, trace elements and REEs

Major oxide geochemistry determination was obtained for selected samples from ~111 to 2.5 cm from core JR175, to characterise the geochemistry of the different sections of the core based on the major lithofacies identified. Presented below are the major, trace and oxide element data considered of most interest to this study.

Firstly, the two main peaks in Ca cps and detrital carbonate contribution recorded in lithofacies 5 and 7 are matched by peaks in CaO% of ~15% and 17% between 15 and 14 cal ka BP and 13 and 11.6 cal ka BP, respectively (Fig. 2.4; SM 2.6), showing that Ca cps is a good proxy for detrital carbonate content, and hence detecting detrital carbonate layers.

The major-element oxide data and La and Sc data is carbonate corrected for the sediments taken from the Ca-rich depths in core JR175 corresponding to BBDC1 (~77 – 60 cm) and BBDC0 (~42 – 24 cm; Table 2.4a). The carbonate correction is based on the average elemental-oxide values for carbonate rocks from Somerset and Devon Islands which are considered representative of the Palaeozoic carbonates on the Canadian Islands and channel floors (this study; Table 2.4b), which are considered to be the likely origin of carbonate associated with detrital carbonate layers in Baffin Bay (Fig. 2.1; Andrews, 1987; Andrews et al., 1998; Andrews & Eberl, 2011; Hiscott et al., 1989; Simon et al., 2014). The decision to carbonate correct these values was done to obtain a better understanding of other potential sources into Baffin Bay than the carbonate rocks of the north and north-west.

Figure 2.4: (Page 47) Foraminifera (counts per 4 ml), Ca (cps), Calcite + dolomite (%), CaO (%), $^{187}Os/^{188}Os$, total Os (ppt), Re (ppb), La/Sc, K_2O/Na_2O, SiO_2/Al_2O_3, and IRD (clasts > 2 mm) for JR175 plotted against the age model determined from Figure 2. Shaded areas and dashed lines represent the different lithofacies and the boundaries between them. See text for discussion.

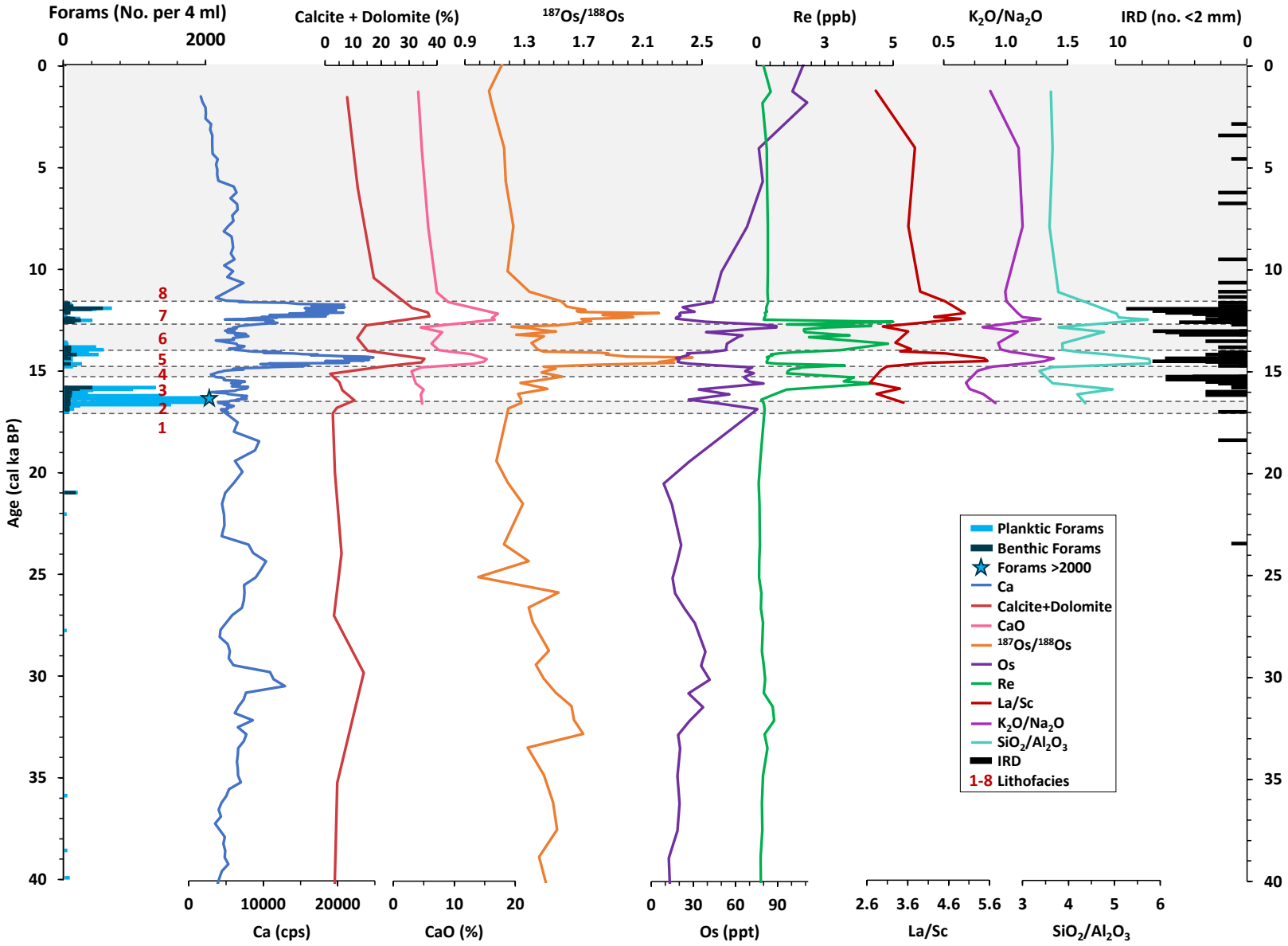
Forams (No. per 4 ml)
0
2000
Calcite + Dolomite (%)
0 10 20 30 40
$^{187}Os/^{188}Os$
0.9 1.3 1.7 2.1 2.5
Re (ppb)
0 3 5
K_2O/Na_2O
0.5 1.0 1.5
IRD (no. <2 mm)
10 0
Age (cal ka BP)
0 5 10 15 20 25 30 35 40
8
7
6
5
4
3
2
1
Planktic Forams
Benthic Forams
Forams >2000
Ca
Calcite+Dolomite
CaO
$^{187}Os/^{188}Os$
Os
Re
La/Sc
K_2O/Na_2O
SiO_2/Al_2O_3
IRD
1-8 Lithofacies
0 10000 20000
Ca (cps)
0 10 20
CaO (%)
0 30 60 90
Os (ppt)
2.6 3.6 4.6 5.6
La/Sc
3 4 5 6
SiO_2/Al_2O_3

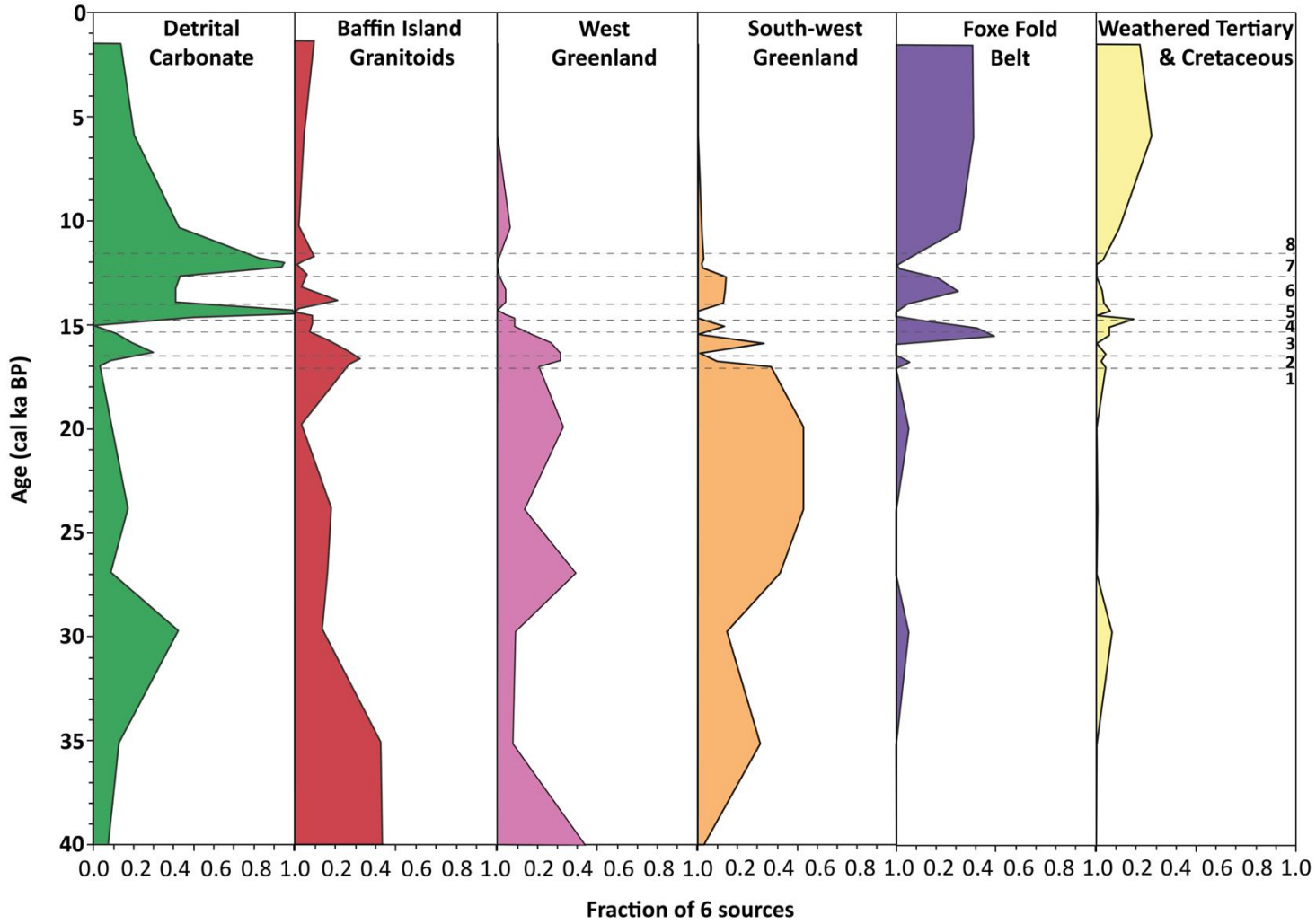

Figure 2.5: Fractions of the six potential sediment provenance sources in each sample analysed from core JR175 against the age model determined in Figure 2. The six sources include: detrital carbonate; igneous and metamorphic bedrock (granitoids) of Baffin Island; granites and granite-gneisses of west Greenland; bedrock from south-west Greenland; rocks from the Foxe Fold Belt, and weathered Tertiary and Cretaceous bedrock. See text for discussion.

The SiO_2/Al_2O_3 values are relatively similar throughout core JR175 (~4.37 to 3.62) except for two peaks over lithofacies 5 (5.77; 14.8 to 14.0 cal ka BP) and lithofacies 7 (5.73; 12.7 to 11.1 cal ka BP), which are coincident with the peaks in Ca cps and $^{187}Os/^{188}Os$ (Fig. 2.4; Table 2.4a). The K_2O/Na_2O values also exhibit limited variation (~0.68 to 1.39), with values being relatively low in the deepest section of the core (~0.68 to 0.92) and peaking again over lithofacies 5 (~1.4) and in lithofacies 7 (~1.3) at 14.4 and 12.5 cal ka BP, respectively. The K_2O/Na_2O values then decrease to the core top to a value of 0.88 (Fig. 2.4). The SiO_2/Al_2O_3 and K_2O/Na_2O data predominantly fall in the greywacke compositional field, with a few depth intervals bearing a more litharenite composition (e.g., 98.5, 72.5, 70.5 and 67.5 cm; Pettijohn et al., 1987).

The La/Sc ratio can be used as an indicator for predominantly mafic rock source types (low La/Sc) versus a predominantly felsic composition source area (high La/Sc; Bhatia & Crook, 1986; Taylor & McLennan, 1985). Across lithofacies 2 to 4 (16.6 to 14.8 cal ka BP), the La/Sc values are constant between 3.5 and 2.5 in core JR175 (Fig. 2.4; Table 2.4a). In lithofacies 5 between 14.8 and 14 cal ka BP, La/Sc peaks to 5.7 before returning to steady values of between 3.0 to 3.7 across lithofacies 6. Another peak in La/Sc up to 5.2 occurs over lithofacies 7 from 12.7 to 11.6 cal ka BP, and then gradually decreases down to a La/Sc value of 2.8 over lithofacies 8 up to the present day. The two large peaks coincide with the peaks in Ca cps, CaO% and a detrital carbonate source.

The carbonate rocks from Somerset and Devon Islands on average contain high CaO (31.7%), MgO (16.8%), with low SiO_2 (4.92%), and < 1% of TiO_2, Fe_2O_3, Al_2O_3, P_2O_5, Na_2O, K_2O, and MnO (Table 2.4b). Of the entire sample set three samples possess Al_2O_3, Fe_2O_3 and K_2O abundances greater than the average and of these, two samples also possess higher than average SiO_2. Additionally, one sample also exhibits higher than average SiO_2 (Table 2.4b). The La/Sc ratio averages at 3.83 (range 2.6 to 4.8) based on the three samples where Sc was above detection (1 ppm; Table 2.4b).

As presented for the major-element data, the REE data described below is carbonate corrected for the sediments taken from the Ca-rich depths in core JR175 corresponding to 15 to 14 cal ka BP and 12.7 to 11.6 cal ka BP (SM 2.7a). Corrected values are based on the average REE values for carbonate rocks from Somerset and Devon Islands (this study; SM 2.8a). The carbonate corrected values are normalised to upper continental crust values (SM 2.7b, 2.8b; McLennan, 2001).

In lithofacies 1 through 4 the heavy REEs (HREEs; Gd to Lu) are fairly flat and depleted compared to the average continental crust. A positive Dy and Eu anomaly is recorded. Between Eu and La the light REEs (LREEs) create a bowl shape (except for the sample at 80.5 cm) and are generally more enriched than the average continental crust (Fig. 2.6a). During lithofacies 5 the HREEs are again fairly flat and slightly more depleted than pre the average continental crust (Fig. 2.6b). A Dy anomaly, although variable, is recorded for all depths. The LREEs overall are enriched relative to average continental crust and although an Eu anomaly is recorded at some depths it is less pronounced than recorded in lithofacies 1 to 4. At 67.5 cm the Eu anomaly is negative. In lithofacies 6 (Fig. 2.6c) the HREEs are fairly flat. A positive Dy anomaly is recorded but less pronounced than in lithofacies 1 to 5. The majority of the LREEs are enriched relative to average continental crust, although at 47.5 cm depth the pattern is more bowl shaped. A very distinctive positive Eu anomaly exists for all samples. The REEs of lithofacies 7 (Fig. 2.6d) overall are more depleted than in lithofacies 5 but follow the same trend in that the HREEs are fairly flat, with only a slight enrichment relative to average continental crust for some LREE (e.g., La to Pr). A positive Dy anomaly is recorded for all samples, with no positive Eu anomaly recorded for the sample at 32.5 cm. Finally, through lithofacies 8 (Fig. 2.6e) the HREEs remain fairly flat and contain a positive Dy anomaly. From Tb to Nd the profile is convex. Negative and positive Pr and Ce anomalies, respectively, is shown for some depths (e.g., 14.5 and 2.5 cm).

Light REE enrichment in terms of La/Yb and Gd/Yb are all > 1 (Fig. 2.6h; SM 2.7b) indicating LREE enrichment over the HREEs. The Gd/Yb values are fairly constant (1.39 and 1.64) throughout the analysed interval of JR175, except for three peaks at 80.5, 70.5, and 54.5 cm to 1.85, 1.69 and 1.76, respectively in lithofacies 4, 5 and 6, respectively. The La/Yb ratios are more variable but are commonly between 2 and 2.2. At 98.5 (lithofacies 3) and 72.5 cm (lithofacies 5) La/Yb values fall to 1.48 and 1.69, respectively. Coinciding with the Gd/Yb peaks, La/Yb also display peaks at 80.5 cm (2.47), 70.5 cm (2.33) and 58.5 cm (2.49), lithofacies 4, 5 and 6, respectively. The Eu anomalies (Eu/Eu*) are variable throughout the analysed interval (0.91 to 1.21; Fig. 2.6g; SM 2.7b). In lithofacies 1 to 4 Eu/Eu* decreases between 110.5 and 80.5 cm from 1.11 to 1.08. Through lithofacies 5 the Eu/Eu* increases slightly then decreases from 1.11 to 0.91 at 67.5 cm. Through lithofacies 6 Eu/Eu* peaks to 1.17 and 1.21 at 58.5 and 44.5 cm, respectively. A decrease in Eu/Eu* to 1.02 occurs between 40 to 20 cm in lithofacies 7. Throughout lithofacies 8 Eu/Eu* varies between 1.04 and 1.08.

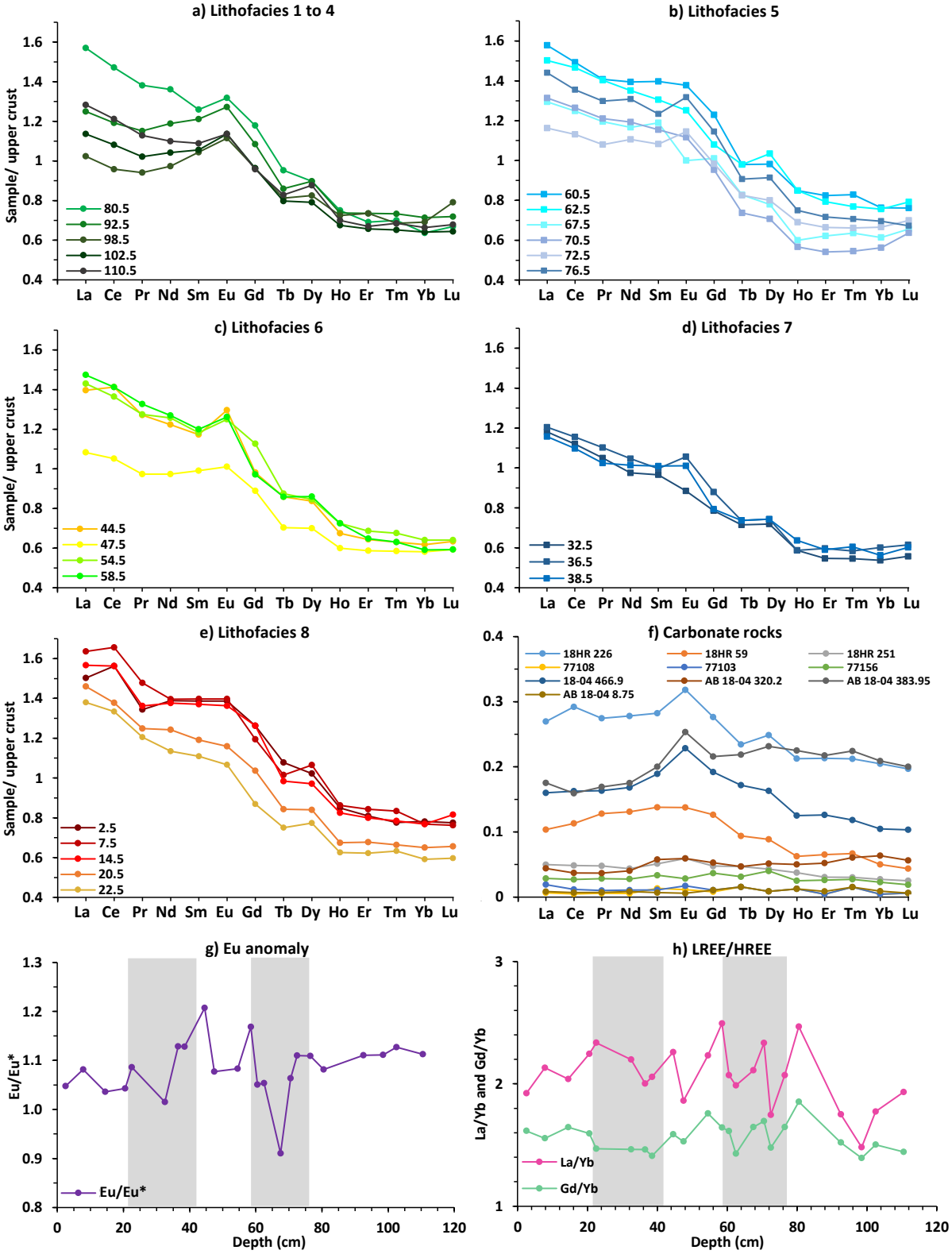

Figure 2.6: REE data normalised to upper crust plotted for the depths corresponding to a) lithofacies 1 to 4, b) lithofacies 5, c) lithofacies 6, d) lithofacies 7, e) lithofacies 8 and f) REE data normalised to upper crust for each carbonate sample analysed from the Somerset and Devon Islands. g) the europium anomaly values (Eu/Eu*) and h) the light rare earth element/ heavy rare earth element (LREE/HREE) ratio in the form of (La/Yb) and Gd/Yb plotted for core JR175 and normalised to upper crustal values. The grey shaded region denotes lithofacies 5 (76 to 59 cm) and lithofacies 7 (42 to 22 cm).

Although variable, the carbonate rocks from Somerset and Devon Islands are depleted in REE compared to upper crustal values (Fig. 2.6f). Six of ten samples possess upper continental crust normalised values of ≤ 0.06 and exhibit flat profiles for both HREE and LREE. The remaining four samples show enrichment in LREE relative to HREE. Sample 18HR59 shows a flat HREE profile with the LREE forming a convex shape. Three samples (18-04 466.9; 18HR 226; AB 18-04 383.95) show flat HREE profiles with REE increasing from Dy through to La. The latter samples all exhibit a pronounced positive Eu anomaly, can be seen with the remaining LREEs forming a bowl shape. Samples 18HR 226 and AB 18-04 383.95 exhibit a positive and negative Ce anomaly, respectively. The carbonate rocks possess La/Yb that varies between 2.07 and 0.69, with one sample recording a value of 4.18 (Average = 1.60; SM 2.8b). The Gd/Yb values vary between 0.68 and 2.53 (Average = 1.61). The Eu/Eu* values in the carbonate rocks vary between 0.68 and 1.58 (Average = 1.10; SM 2.8b).

2.4.5 Re and Os abundance and Os-isotope composition

2.4.5.1 JR175

The abundance of Re and total Os for the sediment from core JR175 vary between 0.07 and 5.01 ppb, and 8.9 and 111 ppt, respectively (Table 2.5). Rhenium levels are overall consistent at a low level (~0.2 to 0.4 ppb), except for two peaks across lithofacies 3 to 4 ~16.6 to 14.6 cal ka BP and in lithofacies 6 from ~14 to 12.4 cal ka BP and where the Re abundance rises to between 4 and 5 ppb (Fig. 2.4). The overall total Os abundance is between 8.92 and 111.1 ppt. Values are ~20 to 50 ppt except for intervals at 16.9 cal ka BP (lithofacies 2), between 15.6 and 14.7 cal ka BP (lithofacies 3 to 4), 13.9 to 13.1 cal ka BP (lithofacies 6) and through lithofacies 1 to the core top, that possess Os abundances between 75 and 111 ppt (Fig. 2.4).

Past seawater Os-isotope compositions are calculated from the present-day $^{187}Os/^{188}Os$ ratio measured in a sedimentary rock by accounting for the amount of post-depositional decay of ^{187}Re to ^{187}Os, assuming that the age of the sample is known and that the sedimentary system remained closed with respect to the two elements throughout its burial history (Cohen et al., 1999; Greg Ravizza & Turekian, 1989). Given the young age and low rhenium of the sediments of the JR175 core, the correction for the radiogenic ingrowth of ^{187}Os to the measured present-day $^{187}Os/^{188}Os$ composition is less than that of the minimum presented $^{187}Os/^{188}Os$ uncertainty of 0.01 (Table 2.5). Therefore, the un-corrected, measured present-day $^{187}Os/^{188}Os$ compositions are discussed below.

The $^{187}Os/^{188}Os$ compositions range between 0.99 and 2.44 and within this range exhibit two distinct radiogenic peaks (Figs. 2.4, 2.7). Before the last glacial maximum (40 – 33 cal ka BP) $^{187}Os/^{188}Os$ values are relatively similar, but overall show a slight decline from 1.45 to 1.32. At the start of the last glacial maximum (~33 cal ka BP), $^{187}Os/^{188}Os$ values increase rapidly to 1.70. Following this there is a gradual decrease to a less radiogenic $^{187}Os/^{188}Os$ value of 0.99 at ~24.8 cal ka BP. The $^{187}Os/^{188}Os$ values then remain roughly constant at ~ 1.1 to 1.2 until ~17.1 cal ka BP (~start of lithofacies 2) where values gradually start to increase again, coincident with what is thought to be the start of GIS retreat. Between ~15.0 to 14.0 cal ka BP (~lithofacies 5), the $^{187}Os/^{188}Os$ values rapidly peak to highly radiogenic value of 2.44 before rapidly decreasing back to 1.43. This peak corresponds very tightly with the first large peak in Ca values, and BBDC1 (Figs. 2.4, 2.7). The $^{187}Os/^{188}Os$ compositions, with the exception of some variation, are then fairly constant between 1.2 and 1.5 over lithofacies 6. Between ~13.1 and 11.7 cal ka BP (lithofacies 7), $^{187}Os/^{188}Os$ values show a rapid increase to 2.21, which is followed by an abrupt decrease to a $^{187}Os/^{188}Os$ value of 1.65 (~12.2 cal ka BP), before a less abrupt decrease back to an $^{187}Os/^{188}Os$ of 1.33. This $^{187}Os/^{188}Os$ peak also corresponds to the second large peak in Ca values and BBDC0, however, the degree of overlap between elevated Ca and radiogenic $^{187}Os/^{188}Os$ is less than shown for the elevated Ca and $^{187}Os/^{188}Os$ seen in lithofacies 5. Further, in contrast to lithofacies 5 coincident with BBDC1, across lithofacies 7 coincident with BBDC0, the $^{187}Os/^{188}Os$ composition trends to more radiogenic values earlier than the rise in Ca, and to less radiogenic values before the decrease in Ca values. From ~11.6 to 0 cal ka BP, coinciding with the Holocene period, $^{187}Os/^{188}Os$ values gradually decrease from 1.33 to 1.15.

A granitic clast from 71 cm (lithofacies 5) from core JR175 possesses a Re abundance of 0.09 ppb and Os of 16.5 ppt, with a $^{187}Os/^{188}Os$ of 1.29. The carbonate clasts from 70 (lithofacies 5), 38 and 29.5 (lithofacies 7) and 8.5 cm (lithofacies 8) from core JR175 have Re abundances between 0.04 and 0.18 ppb, Os abundances ranging from 5.3 to 48.8 ppt, and display a range in $^{187}Os/^{188}Os$ from 0.40 to 3.34 (Table 2.6).

2.4.5.2 DA04

The abundance of Re and total Os for the sediment from core DA04 varies between 0.45 and 11.4 ppb, and 30.2 and 74.5 ppt, respectively (Table 2.5). The $^{187}Os/^{188}Os$ values vary between 0.93 and 1.17 between the analysed interval of 15.3 – 9.1 cal ka BP (Fig. 2.7).

2.4.5.3 Carbonate rocks

Palaeozoic carbonate rock samples from the Turner Cliffs, Ship Point, Bay Fiord, Irene Bay and Allen Bay formations possess Re abundances between 0.03 and 0.36 ppb, and total Os abundances between 1.21 and 16.48 ppt. The $^{187}Os/^{188}Os$ values vary between 1.03 and 9.51 (Table 2.5). No relationship is observed between Os abundance and $^{187}Os/^{188}Os$ composition. For example, the most radiogenic carbonate sample (77156) from Devon Island with a $^{187}Os/^{188}Os$ of 9.51 has a Os abundance of 4.5 ppt, whereas sample AB18-01 383.95 from Somerset Island possesses a less radiogenic $^{187}Os/^{188}Os$ composition (2.91) yet has a Os abundance of 16.5 ppt (Table 2.5).

2.5 Discussion

Overall, core JR175 records sedimentation over a ~50 kyr timespan. Data analysis for the last 40 kyrs is presented as a calibrated age of 39.9 cal ka BP at 154 cm depth which is the deepest radiocarbon dated age included in the formation of the developed Bacon age model (Fig. 2.2). This time period covers several significant events affecting Baffin Bay. These include: the LGM (~33 – 19 Ka; Clark et al., 2009; Ó Cofaigh et al., 2019); Baffin Bay detrital carbonate layers BBDC0 (~12.7 – 11 cal ka BP), BBDC1 (~14.2 – 13.7 cal ka BP), BBDC2 (~25 – 24.7 cal ka BP), BBDC3 (~27.7 – 26.4 cal ka BP) and BBDC4 (~37 – 31.9 cal ka BP; Jackson et al., 2017; Simon et al., 2014); the Bølling-Allerød period (~14.7 – 12.9 cal ka BP; Rasmussen et al., 2006); the Older Dryas (~14 cal ka BP; Rasmussen et al., 2006), and the Younger Dryas (12.9 – 11.7 cal ka BP; Rasmussen et al., 2006). As discussed below, core JR175 preserves a very clear signal of BBDC1 and BBDC0 in lithofacies 5 and 7, respectively, but there appears to be no clear expression of BBDC2, 3 and 4 (Fig. 2.7). The timings of BBDC1 and BBDC0 also coincide with the Bølling-Allerød, Older Dryas, and Younger Dryas events (Fig. 2.7).

One of the key proxies developed by this study is the use of osmium isotopes in this context. The osmium isotopic composition ($^{187}Os/^{188}Os$) of sediments can be used to infer the $^{187}Os/^{188}Os$ of the surrounding waters and the different sources of inputs into the area at the time of deposition (e.g. Peucker-Ehrenbrink & Ravizza, 2000; Rooney et al., 2016). The $^{187}Os/^{188}Os$ of seawater reflects a sensitive interplay of radiogenic Os signatures from continental inputs ($^{187}Os/^{188}Os$ average = ~1.4 but old crystalline basement rocks can be much higher, > 2; Peucker-Ehrenbrink & Jahn, 2001) and unradiogenic Os signatures from mantle/hydrothermal inputs ($^{187}Os/^{188}Os$ = ~0.12; Peucker-Ehrenbrink & Ravizza, 2000). Present-day seawater records an $^{187}Os/^{188}Os$ of ~1.060 ± 0.005, reflecting a balance of continental and mantle inputs and is relatively stable across the global oceans,

although it has been shown that the North Atlantic Ocean possess a slightly less radiogenic $^{187}Os/^{188}Os$ of ~1.04 (Burton et al., 1999; Cohen, 2004; Levasseur, 1998; Peucker-Ehrenbrink & Ravizza, 2000; Rooney et al., 2016; Sharma et al., 1997). The residence time for osmium in the oceans is ~1-50 kyrs, with several studies proposing a residence time of < 10 kyrs (Levasseur et al., 1999; Oxburgh, 1998, 2001; Peucker-Ehrenbrink & Ravizza, 2012; Rooney et al., 2016; Sharma et al., 1997). This means that $^{187}Os/^{188}Os$ responds quickly to environmental changes, so is able to distinguish between shorter and longer-term perturbations in the sediments such as changes in ocean connectivity, weathering, hydrological and glacial cycles (e.g., Cohen, 2004; Peucker-Ehrenbrink & Ravizza, 2000; Rooney et al., 2016).

2.5.1 Pre-Last Glacial Maximum (LGM)

Pre the LGM (> 33 cal ka BP), $^{187}Os/^{188}Os$ values in JR175 are relatively stable, but display a slight decrease from 1.4 at 39.3 ka cal BP to 1.3 at 33.3 ka cal BP (Fig. 2.7). In the same time interval, calcium levels show a slight increase from 3826 to 6648 cps. The TOC (%) levels are also low and stable (< 0.3%) over this time period, with no IRD or large clasts observed in the core and low foraminiferal abundance (Figs. 2.3, 2.4). The $^{187}Os/^{188}Os$ values of 1.3 to 1.4 are more radiogenic than the open ocean at the time (~1; Paquay & Ravizza, 2012; Peucker-Ehrenbrink & Ravizza, 2000) suggesting that there is some flux of radiogenic materials from the surrounding landmasses. Pre 33 cal ka BP the qXRD based SedUnMix data suggests that the predominant sources of sediment to the core site are from W, SW Greenland, and Baffin Island (Fig. 2.5), all of which possess old, continental geologies (Fig. 2.1) with likely radiogenic $^{187}Os/^{188}Os$. This time period however is from before it is thought that the Baffin Bay ice sheets expanded out onto the shelf edges (e.g., Andrews et al., 2015; Briner et al., 2003; Ó Cofaigh et al., 2013), and as $^{187}Os/^{188}Os$ and Ca counts do not greatly fluctuate and no IRD is recorded (Fig. 2.4), it might suggest a steady outwash of material into Baffin Bay through meltwater, sediment flows and other delivery methods, rather than through a large 'event.' Low foraminifera abundance and TOC percentages would also suggest low productivity pre 33 cal ka BP. This time period also covers the proposed timing of BBDC4 (~37 – 31.9 cal ka BP; Jackson et al., 2017; Simon et al., 2014), as well as a number of fluctuations in $\delta^{18}O$ seen in the ice core records (Fig. 2.7). However, no distinctive peak in calcium levels is observed in JR175 over the time interval for BBDC4, and the $^{187}Os/^{188}Os$ and Ca counts do not appear to change in response to fluctuating $\delta^{18}O$ (although sample resolution is comparatively low in this age range, and the age model is less well constrained).

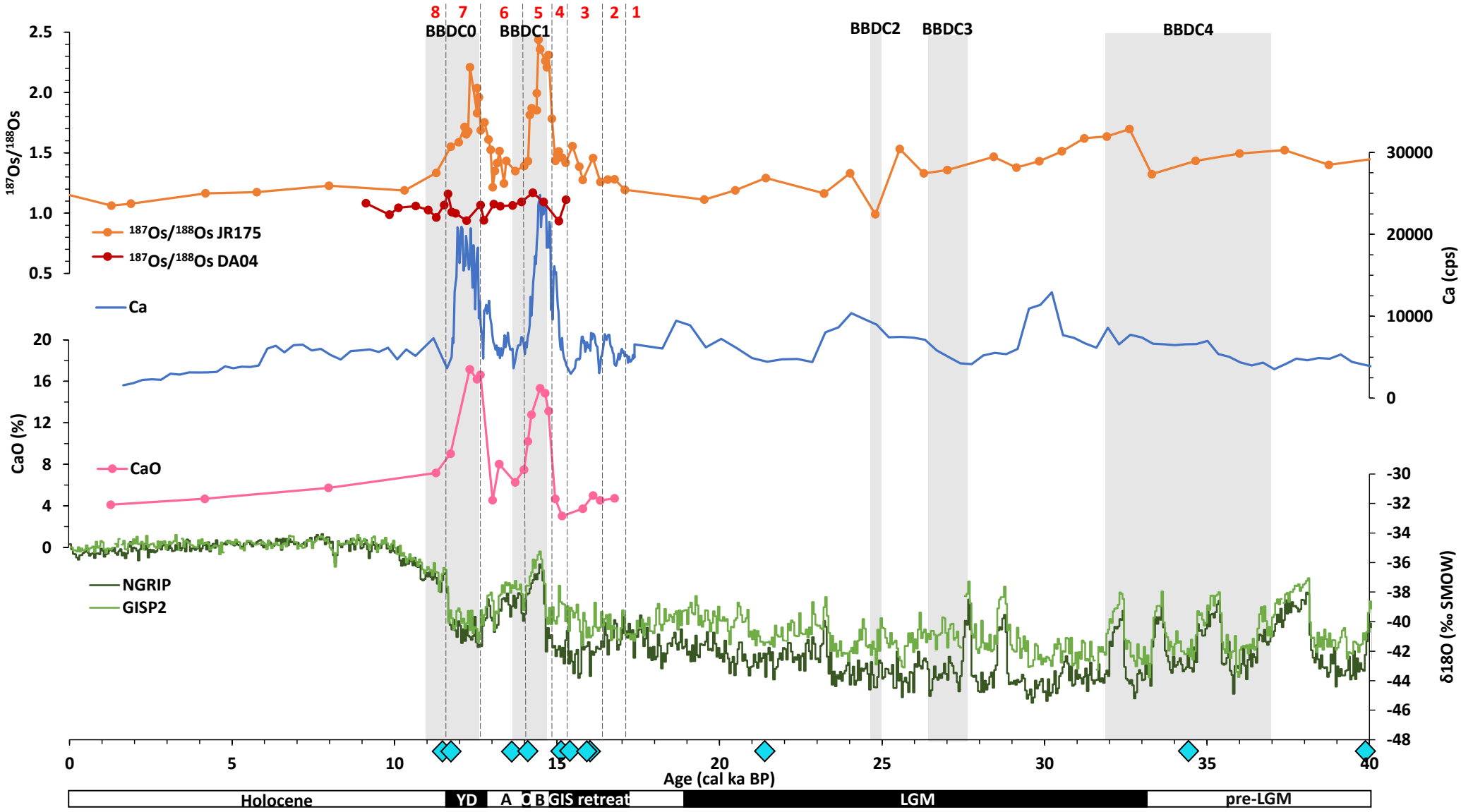
8
7
6
5
4
3
2
1
BBDC0
BBDC1
BBDC2
BBDC3
BBDC4
$^{187}Os/^{188}Os$
$^{187}Os/^{188}Os$ JR175
$^{187}Os/^{188}Os$ DA04
Ca
Ca (cps)
CaO (%)
CaO
NGRIP
GISP2
δ18O (‰ SMOW)
Age (cal ka BP)
Holocene
YD
A
B
GIS retreat
LGM
pre-LGM

Figure 2.7: (Page 56) $^{187}Os/^{188}Os$, Ca (cps), CaO (%) data from core JR175, $^{187}Os/^{188}Os$ for core DA04, and ice core $\delta^{18}O$ values (NGRIP and GISP2) plotted against the age model determined in Figure 2. NGRIP and GISP2 ages corrected from years B2k to years BP to fit with the age model (Data from: Grootes & Stuiver, 1997; Johnsen et al., 1997; Rasmussen et al., 2014; Seierstad et al., 2014; Stuiver & Grootes, 2000). Blue triangles show the positioning of the calibrated radiocarbon ages. Grey shaded boxes are approximate ages of the Baffin Bay detrital carbonate events BBDC4, BBDC3, BBDC2, BBDC1 and BBDC0 (Andrews et al., 1998; Jackson et al., 2017; Simon et al., 2014). The black and white bar shows the approximate timings of the Last Glacial Maximum (LGM; Clark et al., 2009; Ó Cofaigh et al., 2019), initial Greenland Ice Sheet (GIS) retreat (Jennings et al., 2017; Ó Cofaigh et al., 2013), the Bølling oscillation (B), the Older Dryas (O), the Allerød oscillation (A) and the Younger Dryas (YD; Rasmussen et al., 2006). See text for discussion.

2.5.2 Last Glacial Maximum (LGM)

Here, the LGM is referred to as the period between ~33 and 19 ka. A time when globally ice sheets reached their maximum and the eustatic sea levels were at their lowest (Clark et al., 2009; Ó Cofaigh et al., 2019).

At the start of the LGM (~33 cal ka BP) the $^{187}Os/^{188}Os$ abruptly increases from 1.3 to 1.7, and then overall steadily decreases, with the exception of a short-lived decrease from 1.5 to 0.99 between 25.6 to 24.0 cal ka BP, to 1.1 at the end of the LGM (~19 cal ka BP; Fig. 2.7). This abrupt change indicates an influx of more radiogenic Os at the start of the LGM, most likely from Os-rich geologies such as those of west Greenland and Baffin Island, covered by the Greenland and Laurentide Ice Sheets, respectively (Fig. 2.1). The abrupt change in the hydrogenous $^{187}Os/^{188}Os$ composition at ~33 cal ka BP coincides with the timing of maximum ice sheet advance onto the continental shelves of Baffin Bay (Briner et al., 2003; Clark et al., 2009), whereby the core site would have been more proximal to the ice margins and affected by ice stream discharge into central Baffin Bay. A similar $^{187}Os/^{188}Os$ composition response on a smaller scale to advance of a GIS ice stream (Jakobshavns Isbrae) has been reported for the Holocene around Disko Bugt, showing $^{187}Os/^{188}Os$ values increasing during ice-proximal periods (Rooney et al., 2016). Therefore, advance of the GIS/LIS ice margins to their LGM positions is the likely cause of the rise in $^{187}Os/^{188}Os$ composition. The trend to less radiogenic $^{187}Os/^{188}Os$ from ~33 to 19 cal ka BP implies the reduction of input of radiogenic $^{187}Os/^{188}Os$ into the water column. This may be the result of a reduction in drainage/ discharge from the ice sheets (reduced flux of glacially eroded material into Baffin Bay). The lower $^{187}Os/^{188}Os$ may also be, in part, due to an increased influence of an open ocean signal through the Davis Strait. This open ocean signature is recorded in core DA04, although the record of the core does not extend back as far as the LGM.

Minor increases in calcium during the LGM interval occur between 30.9 and 29.2 cal ka BP and 27.4 and 22.8 cal ka BP, the earlier period corresponds to a peak in the detrital

carbonate source fraction recorded at ~30 cal ka BP from the qXRD data (Figs. 2.5, 2.7). The older peak in Ca in the core is dated between the proposed timings of BBDC3 and BBDC4. The temporally broad peak in Ca, in part, coincides with the short-lived BBDC2. A contributing factor could potentially be that the chronology of core JR175 is more poorly constrained in this section compared to other parts of the core due to a low abundance of foraminifera for dating. On top of this, this study uses the updated MARINE20 calibration curve, which was not available for the studies from which the dates for BBDC2, 3 and 4 were obtained (Jackson et al., 2017; Simon et al., 2014). It is likely therefore that the Ca peaks (and detrital carbonate) in JR175 between 30.9 and 29.2 cal ka BP, and 27.4 and 22.8 cal ka BP represents either BBDC3 or 4 and BBDC2, respectively. It is also worth noting that the smaller peaks in Ca in JR175 (30.9 to 29.1, 27.4 to 22.8 and ~20 to 17 cal ka BP) temporally correlate to Hudson Strait Heinrich Events (HE3, HE2 and HE1, respectively; Andrews & Voelker, 2018; Knutz et al. 2011), with the signal potentially being carried north from the Hudson Bay region by ocean currents and icebergs along the West Greenland Current. However, Heinrich Events haven't previously shown a large influence north of the Davis Strait, but some cores in Baffin Bay have previously recorded a detrital signature over the same time period as a Heinrich Event (Andrews & Voelker, 2018 and references therein).

The temporal changes in Ca do not correlate with those described for $^{187}Os/^{188}Os$. This could suggest different temporal ice sheet dynamics between the Innuitian Ice Sheet and the Greenland and/or Laurentide Ice Sheets. This is supported by the qXRD SedUnMix data as the 30 cal ka BP detrital carbonate peak is coincident with lows in the source fractions from Baffin Island and W and SW Greenland (Fig. 2.5). It appears that IIS dynamics over the Palaeozoic carbonate units and subsequent discharge resulting in the carbonate input into Baffin Bay was not in sync with the dynamics of the GIS/LIS during the LGM.

The foraminifera data in core JR175 show very low abundances through the LGM period until ~17 cal ka BP (Fig. 2.4). This suggests relatively low productivity during the LGM due to strong/stable, year-round sea ice cover and hence harsh sea surface conditions would be expected (Jennings et al., 2018). The data show no evidence of spikes in productivity that could be associated with the seasonal break up of sea ice that might produce productivity blooms in the surface waters.

2.5.3 LGM to BBDC1

The time period between the end of the LGM and BBDC1 covers the age range of 19 to ~14.8 cal ka BP comprising sediments of the end of lithofacies 1 through to lithofacies 4 (Figs. 2.7, 2.8). During this time, $^{187}Os/^{188}Os$ values overall increase from 1.1 to 1.5 but fluctuate, and Ca levels overall decrease (7200 to 4700 cps) but again fluctuate (Figs. 2.7, 2.8). This would suggest an increase in the proportion of radiogenic material flux from the surrounding landmasses (i.e., more delivery from the GIS/LIS) and a relative decrease in the amount of carbonate flux (i.e., less delivery from the IIS). The time interval of 19 to 14.8 cal ka BP covers the time period through which the ice sheets surround Baffin Bay are thought to have started to retreat from their LGM positions (e.g., Brouard & Lajeunesse, 2017; Jennings et al., 2017; Simon et al., 2014).

The timing of the retreat of the Greenland Ice Sheet is gradual and diachronous based on estimated timings at different outlets. For example, retreat in Uummannaq Trough is proposed to have been underway by 17.1 cal ka BP, whereas retreat in Disko Trough did not begin until 16.2 cal ka BP (Jennings et al., 2017). In the JR175 core, $^{187}Os/^{188}Os$ compositions begin to steadily increase from ~17.1 cal ka BP. This increase corresponds to the estimated timing for the onset of retreat of some ice streams in western Greenland, which would imply an enhanced release of radiogenic $^{187}Os/^{188}Os$ from the GIS outflows into the water column of Baffin Bay. The increase in $^{187}Os/^{188}Os$ is most likely controlled by the geology underlying the western sector of the GIS. For example, an Archean orthogneiss from Salliaruseq Storøen Island in Uummannaq Fjord records a $^{187}Os/^{188}Os$ value of 2.82 (Rooney et al., 2016). This is also supported by an increase in the proportion of material sourced from west Greenland from 17.1 cal ka BP based on qXRD results (Fig. 2.5). During this time REE profiles from lithofacies 1 to 4 record LREE enrichment and a marked positive Eu anomaly (Fig. 2.6a). A positive Eu anomaly indicates a greater proportion of plagioclase and alkali feldspar (because Eu is common in these minerals; Taylor & McLennan, 1985). Plagioclase and alkali feldspar proportions are greatest within lithofacies 1 to 4 according to qXRD data (Table 2.3). These minerals are synonymous with granites, granodiorites, gneisses and gabbros, typical of the geology of west Greenland and Baffin Island. Along the west Greenland shelf are the major trough mouth fans leading from Disko Bay and Uummannaq, clearly showing the presence of major ice streams flowing to the shelf edge (Fig. 2.1). The Baffin Island shelf does not have these features, which may suggest west Greenland could be the more likely source. Coincident with the trend to more radiogenic $^{187}Os/^{188}Os$ the abundance of IRD recorded in the core increases, between ~17 to 15 cal ka BP (~105 – 85 cm; Figs. 2.3, 2.4).

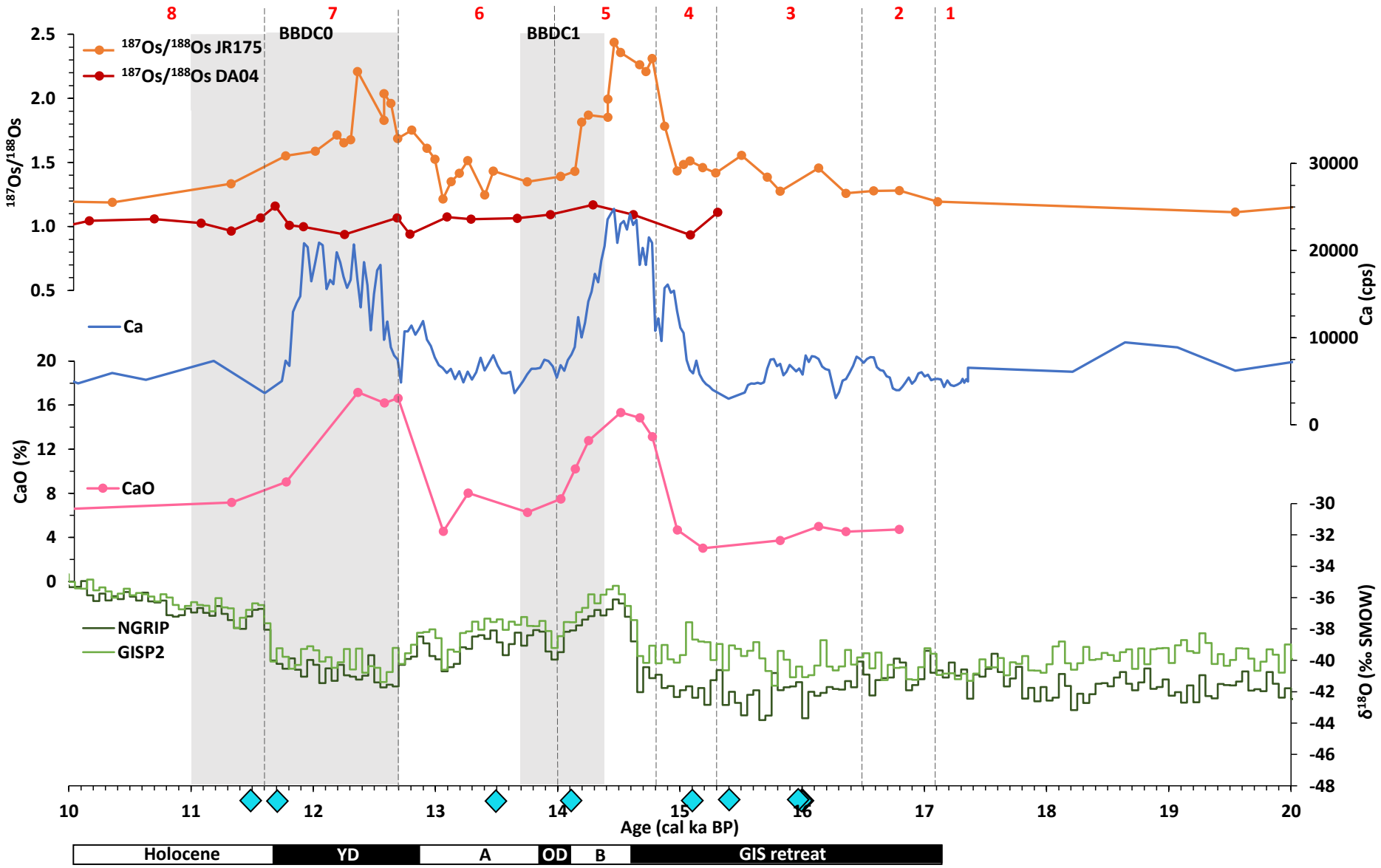
8
7
6
5
4
3
2
1
BBDC0
BBDC1
$^{187}Os/^{188}Os$ JR175
$^{187}Os/^{188}Os$ DA04
$^{187}Os/^{188}Os$
Ca
Ca (cps)
CaO
CaO (%)
NGRIP
GISP2
$\delta^{18}O$ (‰ SMOW)
Age (cal ka BP)
Holocene
YD
A
OD
B
GIS retreat

Figure 2.8: (Page 60) $^{187}Os/^{188}Os$, Ca (cps), CaO (%) data from core JR175, $^{187}Os/^{188}Os$ for core DA04, and ice core $\delta^{18}O$ values from NGRIP and GISP2 plotted against the age model determined in Figure 2 between the ages of 20 to 10 cal ka BP, to enhance the age range of interest (see discussion). NGRIP and GISP2 ages corrected from years B2k to years BP to fit with the age model (Data from: Grootes & Stuiver, 1997; Johnsen et al., 1997; Rasmussen et al., 2014; Seierstad et al., 2014; Stuiver & Grootes, 2000). Blue triangles show the positioning of the calibrated radiocarbon ages. Grey shaded boxes are approximate ages of the Baffin Bay detrital carbonate events BBDC1 and BBDC0 (Andrews et al., 1998; Jackson et al., 2017; Simon et al., 2014). The black and white bar shows the approximate timings for Greenland Ice Sheet (GIS) retreat (Jennings et al., 2017; Ó Cofaigh et al., 2013), the Bølling oscillation (B), the Older Dryas (OD), the Allerød oscillation (A) and the Younger Dryas (YD; Rasmussen et al., 2006). See text for discussion.

The absence of IRD between 15.3 and 14.8 cal ka BP (~85 – 75 cm; Figs. 2.3, 2.4) is consistent with the hypothesis that the lack of IRD following the initial GIS retreat is in response to limited rapid ice calving, with the GIS retreating slowly across the continental shelf due to a buttressing ice shelf, resulting in deposition of coarser-grained material more proximal to the ice margin (Jennings et al., 2017), and hence not reaching further out into Baffin Bay at the JR175 core site. Yet, the $^{187}Os/^{188}Os$ composition continues to rise suggesting a continued flux of radiogenic Os into Baffin Bay. This continued input may be due to continued delivery of the finer sediment fraction and hydrogenous load through meltwater flux still being able to reach beyond the continental shelf, after the coarser grained material is deposited.

In contrast to the trend in $^{187}Os/^{188}Os$ compositions, from 17.1 cal ka BP calcium levels show more variability, but do not appreciably increase, yet calcium oxide levels decrease, which is likely in direct response to the reduction in detrital carbonate content (Figs. 2.4, 2.7). The relatively low carbonate delivery may further support the relative stability along the Innuitian Ice Sheet margins in comparison to the GIS at this time (Jackson et al., 2017; Simon et al., 2014). The fraction of detrital carbonate input determined by SedUnMix partially supports this in that the fraction is low at 17.1 and 15 cal ka BP, but a peak does occur around 16 cal ka BP (although this peak is still relatively low compared to other core intervals; Fig. 2.5). This would suggest therefore that the IIS did not begin to collapse and deliver large quantities of icebergs carrying carbonate material until after the evidence for initial GIS retreat. Perhaps the IIS remained relatively stable for longer, or sea-ice in northern Baffin Bay could have prevented delivery of icebergs further south.

As well as an increase in $^{187}Os/^{188}Os$ and IRD from ~17 cal ka BP, the numbers of foraminifera also increase rapidly, to a peak of 13,000 individuals/4 ml (Fig. 2.4). This rapid increase in foraminiferal abundance suggests a significant peak in productivity. Such productivity spikes can often occur near the edge of sea ice stimulated by seasonal advance/retreat of the sea ice edge (Jennings et al., 2018; Nørgaard-Pedersen et al., 2003).

Therefore, the peak recorded in JR175 from 17 to 16.2 cal ka BP could represent a time when the stability of sea ice decreased around the core site with a more seasonal pattern of advance and retreat of the sea ice margin. Another explanation for the large increase in foraminiferal abundance could be linked to the retreat of the GIS and an increased flux of nutrients due to increased glacial meltwater flux (Jennings et al., 2018). A very large peak in both benthic and planktic foraminifera abundance has also previously been noted in a core from northern Disko trough mouth fan (slightly more southern location to JR175; core HU2008029-12PC), although this peak is dated ~1 kyr earlier than that found in JR175 (Jennings et al., 2018). This could relate to different marine calibration curves utilised between the studies. However, if this increase in abundance is related to retreat of sea ice cover and/or ice margin retreat then the different timings could be showing a diachronous retreat of the sea ice/ ice margin through Baffin Bay from Disko Bay (~18 to 17.5 cal ka BP; Jennings et al., 2018) to JR175 (~17 cal ka BP) further north off the Uummannaq trough mouth fan (Fig. 2.1).

Despite evidence suggesting a GIS source during this period is the most likely, the SedUnMix qXRD data does also show a peak in the contribution from a Baffin Island source (Fig. 2.5), and therefore does not rule the LIS out as a potential source of the $^{187}Os/^{188}Os$ values beginning to increase at 17.1 cal ka BP.

2.5.4 Baffin Bay Detrital Carbonate event 1 (BBDC1)

Studies of numerous cores throughout Baffin Bay have shown two periods of enhanced detrital carbonate delivery between the end of the LGM and present-day. These layers are synchronous across Baffin Bay, with the carbonate sourced from Palaeozoic carbonate outcrops of north-eastern Canada and north-western Greenland in the northern regions of Baffin Bay (Fig. 2.1; Andrews, 1987; Andrews et al., 1998; Hiscott et al., 1989; Jackson et al., 2017; Simon et al., 2014).

Shortly after the LGM an inundation of carbonate material is recorded in Baffin Bay cores, dated to between 14.2 and 13.7 cal ka BP, which is associated with a near doubling in sedimentation rate and abundant dropstones, and is termed BBDC1 (Andrews et al., 1998; Jackson et al., 2017). Using the age model developed in this study, the peak in calcium, calcium oxide and detrital carbonate abundance, that occurs at a core depth between ~60 and 80 cm (lithofacies 5), is dated to between ~15.2 and 13.9 ka cal BP. This age range overlaps with the timing of BBDC1 (Fig. 2.7), though the event recorded in JR175 starts approximately 1000 years before the onset of BBDC1 from previous

studies (e.g., Jackson et al., 2017; Simon et al., 2014). A likely cause for this discrepancy may be due to the age model in this study using the updated MARINE20 calibration curve, which was not available at the time for previous studies. Using the MARINE13 calibration curve, the $^{187}Os/^{188}Os$, Ca and CaO peaks from JR175 match very closely with the published timings of BBDC0 and BBDC1 shown in Figures 2.7 and 2.8.

Coupled with the peak in Ca, CaO and detrital carbonate, an increase in IRD material, TOC (up to 2.8%) and a peak in the La/Sc values (up to 5.72) is recorded, as is the trend to higher $^{187}Os/^{188}Os$ between 15 and 13.7 cal ka BP (Figs. 2.3, 2.4, 2.5, 2.7) indicating the input of radiogenic osmium to the watermass. Although trends with radiogenic $^{187}Os/^{188}Os$ are not coincident with increases in Ca at ~33 cal ka BP, the temporal agreement between the peak in Ca, CaO and $^{187}Os/^{188}Os$ for BBDC1 could indicate the radiogenic $^{187}Os/^{188}Os$ signal is derived from the carbonate, given that the carbonate mineralogy in the core sediment is digested by the Re-Os analytical protocol. Indeed, Re-Os analysis on carbonate rocks sourced from Somerset and Devon Islands yielded an average $^{187}Os/^{188}Os$ of 3.6, although values range between ~1.0 and 9.5 (Table 2.5), which is more radiogenic than the highest $^{187}Os/^{188}Os$ value (2.44) recorded in the BBDC1 section of core JR175 (Fig. 2.8). In contrast to the Somerset and Devon Island carbonate lithologies, a carbonate clast recovered from the BBDC1 interval (70 cm) in the JR175 core is less radiogenic $^{187}Os/^{188}Os$ (~1.6) than the sediment at the same interval (~2.2; Fig. 2.8; Table 2.6).

In the BBDC1 interval, carbonate accounts for on average ~30 to 40% of the mineralogy (calcite + dolomite %; Fig. 2.4). Utilising a progressive, two component mixing model (van der Ploeg et al., 2018) and even considering a carbonate with the most radiogenic $^{187}Os/^{188}Os$ composition (~9.5), and with the highest Os abundance (16.5 ppt) together with a seawater $^{187}Os/^{188}Os$ of ~1.3 (recorded prior to the BBDC1 onset; Fig. 2.8), the carbonate would have to significantly exceed 100% to reach the most radiogenic values recorded in JR175 (2.44). Thus, given the predominantly less radiogenic $^{187}Os/^{188}Os$ compositions of the carbonate lithologies from Somerset Island and that of the clast in the BBDC1 interval of JR175, an alternate source to carbonate is needed for osmium. In addition to the Os mixing modelling, REE data further supports an alternate source for the sediment in this zone and, therefore, the osmium signature, given that all REE abundances are significantly lower (in most case ~90% lower) in the carbonate rocks than they are across the whole core and BBDC1 layer (SM 2.7, 2.8). Further, the carbonate rocks display no, or very little LREE enrichment (Fig. 2.6f) whereas the REE profiles

during BBDC1 in JR175 show high LREE enrichment (Fig. 2.6b). Therefore, the difference in REE abundances and enrichment between the carbonate rocks and JR175 sediments during BBDC1 suggest there must be another significant source of material during this period, other than the dominant carbonate source from the IIS.

Taken together the lines of evidence outlined above suggest that the radiogenic $^{187}Os/^{188}Os$ identified in this interval is not sourced entirely from ice streaming activities of the northern IIS and LIS. An additional and dominant source therefore must be from either western Greenland (GIS) or Baffin Island (LIS). However, as previously noted, the geologies of west Greenland and Baffin Island are very similar and hence it is difficult to differentiate between the two sources (Aksu & Piper, 1979; Andrews et al., 2014; Harrison et al., 2011; Hiscott et al., 1989; Jennings et al., 2018; MacLean et al., 1990; Simon et al., 2014).

After the pause in IRD following the initial retreat in Uummannaq and Disko Troughs at 17.1 and 16.2 cal ka BP, respectively, a rise in Greenlandic IRD recorded in Uummannaq trough occurs at 15.3 cal ka BP (Jennings et al., 2017). This is attributed to iceberg calving, with ice margin retreat by this method beginning at 15.1 cal ka BP. This is coincident, within uncertainty (and up to 1 kyr difference due to marine calibration curves), with the timing of IRD in core JR175 at ~14.8 cal ka BP (Fig. 2.4). This temporal agreement of IRD could represent GIS sourced IRD, suggesting that radiogenic Os in the water column is also principally sourced from ice stream dynamics of the GIS. Larger IRD clasts found in core JR175 include both carbonate and a granite/gneiss over the BBDC1 time interval (Table 2.6). The granite/gneiss clast is less radiogenic ($^{187}Os/^{188}Os = 1.3$) than recorded in the host sediment ($^{187}Os/^{188}Os = 2.2$), which is also less radiogenic than the Archean orthogneiss from Salliaruseq Storøen Island in Uummannaq Fjord ($^{187}Os/^{188}Os = 2.82$; Rooney et al., 2016). However, the clast comprises only quartz and feldspar, and it is biotite that has been shown to possess a radiogenic Os component (Bernhard Peucker-Ehrenbrink & Blum, 1998). Regardless, the clast coupled with the LREE enrichment, positive Eu anomaly, and the high La/Sc ratios recorded in JR175 (Figs. 2.4, 2.6b) would also indicate a predominantly felsic provenance (Bhatia & Crook, 1986; Taylor & McLennan, 1985) such as the Precambrian crystalline rocks along the west coast of Greenland (Fig. 2.1). These factors alongside sediment (with minimal carbonate) deposited proximal to the Jakobshavn Isbrae ice margin in Disko Bugt possessing a $^{187}Os/^{188}Os$ composition of ~2.0 to 2.4 during ice proximal conditions in comparison to ~1.3 to 1.8 during times when the ice margin was more distal (Rooney et

al., 2016), suggests that the radiogenic $^{187}Os/^{188}Os$ values of ~2.0 to 2.5 recorded during BBDC1 in core JR175 (Fig. 2.8) could be achieved solely by a western Greenland source.

A west Greenland source during BBDC layers has been speculated previously, with finer-grained glaciomarine sediments with a mineralogical make-up that potentially matches Uummannaq ice streaming activities in western Greenland (Simon et al., 2014). These finer sediments are also noted to be Ti-rich, and indicate delivery from a lateral source (i.e. GIS or LIS) during the advance and/or retreat of ice streams (Aksu & Piper, 1987; Hiscott et al., 1989). However, no Ti-rich signature is found in core JR175, with lows of TiO_2 occurring over BBDC layers (Table 2.4a). Further, a study investigating the provenance of central Baffin Bay sediments based on radiogenic isotope work of lead, neodymium and strontium determined that the isotope values during the last deglaciation period (since LGM) represent source areas of central-west and south-west Greenland, mainly from the Nagssugtoqidian Mobile Belt and the Archean Block (Kirillova, 2017).

The geography of Baffin Bay may also play a part in sediment delivery to the core site. The continental shelf of west Greenland is much wider (135 – 200 km) than the Baffin Island Shelf (25 – 50 km), and contains a number of troughs leading to large trough mouth fans, whereas the Baffin Island shelf shows little evidence of continental slope canyons (Andrews et al., 2014; Jakobsson et al., 2012; Li et al., 2011; MacLean et al., 1990). Further, there are more major ice streams originating from west Greenland than Baffin Island (Fig. 2.1; Brouard & Lajeunesse, 2017; Jennings et al., 2017; Margold et al., 2018; Simon et al., 2014). This suggests that sediment delivery into Baffin Bay was dominated by transport through the large ice stream scoured cross-shelf troughs from western Greenland ending in the major trough mouth fans at the shelf edge.

However, although certain evidence can be linked to a west Greenland source as the most likely explanation, a partial Baffin Island source cannot be definitively ruled out. The end of glaciation of the Laurentide Ice Sheet on the shelf edge is dated to be a minimum of 15 cal ka BP (Brouard & Lajeunesse, 2017) after reaching its maximum extent around 24 – 20 cal ka BP, with terminating ice margins on the continental shelf during the LGM (Briner et al., 2003, 2006; Ó Cofaigh et al., 2013; Simon et al., 2014). Although smaller than west Greenland, a number of ice streaming outlets existed along Baffin Island into Baffin Bay including for example, Home Bay, Scott Inlet, Buchan Gulf and Merchants Bay (Briner et al., 2003; Brouard & Lajeunesse, 2017; Margold et al., 2018). A previous study on sediment provenance reconstruction using qXRD data with SedUnMix has

suggested that short pulses of coarse Baffin Island sediment occur within BBDC layers (Simon et al., 2014).

It has also been noted that BBDC events occur during both warmer interstadial and cooler stadial cycles, suggesting that the North Atlantic climate may not be the dominant driver of deglaciation events of the LIS, GIS and IIS (Jackson et al., 2017). Laurentide Ice Sheet discharge events have been linked to mainly stadial periods, whereas sediment delivery from the GIS has been linked to retreat due to warmer temperatures both in the atmosphere and through warmer waters entering Baffin Bay (Hiscott et al., 1989; Jennings et al., 2011; Simon et al., 2014). The timing of BBDC1 corresponds to the Bølling-Allerød interstadial period as seen in the NGRIP and GISP2 ice core data (~14.7 – 12.9 cal ka BP; Fig. 2.8; Rasmussen et al., 2006). As this is a time of warmer temperatures, it could indicate retreat of the Greenland Ice Sheet bringing sediment delivery and a radiogenic $^{187}Os/^{188}Os$ glacial melt waters into Baffin Bay preferentially over sediment/water sourced from the Laurentide Ice Sheet.

After the initial peak in foraminiferal abundance between 17 to 16.2 ka cal BP, a further increase in abundance occurs between 16 to 15.5 cal ka BP before a period of no foraminifera, and then another increase beginning at *c.* 14.8 cal ka BP at the start of BBDC1 in JR175 (Fig. 2.4). Foraminifera abundance continues to climb to a peak (at 13.9 cal ka BP) after the initial decline in Ca and $^{187}Os/^{188}Os$ (Fig. 2.4). The peak in abundance is largely due to an increase in planktic foraminifera. This could represent an increase in productivity in the surface waters due to the increased sediment and nutrient flux into Baffin Bay that occurred during BBDC1. Further, after accounting for differences in age relating to different marine calibrations, the foraminifera peaks in JR175 between 16 to 15.5 cal ka BP and between 14.8 to 13.9 cal ka BP may relate to peaks in abundance recorded in core HU2008029-12PC at ~16.2 cal ka BP and ~14 cal ka BP (Jennings et al., 2018).

The DA04 core $^{187}Os/^{188}Os$ record from southern Greenland (Fig. 2.1) over BBDC1 records markedly less radiogenic compositions compared to the JR175 core over the same period, at ~0.9 to 1.2 compared to 1.4 to 2.4 in JR175 (Fig. 2.8). The lower $^{187}Os/^{188}Os$ values recorded in DA04 suggests a greater open marine influence with less, continental derived osmium input through the influence of advancing and retreating ice sheets, as noted at the same core site during the Holocene (Rooney et al., 2016). This also further

supports the idea that when there is increased influence from the open ocean beyond Baffin Bay, a reduction in the radiogenic signal would be expected in core JR175.

2.5.5 Baffin Bay Detrital Carbonate event 0 (BBDC0)

The youngest of the BBDC layers, termed BBDC 0, has previously been dated to have started between ~12.7 and 12.4 ka cal BP, and is considered to be associated with approximately a fourfold increase in sedimentation rates (Andrews et al., 1998; Jackson et al., 2017). The timings for BBDC0 is coincidental with the onset of the Younger Dryas (~12.7 ka cal BP), an event in the northern hemisphere characterised by cooler, stadial like conditions (12.9 – 11.7 cal ka BP; Andrews et al., 1998; Jackson et al., 2017; Jennings et al., 2017; Rasmussen et al., 2006). The end of BBDC0 is dated at ~11 ka cal BP (Jackson et al., 2017). In core JR175, a peak in Ca, CaO and detrital carbonate levels between ~20 and 45 cm depth (lithofacies 7) corresponds to an age range of 13.1 and 11.7 ka cal BP (Fig. 2.8), identifying this excursion as BBDC0.

As shown for BBDC1, there is an increase in $^{187}Os/^{188}Os$ levels over the BBDC0 interval. However, unlike the temporal agreement of Ca, CaO, detrital carbonate and La/Sc with the trend in $^{187}Os/^{188}Os$ for BBDC1, for BBDC0 the $^{187}Os/^{188}Os$ decreases midway through the peak in Ca and CaO (Fig. 2.8). At ~13.0 cal ka BP, the rise in Ca, CaO, and La/Sc is coupled with the rise in $^{187}Os/^{188}Os$, which peaks at 2.2 at 12.3 cal ka BP (Figs. 2.4, 2.8). However, at 12.2 cal ka BP there is an abrupt decrease in $^{187}Os/^{188}Os$ values to ~1.7 and then a more gradual decrease to 1.3 at 11.3 cal ka BP. This is partly mirrored by the trend in La/Sc. Yet, in contrast, calcium levels, remain at their highest until ~11.8 cal ka BP and then abruptly decrease to their lowest values by 11.6 cal ka BP. This asynchronicity further supports differing sources of carbonate and radiogenic Os into Baffin Bay as discussed above for BBDC1. The BBDC0 period is also characterised by higher TOC levels (up to 3.8%) and IRD clasts (Figs. 2.3, 2.4). As with BBDC1, mixing models show that the $^{187}Os/^{188}Os$ values of > 2 cannot be achieved by only carbonate input. The REE patterns during BBDC0 (Fig. 2.6d) are similar to those for BBDC1 (Fig. 2.6b) with LREE enrichment and a positive Eu anomaly, as well as higher SiO_2/Al_2O_3 and K_2O/Na_2O values (Fig. 2.4) suggesting a mature plagioclase and alkali feldspar input. This would therefore suggest a radiogenic, felsic source from west Greenland and/or Baffin Island.

Again, foraminifera abundances increase over BBDC0, indicating increased productivity again most likely driven by increased nutrient delivery from glacial meltwaters (Fig. 2.4).

This peak in abundance is also characterised by high planktic and benthic abundance (earlier peaks tend to be mainly planktic foraminifera). The increase in benthic productivity is most likely associated with an increased flux of food supply from above (surface productivity). The higher TOC levels during this interval suggest the increased surface productivity is even more pronounced than during earlier productivity peaks (BBDC1 and at the onset of shelf edge deglaciation).

Similar to BBDC1, the DA04 $^{187}Os/^{188}Os$ record during BBDC0 is less radiogenic (0.9 to 1.2) than that of JR175 (1.2 to 2.2; Fig. 2.8), again suggesting a greater marine influence over continental influence. A peak in values to 1.2 at 11.7 cal ka BP corresponds in timing to the end of the Younger Dryas period, perhaps an influence of glacial discharge from southern Greenland as temperatures warmed.

Further, in comparison to BBDC1 occurring contemporaneous with the Bølling-Allerød interstadial, BBDC0 and the increase in $^{187}Os/^{188}Os$ occurs at the same time as the Younger Dryas stadial. Hence, ice sheet dynamics in both warmer and cooler periods can lead to influxes causing changes in the water column chemistry. Extensive readvance of Greenland Ice Sheet glacial outlets, and subsequent rapid retreat from ~12.2 cal ka BP is known to have occurred during the Younger Dryas (Jackson et al., 2017; Jennings et al., 2014, 2017; Ó Cofaigh et al., 2013). The carbonate and $^{187}Os/^{188}Os$ excursion could therefore be related to increased sediment delivery during readvance and thickening of glacial outlets across the shelf, combined with their subsequent retreat through breakup and iceberg calving at the end of the Younger Dryas. The end of the Ca, CaO and $^{187}Os/^{188}Os$ peaks are coincident with a rise in $\delta^{18}O$ levels in the Greenland ice cores indicating warming at the end of the Younger Dryas. However, readvance and stabilisation of retreat from the Laurentide Ice Sheet into Baffin Bay has also been noted, for example in the east of Lancaster Sound an ice shelf existed through much of the Younger Dryas until ~12.5 cal ka BP as well as ice re-advance across the Hudson Strait, and deglaciation of the LIS margin on Baffin Island beginning somewhere between 12.5 cal ka BP and 11.5 cal ka BP (Andrews et al., 1996; Furze et al., 2018; Margold et al., 2018).

Combined, the $^{187}Os/^{188}Os$ and Ca data suggest that there was significant flux of radiogenic material, likely from the GIS (although an LIS Baffin Island source cannot be ruled out completely), during the earlier stages of BBDC0. This influx then significantly decreased part way through BBDC0, but the flux of carbonate material from the northern

IIS and NE LIS continued. The abundance of IRD is high throughout this interval, indicating high iceberg delivery from at least one ice sheet continued.

2.5.6 Holocene

At the transition to the Holocene, the Ca, CaO and detrital carbonate content in core JR175 decreases abruptly, and then decreases more gradually to the present day (Figs. 2.5, 2.7). The $^{187}Os/^{188}Os$ values decrease more gradually but reach lower values by the early Holocene, and then record a very slow decrease to the present day from ~1.2 to 1.1, moving closer to open ocean values of ~1.06. This likely reflects a combination of an increased influence of open ocean waters through Davis Strait from the Atlantic (similar $^{187}Os/^{188}Os$ values to those measured from DA04 at the onset of the Holocene) and an overall reduced influx of more radiogenic glacially eroded material as the ice sheets retreated back across the continental shelves around Baffin Bay and in land during this time (e.g., Briner et al., 2013; Jennings et al., 2014; Ó Cofaigh et al., 2013).

The second core analysed, DA04, to the south of the Davis Strait (Fig. 2.1) records $^{187}Os/^{188}Os$ values between 0.9 and 1.2 from 15.3 to 9.1 cal ka BP, throughout BBDC1 and BBDC0 (Fig. 2.7). It shows a higher influence of open ocean marine waters at DA04. The $^{187}Os/^{188}Os$ of JR175 through the Holocene gradually reduces to open ocean values as an increased flux of open ocean $^{187}Os/^{188}Os$ signal enters Baffin Bay via the West Greenland Current (Rooney et al., 2016).

The REE pattern during the Holocene does not record an Eu anomaly (Fig. 2.6e) as seen in previous sections, suggesting reduced plagioclase and alkali feldspar input, and reduced glacial flux as the west Greenland ice sheet and LIS retreat to their current positions. This is further supported by the qXRD SedUnMix model which shows the fraction of west Greenland and south-west Greenland sources decreasing to almost zero through the Holocene (Fig. 2.5). A contribution from Baffin Island, however, remains during this time and slightly increases. This provides further evidence that the $^{187}Os/^{188}Os$ signal is not controlled by a Baffin Island source, as the $^{187}Os/^{188}Os$ continues to decline into the Holocene while the Baffin Island contribution does not. The Holocene records the largest source components as that from the Foxe Fold Belt and from weathered Tertiary and Cretaceous rocks (Fig. 2.5), the latter makes up a large proportion of the present-day shelf, slope, and floor of Baffin Bay (Fig. 2.1).

2.6 Implications and conclusions

In summary, the Ca, CaO and detrital carbonate data presented alongside a robust age model indicate that BBDC1 and BBDC 0 are recorded in the sediments between 15.2 and 13.9 ka cal BP and 13.1 to 11.7 cal ka BP, respectively. BBDCs 2, 3 and 4, however, are not recorded as clearly in the core but are likely linked to the peaks in Ca and detrital carbonate recorded over the LGM. This potentially indicates that they were smaller and less extensive, or that carbonate is poorly preserved during these earlier stages. This study also uses the most up to date marine calibration curve, MARINE20, and hence leads to a slightly different age for BBDC1 (15.2 to 13.9 cal ka BP) and BBDC0 (13.1 to 11.7 cal ka BP).

A mixing model shows that the radiogenic peaks in $^{187}Os/^{188}Os$ coinciding with BBDC1 and the start of BBDC0 are not sourced from the same carbonate rocks as the BBDC layers, and must be originating from either a radiogenic LIS or GIS source, but distinguishing between an LIS vs GIS source is difficult. This is further supported by the very low REE abundances found in the carbonate rocks compared to the markedly higher abundances found in JR175 sediments over the BBDC intervals. The combined data from this study including IRD, La/Sc, REE analysis, SiO_2/Al_2O_3 and K_2O/Na_2O values and the geography of Baffin Bay and ice core records provide a strong argument for a dominant GIS sourced flux during these times (although a Baffin Island contribution cannot be ruled out completely). The short duration of BBDC1 and BBDC0 of ~1000 years would suggest a catastrophic failure of the IIS and GIS leading to increased iceberg discharge and sediment delivery out into Baffin Bay.

BBDC1 is coincident with the Bølling-Allerød period indicating increased glacial meltwater flux and discharge through icebergs during a period of warmer temperatures. Further, the sudden decline in Ca, CaO and $^{187}Os/^{188}Os$ values also corresponds to the timing of the Older Dryas stadial (~14 cal ka BP; Rasmussen et al., 2006), which potentially was enough therefore to slow or halt this break up. Conversely, BBDC0 is coincident with the Younger Dryas stadial, suggesting that increased flux from the ice sheets can occur in both colder and warmer periods. This further agrees with the suggestions that the dynamics of the ice sheets surrounding Baffin Bay are not always in sync and are not directly forced/controlled by North Atlantic-wide climate changes.

The dynamics of the ice sheets surrounding Baffin Bay display both synchronous and asynchronous behaviour. The $^{187}Os/^{188}Os$ values begin to increase ~17.1 cal ka BP, at the

same time as the GIS is thought to have begun to retreat, whereas the Ca and CaO levels during this time remain roughly constant, indicating that the GIS is changing but the IIS and NE LIS is relatively stable. During BBDC1 both the IIS and GIS (and/or LIS) behave synchronously, both responding quickly and dramatically to warmer temperatures during the Bølling-Allerød. During BBDC0 however, the ice sheets respond asynchronously. Again $^{187}Os/^{188}Os$ values begin to rise before Ca, CaO and detrital carbonate, indicating earlier flux from the GIS (and/or LIS) in comparison to the IIS. $^{187}Os/^{188}Os$ values then drop quickly at 12.7 ka cal BP within BBDC0, whilst Ca and CaO levels remain higher for longer. This indicates that flux from the GIS (and/or LIS) stops before flux from the northern IIS does.

In terms of using this information to help understand future possible ice sheet responses to changes in climate, it appears that the GIS begins to respond earlier than the other ice sheets and the dynamic response of the GIS can be linked to periods of both warmer and colder climate, but could also be driven by non-climatic factors. Past responses of the IIS and LIS are likely less useful looking to the future as these ice sheets no longer exist to a great extent.

2.7 Tables

Table 2.1: Locations of the studied cores JR175, BC06 and DA04-31P alongside the locations of carbonate rock samples from Somerset Island.

Sample	Type	Formation	Location	Latitude (°N)	Longitude (°W)	Water depth (m)
JR175-BC06	Box core	-	Baffin Bay	69°56.01	63°03.40	2034
JR175-GC01	Gravity core	-	Baffin Bay	69°56.01	63°03.40	2034
DA04-31P	Piston core	-	Labrador Sea	62°33.78	54°13.11	2525
AB18-04 466.9	Carbonate core sample	Bay Fiord	Somerset Island	73°40.86	94°17.44	-
AB18-04 320.2	Carbonate core sample	Irene Bay	Somerset Island	73°40.86	94°17.44	-
AB18-04 383.95	Carbonate core sample	Lower Allen Bay	Somerset Island	73°40.86	94°17.44	-
AB18-04 8.75	Carbonate core sample	Upper Allen Bay	Somerset Island	73°40.86	94°17.44	-
18HR59	Carbonate outcrop sample	Lower Turner Cliffs	Somerset Island	73°35.32	94°40.59	-
18HR251	Carbonate outcrop sample	Ship Point	Somerset Island	73°35.30	94°39.21	-
18HR226	Carbonate outcrop sample	Upper Turner Cliffs	Somerset Island	73°35.31	94°40.27	-
77108	Carbonate outcrop sample	Cape Phillips/ Allen Bay	Devon Island	74°32.27	89°53.06	-
77103	Carbonate outcrop sample	Cape Phillips/ Allen Bay	Devon Island	74°32.26	89°55.08	-
77156	Carbonate outcrop sample	Cape Phillips/ Allen Bay	Devon Island	74°37.30	90°26.09	-

Table 2.2: Radiocarbon data for core JR175 calibrated in Calib 8.2 using the MARINE20 calibration curve and a reservoir correction of ΔR = 140 ± 30. Calibrated ranges and middle values in cal ka BP.

Lab code	Analysis type	Depth (cm)	Species	^{14}C age ± error (BP)	Calibrated range (1σ)	Calibrated range (2σ)	Middle value (1σ)	Middle value (2σ)
Beta468820	AMS	27-29	C. neoteretis + Trioculina	10560 ± 40	11305 - 11558	11227 - 11687	11432	11457
Beta521060	AMS	38-41	C. neoteretis + Trioculina	10750 ± 30	11625 - 11854	11491 - 11964	11740	11728
Beta470332	AMS	57-59	N. pachyderma	12310 ± 40	13412 - 13591	13320 - 13699	13502	13510
Beta521061	AMS	74-77	C. neoteretis	12800 ± 30	14015 - 14233	13890 - 14389	14124	14140
BE-14923.1.1	MICADAS	97-99	N. pachyderma	13425 ± 78	14999 - 15288	14861 - 15458	15144	15160
Beta483066	AMS	106	N. pachyderma	14080 ± 40	15881 - 16134	15752 - 16252	16008	16002
BE-14924.1.1	MICADAS	106	N. pachyderma	14053 ± 65	15827 - 16113	15685 - 16248	15970	15967
BE-14925.1.1	MICADAS	111-113	N. pachyderma	14047 ± 150	15734 - 16183	15508 - 16411	15959	15960
BE-12425.1.1	MICADAS	118-120	N. pachyderma	13637 ± 139	15210 - 15631	15008 - 15854	15412	15431
BE-12426.1.1	MICADAS	126-128	N. pachyderma + C. neoteretis	18608 ± 209	21122 - 21746	20849 - 21996	21434	21423
Beta483067	AMS	154	N. pachyderma	35850 ± 280	39548 - 40123	39320 - 40420	39836	39870
BE-14926.1.1	MICADAS	168	N. pachyderma	30996 ± 730	33781 - 35267	32920 - 36057	34524	34489

Table 2.3: qXRD data from samples for core JR175. All values in %.

Depth (cm)	Quartz	Alkali Feldspar	Plagioclase	Calcite	Dolomite	Amphibole	Pyroxene	FeO	SiO_2	Kaolinite	Smectite	Illites	Biotite
3	7.7	16.3	10.4	0.0	7.9	1.2	0.0	1.8	10.5	1.3	11.8	13.3	14.3
11	9.8	17.9	10.1	0.0	11.7	0.6	0.5	0.3	12.2	1.8	12.5	14.5	14.0
19	12.9	18.0	13.8	0.1	17.4	1.6	0.0	0.6	8.6	0.2	6.6	14.5	8.1
27	12.6	21.0	9.3	6.7	24.4	1.7	0.6	0.8	5.3	0.0	3.9	9.9	5.0
31	13.4	19.7	8.2	9.4	27.3	1.4	0.5	0.2	5.1	0.0	3.9	8.8	4.5
35	12.1	17.9	8.6	9.1	28.2	1.1	1.1	0.9	6.8	0.0	3.4	3.8	6.1
43	11.7	18.2	14.1	2.8	11.9	3.4	0.7	0.5	8.7	0.2	12.2	12.4	6.5
51	12.5	18.6	16.2	0.1	11.4	2.2	0.0	0.9	10.2	0.8	10.3	7.0	8.4
59	14.5	21.6	13.6	3.0	12.2	2.6	0.0	1.2	7.2	0.8	8.8	12.7	6.1
67	18.4	19.9	6.8	7.1	28.4	0.8	1.3	0.3	9.1	0.0	0.1	6.8	3.8
71	18.3	17.6	8.5	6.5	27.9	0.9	0.7	0.5	8.9	0.0	1.2	6.7	3.3
75	16.9	18.4	9.5	5.6	16.6	1.6	0.8	0.5	11.5	0.5	4.5	10.0	7.2
83	7.5	17.2	18.6	0.0	1.8	4.9	0.0	1.8	10.3	1.5	16.0	15.3	8.6
91	11.5	18.6	19.7	0.3	4.8	2.5	0.7	2.2	14.3	1.4	7.0	13.8	6.8
99	22.9	20.2	24.9	0.8	5.4	3.5	0.5	1.1	9.9	0.0	1.8	7.0	3.0
107	23.0	20.5	17.8	1.1	9.4	2.4	0.6	0.5	13.8	0.3	1.6	8.0	4.2
115	14.7	21.9	21.4	0.9	3.3	3.7	0.2	1.6	11.1	0.7	7.3	10.5	4.6
121	17.9	22.5	24.7	0.3	2.4	4.1	0.6	2.2	9.7	0.7	5.3	8.3	3.5
125	17.5	18.8	32.7	0.6	2.9	4.0	1.9	1.5	11.3	0.0	2.7	4.7	1.6
129	21.9	23.2	27.2	0.7	5.2	4.6	0.7	2.1	6.4	0.0	2.6	4.4	1.7
133	20.2	20.8	31.3	0.4	2.8	3.8	1.2	1.3	11.5	0.0	2.4	3.9	1.3
137	18.3	19.0	14.4	1.1	12.7	2.0	0.4	0.9	9.1	0.0	8.5	5.5	7.2
145	27.0	27.6	20.8	0.4	3.9	2.8	0.2	1.2	9.2	0.0	1.6	4.6	2.4
153	26.3	24.3	24.0	0.8	2.5	2.3	1.2	0.3	13.0	0.0	0.3	4.7	3.0
161	9.8	21.7	21.4	0.3	2.3	3.8	0.0	1.4	12.3	1.1	12.5	10.7	5.0

Table 2.4a: Carbonate corrected major oxide data and La and Sc data from Actlabs for core JR175.

Depth cm	SiO_2 %	Al_2O_3 %	Fe_2O_3 %	MnO %	MgO %	CaO %	Na_2O %	K_2O %	TiO_2 %	SiO_2/Al_2O_3 -	K_2O/Na_2O -	P_2O_5 %	La ppm	Sc ppm	La/Sc -
2.5	48.52	13.42	6.66	0.67	4.83	4.12	3.66	3.21	0.64	3.62	0.88	0.21	45.10	16.00	2.82
7.5	48.41	13.26	5.97	0.47	5.19	4.68	3.06	3.38	0.62	3.65	1.10	0.19	49.10	13.00	3.78
14.5	48.55	13.53	5.81	0.34	5.57	5.74	3.04	3.46	0.65	3.59	1.14	0.20	47.00	13.00	3.62
20.5	67.61	17.90	7.35	0.27	1.08	-3.48	4.55	4.53	0.83	3.78	1.00	0.22	63.03	16.13	3.91
22.5	67.55	15.51	5.81	0.12	1.87	-0.76	3.83	3.85	0.70	4.36	1.01	0.17	59.51	13.20	4.51
32.5	52.75	10.45	3.36	0.09	4.34	11.17	2.64	2.90	0.38	5.05	1.10	0.14	36.63	7.33	4.99
36.5	53.47	10.50	3.45	0.18	4.29	9.76	2.55	2.90	0.39	5.09	1.14	0.12	37.36	8.80	4.25
38.5	56.14	9.80	3.10	0.35	4.01	10.39	2.27	2.92	0.39	5.73	1.28	0.11	35.90	7.33	4.89
44.5	53.73	14.21	5.79	0.06	4.41	4.55	3.59	2.92	0.73	3.78	0.81	0.16	41.90	14.00	2.99
47.5	51.63	10.82	3.93	0.05	6.24	8.03	2.46	2.70	0.48	4.77	1.10	0.12	32.50	9.00	3.61
54.5	51.68	13.38	5.75	0.06	4.95	6.28	3.20	3.01	0.72	3.86	0.94	0.16	42.90	13.00	3.30
58.5	50.21	12.97	4.98	0.06	5.09	7.50	3.01	2.89	0.63	3.87	0.96	0.13	44.20	12.00	3.68
60.5	47.88	11.33	4.12	0.05	5.62	10.22	2.58	2.69	0.50	4.23	1.04	0.13	34.20	10.00	3.42
62.5	65.31	13.63	4.55	0.07	1.42	4.74	3.04	3.49	0.57	4.79	1.15	0.12	46.60	10.27	4.54
67.5	60.63	10.53	2.83	0.07	3.52	8.50	2.29	3.18	0.37	5.76	1.39	0.11	40.15	7.33	5.47
70.5	61.54	10.67	3.26	0.07	3.12	7.78	2.41	3.15	0.38	5.77	1.31	0.11	40.74	7.33	5.55
72.5	66.13	11.46	4.04	0.07	2.02	5.27	2.66	3.18	0.44	5.77	1.20	0.15	36.04	8.80	4.10
76.5	53.71	14.69	6.14	0.07	4.36	4.68	3.32	2.97	0.80	3.66	0.89	0.17	43.20	14.00	3.09
80.5	51.49	15.29	7.88	0.08	4.21	3.03	4.19	3.25	0.85	3.37	0.78	0.17	47.10	16.00	2.94
92.5	56.35	15.42	5.97	0.07	3.47	3.73	3.92	2.67	0.76	3.65	0.68	0.17	37.50	14.00	2.68
98.5	64.39	12.98	3.41	0.06	2.63	4.99	3.35	2.38	0.50	4.96	0.71	0.14	30.70	9.00	3.41
102.5	55.47	13.23	5.12	0.06	3.84	4.53	3.31	2.71	0.67	4.19	0.82	0.15	34.10	12.00	2.84
110.5	59.41	13.59	4.80	0.06	3.55	4.73	3.09	2.84	0.64	4.37	0.92	0.13	38.50	11.00	3.50

Table 2.4b: Major oxide data and La and Sc data from Actlabs for carbonate rocks of Somerset Island and Devon Island.

Sample	SiO_2 %	Al_2O_3 %	Fe_2O_3 %	MnO %	MgO %	CaO %	Na_2O %	K_2O %	TiO_2 %	P_2O_5 %	SiO_2/Al_2O_3 -	K_2O/Na_2O -	La ppm	Sc ppm	La/Sc
18HR 226	18.66	4.04	1.14	0.03	15.89	21.63	0.06	3.00	0.15	0.05	4.62	50.00	8.09	2.00	4.05
18HR 59	2.19	0.72	0.97	0.04	20.41	28.05	0.02	0.54	0.03	0.05	3.04	27.00	3.11	< 1	-
18HR 251	9.02	0.41	0.22	0.01	21.92	26.70	0.03	0.16	0.02	0.01	22.00	5.33	1.49	< 1	-
77108	0.14	0.04	0.04	0.00	21.01	30.14	0.03	0.02	0.00	< 0.01	3.50	0.67	0.19	< 1	-
77103	1.63	0.03	0.01	0.00	4.59	49.05	0.02	0.01	0.00	0.01	54.33	0.50	0.57	< 1	-
77156	1.53	0.36	0.13	0.01	21.33	28.40	0.03	0.19	0.01	0.01	4.25	6.33	0.86	< 1	-
AB18-04 466.9	4.52	1.22	1.08	0.04	20.05	28.33	0.03	0.64	0.04	0.02	3.70	21.33	4.80	1.00	4.80
AB18-04 320.2	1.51	0.47	0.12	0.01	20.75	28.8	0.02	0.20	0.02	< 0.01	3.21	10.00	1.32	< 1	-
AB18-04 383.95	7.59	2.04	0.61	0.03	1.25	47.76	0.03	0.93	0.11	0.04	3.72	31.00	5.26	2.00	2.63
AB18-04 8.75	2.36	0.04	0.03	0.01	21.05	28.94	0.02	0.02	< 0.001	0.02	59.00	1.00	0.25	< 1	-
Average	4.92	0.94	0.44	0.02	16.83	31.78	0.03	0.57	0.04	0.03	16.14	15.32	2.59	1.67	3.83

Table 2.5: Re-Os data presented for box core BC06, gravity core JR175, piston core DA04-31P, and carbonate rock samples. Uncertainty is ± 2 SE.

Sample	Depth (cm)	Re (ppb)	±	Os (ppt)	±	^{192}Os (ppt)	±	^{187}Re/^{188}Os	±	^{187}Os/^{188}Os	±
BC06	0	0.24	0.00	108.60	0.54	39.54	0.21	12.06	0.13	1.15	0.01
JR175	2.5	0.52	0.00	100.66	0.68	37.04	0.34	27.93	0.30	1.06	0.01
	3.5	0.21	0.00	111.06	0.54	40.79	0.22	10.44	0.12	1.08	0.01
	7.5	0.38	0.00	76.72	0.92	27.90	0.57	27.02	0.57	1.16	0.03
	10.5	0.38	0.00	79.43	0.40	28.85	0.16	26.46	0.21	1.17	0.01
	14.5	0.41	0.00	68.21	0.48	24.63	0.22	33.49	0.46	1.23	0.02
	18.5	0.42	0.01	50.06	0.35	18.16	0.16	45.86	0.74	1.19	0.02
	20.5	0.40	0.00	46.03	0.26	16.42	0.10	48.25	0.40	1.33	0.01
	22.5	0.42	0.00	43.99	0.33	15.32	0.14	55.09	0.64	1.55	0.02
	26.5	0.36	0.00	22.35	0.18	7.75	0.08	92.65	1.22	1.59	0.02
	29.5	0.36	0.00	28.43	0.20	9.73	0.08	73.13	0.75	1.71	0.02
	30.5	0.38	0.00	30.85	0.24	10.62	0.10	71.11	0.80	1.65	0.02
	31.5	0.31	0.00	21.18	0.15	7.27	0.06	84.12	0.93	1.68	0.02
	32.5	0.32	0.00	20.11	0.29	6.53	0.14	97.40	2.18	2.21	0.07
	34.5	0.33	0.00	20.82	0.19	7.03	0.08	92.70	1.29	1.83	0.03
	36.5	0.28	0.00	17.77	0.13	5.87	0.05	95.49	1.13	2.04	0.02
	37.5	0.30	0.00	17.62	0.16	5.87	0.07	100.97	1.36	1.96	0.03
	38.5	0.27	0.00	24.76	0.16	8.49	0.06	62.65	0.73	1.69	0.02
	40.5	5.01	0.16	38.36	0.23	13.07	0.08	762.34	24.84	1.75	0.01
	42.5	1.11	0.00	76.99	0.44	26.63	0.15	83.01	0.54	1.61	0.01
	43.5	4.20	0.01	89.36	0.53	31.20	0.19	267.74	1.74	1.53	0.01
	44.5	2.54	0.01	89.09	0.46	32.05	0.18	157.40	0.96	1.26	0.01
	45.5	1.74	0.00	70.77	0.38	25.20	0.14	137.64	0.86	1.35	0.01
	46.5	1.73	0.00	56.83	0.34	20.08	0.13	171.81	1.20	1.42	0.01
	47.5	1.78	0.01	39.17	0.23	13.69	0.09	258.77	1.83	1.51	0.01
	49.5	3.40	0.01	64.99	0.33	23.41	0.13	288.90	1.95	1.25	0.01
	50.5	1.92	0.01	61.98	0.60	21.86	0.31	174.86	2.50	1.43	0.03
	54.5	4.82	0.15	54.07	0.32	19.25	0.12	497.84	15.39	1.35	0.01
	58.5	3.08	0.01	53.26	0.39	18.88	0.18	324.72	3.24	1.39	0.02
	60.5	1.37	0.00	41.78	0.25	14.74	0.10	185.34	1.34	1.43	0.01
	61.5	0.83	0.00	25.63	0.21	8.67	0.09	191.09	2.04	1.81	0.02
	62.5	0.53	0.00	27.35	0.24	9.20	0.10	114.43	1.34	1.87	0.03
	63.5	0.60	0.00	25.98	0.19	8.76	0.07	135.82	1.25	1.85	0.02
	65.5	0.37	0.00	20.78	0.15	6.90	0.06	107.22	1.11	1.99	0.02
	66.5	0.44	0.00	17.78	0.14	5.64	0.05	154.68	1.67	2.44	0.03
	67.5	0.41	0.00	20.07	0.15	6.42	0.05	127.61	1.29	2.36	0.02
	70.5	0.37	0.00	18.80	0.22	6.07	0.10	121.42	2.05	2.26	0.05
	71.5	0.38	0.00	21.14	0.15	6.86	0.06	109.54	1.14	2.21	0.02
	72.5	0.77	0.00	27.50	0.24	8.84	0.09	174.17	1.85	2.31	0.03
	74.5	3.22	0.01	45.51	0.35	15.45	0.14	414.80	3.91	1.78	0.02
	76.5	1.62	0.00	72.04	0.42	25.41	0.16	127.02	0.87	1.43	0.01
	77.5	1.59	0.00	71.01	0.39	24.91	0.14	126.88	0.81	1.48	0.01
	78.5	1.25	0.00	69.26	0.38	24.22	0.13	102.85	0.65	1.51	0.01
	80.5	1.14	0.00	66.94	0.86	23.55	0.49	96.61	2.06	1.46	0.04
	82.5	1.12	0.00	73.22	0.39	25.87	0.14	85.90	0.55	1.42	0.01
	86.5	3.56	0.01	66.17	0.65	23.03	0.32	307.44	4.37	1.56	0.03
	90.5	3.19	0.01	69.92	0.41	24.80	0.15	256.08	1.72	1.38	0.01
	92.5	4.30	0.01	80.14	0.42	28.78	0.16	296.98	1.80	1.27	0.01
	98.5	1.10	0.00	33.96	0.20	11.95	0.08	183.26	1.33	1.46	0.01
	102.5	0.65	0.00	55.70	0.56	20.04	0.28	64.23	0.95	1.26	0.03
	106.5	0.18	0.00	26.60	0.16	9.55	0.07	37.71	0.51	1.28	0.01
	110.5	0.26	0.00	48.65	0.46	17.46	0.25	29.78	0.48	1.28	0.03
	116.5	0.29	0.00	75.70	0.38	27.44	0.15	21.25	0.20	1.19	0.01
	124.5	0.13	0.00	26.95	0.16	9.86	0.07	26.70	0.46	1.11	0.01
	125.5	0.07	0.00	8.92	0.10	3.23	0.06	45.62	1.51	1.19	0.03
	126.5	0.10	0.00	14.68	0.15	5.26	0.09	39.31	0.99	1.29	0.03
	128.5	0.12	0.00	21.24	0.20	7.73	0.11	30.99	0.70	1.16	0.02
	129.5	0.10	0.00	18.45	0.23	6.58	0.14	30.75	0.90	1.33	0.04
	130.5	0.09	0.00	15.19	0.19	5.64	0.12	31.08	0.99	0.99	0.03
	131.5	0.18	0.00	16.95	0.17	5.91	0.09	59.55	1.15	1.53	0.03
	132.5	0.16	0.00	23.81	0.14	8.50	0.06	36.30	0.55	1.33	0.01
	133.5	0.23	0.00	31.09	0.26	11.06	0.13	42.12	0.61	1.36	0.02
	135.5	0.20	0.00	38.61	0.39	13.57	0.20	28.79	0.52	1.47	0.03

	136.5	0.27	0.00	35.64	0.34	12.65	0.18	41.88	0.68	1.38	0.03
	137.5	0.31	0.00	41.65	0.41	14.70	0.21	42.35	0.67	1.43	0.03
	138.5	0.27	0.00	26.52	0.27	9.27	0.14	57.53	0.96	1.51	0.03
	139.5	0.59	0.00	36.93	0.38	12.76	0.18	91.86	1.38	1.62	0.03
	140.5	0.64	0.00	27.27	0.28	9.41	0.14	135.64	2.05	1.64	0.03
	141.5	0.30	0.00	19.21	0.20	6.58	0.10	89.98	1.52	1.70	0.04
	142.5	0.40	0.00	20.51	0.20	7.33	0.11	107.60	1.75	1.32	0.03
	144.5	0.23	0.00	18.63	0.19	6.57	0.10	70.69	1.25	1.43	0.03
	146.5	0.20	0.00	20.23	0.21	7.09	0.11	55.39	1.02	1.49	0.03
	148.5	0.21	0.00	18.69	0.24	6.53	0.14	63.12	1.49	1.52	0.05
	150.5	0.15	0.00	12.58	0.17	4.45	0.10	66.11	1.75	1.40	0.04
	152.5	0.16	0.00	13.33	0.10	4.69	0.05	65.80	1.11	1.45	0.02
	156.5	0.22	0.00	35.11	0.28	12.49	0.14	35.28	0.51	1.36	0.02
	160.5	0.24	0.00	73.97	0.60	26.60	0.30	18.14	0.26	1.26	0.02
	164.5	0.24	0.00	57.91	0.50	20.43	0.14	22.90	0.39	1.43	0.03
DA04	43	11.42	0.03	49.11	0.27	18.03	0.12	125.98	8.75	1.08	0.01
	53	2.20	0.01	56.92	0.30	21.13	0.14	207.44	1.44	0.99	0.01
	57	2.06	0.01	54.36	0.30	20.04	0.14	204.86	1.50	1.04	0.01
	65	2.11	0.01	61.32	0.33	22.57	0.14	185.57	1.27	1.06	0.01
	71	4.85	0.01	44.78	0.30	16.55	0.15	582.97	5.57	1.03	0.01
	75	0.45	0.00	33.92	0.18	12.62	0.09	70.47	0.60	0.97	0.01
	79	1.80	0.00	74.47	0.40	27.39	0.17	130.64	0.90	1.07	0.01
	81	4.30	0.01	60.60	0.30	22.05	0.12	388.20	2.28	1.16	0.01
	83	6.85	0.02	59.46	0.29	22.01	0.12	618.85	3.82	1.01	0.01
	85	6.24	0.02	54.25	0.25	20.11	0.11	617.17	3.57	1.00	0.01
	91	2.18	0.01	63.30	0.28	23.64	0.12	183.51	1.04	0.94	0.01
	99	2.01	0.01	60.23	0.29	22.15	0.12	180.38	1.10	1.07	0.01
	101	1.09	0.00	52.08	0.29	19.44	0.14	111.89	0.86	0.94	0.01
	107	1.09	0.00	35.09	0.17	12.89	0.08	168.78	1.11	1.07	0.01
	111	3.20	0.01	38.07	0.19	14.02	0.08	453.83	2.79	1.06	0.01
	119	1.40	0.00	49.62	0.24	18.25	0.10	152.13	0.96	1.06	0.01
	125	6.68	0.02	45.69	0.23	16.75	0.10	793.71	4.97	1.09	0.01
	133	1.90	0.01	48.07	0.24	17.47	0.10	216.72	1.33	1.17	0.01
	141	0.81	0.00	42.77	0.21	15.68	0.09	103.25	0.67	1.09	0.01
	153	0.51	0.00	31.76	0.17	11.86	0.08	85.10	0.73	0.93	0.01
	159	0.54	0.00	30.16	0.18	11.04	0.08	97.93	0.82	1.11	0.01
AB18-01 466.9	-	0.36	0.00	11.43	0.27	3.64	0.15	196.70	8.36	2.40	0.14
AB18-01 320.2	-	0.03	0.00	5.52	0.15	1.56	0.08	44.08	3.35	3.64	0.23
AB18-01 383.95	-	0.05	0.00	16.48	0.40	4.99	0.21	18.55	1.11	2.91	0.17
18HR251	-	0.08	0.00	7.49	0.16	2.77	0.12	56.35	2.87	1.03	0.06
18HR226	-	0.27	0.00	7.99	0.19	2.58	0.11	210.95	9.48	2.26	0.14
77108	-	0.04	0.00	1.21	0.06	0.34	0.04	240.21	32.36	3.60	0.48
77156	-	0.23	0.00	4.54	0.17	0.84	0.05	551.36	35.44	9.51	0.72

Table 2.6: Re-Os data presented for clast samples located in core JR175. Uncertainty is ± 2 SE.

Sample	Clast type	Depth (cm)	Re (ppb)	±	Os (ppt)	±	^{192}Os (ppt)	±	^{187}Re/^{188}Os	±	^{187}Os/^{188}Os	±
8-9cm W Carb	Carbonate	8.5	0.04	0.00	12.81	0.26	4.90	0.21	14.73	1.50	0.73	0.04
29-30cm A Carb	Carbonate	29.5	0.06	0.00	48.82	0.91	19.45	0.79	6.64	0.44	0.40	0.02
38cm W Carb	Carbonate	38	0.14	0.00	5.28	0.16	1.53	0.10	184.43	12.76	3.34	0.25
70cm W Carb	Carbonate	70	0.18	0.00	14.63	0.32	5.10	0.22	68.71	3.24	1.55	0.09
71cm A Granite	Granite	71	0.09	0.00	16.53	0.35	5.93	0.25	29.96	1.56	1.29	0.07

Chapter 3: Postglacial palaeoceanography of the Baltic Sea Basin

*A version of this paper will be submitted for publication to Boreas co-authored by David Selby of the Department of Earth Sciences, Durham University, Jeremy Lloyd of the Department of Geography, Durham University, Matthias Moros of the Leibniz Institute for Baltic Sea Research Warnemünde, Germany, Jaap Damste from Utrecht University, and Slawomir Dobosz from Szczecin University.

I completed all Re-Os laboratory analysis, data synthesis, literature reviews and formulisation of the manuscript. Co-authors Selby and Lloyd contributed through supervisor discussions and editorial comments on the manuscript. Moros provided access to all core samples and XRF, TIC data, x-ray, and core images as well as through supervisor discussions and editorial comments. Damste provided the BIT index data and Dobosz the diatom data.

3.1 Introduction

The Baltic Sea Basin has had a long glaciological history. The Basin has, throughout the Quaternary, been influenced by the continually shifting ice margins of the Fennoscandian Ice Sheet (FIS; Andrén et al., 2015; Björck, 1995). At the Last Glacial Maximum (LGM), the entire Baltic Basin was covered by the FIS (Rosentau et al., 2017). The retreat of the FIS was not continuous, and over time differing rates of glacio-isostatic uplift as well as glacio-eustatic sea level rise have resulted in changes in basin palaeogeography that defined a series of basin stages called the Baltic Ice Lake, the Yoldia Sea, the Ancylus Lake and the Littorina Sea (Andrén et al., 2008, 2011, 2015; Berglund et al., 2005; Björck, 1995; Jakobsson et al., 2007; Rosentau et al., 2017).

During these different basin stages, connections between the Baltic Basin and the palaeo-North Atlantic (via the North Sea) changed between Öresund and the Great Belt Straits (Baltic Ice Lake, Yoldia Sea, Ancylus Lake and Littorina Sea), and through south-central Sweden (Baltic Ice Lake and Yoldia Sea; Andrén et al., 2011; Björck, 1995; Jakobsson et al., 2007; Rosentau et al., 2017). Due to the altering connections during the Baltic Sea stages, the basin has varied between an isolated freshwater lake, a brackish basin, and a more open marine basin, and hence underwent changes in salinity, freshwater versus marine input, temperature, productivity, and sedimentation (Andrén et al., 2015; Björck, 1995; Rosentau et al., 2017). These changes are subsequently recorded in the geochemistry of the sediments. The Baltic Sea Basin generally experiences high

sedimentation rates (~100-500 cm/1000 years; Andrén et al., 2015) and therefore can provide high resolution records, making it an excellent site for reconstructing longer and shorter timescale climatic oscillations and palaeoenvironments (Andrén et al., 2015; Björck, 1995; Rosentau et al., 2017).

Studies of numerous cores from the Baltic Sea Basin show records of these different sea stages. During the early phase of retreat of the FIS the Baltic Ice lake, a freshwater lake, began to form at ~16 cal ka BP (Andrén et al., 2011; Björck, 1995; Rosentau et al., 2017). At ~13 cal ka BP continued retreat of the FIS allowed a drainage of the lake through south-central Sweden (Andrén et al., 2011; Björck, 1995; Fig. 3.1). During the Younger Dryas (~12.8 cal ka BP) glacial advance re-blocked the channel and the lake level rose once more before a final catastrophic, rapid (1 – 2 years) drainage through south-central Sweden coincident with the end of the Younger Dryas ~11.7 cal ka BP, lowering the lake level by 25 m (Andrén et al., 2008, 2011; Björck, 1995; Jakobsson et al., 2007; Rosentau et al., 2017). Small, short lived, influxes of marine waters into the Baltic Basin through the now narrowing Swedish channels characterise the next sea stage, the brackish to marine Yoldia Sea (~11.7 – 10.7 cal ka BP), before the channels closed as a result of glacio-isostatic uplift (Andrén et al., 2008, 2011; Björck, 1995; Rosentau et al., 2017). This allowed freshwater to build up forming the Ancylus Lake between ~10.7 – 9.7 cal ka BP (Andrén et al., 2011; Berglund et al., 2005; Rosentau et al., 2017). Due to isostatic and eustatic sea-level changes, areas such as Öresund, and the Great Belt Strait began to lower, allowing these channels to enlarge and create an outflow through which the Ancylus Lake was able to drain (Andrén et al., 2011; Rosentau et al., 2017). This new connection out to the North Sea eventually allowed saline marine waters to enter the Baltic Basin as the Fennoscandian Ice Sheet underwent its final retreat resulting in the final stage, the Littorina Sea, from 9.7 cal ka BP lasting up to the present day (Andrén et al., 2011; Berglund et al., 2005; Björck, 1995; Rosentau et al., 2017). However, the accuracy of this timing is disputed and the spread of the marine incursion influence is time-transgressive through the Baltic Basin, in that it alters depending on location in the Baltic Sea Basin (Bennike et al., 2021).

Despite these basin stages being fairly well documented, the exact timings of connection and isolation of the Baltic Basin and interaction with the North Sea in different parts of the Baltic Basin remains debated, and it is difficult to identify the pre-Littorina stages in deeper basins such as the Gotland Basin (Andrén et al., 2008; Berglund et al., 2005; Björck, 1995; Westman et al., 1999). This is largely because microfossils in the deeper

basin cores are rare to absent and organic carbon content is low, which makes the dating of the core sediments very difficult. As such dating from coastal settings are more common due to higher organic matter, but due to numerous changes in water levels over the basins history, these records are discontinuous and hence constraining the age of some Baltic Sea stage intervals is difficult in many of the deeper, sub-basins (Hyttinen et al., 2014; Kögler & Larsen, 1979; Kortekaas, 2007). Further, many of the characteristic stratigraphic markers found in shallower basins relating to regressions and transgressions during the different stages are not found in the deeper basins (e.g. Moros et al., 2002).

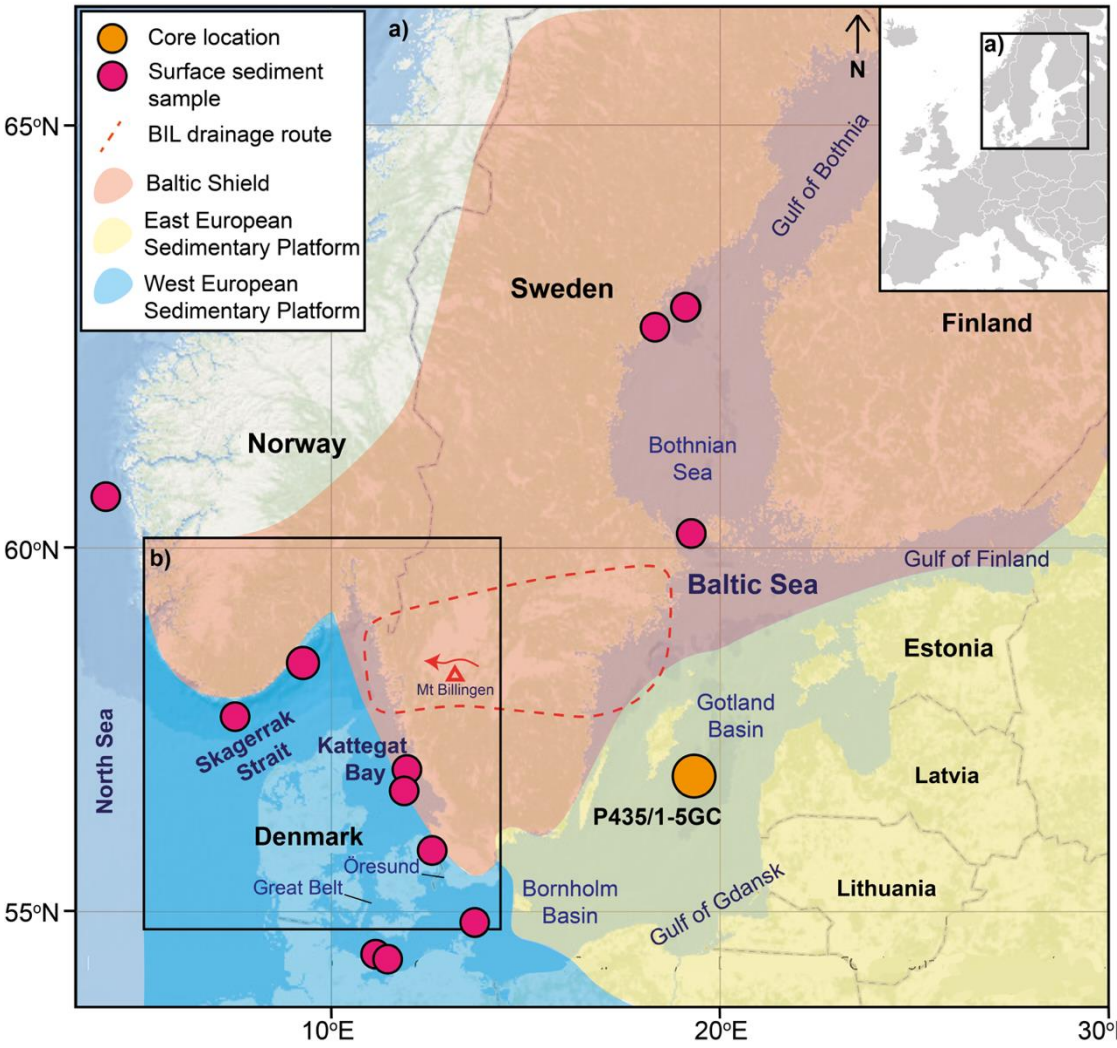

Figure 3.1: Map of the Baltic Sea Basin showing the locations of core P435/1-5 GC and surface sediment samples analysed in this study (pink circles). Colour map from ArcGIS, grey and white Europe map from Wikipedia (https://en.wikipedia.org/wiki/File:Europe_blank_map.png), and the basic geological data is adapted from Peucker-Ehrenbrink & Ravizza (1996) and Rosentau et al. (2017). Dashed, orange line shows the area through south-central Sweden through which the Baltic Ice Lake drained.

This study therefore aims to identify and further understand the evolution of the Baltic Sea Basin stages in a core from the Gotland Basin with the addition a new geochemical proxy, the use of osmium isotopes ($^{187}Os/^{188}Os$), which as yet has not been applied to cores from the Baltic Sea Basin. The $^{187}Os/^{188}Os$ coupled with BIT index (Branched and

Isoprenoid Tetraether index), X-ray fluorescence (XRF) data, diatoms, and core sedimentology provides a multi-proxy geochemical record of the changes in the Baltic Sea Basin during the late Pleistocene and through the Holocene.

Herein, it is shown that $^{187}Os/^{188}Os$ values of surface sediment samples show a clear distinction between the $^{187}Os/^{188}Os$ of present-day North Sea, Kattegat Bay and Skagerrak Strait waters and the $^{187}Os/^{188}Os$ of the present-day Baltic Sea Basin, with the data showing a positive correlation between $^{187}Os/^{188}Os$ and salinity. This relationship was then applied to the long core record. A clear record of the freshwater Ancylus Lake stage and transition into the Littorina Sea stage is shown. However, a record of the weak and short-lived marine ingressions into the Baltic Basin during the Yoldia Sea is not clearly defined. This shows that $^{187}Os/^{188}Os$, BIT index and other geochemical data can identify larger changes between freshwater and marine stages, but it is difficult to identify weak and ephemeral marine ingressions.

3.2 Present day Baltic Sea Basin geography and geology

The Baltic Sea Basin lies between ~53-66^{o} N, 10-20^{o} E and occupies ~373,000 km^2, with a mean depth of 54 m, making it one of the world's largest intracontinental basins, and largest brackish water body (Andrén et al., 2015; Björck, 1995; Rosentau et al., 2017). The Baltic Basin itself is split into a number of different zones and smaller sub-basins including the Gulfs of Bothnia and Finland, the Gotland Basin, Bornholm Basin and a number of other sub-basins (Fig. 3.1; Andrén et al., 2015; Björck, 1995; Tuuling et al., 2011). Connection of the Baltic Sea to the North Sea exists through the narrow and shallow straits between Sweden and Denmark (Öresund, the Great Belt Strait) and then through Kattegat Bay and Skagerrak Strait which, combined act as an estuary (Björck, 1995; Dickens, 2013; Nordberg, 1991; Rosentau et al., 2017; Tuuling et al., 2011).

The salinity in the Baltic is mainly controlled by varying freshwater inputs and a restricted input of marine waters from the North Sea (Andrén et al., 2011). Salinity varies between almost freshwater (0 – 5 PSU) in the Gulfs of Bothnia and Finland, to 6 – 8 PSU in the central Baltic and 10 – 15 PSU in the south Baltic and Danish Straits into the Kattegat (Fig. 3.2; Björck, 1995; Ducrotoy & Elliott, 2008; Jiang et al., 1997; Peucker-Ehrenbrink & Ravizza, 1996; Rosentau et al., 2017). The Baltic Sea drains a large area of 1.6 million km^2, almost four times the size of the sea itself (Andrén et al., 2015; Björck, 1995). It has been calculated that roughly 1.2% of global runoff (435 km^3 freshwater) enters the Baltic

Sea every year, with half originating from rivers draining south/southeast of the Basin, and half draining the Precambrian Shield (Peucker-Ehrenbrink & Ravizza, 1996).

The north, east and west of the Baltic Sea Basin is characterised by crystalline basement or 'shield' (Precambrian: Late Proterozoic – Late Archean), whilst the south and east is dominated by the European sedimentary platform of Phanerozoic age, and a small part of south-western Baltic Sea lies on the west European sedimentary platform of Palaeozoic age (Fig. 3.1; Björck, 1995; Peucker-Ehrenbrink & Ravizza, 1996; Rosentau et al., 2017).

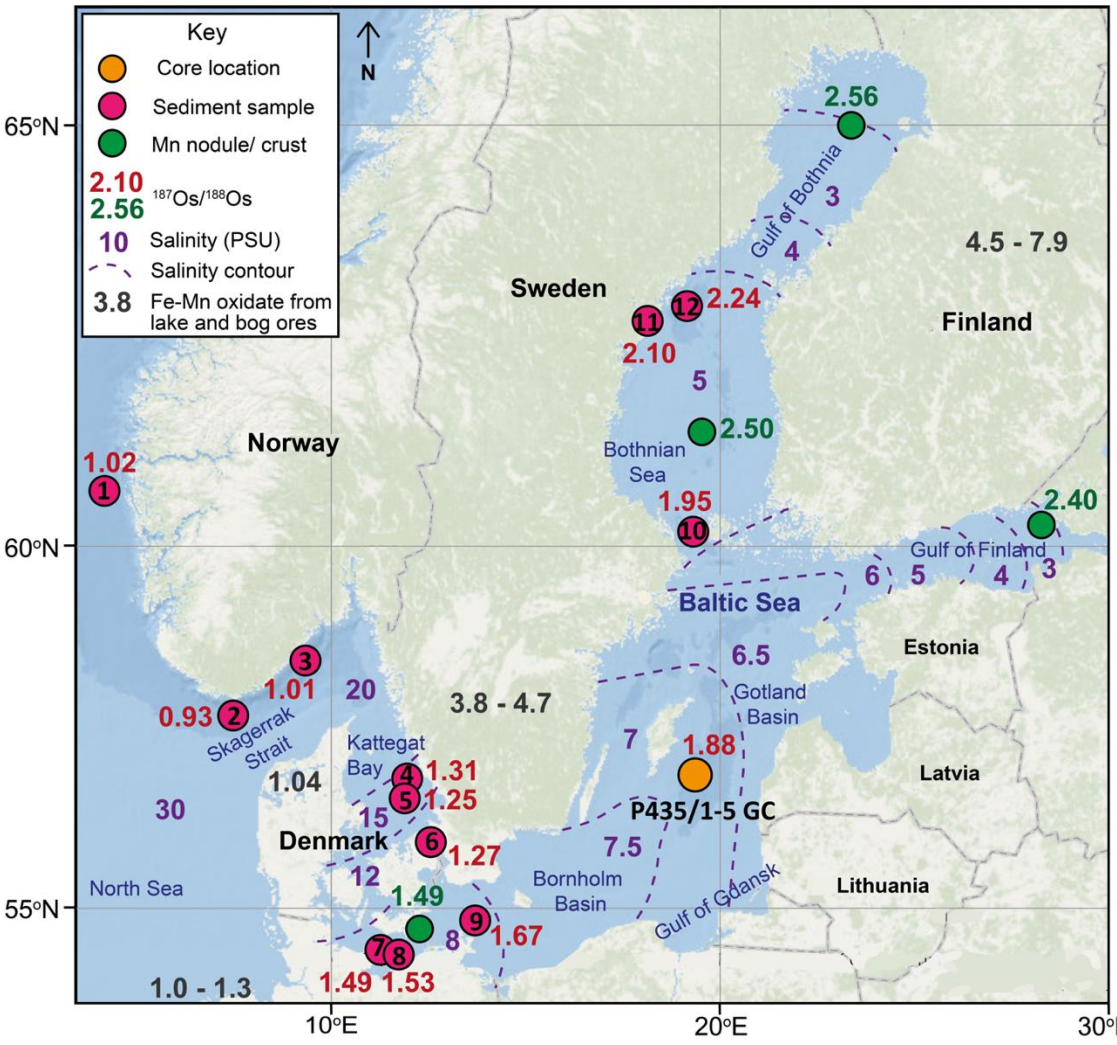

Figure 3.2: $^{187}Os/^{188}Os$ data for surface samples in this study (pink circles), core top sample of P435/1-5 GC, and Mn nodules (green circles; Peucker-Ehrenbrink & Ravizza, 1996) across the Baltic Sea, Skagerrak Strait and the Kattegat. $^{187}Os/^{188}Os$ values are also shown for continental runoff from Finland, south-Sweden, Denmark and northern Germany derived from lake ore and bog ore Fe-Mn oxidates (dark grey values; Peucker-Ehrenbrink & Ravizza, 1996). Estimated salinity across the study area is also plotted in purple (PSU; Sjöqvist et al., 2015). Map sourced from ArcGIS.

3.3 Materials and methods

The analyses undertaken on the central Baltic Sea core and the surface sediment samples are detailed below. For core P435/1-5 GC, XRF scanning, X-radiograph imagery, and Re-Os analysis was undertaken on the whole length of the core (0 – 11 m). BIT index and

TOC, TIC, TC analysis was undertaken between the depths of 2 to 11 m. For the trigger core 303600 TC, BIT index, TOC and XRF data was collected to provide a more accurate understanding of the shallower sediments from 2 m depth to the core top. The Re-Os analysis was also undertaken on all surface sediment samples.

3.3.1 Sample sites

To characterise the present-day $^{187}Os/^{188}Os$ ratio along a marine to brackish to relatively freshwater transition, twelve surface samples were analysed from across the Baltic Sea, Kattegat, Skagerrak, and North Sea (Fig. 3.1; Table 3.1). These samples are a mix of sandy, gritty, muddy to clayey sediments with occasional shelly detritus and larger clasts (which were removed before powdering).

To understand the palaeoceanography and evolution of the Baltic Basin from deglaciation through the Holocene, forty-eight core samples were analysed. The samples analysed in this study are from sediment gravity core P435/1-5 GC collected from the central Baltic (56°57.954 ^{o}N, 19°22.210 ^{o}E) on research cruise RV 'Poseidon' in 2012 (Fig. 3.1; Table 3.1). The core contains 11 m of sediment and is from a water depth of 178 m. This core was chosen due to its central and relatively deep location, with its continuous sedimentation sequence (discussed below). As well as the gravity core a trigger core was also taken at the same locality, core 303600 TC (trigger core) containing 4 m of sediment.

3.3.2 XRF and X-radiograph

The semi-quantitative distribution of K, Ti, and Ca for the core sections was determined by X-ray fluorescence (XRF) core scanning (ITRAX XRF Core Scanner, COX; e.g. Croudace et al., 2006) at the Leibniz-Institute for Baltic Sea Research Warnemünde (IOW). Core surfaces were cleaned, smoothed, and covered with a thin plastic foil to avoid evaporation during measurements. A Cr-tube was used operating at 30 kV and 30 mA with an exposure time of 15 seconds per step. Step size was 1 mm. The ITRAX Core Scanner is also able to produce an x-ray radiographic image (200µm steps at 60 kV and 25 mA).

3.3.3 TC, TIC, TOC

Total carbon (TC) and total inorganic carbon (TIC) was determined at ~3 cm intervals using 100 mg of freeze-dried sediment that was diluted with 40% H_3PO_4 and incinerated at 1200 °C on a Multi Elemental Analyser 4000 from Analytik Jena at IOW. Total organic carbon (TOC) was calculated based on TOC (wt. %) = TC (wt. %) – TIC (wt. %).

3.3.4 Diatoms

Diatom identification was undertaken at the University of Szczecin. Analysis focussed on the identification of general trends in ecology of diatoms present, rather than a detailed abundance of individual species. Between 11 and 2 m, samples 1 cm thick were analysed every 9 to 12 cm. The diatoms present were classified as either brackish or freshwater.

3.3.5 BIT index

The BIT (Branched and Isoprenoid Tetraether) index records the abundance of certain branched glycerol dialkyl glycerol tetraethers (bGDGTs) obtained from terrestrial organisms, compared to an isoprenoid GDGT called 'crenarchaeol' which marine Archaea produce (Kim et al., 2006; Sinninghe Damsté et al., 2002). This therefore allows basic changes between a comparatively more terrestrial (value of 1) versus more marine environment (value of 0) to be inferred. Sediment samples were freeze-dried, ground, homogenised (with a pestle and mortar), and extracted using DionexTM accelerated solvent extraction (ASE). Sample treatment and BIT index calculation is described in detail in Warden et al. (2018). In brief, 1 to 3 g of sediments were extracted at 100 ^{o}C and 1500 psi pressure with a solvent mixture of dichloromethane (DCM):methanol (9:1, v:v) for 5 minutes each, then concentrated with a Caliper Turbovap_LV, dried over anhydrous Na_2SO_4 and blown over N_2. An internal standard (1 mg C46 GDGT; Huguet et al., 2006) was added to the total lipid extract to quantify the GDGTs before separation into three fractions over an Al_2O_3 column (activated for 2 h at 150 ^{o}C): an apolar fraction (hexane:DCM; 9:1, v:v); a ketone fraction (hexane:DCM; 1:1, v:v); and a polar fraction (DCM:MeOH; 1:1, v:v). The polar fraction contains the GDGTs and was dried under N_2 then re-dissolved in hexane: isopropanol (99:1, v:v; 10 mg ml^{-1} concentration) before being passed through a 0.45 mm PTFE filter and analysed with ultra-high performance liquid chromatography-atmospheric pressure positive ion chemical ionization–mass spectrometry (UHPLC-APCI-MS; Hopmans et al., 2016). Selected ion monitoring of specific ions was used to quantify crenarchaeol and the bGDGTs. The concentration of brGDGTs were normalised on the total organic carbon (TOC) content. The BIT Index was then calculated according to De Jonge et al. (2016).

3.3.6 Rhenium-osmium (Re-Os) isotope analysis

In this study 48 samples from P435/1-5 GC and 12 surface sediment samples were analysed for their Re-Os chemistry. Each sampled interval records 1 cm of stratigraphy. The samples were dried at 60 ^{o}C overnight and then powdered using an agate pestle and mortar. The Re-Os analysis is based on established methods (Selby & Creaser, 2003).

Approximately 1 g of powdered sample is sealed into a Carius tube with 8 mL CrO_3 4N H_2SO_4 and a pre-determined amount of tracer solution (enriched in ^{185}Re and ^{190}Os) then is heated at 220 ^oC for 48 h in an oven. The Carius tubes are opened, and a solvent extraction is undertaken using 9 mL chloroform ($CHCl_3$) to separate the Os for back extraction into 3 mL HBr. Purification of the Re fraction is achieved using a 5N NaOH – acetone extraction, and HCl-HNO_3 anion bead chromatography. The osmium fraction is further purified by a H_2SO_4-CrO_3-HBr microdistillation. The Os and Re fractions are loaded into a ThermoScientific TRITON mass spectrometer on Pt and Ni filaments, respectively, and analysed using negative thermal ionisation mass spectrometry (NTIMS). The isotopic composition of Re is determined using Faraday collectors in static mode, and the Os composition with an electron multiplier in dynamic mode.

Total analytical protocol blanks are similar throughout the study (Re = 19.04 ± 4.67 ppt, Os = 0.08 ± 0.05 ppt, with a $^{187}Os/^{188}Os$ of 0.27 ± 0.20; 1 S.D, N = 8). The long-term reproducibility of the Re-Os isotopic measurements were monitored using Re and Os standard solutions. A 50 pg osmium standard solution (DROsS - Durham Romil Osmium Standard) yielded $^{187}Os/^{188}Os$ values of 0.16080 ± 0.00025 (1 S.D., N = 25), which is in agreement with proposed values for the solution and the laboratory running average (Luguet et al., 2008; Nowell et al., 2008; 0.16082 ± 0.0006 1 S.D; N = 816). The 125 pg rhenium standard solution (Restd) yielded $^{185}Re/^{187}Re$ values of 0.59834 ± 0.00063 (1 S.D., N = 25), which agrees the laboratory average (0.59861 ± 0.0015 1 S.D; N = 720).

3.4 Results

3.4.1 Lithofacies

Based on the sedimentological features and x-radiograph imagery the core sediments are divided into 8 lithofacies (Fig. 3.3).

3.4.1.1 Lithofacies 1

The lower portion of the core between 11.1 to 9.2 m consists of brown clay with relatively thick banding clearly visible in the x-radiograph images that varies between <1 cm and ~5 cm in thickness (Fig. 3.3). The banding seen in the x-radiographs is often slightly disturbed through this lithofacies.

3.4.1.2 Lithofacies 2

Between 9.2 and 6.1 m the brown coloured clay becomes slightly lighter in colour and the laminations picked out by the x-radiograph become much finer, all consistently <1

cm thickness. At ~6.35 m a ~2 cm thick dark band is present in the x-radiographs, and can also be seen clearly in the core photograph as a cream-coloured layer and is identified as a carbonate layer (Fig. 3.3). There is a disturbance to the sequence, interrupting the varves, observed in the x-rays at 8.8 m.

3.4.1.3 Lithofacies 3

From the depths of 6.1 to 3.95 m the sediments are characterised by smooth, brown-grey coloured clays that appear homogenous and featureless in the core photo (Fig. 3.3). The x-radiograph image shows very fine (< 0.5 cm thickness) and regular laminations.

3.4.1.4 Lithofacies 4

Between 3.95 and 2.9 m the laminations become less clear and tend to be thicker and often not so complete and disturbed (Fig. 3.3). This lithofacies also records a shift in colour to blue-grey clay with some silty and sandy layers and some darker orange-brown bands. The darker orange-brown bands relate to dark bands in the x-radiograph image and may relate to iron and sulphide bands.

3.4.1.5 Lithofacies 5

Between the depths of 2.9 to 2.3 m the sediments remain a blue-grey coloured clay, but the laminations become more regular (less disturbed) and thinner (Fig. 3.3).

3.4.1.6 Lithofacies 6

Lithofacies 6 (2.3 – 0.9 m) is characterised by a colour change to brown clays (Fig. 3.3). Very clear, undisturbed, very fine laminations are visible in the core and x-rays up to 0.9 m, except for between 1.89 and 1.85 m and 1.73 and 1.59 m where laminations are absent.

3.4.1.7 Lithofacies 7

From 0.9 to 0.2 m the fine and undisturbed laminations disappear, with the sediments exhibiting a more homogeneous/massive structure (Fig. 3.3). Occasional laminations or bands are present, but are rare.

3.4.1.8 Lithofacies 8

Finally, between 0.2 and 0 m dark brown coloured sediments are recorded that exhibit fine laminations (Fig. 3.3).

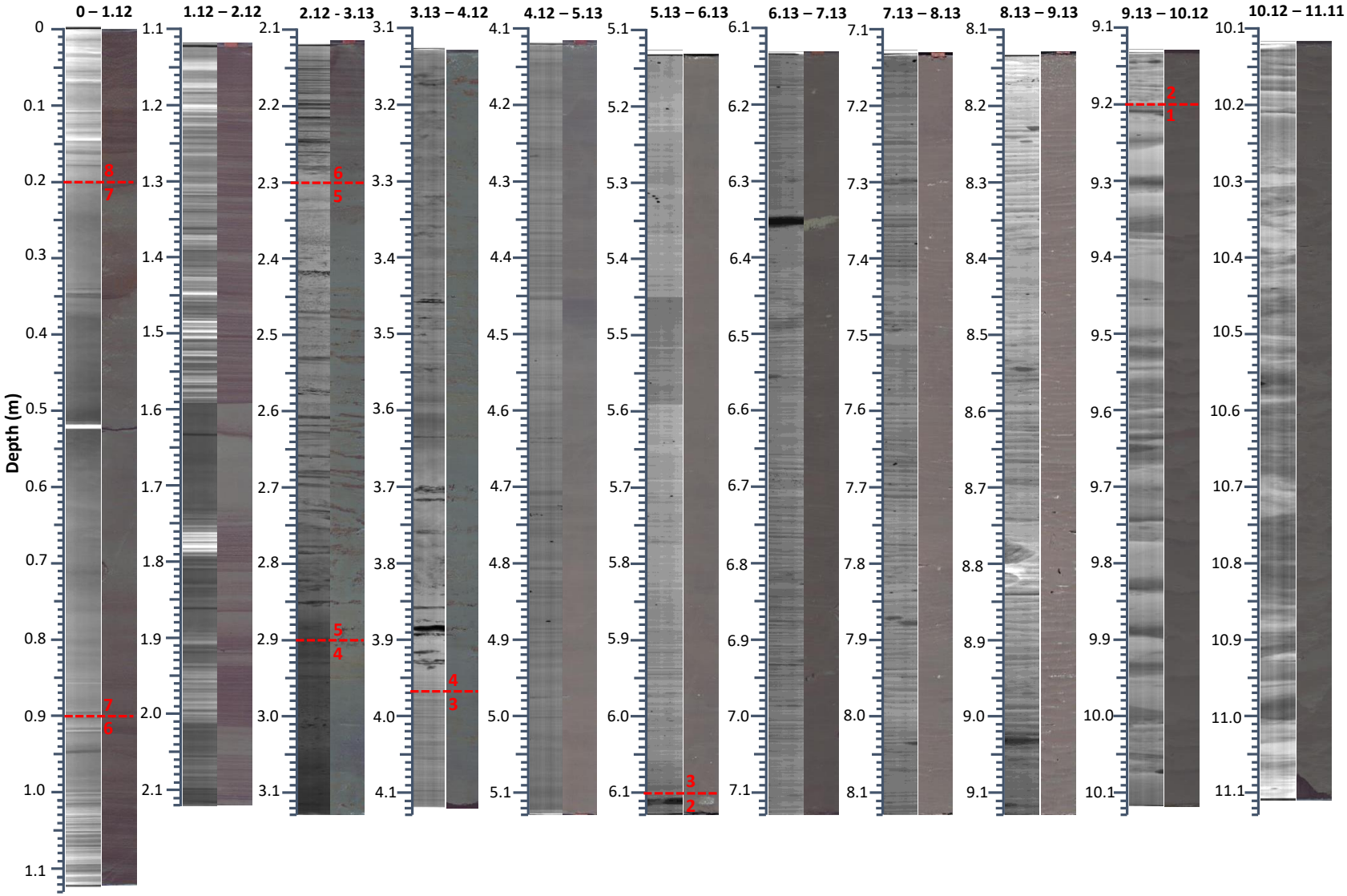

Figure 3.3: X-radiograph images and core images of P435/1-5 GC. Dotted lines represent lithofacies boundaries, see text for discussion

3.4.2 XRF

A whole suite of elemental data was collected through XRF analysis but here only elements of particular interest in relation to their use as a proxy to identify Baltic Sea stages are discussed (calcium - Ca, and the potassium/titanium – K/Ti ratio). These proxies are utilised due to their use to track terrigenous input, clay input, and carbonate content (Rothwell & Croudace, 2015).

In P435/1-5 GC Ca counts start off at 320,000 cps at 11.1 m and decrease to ~90,000 cps at ~9.2 m (lithofacies 1) where they stay until decreasing down to 16,000 cps at 6 m, with the exception of a spike (~500,000 cps) at 6.35 m representing the carbonate layer picked out in lithofacies 2 (Fig. 3.4; SM 3.1). This value remains very flat staying around 1700 to 1800 cps until 4.1 m where Ca counts abruptly increase to 350,000 cps in lithofacies 4 before decreasing back to 12,000 cps at 2.8 m and then decreasing gradually up to the surface of the core to 4000 cps, minus an excursion to 48,000 cps at 2.2 m.

The K/Ti ratio starts off ~2.4 at 11.1 m (Fig. 3.4; SM 3.1). The ratio then gradually decreases to ~1.8 until 7.2 m where the ratio increases to ~2.2 before continuing to decrease gradually to ~1.7 at 5.2 m through lithofacies 1 to 3. Between 5.2 – 4.5 m K/Ti rises to ~2.2 and then decreases back to ~1.7. Values then increase gradually until ~3.3 m where the K/Ti ratio increases quickly to a value of 2.9 at 3 m before decreasing quickly again to ~2.0 at 2.7 m. From 2.7 m through lithofacies 5 to 8, the K/Ti ratio gradually decreases (with a small increase to 1.8 at 0.6 m) to ~1.5 at the core top (present day).

3.4.3 TC, TIC, TOC

Total inorganic carbon (TIC) at the core bottom (11.1 m) is 3.59% (Fig. 3.4; SM 3.2a). The TIC fluctuates but overall decreases gradually down to 0.16% at 7.2 m. The TIC then peaks to 1.34% at 6.9 m before decreasing gradually down to 0 at 5.8 m where the levels remain across lithofacies 3 to 6 until the last analysed part of the core at 2 m.

Core P435/1-5 GC shows that from the core bottom (11.1 m) to 8.9 m total organic carbon (TOC) fluctuates between 0.52 and 0.08% with one larger peak of 2.48% at 9 m (Fig. 3.4; SM 3.2a, b). From 8.9 m TOC levels very gradually increase from 0.13 to 0.3% at 6 m. TOC continues to gradually increase to 0.4% and then to 0.60% at 2.9 m, with a small peak of 1.2% recorded at 3.9 m, and then begin to increase more abruptly to 1.5%. Finally, in lithofacies 6 the TOC levels quickly and dramatically increase to 13.2% at 2 m. Core 303600 TC then shows TOC levels decrease to 4% at 1.6 m, increase to 11.5% at 1.1 m,

decrease again to 4% between 0.8 and 0.3 m, and finally peak again to 12% at 0.1 m before decreasing to 6% at the core top. Overall TOC values are much higher in lithofacies 6 to 8.

3.4.4 Diatoms

Core P435/1-5 GC displays limited occurrences of diatoms (Fig. 3.4; SM 3.3). From 11.1 to 3.8 m diatoms are absent. Fresh water diatoms are recorded at depths of 3.705 and 3.585 m. No diatoms are found between the depths of 3.5 and 3.2 m. Freshwater diatoms are recorded between 3.1 and 2.1 m. The occurrence of brackish diatoms is then noted at 1.995 m.

3.4.5 BIT index

In core P435/1-5 GC the BIT index values begin at 0.7 at 11.1 m and remain approximately constant except for a few fluctuations until 9.7 m where the values then decrease to 0.41 at 8.1 m before a slight increase to 0.57 at 7.2 m, and then continuing to decrease to 0.3 at 5.8 m (Fig. 3.4; SM 3.4a, b). A small peak of 0.52 occurs at 5.1 m before a shallow increase between 5.0 and 3.9 m from 0.34 to 0.39. The BIT index value then abruptly drops in lithofacies 4 to 0.14 at 3.9 m before rapidly increasing up to 0.6 at 3.7 m and decreasing back down to 0.38 at 3.6 m. Values then decrease down to 0.22 at 3.1 m before rapidly increasing up to 0.83 at 2.9 m and decreasing rapidly back down to 0.03 at 2 m. Core 303600 TC shows BIT index values then remain between 0.07 and 0.01 from 2 m to the core top.

3.4.6 Re-Os

3.4.5.1 Surface sediment samples

The Re-Os surface sediment data is presented in Figure 3.2 and Table 3.2. For the surface samples the Re and total Os abundances vary between 0.81 and 4.20 ppb, and 16 and 167 ppt, respectively. The $^{187}Os/^{188}Os$ values range between 0.93 and 2.25 (Fig. 3.2; Table 3.2). The $^{187}Os/^{188}Os$ values in the Skagerrak and off western Norway (samples 1 – 3; Fig. 3.2) are low ~1. Moving through the Kattegat into the southwest of the Baltic Sea values increase from ~1.25 to 1.67 (samples 4 – 9; Fig. 3.2). In the mid Baltic Sea and northern Baltic Sea values increase to 1.88 and 1.95 and then further to 2.10 and 2.24, respectively (samples P435/1-5 GC – 10 and 11 – 12, respectively; Fig. 3.2).

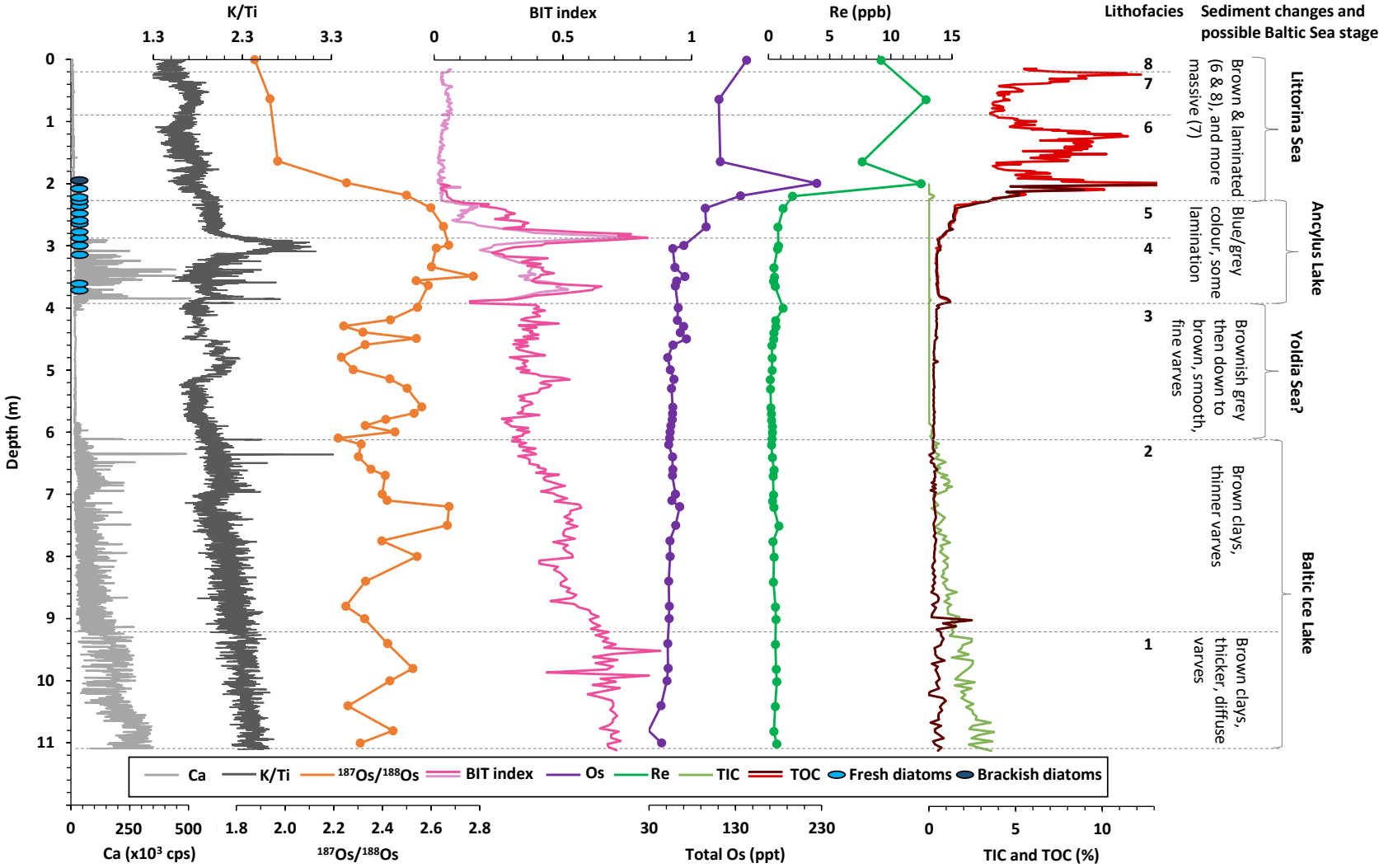

Figure 3.4: Calcium (cps), fresh and brackish diatoms, K/Ti, $^{187}Os/^{188}Os$, BIT index, total Os (ppt), Re (ppb), TIC (%) and TOC (%) data for core P435/1-5 GC against depth. Lighter coloured lines for BIT index and TOC represent data from trigger core 303600. Dashed lines show changes in the visible properties of the core and are divided into eight lithofacies.

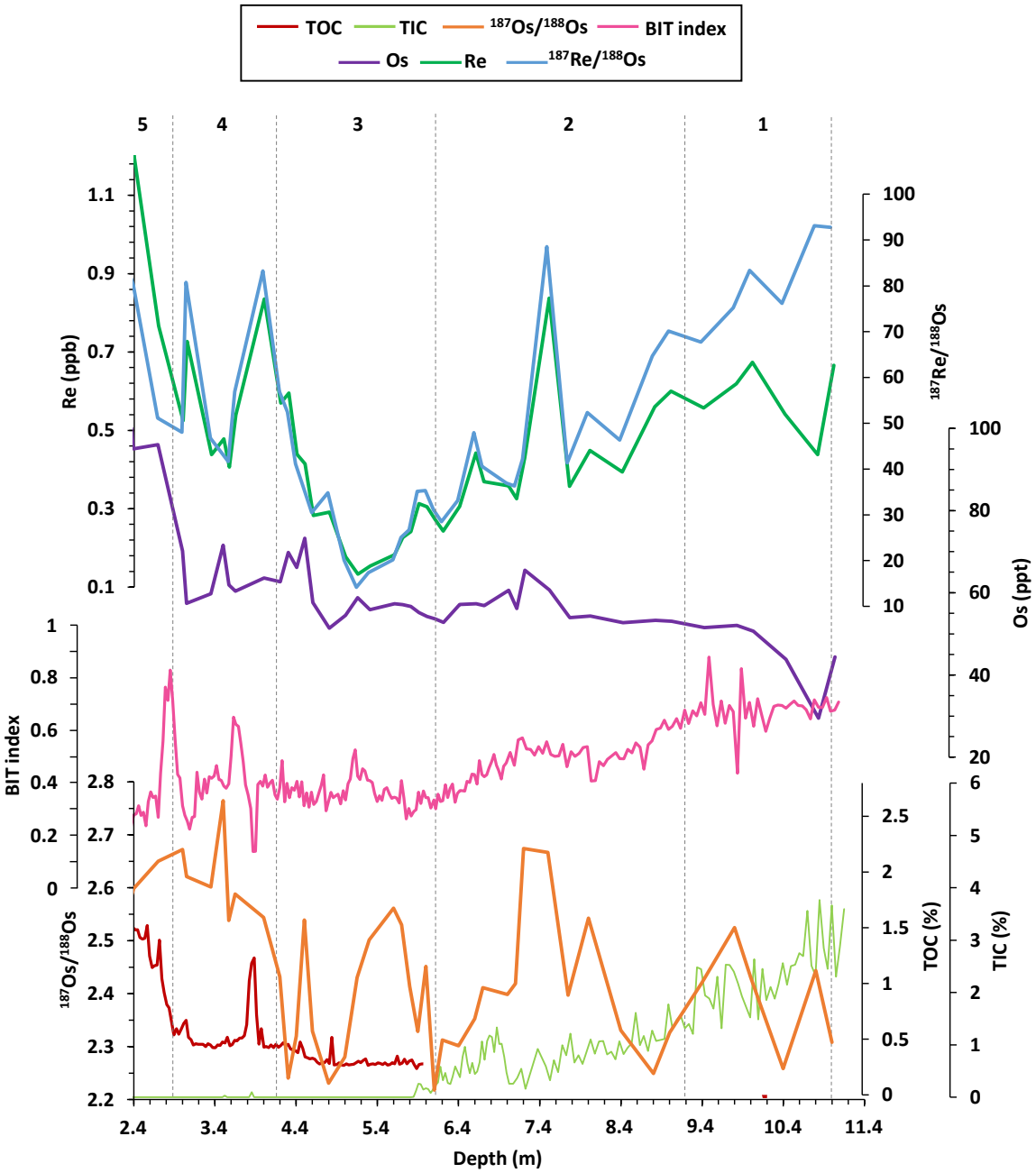

Figure 3.5: TOC (%), TIC (%), $^{187}Os/^{188}Os$, BIT index, Os (ppt), Re (ppb) and $^{187}Re/^{188}Os$ data for the depths of 2.4 m to 11.1 m in core P435/1-5 GC to show the finer details in trends recorded between these depths. Dashed lines show the changes in lithofacies, see text for discussion.

3.4.5.2 Core sediment samples

The Re-Os core data is presented in Figures 3.4, 3.5 and Table 3.2. The Re and Os abundances vary between 0.13 and 12.9 ppb and 44 and 224 ppt, respectively within the core. Total Os abundances remain low and constant in lithofacies 1 and 2 at ~55 ppt up to ~4.6 m where abundances rise slightly to ~65 ppt until 3 m in lithofacies 4 where abundances rise to a peak of 224 ppt at 2 m in lithofacies 6 then decrease to between 65 and 143 ppt to the core top (Figs. 3.4, 3.5). The Re abundances are relatively stable across lithofacies 1 to 5 between 11 and 2.4 m averaging around 0.5 ppb (although a slight decreasing trend of 0.7 to 0.1 ppb is observed between 11 and 5.1 m), before rising rapidly to an average of ~11 ppb in lithofacies 6 to 8 between 2 m and the core top (Fig. 3.4, 3.5). The $^{187}Os/^{188}Os$ values range between 1.88 and 2.76. In lithofacies 1 the $^{187}Os/^{188}Os$ values start at 2.31 at 11 m which increases to 2.44 before decreasing to 2.26 at 10.4 m. The $^{187}Os/^{188}Os$ then increases to 2.53 at 9.8 m and declines to 2.25 at 8.8 m. The $^{187}Os/^{188}Os$ values then rise (with a brief dip at 7.75 m) to 2.67 at 7.2 m before abruptly decreasing to 2.42 and then gradually decreasing to 2.22 at 6.1 m. In lithofacies 3 another peak in $^{187}Os/^{188}Os$ values occurs between 6.1 and 4.8 m with values rising to 2.56 and dropping back to 2.32. A very abrupt peak in $^{187}Os/^{188}Os$ values up to 2.54 and back down occurs between 4.8 and 4.3 m. At 4.3 m the $^{187}Os/^{188}Os$ increase to ~2.6 and remain radiogenic between 4.0 and 2.2 m in lithofacies 4 and 5, with a peak of 2.77 at 3.5 m. The $^{187}Os/^{188}Os$ values then decrease sharply to 1.97 in lithofacies 6 from 2.2 to 1.65 m and then gradually decrease to the lowest $^{187}Os/^{188}Os$ value recorded of 1.88 at the surface (2 cm) of the core.

3.5 Discussion

3.5.1 Defining the $^{187}Os/^{188}Os$ of the present-day Baltic Sea basin

This study utilises the understanding of the present-day environment and sediment geochemistry in the Baltic Sea to investigate the evolution of the Baltic Sea Basin through the Late Quaternary and Holocene. Specifically, focusing on the connection and isolation of the Baltic basin from the North Sea and tracking the changes between sea stages from the Baltic Ice Lake to the Yoldia Sea, the Ancylus Lake and into the Littorina Sea. In addition to sediment characteristics and geochemistry (lithology, total organic carbon, XRF), this study also uses biomarkers (BIT index), and sediment osmium isotope ($^{187}Os/^{188}Os$) analysis to infer the water $^{187}Os/^{188}Os$ composition of the Baltic Basin (Ravizza & Turekian, 1989; Cohen et al., 1999) and to investigate basin evolution. As such it is critical to understand the present-day $^{187}Os/^{188}Os$ signature of the Baltic and North Sea to assess the potential of $^{187}Os/^{188}Os$ to track the different sea stages through

exchanges between the two. The $^{187}Os/^{188}Os$ proxy allows the differentiation between long- and short-term changes in the environment due to the relatively short residence time of osmium in the oceans of 1 to 50 kyrs, with some studies noting a residence time of < 10 kyrs (Levasseur et al., 1999; Oxburgh, 1998, 2001; Peucker-Ehrenbrink & Ravizza, 2012; Rooney et al., 2016; Sharma et al., 1997). The $^{187}Os/^{188}Os$ signature of present-day oxic seawater has an average value of 1.060 ± 0.005 and is relatively stable across the global oceans (Burton et al., 1999; Cohen, 2004; Levasseur, 1998; Peucker-Ehrenbrink & Ravizza, 2000; Rooney et al., 2016; Sharma et al., 1997). Furthermore, spatial and temporal variations in $^{187}Os/^{188}Os$ can exist that reflect local influences in the ocean chemistry due to variations in terrestrial sources, especially in more isolated/restricted seawater basins (e.g., Burton et al., 2010; Chen et al., 2009; Gannoun & Burton, 2014; Paquay & Ravizza, 2012; Peucker-Ehrenbrink & Ravizza, 2012; Rooney et al., 2016). For example, significant variation from the global ocean $^{187}Os/^{188}Os$ signature is recorded in a core from Disko Bugt (west of Greenland) due to influx of glacially eroded material from the Precambrian terranes of west Greenland during glacial advance ($^{187}Os/^{188}Os$ values 2.2 to 2.4; Rooney et al., 2016). The $^{187}Os/^{188}Os$ system has also been applied to the Mediterranean Sea across the Messinian Salinity Crisis (Kuroda et al., 2016). The data show that before the event $^{187}Os/^{188}Os$ values were similar to open marine values at the time, whilst $^{187}Os/^{188}Os$ values of evaporates during the crisis record unradiogenic values (~0.8 to 0.2), attributed to restricted influence of the North Atlantic and/or unradiogenic material resulting from weathering of ultramafic ophiolites common around the Mediterranean (Kuroda et al., 2016). The surrounding geology and variations in flux of material, as well as marine influence is therefore important in understanding the $^{187}Os/^{188}Os$ of sediments through a core section. The Baltic Sea Basin is an example of where the $^{187}Os/^{188}Os$ of the surrounding geologies differs significantly to that of an open marine signal and is discussed below.

The geology of the Baltic Sea catchment is dominated by the Precambrian crystalline basement (Baltic Shield; Fig. 3.1) comprising rocks and runoff with a highly radiogenic $^{187}Os/^{188}Os$ signature of ~3.6 to 7.9 (Peucker-Ehrenbrink & Ravizza, 1996). Freshwater runoff from the Baltic Shield would therefore potentially deliver a radiogenic signal into the Baltic Basin, and with a potentially even greater radiogenic signature due to preferential weathering of felsic matrices that possess a more radiogenic $^{187}Os/^{188}Os$ composition (Bernhard Peucker-Ehrenbrink & Blum, 1998). This is demonstrated by present-day sediment and Mn nodule $^{187}Os/^{188}Os$ compositions of the Baltic Basin (Fig. 3.2; this study; Peucker-Ehrenbrink & Ravizza, 1996).

The present-day Baltic Sea $^{187}Os/^{188}Os$ compositions can be determined from modern surface sediment samples. At present the Baltic Sea possesses $^{187}Os/^{188}Os$ compositions ranging from 1.3 in Kattegat Bay through to 2.6 in the Gulf of Bothnia (N = 4 Mn nodules; Peucker-Ehrenbrink & Ravizza, 1996, N = 10 surface sediments; this study; Fig. 3.2). The $^{187}Os/^{188}Os$ compositions for the Baltic Sea in general are significantly more radiogenic than those from the North Sea and Skagerrak (~0.9 to 1.0, N = 3 surface sediments; this study; Fig. 3.2). The significant increase in the $^{187}Os/^{188}Os$ composition moving from the Skagerrak through the Kattegat into the Baltic Sea from the narrow straits around Denmark to the south-central Baltic Sea is due, in part, to decreased marine influence from the North Sea. This is shown by the decrease in salinity from normal marine values in the North Sea (30 – 35 PSU) to 30 to 15 PSU through the Skagerrak and Kattegat, 10 PSU in the south Baltic Sea, 8 to 6 PSU in the Central Baltic, and then almost fresh water at 0.5 PSU in the outer Gulf of Finland and Gulf of Bothnia (Fig. 3.2; Ducrotoy & Elliott, 2008; Jiang et al., 1997). The decreasing salinity indicates an increased influence of freshwater runoff from the land, and hence an increased supply of terrestrially sourced radiogenic material from the Precambrian Baltic Shield which possesses $^{187}Os/^{188}Os$ between 3.6 and 7.9 (Peucker-Ehrenbrink & Ravizza, 1996). The link between $^{187}Os/^{188}Os$ and freshwater versus seawater input can be clearly seen when plotted against salinity (Fig. 3.6). The $^{187}Os/^{188}Os$ values show a moderate increase with a decrease in salinity between the North Sea and the Danish Straits. From the Danish Straits the $^{187}Os/^{188}Os$ values become progressively more radiogenic through the central and northern regions of the Baltic Sea, corresponding to the dramatic reduction in marine influence through the narrow Danish Straits. The new $^{187}Os/^{188}Os$ data presented here show a clear link between a more radiogenic $^{187}Os/^{188}Os$ signature preserved in surface sediments and increased freshwater/terrestrial flux. Based on this it is concluded that sediment $^{187}Os/^{188}Os$ compositions have the potential to identify periods of isolation from an ocean signal (i.e., from the North Sea) driven by the relative increase in the flux of terrestrially eroded material into the basin and reduced dilution by marine incursion. As such, the present-day $^{187}Os/^{188}Os$ signature contrast between the North Sea and the Baltic Sea implies that periods of Baltic Sea isolation (e.g., during the Baltic Ice Lake), would be characterised by a more radiogenic $^{187}Os/^{188}Os$ signature. This would be similar to the present-day $^{187}Os/^{188}Os$ composition of the Baltic Sea extremities, and thus starkly different to that of the Late Pleistocene and Holocene global ocean (ca. 1; Paquay & Ravizza, 2012; Rooney et al., 2016).

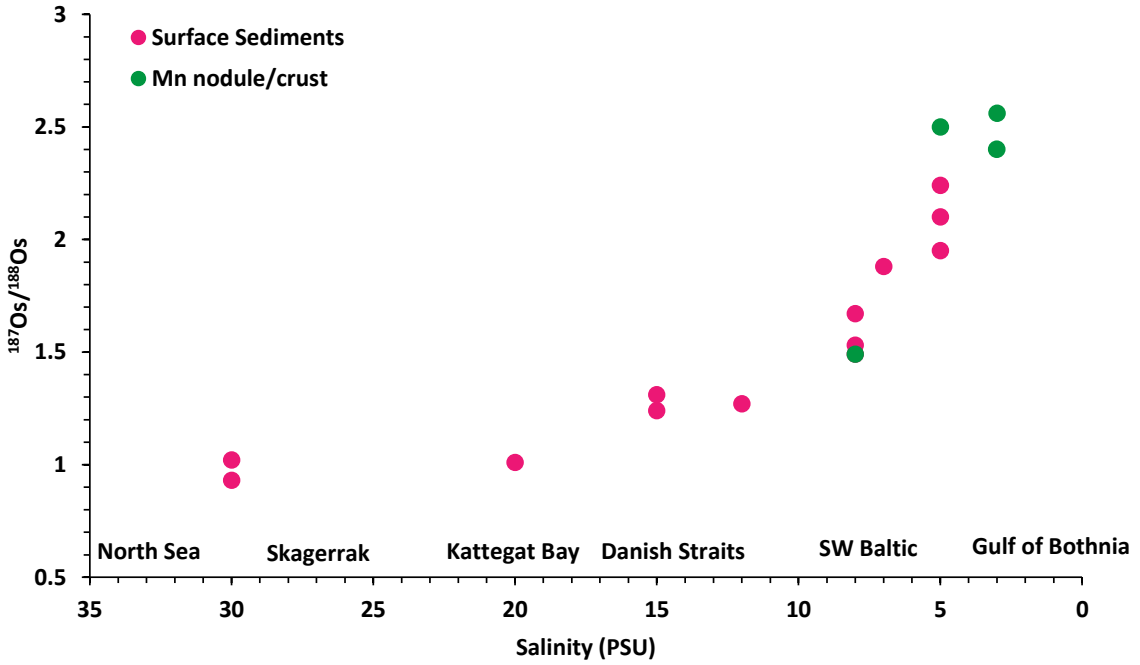

Figure 3.6: $^{187}Os/^{188}Os$ for the surface samples analysed in this study and Mn nodules (Peucker-Ehrenbrink & Ravizza, 1996) plotted against salinity (PSU; Sjöqvist et al., 2015) moving through the North Sea, Skagerrak, Kattegat Bay, through the Danish Straits into the Baltic Sea and moving northwards.

3.5.2 A record of the Baltic Sea stages

In Chapter 4 it is shown that the use of osmium isotopes coupled with other geochemical techniques can track the drainage of the Baltic Ice Lake into the Skagerrak through an influx of radiogenic waters. Below, the $^{187}Os/^{188}Os$ proxy alongside XRF, sedimentology and BIT index is discussed with respect to tracking the different sea stages recorded in the central Baltic.

As with many other cores from the Baltic region, the core utilised in this study lacks any datable material (this study; Hyttinen et al., 2014; Kortekaas, 2007). Thus, any discussion of the ages of sediments in core P435/1-5 GC below are based solely on correlation of changes in sedimentology (which, basin wide have been attributed to the different stages) and any accompanying geochemical changes ($^{187}Os/^{188}Os$, BIT index and XRF) further linking the sediments to Baltic Sea stages. Across the Baltic Sea Basin changes in the sedimentology of cores and certain geochemical characteristics are linked to the different Baltic Sea stages. The Baltic Ice Lake is distinguished by characteristic deposits of glacio-lacustrine clays of a brown colour, showing varves, and these sediments tend to be Ca rich and record deposition between ~16 to 11.7 cal ka BP (Moros et al., 2002; Rosentau et al., 2017). The transition into the Yoldia Sea stage is represented by a change to more brown-grey clays with thinner laminations and records deposition between ~11.7 and 10.7 cal ka BP. The transition into the Ancylus Lake (~10.7 and 9.7 cal ka BP) is characterised by a clear change in the colour of sediments to a distinctive blue/grey colour with some

laminations, representing lacustrine deposits (Kögler & Larsen, 1979; Rosentau et al., 2017). Finally, during the Litorrina Sea sediments return to olive-grey to brown colour with abundant laminations (Andrén et al., 2000; Moros et al., 2002; Rosentau et al., 2017). Although no absolute age constraints can be placed on the sediments of core P435/1-5 GC, as discussed below the transitions into the Ancylus Lake and the Littorina Sea stages are shown clearly by the data. However, marking the end of the Baltic Ice Lake and the Yoldia Sea stages, is not definitive, and thus arguments are presented regarding the possible positions of the stage transitions.

3.5.2.1 Baltic Ice Lake (16 – 11.7 cal ka BP) and Yoldia Sea (11.7 – 10.7 cal ka BP)

The freshwater Baltic Ice Lake began to form ~16 cal ka BP due to a damming effect as isostatic rebound lifted the channels through the Danish Straits above sea level (Andrén et al., 2011; Björck, 1995; Rosentau et al., 2017). At ~13 cal ka BP retreat of the FIS allowed the first drainage of the lake through channels in south-central Sweden (Andrén et al., 2011; Björck, 1995; Fig. 3.1). During the Younger Dryas (~12.8 cal ka BP) it is thought that glacial advance re-blocked the south-central Swedish channel. Due to the constriction of the Swedish channel, the Baltic Ice Lake level rose once more before a final catastrophic, rapid (1 – 2 years) drainage through south-central Sweden coincident with the end of the Younger Dryas ~11.7 cal ka BP, lowering the lake level by 25 m (Andrén et al., 2008, 2011; Björck, 1995; Jakobsson et al., 2007; Rosentau et al., 2017). After the large final drainage, small, short-lived, influxes of marine waters were able to flow back into the Baltic Basin through the now narrowing Swedish channels. This marks the next stage in the Baltic Basin history, the Yoldia Sea (~11.7 – 10.7 cal ka BP; Andrén et al., 2002, 2011; Björck, 1995; Rosentau et al., 2017). The Yoldia Sea is a stage that is challenging to define in Baltic Sea sediment cores, as the marine incursions are relatively short-lived and likely lead to rather moderate change in basin salinity, and hence is difficult to detect and accurately date, especially in areas not directly proximal to the south-central Sweden channels (Andrén et al., 2008; Kortekaas, 2007; Rosentau et al., 2017). The geochemical data should therefore show a freshwater signal during the Baltic Ice Lake stage, and potentially a brief change to a more marine signature representing the Yoldia Sea stage. During the Baltic Ice Lake, characteristic deposits of glacio-lacustrine clays of a brown colour, and showing varves, are found in numerous cores across the Baltic Basin (Rosentau et al., 2017), including core P435/1-5 GC. A trend to more brown-grey coloured clays with thinner laminations are then associated with the end of the Baltic Ice Lake stage and the start of the Yoldia Sea stage (Rosentau et al., 2017), although the

change in sediment colour is not directly linked to the incursion of saline marine waters (Andrén et al., 2008).

Typical Baltic Ice Lake sediments are seen in core P435/1-5 GC in lithofacies 1 and 2, from the deepest part of the core (11.1 m) to ~6.1 m (Figs. 3.3, 3.4). During this time, the BIT index values are at their highest for the whole core, but overall, gradually decreasing from 0.7 to 0.3 (11 – 6 m) with peaks of 0.8 (9.9 m) and 0.9 (9.5 m; Fig. 3.4). The BIT index varies between 0 and 1, with 0 representing an entirely marine end member, and 1 representing a terrestrial/soil organic matter end member (Kim et al., 2006; Wang et al., 2013; Warden et al., 2018). This would therefore imply a decreasing terrestrial flux over time from 11 to 6 m. During this same period, $^{187}Os/^{188}Os$ values are radiogenic but quite variable, ranging between 2.2 and 2.7 (Fig. 3.4). The high $^{187}Os/^{188}Os$ values in general suggest a predominantly continental source, originating from old geologies such as the Baltic Shield. Trends towards lower $^{187}Os/^{188}Os$ values as seen at depths of ~10.5, 9.0 and 6.5 m in core P435/1-5 GC could occur for several reasons. Less radiogenic $^{187}Os/^{188}Os$ compositions can be as a result of input of more mafic, mantle or hydrothermal sources ($^{187}Os/^{188}Os$ = ~0.12; Peucker-Ehrenbrink & Ravizza, 2000), greater input from the sedimentary platforms to the south and south-west of the Baltic Basin ($^{187}Os/^{188}Os$ runoff = 1 – 1.3; Peucker-Ehrenbrink & Ravizza, 1996), or also as a result of increased marine influence ($^{187}Os/^{188}Os$ = ~1.06; Burton et al., 1999; Cohen, 2004; Levasseur, 1998; Peucker-Ehrenbrink & Ravizza, 2000; Rooney et al., 2016; Sharma et al., 1997). Mafic/mantle rock types and hydrothermal deposits are not dominant in the Baltic Basin catchment (Fig. 3.1; Björck, 1995; Peucker-Ehrenbrink & Ravizza, 1996; Rosentau et al., 2017) and, if this section does represent the Baltic Ice Lake, a marine influence has not previously been noted over this time period (Andrén et al., 2011; Björck, 1995; Rosentau et al., 2017). Variability in $^{187}Os/^{188}Os$ between 11 and 6.1 m therefore is most likely caused by changes in flux of material from the continent, perhaps increased weathering and delivery of material derived from a particularly radiogenic or less radiogenic geology (i.e., Baltic Shield vs. European Sedimentary Platform), and/or ice calving events bringing in increased amounts of dissolved materials closer to the core site. The range in $^{187}Os/^{188}Os$ values between 2.2 and 2.7 are also very similar to the modern end member values recorded in surface sediments and Mn-nodules in the Gulf of Bothnia and Gulf of Finland (Fig. 3.2), which are representative of virtually freshwater conditions (more similar to the Ice Lake conditions) and hence provides further evidence the variability in $^{187}Os/^{188}Os$ is less likely to be from a marine source.

Between 11 and 8 m the BIT index and $^{187}Os/^{188}Os$ appear independent of one another, but from 8 m onwards the two proxies begin to follow the same trend of peaks and troughs (Fig. 3.4). This provides further evidence that from 8 m onwards the $^{187}Os/^{188}Os$ ratio is capable of recording terrestrial versus marine signals, and that other factors could be contributing to the initial decrease in the BIT index, not necessarily increased marine influence. The mismatch in the deeper parts of the core could relate to complicated ice and water dynamics occurring during the Baltic Ice Lake. It has been noted that the terrestrial related bGDGTs associated with a higher BIT index are able to be produced in situ in lake environments as well as being derived from terrestrial organic matter (Warden et al., 2018 and references therein), which could explain the higher BIT index and mismatch to $^{187}Os/^{188}Os$ in the deepest part of the core. It has also been noted that occurrences of the marine type GDGT (crenarchaeol) have been found in river water (Kim et al., 2006), which could also contribute to fluctuations towards lower BIT index values and may represent river water influxes as the retreat of the FIS frees up more river valleys and channels.

The abundance of calcium (cps) is also high over the interval of 11 to 6.1 m, and the TIC levels also follow the calcium signal, implying it is a carbonate source (Fig. 3.4). Higher TIC and calcium in the form of carbonate is common in sediments of the Baltic Ice Lake in cores around the Baltic Sea and generally records higher TIC values (Bennike & Jensen, 1995; Moros et al., 2002).

A trend to more Yoldia Sea style sediments (brown-grey clay) is seen in lithofacies 3 between depths of ~6.1 to 3.95 m in core P435/1-5 GC (Fig. 3.3). The Yoldia Sea records a freshwater stage, followed by a marine incursion, and then back to a freshwater stage (Andrén et al., 2002). The marine incursions are thought to be quite ephemeral and small-scale, lasting only ~100 to 350 years (Andrén et al., 2002; Björck, 1995; Rosentau et al., 2017). Although relatively weak, the marine inflows have been shown to have reached the north-western Baltic and the eastern Gotland Basin, close to the core P435/1-5 GC site (Andrén et al., 2008). Between the depths of 6.1 and 3.95 m there are two lows in $^{187}Os/^{188}Os$ down to a ratio of 2.2 (Figs. 3.4, 3.5). These lower values could indicate an increased marine influence, although still relatively weak as $^{187}Os/^{188}Os$ values do not reach present surface sediment values of 1.88 where there is a continued marine influence. The $^{187}Os/^{188}Os$ values of 2.2 however are very similar to the lows recorded in the deeper sections of the core, attributed to less flux of radiogenic material from the continent, or a change in dominant source to a less radiogenic area. This therefore could not be ruled out

as the case for the low values within lithofacies 3 (which are tentatively interpreted as the Yoldia Sea sediments). The BIT index between 6 and 3.95 m is relatively constant between 0.3 and 0.4, with a peak of 0.5 at ~5.15 m. Whilst this does indicate a mixture of marine and terrestrial sources, there is no distinctive 'event' that could be interpreted as a clear, isolated period of marine incursion. Total Os abundances are also relatively stable between 11 to 4.25 m (~50 ppt), interestingly however, the Re abundance (and therefore also the $^{187}Re/^{188}Os$ ratio) gradually decreases (Re ~0.6 to 0.1 ppb; $^{187}Re/^{188}Os$ ~93 to 15), reaching a low at 5.15 m, before beginning to increase at 4.6 m (Fig. 3.5). The reason for the latter is not clear, but the decrease in Re abundance also correlates with the start of the decrease in the $^{187}Os/^{188}Os$, and the start of the decrease in the BIT index from 0.5 to 0.3. The depth of 5.15 m is also coincident with the start of a small peak in K/Ti, due to a distinct decrease in Ti (cps) and small peak in K (cps; SM 3.1). This could represent a decrease in terrestrially sourced material and a small peak in K could tentatively be linked to a more marine source due to potassium salts (Rothwell & Croudace, 2015). The peak in K/Ti also overlaps the same depth interval (5.15 to 4.5 m) as the low in $^{187}Os/^{188}Os$. During this time there is also a distinct low in Ca cps.

Based on the evidence presented in this study, the coincidence of a decrease in Re, $^{187}Os/^{188}Os$, BIT index, a peak in K/Ti, and a reduction in Ca all indicate a change in conditions, potentially associated with increased marine influence, hence the marine incursion phase of the Yoldia Sea is tentatively placed between the depths of 5.15 to 4.5 m. However, as mentioned previously, due to the short and weak nature of the marine inflow it is not possible to definitively detect such ephemeral marine incursions. Identification of the Yoldia Sea stage is further complicated by the nature of variable marine incursions through this stage - the marine input is between two Yoldia Sea freshwater stages. Based on the proxies used here, it would be very difficult/impossible to differentiate between the freshwater Yoldia Sea stages and the Baltic Ice Lake phase. Therefore, the changes mentioned above linked to the marine incursion may be purely coincidental. Further, no diatoms were recorded over the suggested interval of the Baltic Ice Lake and Yoldia Sea in core P435/1-5 GC, which may also have helped distinguish between a freshwater and brackish water setting (Fig. 3.4). It has been noted previously that diatoms are rare during these intervals with dissolution and diagenesis likely affecting preservation (e.g., Andrén et al., 2011). Further, the marine incursion during the Younger Dryas may have been too weak and short lived to permit brackish-marine diatoms.

It may be likely that during the Baltic Ice Lake stage and transition through the Yoldia Sea there was too much variation in amount of material being washed into the Baltic Basin from the radiogenic Baltic Shield catchment meaning that any clear signal of the marine incursions of the Yoldia Sea, especially in the $^{187}Os/^{188}Os$ signal, is diluted and masked. During this time there would have been significant meltwater input from the FIS eroding material and carrying glacially eroded rock flour, changing the amount and source of material from the catchment which could explain the larger variability in the $^{187}Os/^{188}Os$ signal through 11.1 to ~4 m, as runoff from the Precambrian shield possesses a wide range of variability in $^{187}Os/^{188}Os$ (3.6 to 7.9; Peucker-Ehrenbrink & Ravizza, 1996).

3.5.2.2 Ancylus Lake (10.7 – 9.7 cal ka BP)

Due to isostatic uplift the channels over south central Sweden closed, allowing the development of the freshwater Ancylus Lake (Andrén et al., 2002, 2011; Berglund et al., 2005; Björck, 1995; Rosentau et al., 2017). Sediments of this stage have a distinctive blue/grey colour with some laminations representing lacustrine deposits (Kögler & Larsen, 1979; Rosentau et al., 2017). Sediments of this nature are seen in lithofacies 4 and 5 between 3.95 and 2.3 m in P435/1-5 GC.

Between 4.25 and 3.6 m the $^{187}Os/^{188}Os$ values increase from 2.2 to 2.6 (Fig. 3.4). The $^{187}Os/^{188}Os$ values peak at 2.8 then remain between 2.6 and 2.7 until 2.4 m. These values are more radiogenic than the northernmost present-day Baltic Sea sediment sample values (2.1 – 2.3), representing the most freshwater influenced values of the present Baltic Sea. The $^{187}Os/^{188}Os$ values of 2.6 to 2.8 therefore would represent a much lower marine influence than the present-day, with more influence of run-off and meltwater from the FIS moving over the Baltic Shield. Coincident with the radiogenic $^{187}Os/^{188}Os$ values, the BIT index is generally higher and shows peaks of 0.6 and 0.8 at 3.6 m and 2.9 m, respectively. These BIT values indicate a greater flux of terrestrial/freshwater material and a more continental input (Kim et al., 2006; Wang et al., 2013; Warden et al., 2018). A peak in the K/Ti ratio also occurs between 3.2 and 2.8 m, which roughly matches lithofacies 4 where the laminations/varves become less frequent and more disturbed. The main peak is due to a fall in Ti (cps; SM 3.1). The increase in Ca (cps) between 4 and 3 m over lithofacies 4 is a due to the presence of gypsum, not related to carbonate content as the TIC values remain level around 0% over this period.

Freshwater diatoms are also recorded at the start of lithofacies 4 at 3.7 and 3.6 m. Freshwater diatoms are also found at various intervals between 3.1 and 2.1 m (Fig. 3.4), indicating that these depths correspond to a more freshwater environment. However, freshwater diatoms (or brackish diatoms), are not found during the 4 to 3 m interval where the presence of gypsum is found (Fig. 3.4). It is not clear as to the cause of this gypsum deposition, but perhaps this altered the conditions enough to prevent diatom growth or to not allow the preservation of diatoms during this time.

Geochemical evidence between ~4 and 2.3 m therefore indicates a freshwater Baltic Basin phase, the Ancylus Lake. Further, the use of $^{187}Os/^{188}Os$ and the BIT index together provide a strong indicator of freshwater conditions in the Baltic Basin at this time with an increased flux of material from the surrounding landmasses and no dilution by marine waters.

3.5.2.3 Littorina Sea (9.7 – present cal ka BP)

Due to the combination of glacio-isostatic and glacial-eustatic changes, areas through the Danish Straits such as Öresund and the Great Belt began to lower, enlarging the channels between the Baltic and the North Sea and allowing the Ancylus Lake to drain, but also permitting the influx of marine waters into the Baltic Basin forming the Littorina Sea stage (Andrén et al., 2011; Rosentau et al., 2017). The timing of this change is, however, disputed and time-transgressive (Bennike et al., 2021). The Littorina Sea represents a change after the drainage of the Ancylus Lake to brackish conditions, as saline marine waters were able to flow freely into the Baltic Basin through the Danish Straits as the FIS retreated and finally disappeared (Andrén et al., 2011; Berglund et al., 2005; Björck, 1995; Rosentau et al., 2017). The stage is represented in cores across the Baltic Basin by olive-grey to brown, laminated sediments (Moros et al., 2002; Rosentau et al., 2017) that are also observed in P435/1-5 GC in lithofacies 6 to 8 from ~2.3 m to the core top.

From ~2.8 m the $^{187}Os/^{188}Os$ values abruptly decrease from 2.60 to 1.97 and then gradually to 1.88 at the core top for the present-day value (Fig. 3.4). This indicates a decrease in radiogenic, terrestrially sourced material from freshwater flux and an increased influence from open marine waters, bringing $^{187}Os/^{188}Os$ values down to 1.88 and in line with other surface samples taken from the present-day around the Baltic Sea (Fig. 3.2). Such an abrupt decline in $^{187}Os/^{188}Os$ suggests marine waters were able to enter and circulate into the Baltic Basin rapidly after the end of the Ancylus Lake stage. The BIT index measurements between 2.8 to 2.0 m decline from 0.83 to their lowest at 0.03

and then remain at approximately this level until the core top. A value of 0 for the BIT index represents a marine end member (Kim et al., 2006; Wang et al., 2013; Warden et al., 2018). Thus, the abrupt decline and then levelling in the BIT index in P435/1-5 GC represents increased and continuous influence of marine waters. A sudden decrease in the BIT index between the Ancylus Lake and Littorina Sea stages has also been noted in sedimentary successions from the Arkona and Gotland Basins (Warden et al., 2018). Contemporaneously, TOC levels begin to increase significantly for the first time over the length of the core at 2.8 m, and then much more rapidly at 2.4 m rising from < 2% to 13%, after this point TOC values fluctuate but remain considerably higher in lithofacies 6 to 8 (average ~ 6%) compared to the previous lithofacies (average ~ 0.5%). This is likely a result of increased productivity due to general climate amelioration, and a reduction of meltwater influx diluting the organic material produced from in situ productivity. Increasing TOC values are found from sediments of the Littorina Sea stage across many cores around the Baltic Sea (Andrén et al., 2000; Kögler & Larsen, 1979; Moros et al., 2002). Total Os and Re values raise to their highest levels coincident with the rise in TOC and decrease in $^{187}Os/^{188}Os$ and BIT index, to 224 ppt and 12 ppb, respectively (Fig. 3.4). Rhenium and osmium are organophilic and so are concentrated into organic-rich sediments during deposition from seawater, so the increasing abundance of Re and Os could relate to chelation by the organic matter associated with increased salinity related to the marine incursion into the basin (Cohen et al., 1999; Cohen, 2004; Ravizza & Turekian, 1989; Selby et al., 2013; Selby & Creaser, 2003). The K/Ti levels reach their lowest, decreasing to 0.24, representing a fall in both Ti and K hinting at a decrease in terrestrially sourced material as there is increased mixing with a more marine signal (Rothwell & Croudace, 2015). Finally, at the transition into lithofacies 6 (~2 m) the first occurrence of brackish diatoms are recorded. Diatom analysis was not undertaken from 2 m to the surface, but abundant brackish to marine diatoms are found throughout the Baltic Sea in core sediments deposited during the Littorina Sea stage (e.g., Andrén et al., 2011; Moros et al., 2002).

Lower (less radiogenic) $^{187}Os/^{188}Os$, low BIT index, high TOC levels and the first occurrence of brackish diatoms recorded across the sedimentology changes in lithofacies 6 to 8 (~2.3 to 0 m) in combined cores P435/1-5 GC and 303600 TC therefore describe increased and continued marine influence, indicating that this represents the brackish Littorina Sea stage of the Baltic Sea Basin history.

3.6 Implications and conclusions

Through combining modern day surface sediment data with past core records this study demonstrates the potential usefulness of osmium isotopes for reconstructing the drainage history of the Baltic Sea Basin and its connection to the open ocean. This technique has the potential to be applied to other similarly restricted basins. A strong correlation between salinity and $^{187}Os/^{188}Os$ is recorded showing this proxy can be used to differentiate between a largely marine environment and a largely freshwater environment as demonstrated for the opening of the Atlantic 36 million years ago (Poirier & Hillaire-Marcel, 2011).

This study demonstrates the first use of osmium isotopes and BIT index combined with other geochemical techniques such as XRF, sedimentology and TIC, TOC content to prove they are useful in tracking the different sea stages of the Baltic Sea Basin. It is shown that the use of $^{187}Os/^{188}Os$ is highly effective in distinguishing between freshwater and marine phases where there are large and longer-term drainage or inflow events, but not as effective at tracking weak and short-term changes in marine influence, described below.

Between 11.1 and 6.1 m the core contains glacial brown varved clays attributed to the Baltic Ice Lake, and at the same time radiogenic $^{187}Os/^{188}Os$ values and a high BIT index are recorded as well as a relatively high Ca content. These all indicate a largely freshwater environment with no marine influence, further implying that these sediments represent deposition during the Baltic Ice Lake.

Between 6.1 and 3.95 m the sedimentology turns to brown-grey laminated clays attributed to the Yoldia Sea stage. At 5.15 m a contemporaneous decrease in Re, $^{187}Os/^{188}Os$, BIT index, and a peak in K/Ti, all indicate a change in conditions and are tentatively attributed to the marine incursion phase of the Yoldia Sea. It is likely that large fluxes in material and changes in origin of the source material over the radiogenic Precambrian Shield were too strong and hence diluted and masked the weak, short marine signal during the incursions in the Yoldia Sea.

Between 3.95 and 2.3 m P435/1-5 GC records blue-grey coloured lacustrine clays with varying varves and laminations attributed to the Ancylus Lake stage. Radiogenic $^{187}Os/^{188}Os$ values and a high BIT index infer an increase in the flux of terrestrially

sourced material and a greater freshwater influence with no marine influx, further linking these sediments to the freshwater Ancylus Lake stage.

Finally, from 2.3 m to the core top, olive-brown, clays/ muds are synonymous of the Littorina Sea stage. Alongside this, $^{187}Os/^{188}Os$ values decrease to match the present-day surface sediments and remain lower, the BIT index also decreases close to 0 and therefore both imply a large and continued influx of marine waters into the Baltic Sea Basin. Organic carbon content also increases and remains high for the first time in the core as do Re and Os concentrations, likely linked to the increase in organic matter and salinity, and likely represents an increase in in-situ productivity as there is a decreased flux of glacial freshwater outwash to dilute it.

3.7 Tables

Table 3.1: Details of surface sediment samples and the P435/1-5 GC and 303600 trigger core of the central Baltic.

Core/Sample	Map Code	Depth (cm)	Latitude (°N)	Longitude (°E)	Water Depth (m)
P435/1-5 GC	P435/1-5 GC	0 - 1100	56°57.954	19°22.210	178
303600 TC	P435/1-5 GC	0 - 400	56°57.954	19°22.210	178
EMB046/8-4 FC	1	0	60°48.68	03°45.19	338
EMB046/10-1	2	0.5-1	57°49.75	07°17.62	457
EMB046/20-2	3	0.5-1	58°31.59	09°29.09	532
242970-4	4	3.5	56°43.580	11°49.800	46
318170-3	5	1	56°36.158	11°46.522	36
348250	6	0-0.5	55°56.54	12°42.85	26
317990 MUC	7	0-1	54°18.596	11°25.571	23
317980	8	0-1	54°14,996	11°30.008	24
318320-2	9	0	54°49.786	13°39.365	45
MSM51/2/53-4	10	0	60°06.927	19°17.925	245
P435-8-3-FC	11	0-1	62°46.690	18°2.973	89
P435/10-2 MUC 1AW	12	0	62°52.169	19°2.562	213

Table 3.2: Synopsis of the Re-Os data for core P435/1-5 GC and surface sediment samples. Uncertainty is 2SE.

Batch/Sample	Depth (cm)	Re (ppb)	±	Os (ppt)	±	^{192}Os (ppt)	±	^{187}Re/^{188}Os	±	^{187}Os/^{188}Os	±
Surface samples											
EMB046/8-4 FC (Map 1)	0	1.0	0.0	135.3	0.6	50.0	0.3	39.6	0.2	1.02	0.01
EMB046/10-1m (Map 2)	0.5-1	1.3	0.0	166.8	1.1	62.3	0.5	40.5	0.4	0.93	0.01
EMB046/20-2 (Map 3)	0.5-1	0.8	0.0	165.5	0.8	61.3	0.3	26.2	0.2	1.01	0.01
242970-4 (Map 4)	3.5	1.7	0.0	16.1	0.1	5.8	0.0	595.6	5.3	1.31	0.01
318170-3 (Map 5)	1	3.9	0.0	78.0	0.4	28.1	0.2	275.7	1.7	1.25	0.01
348250 (Map 6)	0-0.5	2.8	0.0	88.7	0.4	31.9	0.1	175.9	0.9	1.27	0.01
317990 MUC (Map 7)	0-1	4.2	0.0	110.4	0.6	38.7	0.2	215.9	1.2	1.49	0.01
317980 (Map 8)	0-1	4.0	0.0	80.6	0.4	28.1	0.1	285.7	1.4	1.53	0.01
318320-2 (Map 9)	0	3.5	0.0	61.4	0.3	21.1	0.1	330.4	1.7	1.67	0.01
MSM51/2/53 (Map 10)	0	1.1	0.0	139.4	0.7	46.5	0.2	45.6	0.2	1.95	0.01
P435-8-3-FC (Map 11)	0-1	1.1	0.0	104.8	0.6	34.4	0.2	65.5	0.4	2.10	0.02
P435/10-2 MUC 1AW (Map 12)	0	0.9	0.0	117.1	1.0	37.9	0.3	46.8	0.4	2.24	0.03
P435/1-5 GC samples											
RO967-2_P435/1-5GC 2cm	2	9.2	0.0	143.0	0.7	48.1	0.2	380.7	1.8	1.87	0.01
RO1001-1_P435/1-5GC 0.65m	65	12.9	0.0	110.8	0.6	37.0	0.2	692.7	3.6	1.94	0.01
RO968-1_P435/1-5GC 1.65m	165	7.7	0.1	112.5	0.6	37.5	0.2	406.4	3.2	1.97	0.01
RO1098-1_P435/1-5 GC 200cm	200	12.5	0.0	224.2	1.7	72.5	0.6	342.3	2.7	2.25	0.02
RO1078-2_P435/1-5GC 220cm	220	2.0	0.0	135.9	1.0	42.9	0.3	91.0	0.6	2.50	0.02
RO1001-2_P435/1-5GC 2.4m	240	1.2	0.0	95.0	0.8	29.7	0.3	80.2	2.6	2.60	0.03
RO1057-2_P435/1-5GC 2.7m	270	0.8	0.0	96.1	0.7	29.8	0.2	51.1	0.5	2.65	0.02
RO967-3_P435/1-5GC 3m	300	0.5	0.0	70.1	0.6	21.7	0.2	48.0	0.5	2.67	0.03
RO1001-3_P435/1-5GC 3.05m	305	0.7	0.0	57.4	0.4	17.9	0.1	80.8	0.6	2.62	0.02
RO1078-3_P435/1-5GC 335cm	335	0.4	0.0	59.8	0.5	18.7	0.2	46.7	0.5	2.60	0.03
RO1111-1_P435/1-5GC 350cm	350	0.5	0.0	71.5	0.6	22.0	0.2	43.3	0.4	2.76	0.03
RO1098-2_P435/1-5 GC 357cm	357	0.4	0.0	61.9	0.5	19.4	0.2	41.6	0.4	2.54	0.03
RO1001-4_P435/1-5GC 3.65m	365	0.5	0.0	60.4	0.5	18.9	0.1	56.9	0.5	2.59	0.03
RO967-4_P435/1-5GC 4m	400	0.8	0.0	63.6	0.5	20.0	0.2	83.2	0.8	2.54	0.03
RO1078-4_P435/1-5GC 420cm	420	0.6	0.0	62.7	0.5	19.9	0.2	56.9	0.5	2.43	0.03
RO1001-5_P435/1-5GC 4.3m	430	0.6	0.0	69.8	0.5	22.6	0.2	52.4	0.5	2.24	0.02

RO1124-2_P435/1-5 GC 440cm	440	0.4	0.0	66.2	0.5	21.2	0.2	41.1	0.4	2.32	0.02
RO1111-2_P435/1-5GC 450cm RPT	450	0.4	0.0	73.2	0.6	23.0	0.2	35.8	0.3	2.54	0.03
RO1124-3_P435/1-5 GC 460cm	460	0.3	0.0	57.6	0.4	18.5	0.1	30.5	0.3	2.33	0.02
RO1057-3_P435/1-5GC 4.8m	480	0.3	0.0	51.4	0.4	16.6	0.1	34.8	0.4	2.23	0.02
RO967-5_P435/1-5GC 5m	500	0.2	0.0	54.5	0.5	17.6	0.2	20.1	0.3	2.28	0.03
RO1093-2_P435/1-5 GC 515cm RPT	515	0.1	0.0	58.8	0.5	18.7	0.2	14.2	0.3	2.43	0.03
RO1057-4_P435/1-5GC 5.3m	530	0.2	0.0	55.9	0.5	17.6	0.2	17.3	0.3	2.50	0.03
RO1078-5_P435/1-5GC 560cm	560	0.2	0.0	57.3	0.5	18.0	0.2	20.2	0.3	2.56	0.03
RO1057-5_P435/1-5GC 5.7m	570	0.2	0.0	57.1	0.5	18.0	0.2	25.1	0.3	2.53	0.03
RO1098-3_P435/1-5 GC 580cm	580	0.2	0.0	56.7	0.4	18.0	0.1	26.7	0.3	2.41	0.03
RO1098-4_P435/1-5 GC 590cm	590	0.3	0.0	55.2	0.4	17.7	0.1	35.1	0.5	2.33	0.03
RO1111-3_P435/1-5GC 600cm RPT	600	0.3	0.0	54.2	0.4	17.2	0.1	35.3	0.4	2.45	0.03
RO1078-6_P435/1-5GC 610cm	610	0.3	0.0	53.6	0.4	17.4	0.1	31.1	0.4	2.22	0.02
RO1078-7_P435/1-5GC 620cm	620	0.2	0.0	52.8	0.4	17.0	0.1	28.5	0.3	2.31	0.03
RO1124-4_P435/1-5 GC 640cm	640	0.3	0.0	57.2	0.5	18.4	0.2	33.1	0.4	2.30	0.03
RO1034-2_P435/1-5GC 6.6m	660	0.4	0.0	57.3	0.4	18.3	0.1	48.0	0.4	2.35	0.02
RO1057-6_P435/1-5GC 6.7m	670	0.4	0.0	56.9	0.4	18.1	0.1	40.6	0.3	2.41	0.02
RO967-6_P435/1-5GC 7m	700	0.4	0.0	60.6	0.5	19.3	0.2	36.9	0.4	2.40	0.03
RO1087-3_P435/1-5GC 710cm	710	0.3	0.0	56.2	0.5	17.9	0.1	36.3	0.4	2.42	0.03
RO1078-8_P435/1-5GC 720cm	720	0.4	0.0	65.5	0.6	20.3	0.2	42.2	0.4	2.67	0.03
RO1098-5_P435/1-5 GC 750cm	750	0.8	0.0	60.7	0.5	18.8	0.2	88.5	0.9	2.67	0.03
RO1087-4_P435/1-5GC 775cm	775	0.4	0.0	54.0	0.4	17.2	0.1	41.3	0.4	2.40	0.03
RO1034-3_P435/1-5GC 8m REPEAT	800	0.4	0.0	54.4	0.4	17.1	0.1	52.3	0.5	2.54	0.03
RO1078-9_P435/1-5GC 840cm	840	0.4	0.0	52.7	0.4	16.9	0.2	46.3	0.5	2.33	0.03
RO1111-4_P435/1-5GC 880cm	880	0.6	0.0	53.3	0.4	17.2	0.2	64.7	0.7	2.25	0.03
RO1034-4_P435/1-5GC 9m	900	0.6	0.0	53.1	0.4	17.0	0.1	70.1	0.6	2.33	0.03
RO1087-5_P435/1-5GC 940cm	940	0.6	0.0	51.5	0.4	16.4	0.1	67.7	0.7	2.42	0.03
RO1098-6_P435/1-5 GC 980cm	980	0.6	0.0	52.0	0.4	16.4	0.1	75.2	0.7	2.52	0.03
RO968-3_P435/1-5GC 10m	1000	0.7	0.0	50.6	0.4	16.1	0.1	83.4	0.8	2.43	0.03
RO1111-5_P435/1-5GC 1040cm RPT	1040	0.5	0.0	43.8	0.4	14.1	0.1	76.2	0.8	2.26	0.03
RO1111-6_P435/1-5GC 1080cm	1080	0.4	0.0	29.5	0.3	9.4	0.1	93.1	1.0	2.44	0.03
RO1034-5_P435/1-5GC 11m	1100	0.7	0.0	44.4	0.4	14.3	0.1	92.8	0.9	2.31	0.03

Chapter 4: First evidence from the open Skagerrak of the absolute timing for the onset of Baltic Ice Lake drainage and evolution to the Baltic Sea since the LGM: Insights from radiocarbon ages, trace element and osmium geochemistry

*A version of this paper will be submitted for publication to Boreas co-authored by David Selby of the Department of Earth Sciences, Durham University, Jeremy Lloyd of the Department of Geography, Durham University, Matthias Moros of the Leibniz Institute for Baltic Sea Research Warnemünde, Germany, Ole Bennike and Jørn Bo Jensen of the Geological Survey of Denmark and Greenland (GEUS), Denmark, and Thomas Blanz and Ralph R. Schneider of the Department of Geology, Kiel University.

I completed all Re-Os laboratory analysis, data synthesis, literature reviews and formulisation of the manuscript. Co-authors Selby and Lloyd contributed through supervisor discussions and editorial comments on the manuscript. Moros provided access to all core samples and XRF, sand content and TIC data, as well as supervisor discussions and editorial comments. Bennike and Bo Jensen contributed radiocarbon dating and scientific background. Blanz and Schneider conducted the $\%C_{37:4}$ biomarker analysis.

4.1 Introduction

Throughout the Quaternary the paleogeography of the Baltic Sea Basin has been continually influenced by the changing ice sheet dynamics of the Fennoscandian Ice Sheet (FIS; Andrén et al., 2015; Björck, 1995). Thus, the sediments deposited in the basin record several different paleogeographic settings (referred to as Baltic Sea stages; Björck, 1995; Rosentau et al., 2017) since the Last Glacial Maximum (LGM). These include: the Baltic Ice Lake, the Yoldia Sea, the Ancylus Lake, and the Littorina Sea stages (Björck, 1995; Rosentau et al., 2017). However, the exact timings and transitions of these stages in different parts of the Basin and surrounding areas remain debated (Berglund et al., 2005; Björck, 1995).

Following initial retreat of the FIS after the LGM the Baltic Basin records a lake environment known as the Baltic Ice Lake from ~16 cal ka BP (Andrén et al., 2011; Björck, 1995; Rosentau et al., 2017). In response to continued recession of the FIS at ~13 cal ka BP the first drainage of the Baltic Ice Lake took place through south-central Sweden lowering the lake level by 5 – 10 m (Andrén et al., 2011; Björck, 1995; Fig. 4.1).

Drainage through these channels is proposed to have continued until the Younger Dryas, ~12.8 cal ka BP when glacial readvance blocked the channels once more and the ice lake level began to rise again. The final drainage of the Baltic Ice Lake is proposed to have occurred around the end of the Younger Dryas at ~11.7 cal ka BP with an extremely rapid (potentially < 1-2 years) and large discharge of freshwater through south central Sweden channels, lowering the lake level by 25 m, marking the end of the Baltic Ice Lake stage (Andrén et al., 2008, 2011; Björck, 1995; Jakobsson et al., 2007; Rosentau et al., 2017).

Following this drainage the next phase in the Baltic Basin history (the Yoldia Sea) is characterised by connection to the North Sea between *c.* 11.7 – 10.7 cal ka BP. Records of this phase show small incursions of marine waters into the Baltic through the narrowing south central Swedish channels lasting only ~ 100 – 350 years before isostatic uplift started to close off connections to the North Sea and the Baltic Basin became dominated by freshwater conditions – the Ancylus Lake stage (Andrén et al., 2008, 2011; Björck, 1995; Rosentau et al., 2017). The freshwater Ancylus Lake stage occurred between 10.7 – 9.7 cal ka BP with a freshwater lake once again increasing the water level in the Basin to ~10 m above sea level (Andrén et al., 2011; Berglund et al., 2005; Rosentau et al., 2017). Isostatic rebound in the north meant land in the south began to lower. This, alongside ongoing glacioeustatic sea-level rise, led to the opening and enlarging of outlets from the Baltic around the Danish Straits such as Öresund and the Great Belt through which some of the lake was able to drain into the Kattegat (Andrén et al., 2011; Rosentau et al., 2017). Some debate remains over whether the end of the Ancylus Lake stage was characterised by a large rapid drainage event (such as with the Baltic Ice Lake as noted by Björck (1995) and references therein), or whether the drainage occurred gradually through these newly developed channels in the south. Research in the last decade, citing evidence such as limited erosion, implies a more gradual drainage (Andrén et al., 2011; Lemke et al., 2001; Rosentau et al., 2017). The final stage in the Baltic Basin history, known as the Littorina Sea (lasting to present-day), is characterised by saline waters entering the basin through the Great Belt and Öresund Straits in a time-progressive manner and the final remnants of the Fennoscandian Ice Sheet melted allowing more continuous connection to the North Sea (Andrén et al., 2011; Bennike et al., 2021; Berglund et al., 2005; Björck, 1995; Rosentau et al., 2017).

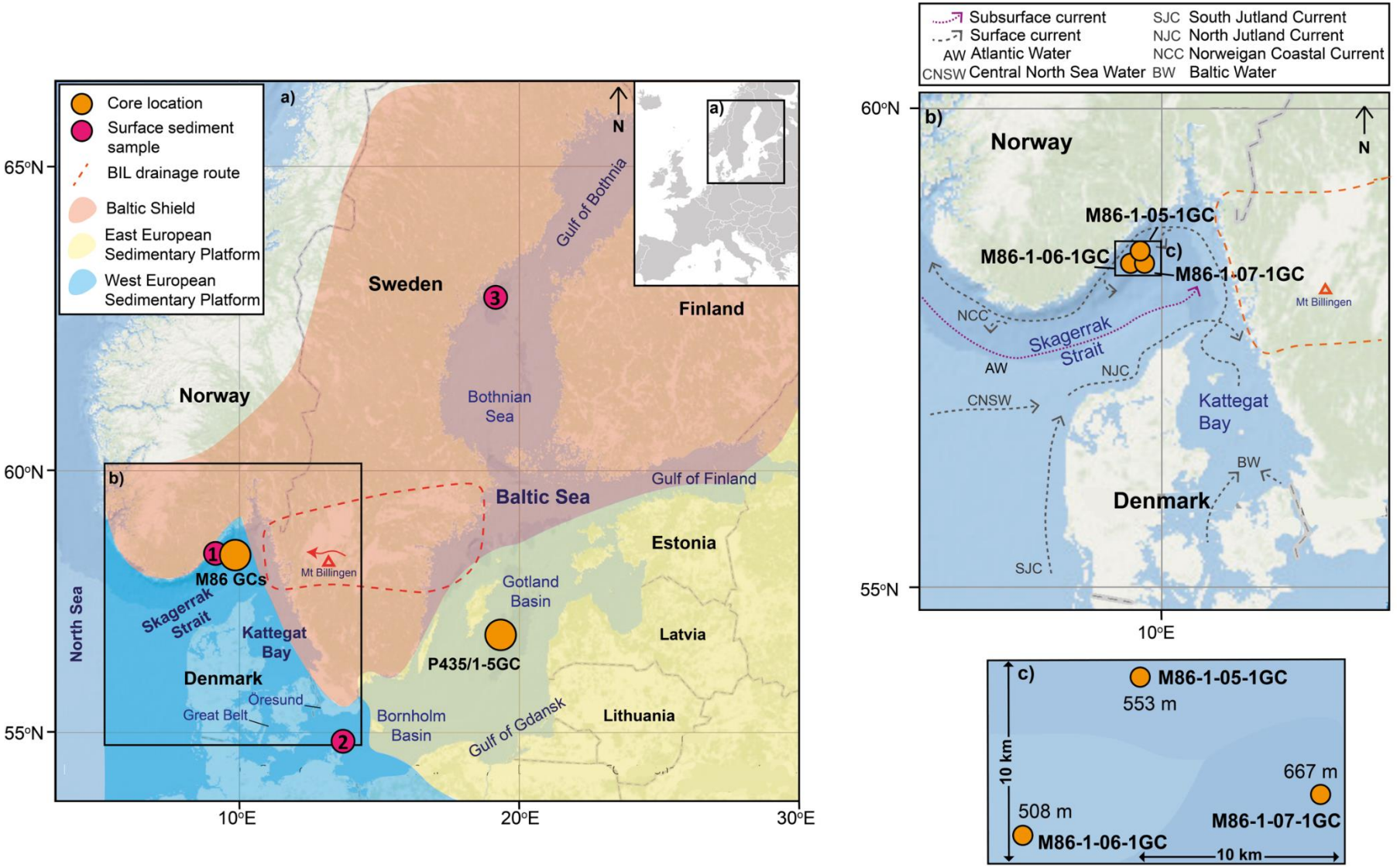
Core location
Surface sediment sample
BIL drainage route
Baltic Shield
East European Sedimentary Platform
West European Sedimentary Platform
a)
b)
N
Sweden
Finland
Norway
Gulf of Bothnia
Bothnian Sea
Baltic Sea
Gulf of Finland
Estonia
Latvia
Lithuania
Gotland Basin
Bornholm Basin
Gulf of Gdansk
North Sea
Skagerrak Strait
Kattegat Bay
Denmark
Öresund
Great Belt
Mt Billingen
M86 GCs
P435/1-5GC
1
2
3
65°N
60°N
55°N
10°E
20°E
30°E
Subsurface current
Surface current
AW Atlantic Water
CNSW Central North Sea Water
SJC South Jutland Current
NJC North Jutland Current
NCC Norweigan Coastal Current
BW Baltic Water
M86-1-05-1GC
M86-1-06-1GC
M86-1-07-1GC
c)
NCC
AW
CNSW
SJC
NJC
BW
553 m
667 m
508 m
10 km

Figure 4.1: (Page 112) Map of the Baltic Sea, Kattegat and Skagerrak showing: a) Locations of all surface gravity cores including three from the Skagerrak and one from the central Baltic Sea and the three surface sediment samples, dominant geology types and the area in south central Sweden around Mt. Billingen through which the Baltic Ice Lake is thought to have drained; b) detail of the inset map of the Kattegat and Skagerrak showing the three cores and also the dominant surface and subsurface currents in the area. The main subsurface current is that of Atlantic Water (AW), the remaining surface currents include Central North Sea Water (CNSW), the South Jutland Current (SJC) the North Jutland Current (NJC), the Norwegian Coastal Current (NCC) and Baltic Water (BW); and c) map showing the geographic position between the three Skagerrak cores and their depths below sea level. Colour maps from ArcGIS, grey and white Europe map from Wikipedia (https://en.wikipedia.org/wiki/File:Europe_blank_map.png), current and subsurface currents adapted from Gyllencreutz (2005), geological data from Peucker-Ehrenbrink & Ravizza (1996) and Rosentau et al. (2017).

Due to narrow connections between the Baltic and the North Sea, via Kattegat Bay and the Skagerrak through the Straits of Öresund and the Great Belt, the present-day Baltic Sea is a restricted basin that exhibits distinct salinity gradients and stratification changes (Fig. 4.1; Andrén et al., 2015; Björck, 1995; Nordberg, 1991). The Baltic Sea waters exhibit a distinct geochemical signature in comparison to that of the more open ocean setting of the North Sea. For example, the Baltic Sea waters generally possess lower trace metal concentrations (e.g., cadmium, copper, nickel, iron and zinc) in comparison to the North Sea (Dutton et al., 1973; Magnusson & Westerlund, 1980). Within the Baltic Sea, salinity decreases from 12 PSU in the Danish Straits, 5 – 8 PSU in the Central Baltic, and is almost fresh water at < 4 PSU in the Gulfs of Finland and Bothnia, all compositions being much lower compared to the Kattegat at 30 – 20 PSU in the north and 15 PSU in the south, and the North Sea at 30 – 35 PSU (Ducrotoy & Elliott, 2008; Jiang et al., 1997; Sjoqvist et al., 2015). This distinction between the Baltic Sea Basin and the more open ocean of the North Sea and the Skagerrak permits the possibility to track inflow and outflow events between the two basins and through the different sea stages.

This study focuses on the final drainage of the Baltic Ice Lake stage. The outflow of this drainage is recorded in sediments and erosional features over south-central Sweden, the Baltic Sea Basin and in the Kattegat in both terrestrial and marine records (Andrén et al., 2002; Björck, 1995; Johnson et al., 2010; Rosentau et al., 2017). However, in many studies from the Skagerrak, evidence of the final drainage of the Baltic Ice Lake is limited, with many cases showing no changes in faunal assemblages, sedimentology, or total organic carbon (TOC) levels (Bodén et al., 1997; Dickens, 2013; Erbs-Hansen et al., 2011; Gyllencreutz, 2005; Jiang et al., 1997; Knudsen et al., 1996). This could be due to several reasons including lower sedimentation rates and the relatively short-lived drainage event (1-2 years; Jakobsson et al., 2007; Rosentau et al., 2017).

Here, this study shows the first evidence of the Baltic Ice Lake drainage from cores in the open Skagerrak. This study combines radiocarbon dating, X-ray fluorescence (XRF), biomarker and osmium-isotope geochemistry to show the hydrogenous chemical signature of the waters draining from the Baltic Ice Lake and the impact this had on water masses in the Skagerrak as well as the sedimentological and detrital changes, to provide accurate constraints on the timing and duration of the Baltic Ice Lake drainage into the Skagerrak.

This study shows that between ~12 to 11.6 cal ka BP the final Baltic Ice Lake drainage through south-central Sweden is characterised by a marked geochemical signature within the Skagerrak. Post 11.6 cal ka BP a more open marine geochemical signature is recorded. Additionally, no geochemical change is shown over the proposed timing of the Ancylus Lake stage (10.7 – 9.7 cal ka BP) supporting the hypothesis of a more gradual drainage of the Baltic Basin at this time.

4.2 Geographical and geological setting of the present-day Baltic Sea Basin and Skagerrak Strait

The Baltic Sea Basin is one of the Earth's largest intracontinental basins and the largest brackish water body (~373,000 km^2; Andrén et al., 2015; Björck, 1995; Rosentau et al., 2017). The basin is split into several zones, including the Gulfs of Bothnia and Finland as well as the Gotland Basin, Bornholm Basin and Bothnian Sea, each of these containing a number of smaller sub-basins (Björck, 1995; Tuuling et al., 2011; Fig. 4.1). Connections to the marine waters of the North Sea are through the narrow and shallow Straits between Sweden and Denmark. All present-day exchanges between the North and Baltic Seas must first pass through the connected water ways of the Skagerrak Strait and Kattegat Bay, which together act as a large estuary (Nordberg, 1991; Tuuling et al., 2011). The oceanward Skagerrak Strait, lying south of Norway and south-west Sweden and north of Denmark, has a maximum depth of 700 m (Nordberg, 1991). Present-day detritus derived from the Baltic Sea, Kattegat Bay, and from the North Sea, is deposited within the Skagerrak largely due to a reduction in water mass velocity as the water masses mix (e.g., Rodhe & Holt, 1996). As a result the Skagerrak has a relatively high sedimentation rate of up to 1 cm per year (Bøe et al., 1996; Gyllencreutz, 2005).

The geological setting of the Baltic Sea Basin (Fig. 4.1) is dominated by the Precambrian crystalline basement (the Baltic shield), which ranges in age from Late Proterozoic in the

south to Late Archean in the northeast over Sweden, Finland and into Russia (Peucker-Ehrenbrink & Ravizza, 1996; Rosentau et al., 2017). The south and south-east of the Baltic Sea is dominated by the Phanerozoic age European Sedimentary Platform, with a small region in the south west comprising the Palaeozoic aged Western European Sedimentary Platform (Björck, 1995; Peucker-Ehrenbrink & Ravizza, 1996; Rosentau et al., 2017). These sediments consist mainly of clastic and calcareous rocks with some sandstone and clayey deposits in the east (Rosentau et al., 2017). In contrast, the Skagerrak Strait mainly lies on the Western European Sedimentary Platform with the very north of the area in the Baltic shield (Rosentau et al., 2017; Solheim & Grønlie, 1983; Tuuling et al., 2011).

4.3 Materials and methods

The analysis of three cores from the Skagerrak, alongside surface sediment samples and sediment samples from a central Baltic Sea core are detailed below. All three Skagerrak cores underwent XRF scanning analyses on the whole record, with specific intervals analysed for sand content (%) and rhenium-osmium analyses. Radiocarbon dates were obtained for cores M86-1-07-1 GC and M86-1-05-1 GC. Measurements of total inorganic carbon (%) and an alkenone biomarker ($\%C_{37:4}$) were conducted for core M86-1-06-1 GC. Due to logistical constraints on the number of analyses that could be completed, the latter analyses were only undertaken for M86-1-06-1 GC, focussing on the interval of core over the region of enhanced Ti/Ca and sand content. All surface sediment samples and samples from the central Baltic Sea core underwent Re-Os analysis.

4.3.1 Sample sites

To investigate the timing and extent of the drainage of the Baltic Ice Lake into the Skagerrak Strait in response to ice sheet recession, three gravity cores were studied. These cores were obtained from the Skagerrak Strait in 2011 by the R/V 'Meteor' cruise (M86-1-07-1 GC, M86-1-06-1 GC and M86-1-05-1 GC; Table 4.1; Fig. 4.1; Arz, 2011). The core sites in the Skagerrak were chosen for this study to search for a Baltic Ice Lake signal in the central Skagerrak, and the sites are proximal to the outflow channels that bisected south central Sweden through which the Baltic Ice Lake drained (Andrén et al., 2011; Björck, 1995; Rosentau et al., 2017; Fig. 4.1a). The three cores are collected within a 60 km^2 region. Although the core sites are spatially close, they were taken from different water depths, and importantly different distances from the outflow channel through which the Baltic Ice Lake drained (Table 4.1; Fig. 4.1c).

Core M86-1-07-1 GC (58°26.370 °N/ 09°43.530 °E), comprising 8.1 m of sediment, taken from water depth of 667 m, represents the most proximal depositional site to the Baltic Ice Lake drainage through south central Sweden. Core M86-1-05-1 GC (58°29.513 °N/ 09°34.787 °E) comprising 8.3 m of sediment was obtained from a water depth of 553 m, ~10 – 11 km north-west of M86-1-07-1 GC, thus slightly more distal to the Baltic Ice Lake drainage. Core M86-1-06-1 GC (58°25.756 °N/ 09°28.551 °E) comprising 6.6 m of sediment was obtained from a water depth of 508 m and is ~14 – 15 km west of M86-1-07-1 GC and 9 – 10 km south-west of M86-1-05-1 GC and is the most distal of the three cores (Fig. 4.1; Table 4.1).

A fourth core P435/1-5 GC (56°57.954 °N/ 19°22.210 °E) from the central Baltic (Fig. 4.1; ~60 – 70 km east of south Gotland Island) is also studied to provide insight into the $^{187}Os/^{188}Os$ ratio for the Baltic Sea during the Baltic Ice Lake stage. This core was collected during the RV 'Poseidon' cruise in 2012. It consists of 11 m of sediment from a water depth of 178 m. Five samples were analysed over a short section of core (7.2 – 10 m) identified sedimentologicaly as representing the Baltic Ice Lake stage in the record (typical brown glacio-lacustrine origin clays with varying varves; Rosentau et al., 2017).

In addition to the sediment cores, 3 surface sediment samples were collected from the Skagerrak Strait, and the south-west and north Baltic Sea to assess the variability of the $^{187}Os/^{188}Os$ ratio along a marine to brackish to relatively freshwater transition (Table 4.1; Fig. 4.1).

4.3.2 XRF analysis

The semi-quantitative distribution of a range of elements for the core sections was determined by XRF core scanning (ITRAX XRF Core Scanner, COX; e.g. Croudace et al., 2006) at the Leibniz-Institute for Baltic Sea Research Warnemünde (IOW). Core surfaces were cleaned, smoothed, and covered with a thin plastic foil to avoid evaporation during measurements. A Cr-tube was used operating at 30 kV and 30 mA with an exposure time of 15 seconds per step. Step size was 1 mm. Of particular interest were the elements K, Ti, and Ca, selected for their use as proxies relating to terrigenous vs. biogenic input, ice rafting and differing sediment sources (Demina et al., 2019; Kylander et al., 2011; Rothwell & Croudace, 2015).

4.3.3 Sand abundance

Core sediment samples (at 1 cm intervals and approx. 20 to 30 g) were freeze-dried, weighed, wet sieved at 63 µm grain size, then dried and weighed again to determine the sand content (wt. %) at the IOW. Depth intervals for sand sieving were selected between 6 and 8.5 m based on XRF scanner results, specifically based on peaks in Ti/Ca which record a potential 'event.' See below discussion.

4.3.4 Total inorganic carbon (TIC) %

For core M86-1-06-1 GC, TIC was determined at ~2 cm intervals using 100 mg of freeze-dried sediment that was diluted with 40% H_3PO_4 and incinerated at 1200 °C on a Multi EA4000 from Analytik Jena at IOW.

4.3.5 Biomarker alkenones (%$C_{37:4}$)

The biomarker alkenone %$C_{37:4}$ analyses for reconstruction of freshwater influence were performed at the Biomarker Laboratory at the Institute of Geosciences, Kiel University, at a sample interval of c. 2 cm (44 samples) in the core depth range of 570 - 670 cm in M86-1-06-1 GC only. Long-chained alkenones (C_{37}) were extracted from homogenised, 2 to 3 grams of bulk sediment, using an Accelerated Solvent Extractor (Dionex ASE-200) with a mixture of 9:1 (v/v) of dichloromethane:methanol (DCM:MeOH) at 100 °C and 100 bar N_2 (g) pressure for 20 minutes. Extracts were cooled to about -20 °C and subsequently taken to near dryness by vacuum rotary evaporation at 20 °C and 65 mbar. A multi-dimensional, double gas column chromatography (MD-GC) with two Agilent 6890 gas chromatographs were used for $C_{37:2}$, $C_{37:3}$ and $C_{37:4}$ identification and quantification (Etourneau et al., 2010). Quantification of the individual compounds was achieved with the addition of an internal standard prior to extraction (cholestane [$C_{37}H_{48}$] and hexatriacontane [$C_{36}H_{74}$]). The relative proportions were obtained using the peak areas of the two different compounds. The specific proportion of tetra-unsaturated C_{37} ketones relative to the sum of alkenones (%$C_{37:4}$) was used. This ratio serves as an indicator of the presence of lower surface salinities in polar and subpolar waters (Bendle et al., 2005; Moros et al., 2016; Rosell-Melé, 1998; Rosell-Melé et al., 2002; Sicre et al., 2002) and has successfully been used for the reconstruction of mid to late Holocene Baltic Sea outflow changes in the study area (Krossa et al., 2015).

4.3.6 Rhenium-osmium (Re-Os) analysis

Fifty-seven down-core sediment samples from four cores were analysed for Re-Os along with the three surface samples. Twenty-four samples from core M86-1-07-1 GC, 17 from

M86-1-05-1 GC, 11 from M86-1-06-1 GC, and 5 from P435/1-5 GC (Table 4.2). Each sampled interval records 1 cm of stratigraphy. The samples were dried at 60 ^{o}C overnight and then powdered using an agate pestle and mortar. The Re-Os analytical protocol is based on established methods (Selby & Creaser, 2003) and was carried out at Durham University (Laboratory of Source Rock and Sulfide Geochemistry and Geochronology and the Arthur Holmes Laboratory). Approximately 1 g of powdered sample is sealed into a Carius tube with 8 mL CrO_3 4N H_2SO_4 and a pre-determined amount of tracer solution (enriched in ^{185}Re and ^{190}Os) and heated at 220 ^{o}C for 48 h in an oven. The Carius tubes are opened, and a solvent extraction is undertaken using 9 mL chloroform ($CHCl_3$) and back extraction into 3 mL HBr. Further purification of the Os fraction is achieved by a H_2SO_4-CrO_3-HBr microdistillation. Purification of the Re fraction from the Os extracted CrO_3 4N H_2SO_4 is obtained using a 5N NaOH – acetone extraction, which is then further purified using HCl-HNO_3 anion bead chromatography. The Os and Re fractions are loaded into a ThermoScientific TRITON mass spectrometer on Pt and Ni filaments, respectively, and analysed using negative thermal ionisation mass spectrometry (NTIMS). The isotopic composition of Re is determined using Faraday collectors in static mode, and the Os composition with an electron multiplier in dynamic mode.

Total analytical protocol blanks (N = 8) are 19.04 ± 4.67 ppt for Re, 0.08 ± 0.05 ppt for Os, with a ^{187}Os/^{188}Os of 0.27 ± 0.20; 1 S.D. To monitor the reproducibility of the Re-Os isotopic analyses over the long term, Re and Os standard solutions are analysed with every sample set. A 50 pg osmium standard solution (DROsS - Durham Romil Osmium Standard) gives ^{187}Os/^{188}Os values of 0.16080 ± 0.00025 (1 S.D., N = 25), which is in agreement with proposed values for the solution and the laboratory running average (Luguet et al., 2008; Nowell et al., 2008; 0.16082 ± 0.0006 1 S.D; N = 816). The 125 pg rhenium standard solution (Restd) yields ^{185}Re/^{187}Re values of 0.59834 ± 0.00063 (1 S.D., N = 25), which agrees with the laboratory running average (0.59861 ± 0.0015 1 S.D; N = 720).

4.3.7 Radiocarbon dating

Thirteen radiocarbon dates were obtained, seven from core M86-1-05-1 GC, five from M86-1-07-1 GC and one from M86-1-06-1 GC (Table 4.3). All analyses were on a mix of benthic foraminifera species with one mollusc from core M86-1-06-1 GC. Analysis was undertaken at the Poznań Radiocarbon Laboratory in Poland (Poz-) and the Laboratory of Ion Beam Physics at Eidgenössische Technische Hochschule in Zürich, Switzerland (ETH-) using accelerator mass spectroscopy (AMS). The raw ^{14}C ages were

calibrated using the CALIB 8.2 software (Stuiver et al., 1998, 2021). A ΔR value of -150 was used (to be consistent with Heier-Nielsen et al., 1995) with the MARINE20 calibration curve (now an inbuilt ΔR of 550; Heaton et al., 2020) to give the values listed in Table 4.3. BACON age-depth modelling software (Blaauw & Christen, 2011) using a ΔR value of -150 was used to calibrate and create an age-depth model from the raw ^{14}C ages using the MARINE20 calibration curve for cores M86-1-05-1 GC and M86-1-07-1 GC (Table 4.3; SM 4.1). For core M86-1-06-1 GC a calibration curve is created based on tie points to the data and age models for core M86-05-1 GC (SM 4.1c; see results section 4.4.6).

4.4 Results

4.4.1 XRF

From the range of elemental data measured through XRF scanning, presented are the ratios of Ti/Ca and K/Ti (a relative measure of terrestrial vs marine sourced material; Demina et al., 2019; Kylander et al., 2011; Rothwell & Croudace, 2015).

In core M86-1-07-1GC, except for two peaks, the Ti/Ca ratio is relatively constant between 0.2 and 0.3 (Fig. 4.2a; SM 4.2b). The first peak occurs between 7.3 and 7.7 m reaching a maximum Ti/Ca of 0.4, driven by a decrease in Ca. A second broader peak occurs between 4.5 and 2.5 m with a maximum Ti/Ca of 0.35. The Ti/Ca in cores M86-1-05-1GC and M86-1-06-1GC (Figs. 4.2b, c; SM 4.2a, c) mirrors the pattern observed in M86-1-07-1GC, although is less pronounced in core 05. For M86-1-05-1GC, the first narrow peak occurs between 8.0 and 7.3 m, reaching a maximum Ti/Ca of 0.28, the second peak being broader, occurring over ~3 m between 6 and 3 m, with a maximum Ti/Ca of 0.3 at ~4.5 m. The Ti/Ca values then remain relatively constant in the upper 3 m at ~0.25. Similarly, for M86-1-06-1GC, the Ti/Ca shows both the relatively abrupt and short-lived peak (maximum of 0.6 at 6 m) and broader peak (maximum of 0.3 between 5 and 3 m) peaks. The Ti/Ca ratio then slowly decreases to 0.2 and remains relatively constant in the upper 2 m of the core.

In cores M86-1-07-1 GC and M86-1-05-1 GC the K/Ti overall steadily decreases from core bottom (1.98 / 1.83) to top (1.38 / 1.44), respectively (Figs. 4.2a, b; SM 4.2a, b). In both cores an abrupt peak in K/Ti of 2.06 over 6.9 – 6.4 m and 2.1 over 8.1 – 7.5 m is observed, respectively, due to both lower Ti levels and higher in K levels. In M86-1-06-1 GC (Fig. 4.2c; Table 4.2c) the K/Ti overall decreases steadily from the core bottom (~1.9) to the top (~1.5), which is interrupted by decreasing and increasing values, with a

peak of 2.02 shown between 6.03 and 5.7 m. The K/Ti then continue to steadily decrease to the top of the core.

4.4.2 Sand analysis and sedimentology

Relatively homogenous brownish, silty, clayey sediments, which are interrupted by more sandy sections as described below, characterise the sedimentology of all three Skagerrak cores. The P435/1-5 GC samples are taken from a section of glacial, brown, varved, clays considered to record sedimentation during the Baltic Ice Lake (Rosentau et al., 2017). The three surface samples analysed are a mix of sandy, gritty, muddy to clayey sediments with occasional shelly detritus and larger clasts (which were removed prior to powdering).

In core M86-1-07-1 GC the sand content is 1 to 2% between 8.1 and 7.4 m. After this there is a sharp increase to 8.5% at 7.1 m (Fig. 4.2a; SM 4.3). The sand content then abruptly declines to < 1% at 6.9 m and stays at this level to 6 m. The trend observed in M86-1-07-1GC is mirrored in core M86-1-06-1GC, with a sand content of ~1 to 2% between 6.7 and 6.3 m (Fig. 4.2c; SM 4.3), interrupted by a rise to 4 % at 6.25m. A sharp peak then occurs between 6.2 and 5.9 m where the sand content reaches 7.8% before decreasing to < 1% at 5.7 m. In contrast, core M86-1-05-1GC is characterised by < 1% sand in the analysed interval between 8.4 m and 6.4 m (Fig. 4.2b; SM 4.3).

4.4.3 TIC (%)

Analysed for core M86-1-06-1 GC only, TIC% is relatively stable between 6.7 and 6.2 m at ~1.0% apart from three short lived peaks at 6.65 m (1.2%), 6.38 m (1.1%) and 6.21 m (1.2%). TIC levels then decrease rapidly to 0.6% at 6.1 m before rising back to 1.3% at 5.9 m and remaining broadly at ~1.3% until 5.7 m (Fig. 4.2c; SM 4.4). The decrease in TIC% corresponds to the peak in Ti/Ca ratio (Fig. 4.2c) showing the driving force is a reduction in calcium/calcite.

4.4.4 Biomarkers

The $\%C_{37:4}$ increases in core M86-1-06-1 GC from 5.2 to 8.6% between the depths of 6.7 and 6.5 m before decreasing to 5.9% at 6.3 m. The $\%C_{37:4}$ then increases to a maximum of 11% at 6.1 m and then drops off to 4% at 5.8 m (Fig. 4.2c; SM 4.4).

4.4.5 Re-Os

Presented below are the Re-Os abundance and isotopic characteristics of the analysed samples of the four cores. Given the age of the analysed sediment (ca. ≤ 14 kyrs) and

relatively low Re abundance, any age correction for the radiogenic ^{187}Os ingrowth from ^{187}Re decay since sediment deposition is less than that of the individual sample $^{187}Os/^{188}Os$ 2SE uncertainty (Table 4.2) and also sample reproducibility of in-house reference samples (Du Vivier et al., 2014; Sproson et al., 2021 in press). As such, age-corrected $^{187}Os/^{188}Os$ values are not presented.

4.4.5.1 Core M86-1-07-1 GC

The Re abundances gradually increase from 0.77 ppb at the base of the core to 1.74 ppb at the top. This gradual increasing trend is interrupted by two peaks at 6.75 m (3.59 ppb) and 3 m (5.09 ppb; Fig 4.2a). The total Os abundance varies between 70.0 and 145 ppt and shows a gradual increase from core bottom to top. The $^{187}Os/^{188}Os$ values range between 1.07 and 1.45 with an overall decreasing trend from approximately 1.4 to 1.5 at the base of the core to 1.1 at the top of the core (8.1 – 0 m), with a sharp decrease between 7 and 6.5 m. The $^{187}Os/^{188}Os$ values then remain relatively stable from 5.5 m to the core top (Fig. 4.2a; Table 4.2).

4.4.5.2 Core M86-1-05-1 GC

The Re abundances vary between 1.07 and 3.63 ppb, with the highest values occurring in the interval between 8 and 7 m. The total Os abundance varies between 74.3 and 90.6 ppt and increases steadily from core bottom to top. The $^{187}Os/^{188}Os$ values and trend up core are similar to M86-1-07-1 GC, showing an abrupt decrease in $^{187}Os/^{188}Os$ between 7.8 and 7.5 m from ~1.31 to 1.20, and then remaining relatively stable (1.17 – 1.12) for the rest of the core (Fig. 4.2b; Table 4.2).

4.4.5.3 Core M86-1-06-1 GC

Rhenium-Os measurements were only taken in the lower parts of this core to cover the Baltic Ice Lake drainage period and provide a correlation between all three Skagerrak cores. The Re abundances vary between 1.08 and 3.36 ppb, with two peaks of 2.83 ppb and 3.36 ppb at 5.95 m and 6.3 m, respectively. The total Os abundance varies between 63.6 and 85.1 ppt and generally increases from 6.5 and 5.4 m. The $^{187}Os/^{188}Os$ composition and profile again is similar to the other two cores, showing an abrupt decrease between 6.1 and 5.4 m from ~1.55 to 1.17 (Fig. 4.2c; Table 4.2)

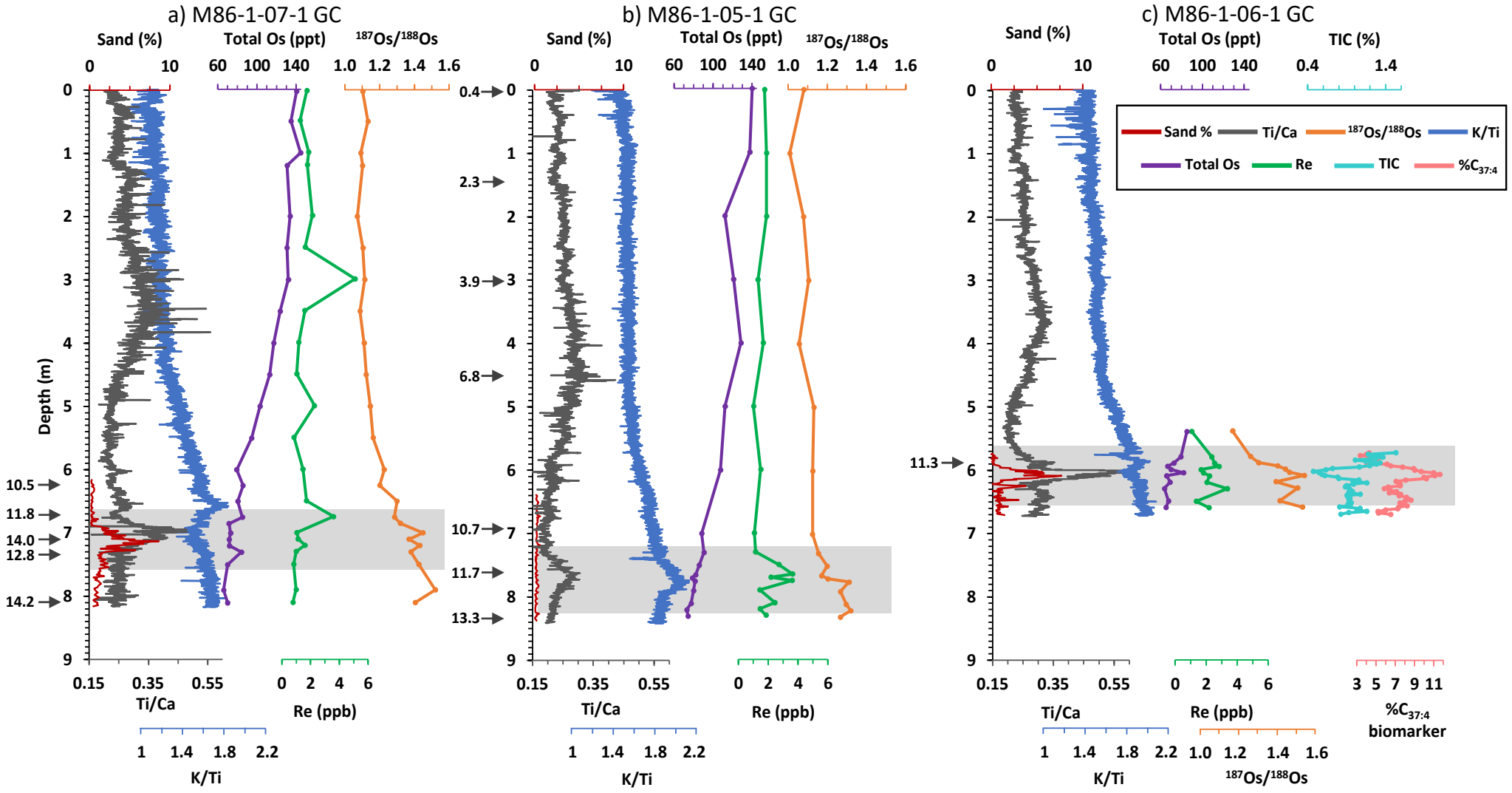
a) M86-1-07-1 GC
b) M86-1-05-1 GC
c) M86-1-06-1 GC
Sand (%)
Total Os (ppt)
187Os/188Os
TIC (%)
Depth (m)
Sand %
Ti/Ca
K/Ti
Total Os
Re
TIC
%C37:4
Re (ppb)
%C37:4 biomarker
10.5
11.8
14.0
12.8
14.2
0.4
2.3
3.9
6.8
10.7
11.7
13.3
11.3

Figure 4.2: (Page 122) Sand content (%), Ti/Ca ratio, K/Ti ratio, Total Os (ppt), Re (ppb), and $^{187}Os/^{188}Os$ ratio plotted against depth (m) for Skagerrak cores a) M86-1-07-1 GC, b) M86-1-05-1 GC and c) M86-1-06-1 GC, the latter also including Total Inorganic Carbon (TIC) content (%) and $\%C_{37:4}$ biomarker index. The grey shaded area represents the proposed time of the Baltic Ice Lake drainage. Blue diamond symbols represent depths for which radiocarbon ages are determined.

4.4.5.4 Core P435/1-5 GC

Five samples from this core were analysed for Re-Os to characterise the isotopic signature of the Baltic Ice Lake stage for comparison with the data obtained from the Skagerrak cores. The Re abundances range between 0.43 and 0.67 ppb, with the total Os abundances varying between 50.6 to 66.5 ppt. The $^{187}Os/^{188}Os$ values range between 2.67 and 2.25 (Table 4.2).

4.4.5.5 Surface samples

For the surface samples the Re and total Os abundances vary between 0.81 and 3.50 ppb, and 61.37 and 165.54 ppt, respectively (Table 4.2). The $^{187}Os/^{188}Os$ values are 1.01 for the Skagerrak sample (map code 1), 1.67 for the sample from the south-west Baltic Sea (map code 2), and 2.24 for the northern Baltic Sea sample (map code 3; Fig. 4.1).

4.4.6 Radiocarbon dating

Table 3 shows the depths, ^{14}C ages and calibrated ages for the three Skagerrak cores. For core M86-1-05-1 GC the seven mixed benthic foraminifera samples yield calibrated dates in stratigraphic order, ranging from 13.3 cal ka BP (834.8 cm) to 0.4 cal ka BP (5.5 cm). An interpolated age model based on a Bayesian modelling approach using the BACON software program is presented in Figure 4.3. Core M86-1-05-1 GC possesses radiocarbon dates for the length of the core that are used to produce the age model. For core M86-1-07-1 GC, good age constraints through radiocarbon dating exists for 625 – 810 cm (~10 – 14 cal ka BP), the most important section of the core in this study. To extrapolate this up to surface level a constant sedimentation rate has been assumed between the most recent radiocarbon date at 625 cm and the surface. For core M86-1-07-1 GC, four of the five dates, except for the date at 710 cm, are in stratigraphic order (Fig. 4.3). The sample at 710 cm (14 cal ka BP) does not conform to stratigraphic order. The BACON age model forces superposition to be upheld and derives a new interpolated age for the 710 cm level (Fig. 4.3). The older date from 710 cm in M86-1-07-1 GC may be due to reworking of sediments as this sample comes from an interval with a peak in sand content (see section 4.4.2; Fig. 4.2).

For core M86-1-06-1 GC a single calibrated date of 11.3 cal ka BP was determined for a mollusc at 590 cm. To develop an age model for this core, Ti/Ca trends were correlated between M86-1-06-1 GC and core M86-1-05-1 GC, which possesses radiocarbon dates from the whole length of the core, and no age inversions due to potential re-working of sediments. The single mollusc age of 11.3 cal ka BP coincides roughly with the base of the large decrease in Ti/Ca in M86-1-06-1 GC and is coincident in timing with the base of the large decrease in Ti/Ca in M86-1-05-1 GC (Figs. 4.4, 4.5). Further tie points correlated between cores M86-1-06-1 GC and M86-1-05-1 GC are: the beginning of the peak in Ti/Ca at 8.1 m and 6.2 m, respectively (~12.3 cal ka BP), the peak in Ti/Ca at 7.7 m and 6.0 m, respectively (~11.7 cal ka BP), the more gradual peak in Ti/Ca at 4.5 m and 3.7 m, respectively (~6.7 cal ka BP), and the dip in Ti/Ca at 1.4 m and 1.0 m, respectively (~2.2 cal ka BP; Figs. 4.2, 4.4, 4.5). These tie points were then input into the BACON software (with no calibration necessary) alongside the mollusc radiocarbon date (to be calibrated) to produce an age-depth model for core M86-1-06-1 GC (Figs. 4.3, 4.4, 4.5). To try to account for errors relating to corelation of the tie points and potential offsets between the two cores, an error of 200 years was also added alongside the ages input into BACON.

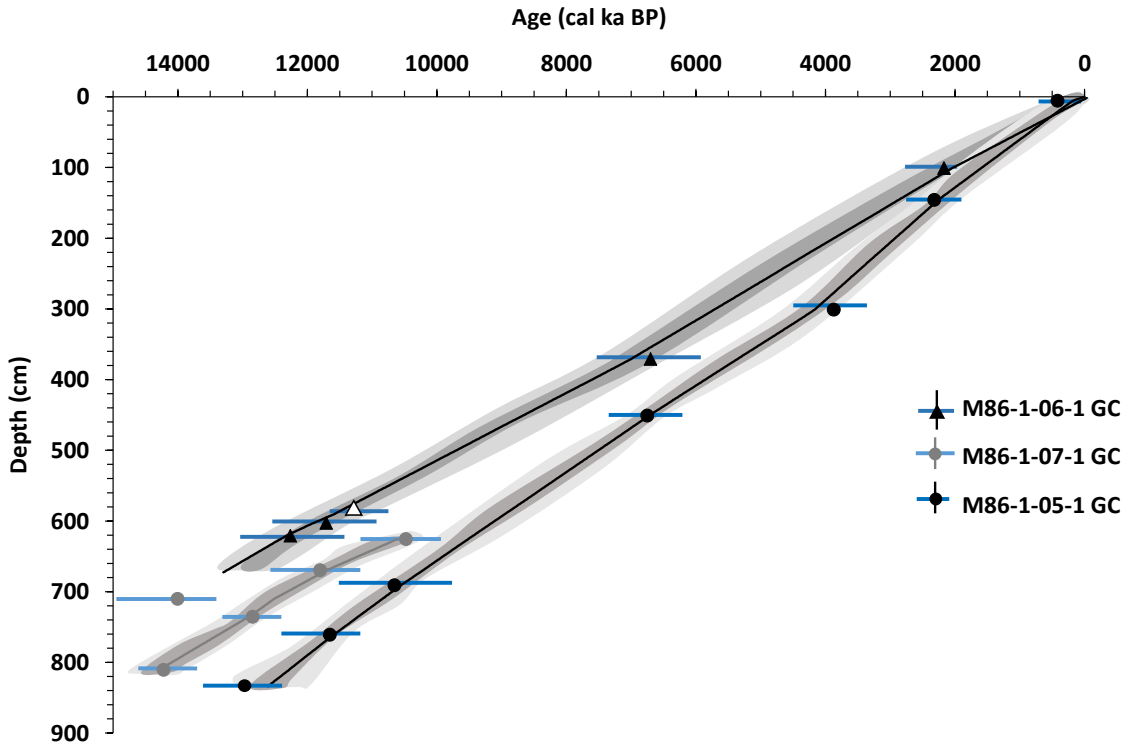

Figure 4.3: Age models developed for the three Skagerrak cores. The age models for cores M86-1-05-1GC and M86-1-07-1GC are based on Bayesian modelling of radiocarbon dates using the BACON software and MARINE20 calibration curve. Blue lines show the calibration range of the raw input ^{14}C ages for cores M86-1-05-1GC and M86-1-07-1GC. The grey area shows 95% confidence limits with darker grey indicating the more likely calendar ages (Blaauw & Christen, 2011). For core M86-1-06-1GC data points represent correlation tie points shown by triangle symbols (white = mollusc, black = tie point), based on comparison to the data and age model presented for core M86-1-06-1GC (see text section 4.4.6).

4.5 Discussion

This study focusses on evidence in the Skagerrak for the final drainage of the Baltic Ice Lake using detrital and hydrogenous geochemical techniques. In addition to sediment characteristics and geochemistry (% sand, total inorganic carbon, trace elements) and biomarkers ($\%C_{37:4}$), this study utilises sediment osmium isotope ($^{187}Os/^{188}Os$) analysis to infer the water $^{187}Os/^{188}Os$ composition of the Baltic Basin at the time of sediment deposition (Ravizza & Turekian, 1989; Cohen et al., 1999). The $^{187}Os/^{188}Os$ proxy allows the differentiation between long- and short-term changes in the environment due to the relatively short residence time of osmium in the oceans of 1 to 50 kyrs, with several studies noting a residence time of < 10 kyrs (Levasseur et al., 1999; Oxburgh, 1998, 2001; Peucker-Ehrenbrink & Ravizza, 2012; Rooney et al., 2016; Sharma et al., 1997). The average $^{187}Os/^{188}Os$ of present-day oxic seawater is relatively stable across the global oceans, with an average value of 1.060 ± 0.005 (Burton et al., 1999; Cohen, 2004; Levasseur, 1998; Peucker-Ehrenbrink & Ravizza, 2000; Rooney et al., 2016; Sharma et al., 1997). However, it has also been shown that the North Atlantic Ocean possesses a slightly less radiogenic $^{187}Os/^{188}Os$ composition (1.04), and that there are still some spatial and temporal variations in $^{187}Os/^{188}Os$ that reflect local influences in the ocean chemistry, especially in more isolated/restricted seawater basins (e.g. Burton et al., 2010; Chen et al., 2009; Gannoun & Burton, 2014; Paquay & Ravizza, 2012; Peucker-Ehrenbrink & Ravizza, 2012; Rooney et al., 2016). The Baltic Sea is an additional example which is discussed in detail below.

The geology of the Baltic Sea catchment is dominated by the Precambrian crystalline basement. Previous research has shown runoff from these areas to possess a highly radiogenic $^{187}Os/^{188}Os$ signature of ~3.6 to 7.9 (Peucker-Ehrenbrink & Ravizza, 1996). Freshwater runoff from the catchment would therefore deliver this radiogenic, and a potentially even higher signature (due to preferential weathering of radiogenic felsic matrix; Bernhard Peucker-Ehrenbrink & Blum, 1998), into the Baltic Basin. This is demonstrated by present-day sediment $^{187}Os/^{188}Os$ compositions. Sample 1 from the Skagerrak possesses a $^{187}Os/^{188}Os$ of 1.01 (Fig. 4.1), extremely close to open ocean values (1.06). Sample 2 from the south-west Baltic Sea has a $^{187}Os/^{188}Os$ of 1.67 representing a decreased marine influence, shown by decreasing salinity values of 30 to 15 PSU in the Skagerrak through to 8 PSU in the southern Baltic Sea (Ducrotoy & Elliott, 2008; Jiang et al., 1997). Finally, sample 3 from the north Baltic Sea, characterised by almost fresh water at 5 PSU, possesses a much more radiogenic $^{187}Os/^{188}Os$ value of 2.24, representing an increased influence of radiogenic runoff from the Precambrian Shield. This therefore

shows a clear difference between the $^{187}Os/^{188}Os$ of an open marine signature in the Skagerrak, to a more isolated Baltic Sea Basin. Based on this the $^{187}Os/^{188}Os$ ratio has the potential to record outwash and inflow exchanges between the Baltic Sea Basin and the Skagerrak/North Sea.

During the freshwater Baltic Ice Lake phase, the Baltic Basin was isolated from marine influence, and therefore a radiogenic $^{187}Os/^{188}Os$ signature is expected to characterise the basin during these times. The present-day north Baltic Sea sample (sample 3) records an almost freshwater salinity signal (~5 PSU), it would be expected that the waters of the Baltic Ice Lake would therefore record a $^{187}Os/^{188}Os$ value close to this (2.24). Indeed, this point is clearly supported by the sediments analysed from core P435/1-5GC from the central Baltic Sea. The $^{187}Os/^{188}Os$ values measured within the clay considered to record deposition during the Baltic Ice Lake are highly radiogenic (2.25 to 2.67) and reflect the radiogenic $^{187}Os/^{188}Os$ derived from the Precambrian Baltic Shield which is delivered by runoff to the Baltic Ice Lake with minimal input from the North Sea. The $^{187}Os/^{188}Os$ of the Baltic Ice Lake phase (2.25 to 2.67) is very different to that of the Late Pleistocene and Holocene global ocean (ca. 1; Paquay & Ravizza, 2012; Rooney et al., 2016).

4.5.1 New insights for Baltic Ice Lake drainage into the Skagerrak Basin

Since the Last Glacial Maximum (LGM) the most significant change to the Baltic Basin was the drainage of the isolated, freshwater Baltic Ice Lake via a channel trending E-W through south-central Sweden that opened into the Skagerrak Strait. The current understanding is that the drainage began at ~ 13 cal ka BP, and then paused coincident with the Younger Dryas cold phase (~12.8 cal ka BP) due to glacial advance, followed by a catastrophic drainage occurring at the end of the Younger Dryas (11.7 cal ka BP), which lowered the lake level by 25 m (Andrén et al., 2008, 2011; Björck, 1995; Rosentau et al., 2017). The channel outlet through south central Sweden closed as a result of isostatic uplift at ~10.3 cal ka BP (Björck, 1995; Gyllencreutz, 2005; Rosentau et al., 2017). However, evidence of this drainage from within the open Skagerrak is limited (Bodén et al., 1997; Dickens, 2013; Erbs-Hansen et al., 2011; Gyllencreutz, 2005; Jiang et al., 1997; Knudsen et al., 1996). This study presents evidence from three central Skagerrak cores clearly showing an ‘event’ coincident in timing to the final outwash of the Baltic Ice Lake.

Figure 4.4: (Page 127) Sand content (%), Ti/Ca, K/Ti, and $^{187}Os/^{188}Os$ ratio plotted against ages obtained from age modelling using the Bacon software for the whole of cores a) M86-1-07-1 GC, b) M86-1-05-1 GC and c) M86-1-06-1 GC. The latter also includes biomarker $\%C_{37:4}$ data and TIC %.

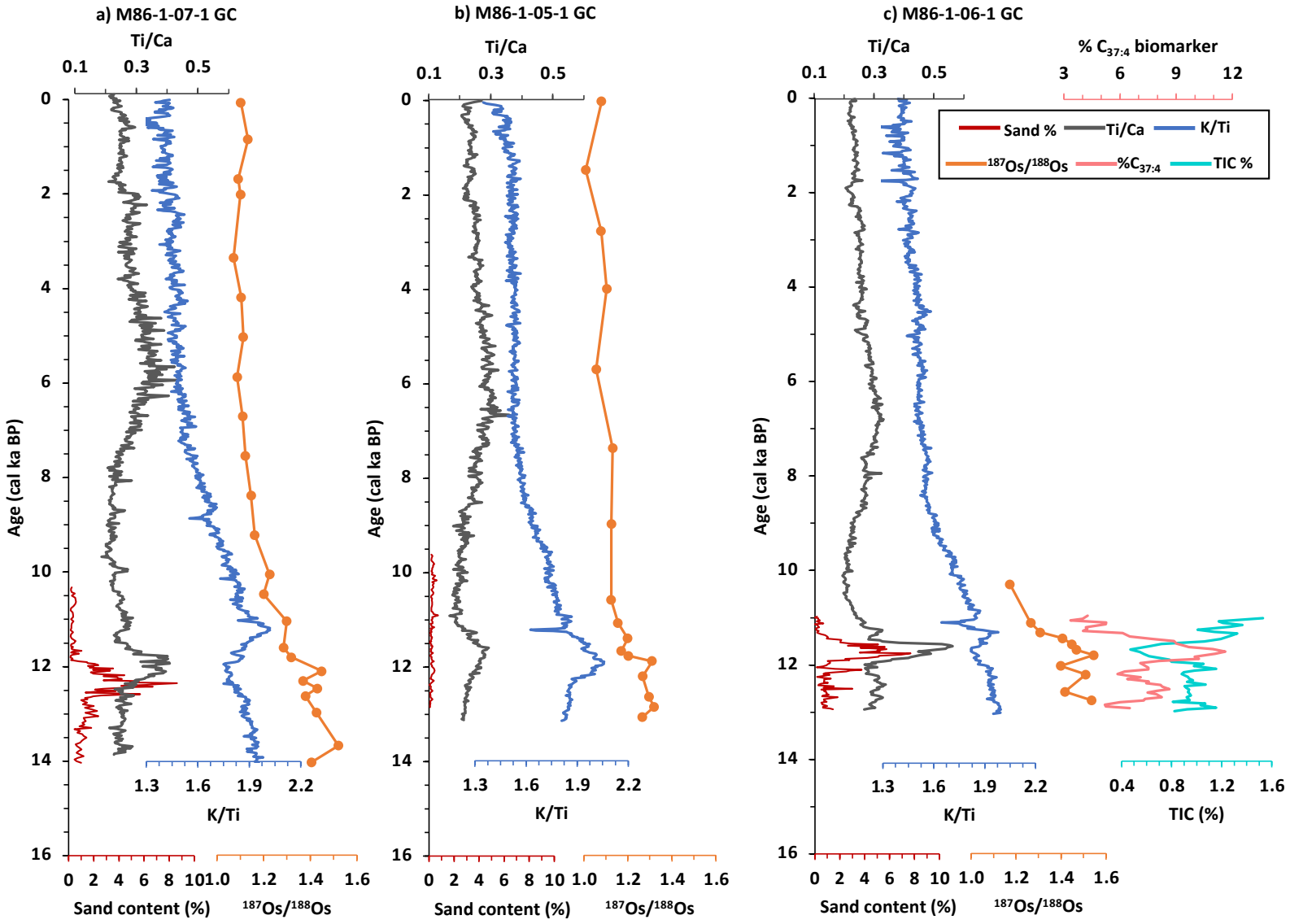
a) M86-1-07-1 GC
b) M86-1-05-1 GC
c) M86-1-06-1 GC
Ti/Ca
% C37:4 biomarker
Sand %
Ti/Ca
K/Ti
187Os/188Os
%C37:4
TIC %
Age (cal ka BP)
K/Ti
TIC (%)
Sand content (%)
187Os/188Os

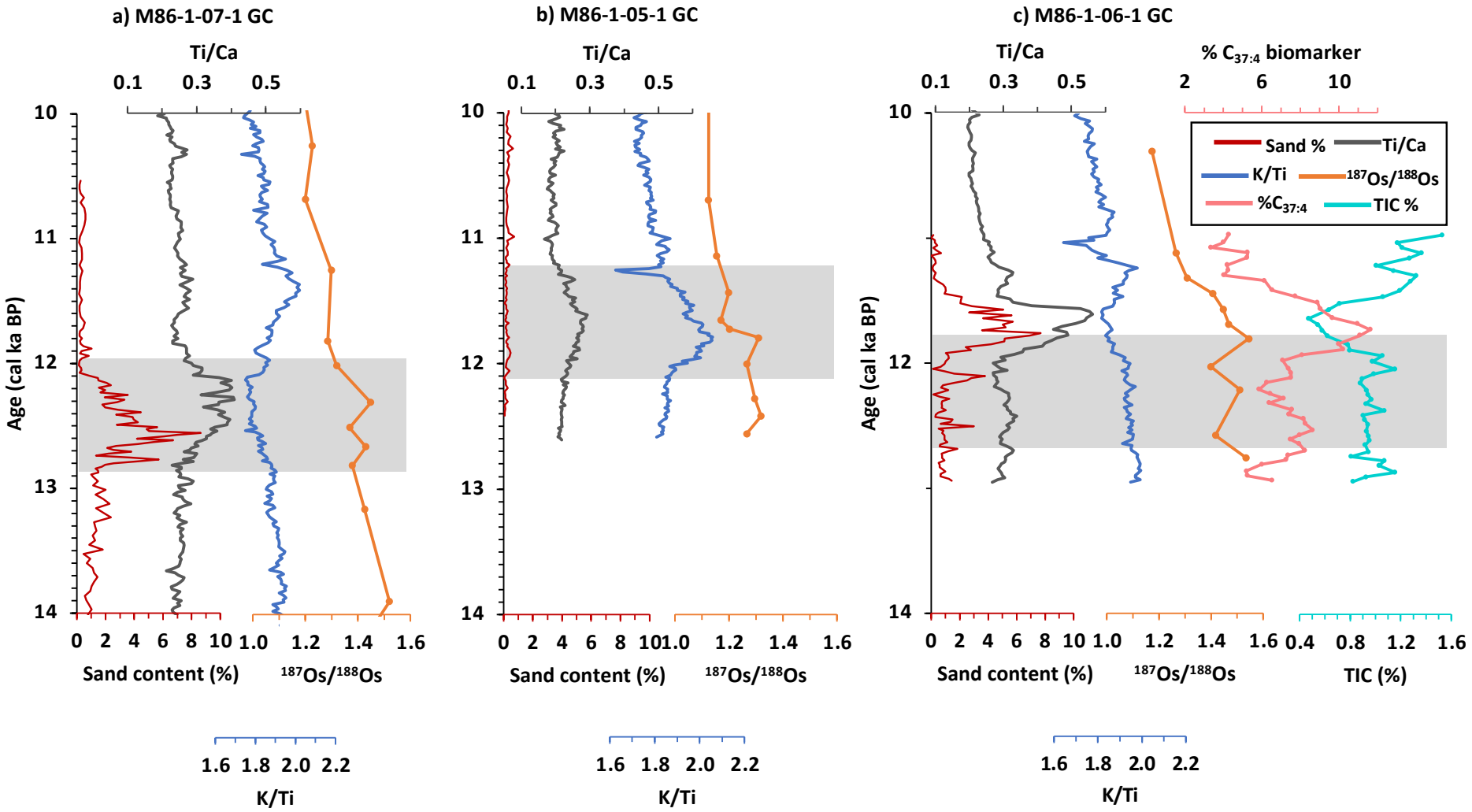

Figure 4.5: Sand content (%), Ti/Ca, K/Ti and $^{187}Os/^{188}Os$ ratio plotted against ages obtained from age modelling using the Bacon software for the time interval of 14 to 10 cal ka BP for cores a) M86-1-07-1 GC, b) M86-1-05-1 GC and c) M86-1-06-1 GC. The latter also includes biomarker $\%C_{37:4}$ data and TIC %. Shaded areas indicate proposed timing of the Baltic Ice Lake drainage.

In core M86-1-07-1 GC between 13 and 11.7 cal ka BP, the $^{187}Os/^{188}Os$ compositions are more radiogenic (1.3 to 1.5; Figs. 4.4, 4.5) than contemporaneous and present-day average open marine values (~1; Burton et al., 1999; Cohen, 2004; Levasseur, 1998; Peucker-Ehrenbrink & Ravizza, 2000; Paquay & Ravizza, 2012; Rooney et al., 2016; Sharma et al., 1997; this study), but are less radiogenic than the $^{187}Os/^{188}Os$ compositions of the Baltic Ice Lake waters (~2.2 – 2.7; this study) inferred from core sediments deposited in the central Baltic during the Baltic Ice Lake stage, and also less radiogenic than present-day Baltic Sea surface sediments. Likewise for core M86-1-05-1 GC between 12.6 and 11.6 cal ka BP, the $^{187}Os/^{188}Os$ are also more radiogenic (1.3 to 1.2) than open marine values. The radiogenic $^{187}Os/^{188}Os$ compositions (1.3 to 1.5) between 13 and 11.6 cal ka BP in the Skagerrak (Figs. 4.4, 4.5) therefore indicate a mixing of the two different water sources - marine waters from the North Sea and waters drained from the Baltic Ice Lake. In addition to the radiogenic $^{187}Os/^{188}Os$ compositions between 13 and 11.7 cal ka BP, a radiogenic signature is recorded pre 13 cal ka BP to the bottom of the core which is dated at 14.1 cal ka BP (Figs. 4.4, 4.5). This suggests that there was a continuous radiogenic source of osmium into the Skagerrak between 14.1 and 11.7 cal ka BP implying that outflow from the Baltic Ice Lake was occurring prior to ~13 cal ka BP, and that glacial readvance during the Younger Dryas, ~12.8 cal ka BP, did not fully block the outflow channels across south-central Sweden.

The radiogenic $^{187}Os/^{188}Os$ signature and freshwater signal before 13 cal ka BP could be due to either a radiogenic source of osmium from earlier drainage/outflow of the Baltic Ice Lake, or from glacial meltwater flux from the retreating FIS across Sweden and Norway over the Baltic Shield. In the Skagerrak area, iceberg calving ended between ~11.6 and 10.2 cal ka BP (Gyllencreutz, 2005), which coincides with slightly less radiogenic $^{187}Os/^{188}Os$ values (1.2 to 1.3) compared to the pre 12 cal ka BP $^{187}Os/^{188}Os$ values of 1.3 to 1.5 (Fig. 4.4). Further, in southeast Norway at ~10.2 cal ka BP, a major flood from the Glomma River Valley occurred (Erbs-Hansen et al., 2011; Gyllencreutz, 2005; Longva & Bakkejord, 1990; Longva & Thoresen, 1991). If the radiogenic osmium isotope values seen in all three cores pre 12 cal ka BP were wholly due to glacial inputs/outwash from a non-Baltic Ice Lake source, i.e., southern Norway or Sweden, a radiogenic $^{187}Os/^{188}Os$ peak over the period of the Glomma flood would be expected. However, no increase in $^{187}Os/^{188}Os$ is observed at ~10.2 cal ka BP in the most analysed core (M86-1-07-1 GC; Fig. 4.4a). Therefore, it is proposed that the radiogenic $^{187}Os/^{188}Os$ composition is being sourced, at least partly, from drainage of the Baltic Ice Lake before the beginning of the drainage event at 13 cal ka BP, with this drainage occurring syn/pre

14.1 cal ka BP. Indeed, large amounts of freshwater drainage through the Öresund Strait and lower Danish valleys did occur prior to the opening of the drainage channel located through south-central Sweden (Andrén et al., 2011; Bergsten & Nordberg, 1992). This would suggest that $^{187}Os/^{188}Os$ values are effective in recording inputs of more radiogenic fresh water from the Baltic Ice Lake into the Skagerrak but are not necessarily able to distinguish between general drainage and larger, more catastrophic drainage events originating from the same basin.

Core M86-1-06-1 GC records peaks in $\%C_{37:4}$ biomarkers (Figs. 4.4c, 4.5c) between 12.9 and 12.2 cal ka BP, and 12.2 and 11.3 cal ka BP. The biomarker proxy ($\%C_{37:4}$) records the influences of freshwater, being an indicator of lower surface salinities (Bendle et al., 2005; Moros et al., 2016; Rosell-Melé, 1998; Rosell-Melé et al., 2002; Sicre et al., 2002) and has successfully been used to show changes in the outflow from the Baltic Sea into the Kattegat during the mid to late Holocene (Krossa et al., 2015). The younger peak in $\%C_{37:4}$ mirrors the stratigraphic position of the peaks in % sand content and Ti/Ca, and the steady decline in $^{187}Os/^{188}Os$ from 1.55 to 1.31. The older peak in $\%C_{37:4}$ would indicate a lower salinity, freshwater source was entering into the Skagerrak prior to the final catastrophic drainage at ~ 11.7 cal ka BP, which is supported by the $^{187}Os/^{188}Os$ data.

At the proposed start of the Baltic Ice Lake drainage ~13 cal ka BP, core M86-1-07-1 GC records stable Ti/Ca and sand content levels. At ~12.8 cal ka BP there is a sharp rise in sand content, a rise in Ti/Ca levels and the $^{187}Os/^{188}Os$ values remain radiogenic (Figs. 4.4a, 4.5a). The increase in % sand content implies an increase in detritus/sediment delivery to the Skagerrak over a time interval of ~700 to 1000 years. The short time interval implies that the sand input occurred as the result of ephemeral high energy flow(s). The Ti/Ca is often used as a proxy for terrestrial input (e.g. Rothwell & Croudace, 2015). In this case it is a decrease in Ca abundance causing the Ti/Ca peak, as shown by the decrease in TIC% (SM 4.4; Fig. 4.5). A lowering in Ca abundance would suggest a change in productivity and biogenic production (Demina et al., 2019; Rothwell & Croudace, 2015), which could have been driven by an influx of cold ice-melt waters. It has also been noted that finer grained Baltic Ice Lake sediments are known to have a high carbonate content (Bennike & Jensen, 2013; Gyllencreutz, 2005; Kögler & Larsen, 1979; Moros et al., 2002). In cores M86-1-07-1 GC and M86-1-06-1 GC, a slight fall in the K/Ti ratio occurs contemporaneously with the peaks in Ti/Ca, and then is followed by an increase in K/Ti, partly driven by an increase in K, as Ti/Ca levels decrease once more (Fig. 4.2a, c). In core M86-1-05-1 GC however, no sand content peak is recorded and the

peaks in Ti/Ca and K/Ti stratigraphically overlap (Fig. 4.2b). The contemporaneous peaks in M86-1-05-1 GC alongside the offset peaks in cores M86-1-07-1 GC and M86-1-06-1 GC between Ti/Ca and K/Ti therefore suggests that the K/Ti ratio is controlled by relative clay content minerals (Diekmann et al., 2008; Hepp et al., 2006; Rothwell & Croudace, 2015). An increase in Ti/Ca and decrease in TIC%, as well as a decrease K/Ti therefore implies a decrease in both carbonate and clay, perhaps due to the high energy outflow changing the depositional environment and preventing the accumulation of Ca-rich clayey Baltic sediments at the core sites, depositing only larger, coarser materials noted by the sand contents. Then, with a decrease in flow energy, deposition of finer sediments occurred, that result in a peak in K/Ti and return of Ti/Ca and TIC% levels to 'pre-event' conditions. Thus, the correlations noted between proxies controlled by both detritus (e.g., % sand content, Ti/Ca, and K/Ti) and hydrogenous load (e.g., $^{187}Os/^{188}Os$ and $\%C_{37:4}$) in cores M86-1-07-1 GC and M86-1-06-1 GC between 12.7 to 11.7 cal ka BP suggests that this high energy event recorded is the catastrophic drainage of the Baltic Ice Lake into the Skagerrak. The timing of the peak in Ti/Ca and K/Ti in core M86-1-05-1 GC, however, is ~1000 years earlier (~11.7 cal ka BP) than that of M86-1-07-1 GC. As mentioned previously, core M86-1-07-1 GC contains an age inversion, which may affect the age-depth model, and hence M86-1-05-1 GC was deemed to be the most accurate model and is used to form the age-depth model of M86-1-06-1 GC, alongside the mollusc age which agrees in timing to M86-1-05-1 GC. This further eludes to the large catastrophic event seen in the data is recording the final drainage of the Baltic Ice Lake into the Skagerrak at 11.7 cal ka BP. The data therefore also suggests that the earlier, smaller, initial drainage of the Baltic Ice Lake at ~13 cal ka BP was not large enough to produce a visible detrital signature in the Skagerrak, but sufficient enough to permit a hydrogenous signature (e.g., $^{187}Os/^{188}Os$ and potentially $\%C_{37:4}$). Further, Ti/Ca, sand content levels and $\%C_{37:4}$ values have all returned to 'normal' in M86-1-05-1 GC and M86-1-06-1 GC by ~11.4 cal ka BP with their peaks beginning to decline by ~11.6 cal ka BP.

Coincident with the decline in % sand content, Ti/Ca and $\%C_{37:4}$ at ~ 11.6 cal ka BP is a trend to less radiogenic $^{187}Os/^{188}Os$ (Fig. 4.4). Although the sand and Ti/Ca levels return to pre 'event' levels by ~11 cal ka BP, the $^{187}Os/^{188}Os$ composition remains slightly more radiogenic (~1.1) than open ocean values until ~9 – 8 cal ka BP. This may suggest that although the main outflow event has ceased by ~11.6 cal ka BP and any detritus and detrital component has settled quickly, the water mass is still receiving some radiogenic osmium input, perhaps from a continued more gradual outflow from the Baltic Ice Lake.

Of interest is the lack of any change in % sand content, which is at < 1%, between 13 – 11.5 cal ka BP in core M86-1-05-1 GC, although both an increase in Ti/Ca, and radiogenic $^{187}Os/^{188}Os$ values are present across the same period (Figs. 4.4b, 4.5b). The Ti/Ca and $^{187}Os/^{188}Os$ proxies reflect the hydrogenous component of the water mass rather than the detrital component, which is reflected by the % sand content. The absence of any change in % sand content implies that the depositional site of core M86-1-05-1 GC, which is more northerly compared to the other two core sites (Fig. 4.1c), was outside the main debris outflow pathway associated with the drainage of the Baltic Ice Lake through south-central Sweden that was captured by cores M86-1-06-1 GC and M86-1-07-1 GC (Fig. 4.5).

4.5.2 Further implications

4.5.2.1 Ancylus Lake drainage

The nature of the drainage of the Ancylus Lake (10.7 – 9.7 cal ka BP) remains debated as to whether it was a single large outwash event, or was a slower, more gradual lowering of lake level draining through smaller channels around Öresund and northern Denmark (Andrén et al., 2011; Lemke et al., 2001; Rosentau et al., 2017). Following the changes in Ti/Ca, K/Ti, % sand content, $\%C_{37:4,}$ and radiogenic $^{187}Os/^{188}Os$ corresponding to the Baltic Ice Lake drainage, all the proxy values decrease (with $^{187}Os/^{188}Os$ becoming less radiogenic trending towards open ocean values) and remain relatively stable during the proposed timing of the end of the Ancylus Lake stage, ~9.7 cal ka BP (Fig. 4.4). Given the absence of any significant or abrupt change in the proxies presented in this study from the Skagerrak, the hypothesis that the drainage of the Ancylus Lake occurred gradually and potentially through smaller channels further south (Andrén et al., 2011; Lemke et al., 2001; Rosentau et al., 2017) is supported, rather than through a catastrophic event.

4.5.2.2 Conservative versus non-conservative behaviour of Os

In contrast to Re, whose abundances remain relatively stable from core bottom to top (0.76 to 1.74 ppb and 1.84 to 1.75 ppb for M86-1-07-1 GC and M86-1-05-1 GC, respectively), the abundance of osmium (total Os ppt) increases from core bottom to top (70 to 140 ppt and 74 to 140 ppt in M86-1-07-1 GC and M86-1-05-1 GC, respectively and 65 to 85 in M86-1-06-1 GC between 6.6 and 5.4 m; Fig. 4.2). The total Os values are relatively stable near the base of the core until ~600 cm (~10 cal ka BP) in M86-1-07-1 GC, and ~700 cm depth (~10.5 cal ka BP), before beginning to increase (post 10 cal ka BP). Rising total Os values coincide with an increase in $\%C_{37:4}$ and the decrease and then

gradual lowering of $^{187}Os/^{188}Os$ values to a more open marine signature (Fig. 4.2). This is therefore inferred to represent an increased marine influence and therefore increased water column salinity. In the Skagerrak water column salinity would have been slightly lower during the Baltic Ice Lake drainage phase in response to the freshwater inputs (high $^{187}Os/^{188}Os$ and low $\%C_{37:4}$). A decrease in freshwater input and an increase in marine influence would result in an increase in salinity after the Ice Lake drainage. Although the conservative or non-conservative (increases or no trend with salinity, respectively) behaviour of osmium is debated, based on studies from different global locations (Levasseur et al., 2000; Ownsworth et al., 2019; Sproson et al., 2018; Turekian et al., 2007), the relationship observed in this study appears to support the conservative behaviour of osmium.

4.6 Conclusion

Utilising three cores from the Skagerrak, this study presents the first temporally constrained evidence of the final Baltic Ice Lake drainage in this area. Based on the proxies presented here (% sand content, Ti/Ca, TIC, K/Ti, $\%C_{37:4}$, and $^{187}Os/^{188}Os$) a large catastrophic event is recorded by an short-term peak in detrital sand material, Ti/Ca content due to decreased fine-grained Ca-rich material, as well as decreased K/Ti indicating less clay deposition due to a higher energy environment, and increased freshwater ($\%C_{37:4}$, and $^{187}Os/^{188}Os$). These changes occur at an age of ~11.7 cal ka BP, the same age as the timing of the final drainage of the Baltic Ice Lake. It is also suggested that the earlier, initial drainage of the Baltic Ice Lake timed at ~13 cal ka BP was not large enough to produce a large detrital signature in the Skagerrak, but may still be recorded in the $\%C_{37:4}$, and $^{187}Os/^{188}Os$ hydrogenous load.

4.7 Tables

Table 4.1: List of core and surface sediment sample localities, including the depth of the cores/ depth of the surface sediment samples, the water depths and their latitudes and longitudes.

Type	Name	Map Code	Depth (cm)	Latitude (°N)	Longitude (°E)	Water Depth (m)
Core	M86-1-07-1GC	M86 GC	0-810	58°26.370	09°43.530	667
	M86-1-05-1GC	M86 GC	0-830	58°29.513	09°34.787	553
	M86-1-06-1GC	M86 GC	0-660	58°25.756	09°28.551	508
Core	P435/1-5 GC	P435/1-5	720-1000	56°57.954	19°22.210	178
Surface	EMB046/20-2	1	0.5-1	58°31.59	09°29.09	532
sample	318320-2	2	0	54°49.786	13°39.365	45
	P435/10-2 MUC 1AW	3	0	62°52.169	19°2.562	213

Table 4.2: Re-Os analysis data from core samples and surface sediments. Uncertainty is ± 2SE.

	Batch/Sample	Depth (cm)	Re (ppb)	±	Os (ppt)	±	^{192}Os (ppt)	±	^{187}Re/^{188}Os	±	^{187}Os/^{188}Os	±
M86-1-07-1GC	**RO1057-1_M86-1-7 3cm**	3	1.7	0.0	140.3	0.7	51.4	0.3	67.3	0.4	1.10	0.01
	RO1093-3_M86-1-7 50cm	50	1.3	0.0	134.7	0.6	49.2	0.2	51.3	0.3	1.13	0.01
	RO1034-6_M86-1-7 1m	100	1.9	0.0	144.5	0.8	53.0	0.3	69.9	0.5	1.09	0.01
	RO1062-1_M86-1-7 1.2m	120	1.8	0.0	130.8	0.6	47.9	0.3	73.4	0.4	1.10	0.01
	RO1111-7_M86-1-7 200cm	200	2.1	0.0	133.8	1.0	49.2	0.5	85.8	1.0	1.07	0.02
	RO1111-8_M86-1-7 250cm	250	1.6	0.0	130.6	0.6	47.8	0.2	67.5	0.4	1.10	0.01
	RO1034-7_M86-1-7 3m	300	4.8	0.0	132.0	0.6	48.3	0.3	209.7	1.2	1.11	0.01
	RO1087-7_M86-1-7 3.5m	350	1.6	0.0	123.6	0.6	45.4	0.2	69.9	0.4	1.09	0.01
	RO1034-8_M86-1-7 4m	400	1.2	0.0	117.2	0.6	42.9	0.3	54.4	0.4	1.11	0.01
	RO1062-3_M86-1-7 4.5m	450	1.0	0.0	112.9	0.6	41.3	0.2	50.0	0.3	1.12	0.01
	RO1062-4_M86-1-7 5m	500	2.3	0.0	103.0	0.6	37.5	0.2	119.8	0.8	1.15	0.01
	RO1093-6_M86-1-7 550cm	550	0.8	0.0	94.5	0.5	34.4	0.2	48.5	0.3	1.16	0.01
	RO1034-9_M86-1-7 6m	600	1.5	0.0	79.3	0.4	28.6	0.2	101.7	0.7	1.23	0.01
	RO1172-2_M86-1-7 625cm	625	2.8	0.0	85.7	0.5	31.0	0.2	177.9	1.2	1.20	0.01
	RO1062-5_M86-1-7 6.5m	650	1.7	0.0	80.4	0.5	28.8	0.2	118.1	0.8	1.30	0.01
	RO1111-9_M86-1-7 675cm	675	3.6	0.0	85.1	0.5	30.5	0.2	233.9	1.8	1.29	0.01
	RO1174-8_M86-1-7 685cm	685	1.6	0.0	71.5	0.4	25.6	0.2	122.4	0.9	1.32	0.01
	RO1062-6_M86-1-7 7m	700	1.0	0.0	73.1	0.4	25.7	0.2	80.8	0.6	1.45	0.01
	RO1087-8_M86-1-7 7.1m	710	1.1	0.0	71.7	0.4	25.5	0.2	87.9	0.6	1.37	0.01
	RO1098-8_M86-1-7 720cm	720	1.6	0.0	72.0	0.4	25.4	0.2	125.7	0.9	1.43	0.01
	RO1093-8_M86-1-7 730cm	730	1.0	0.0	84.2	0.5	29.9	0.2	66.1	0.5	1.38	0.01
	RO1062-8_M86-1-7 7.5m	750	0.8	0.0	70.0	0.4	24.7	0.2	65.9	0.5	1.43	0.01
	RO1172-5_M86-1-7 790cm	790	1.0	0.0	65.9	0.4	23.0	0.2	84.9	0.7	1.52	0.02
	RO1062-9_M86-1-7 8.1m	810	0.8	0.0	70.0	0.4	24.8	0.2	61.7	0.5	1.40	0.01
M86-1-05-1GC	**RO1174-1_M86-1-5 0cm**	0	1.8	0.0	140.1	0.6	51.4	0.2	67.7	0.4	1.08	0.01
	RO1174-2_M86-1-5 100cm	100	1.9	0.0	137.8	0.6	51.0	0.2	73.3	0.4	1.01	0.01
	RO1179-2_M86-1-5 200cm	200	1.9	0.0	112.1	0.5	47.0	0.2	90.7	0.5	1.08	0.01
	RO1174-4_M86-1-5 300cm	300	1.3	0.0	121.0	0.6	44.3	0.2	58.5	0.3	1.10	0.01
	RO1174-5_M86-1-5 400cm	400	1.7	0.0	128.5	0.6	47.3	0.3	69.8	0.4	1.06	0.01
	RO1174-6_M86-1-5 500cm	500	1.0	0.0	112.3	0.6	41.0	0.2	48.7	0.3	1.13	0.01
	RO1174-7_M86-1-5 600cm	600	1.5	0.0	107.6	0.6	39.3	0.2	75.5	0.5	1.13	0.01
	RO1124-1_M86-1-5 7m RPT	700	1.1	0.0	88.3	0.6	32.3	0.2	65.7	0.5	1.12	0.01
	RO1114-4_M86-1-5 7.3m	730	1.1	0.0	90.6	0.5	33.0	0.2	69.1	0.5	1.16	0.01

	RO1114-5_M86-1-5 7.5m	750	2.7	0.0	85.8	0.5	31.1	0.2	172.8	1.3	1.20	0.01
M86-1-05-1GC continued	**RO1114-6_M86-1-5 7.65m**	765	3.6	0.0	82.2	0.5	29.9	0.2	241.8	2.0	1.17	0.01
	RO1179-3_M86-1-5 770cm	770	2.2	0.0	78.7	0.4	28.5	0.2	152.1	1.1	1.20	0.01
	RO1114-7_M86-1-5 7.75m	775	3.6	0.0	81.5	0.5	29.2	0.2	245.4	1.6	1.31	0.01
	RO1114-8_M86-1-5 7.9m	790	1.4	0.0	79.9	0.5	28.7	0.2	99.5	0.7	1.27	0.01
	RO1172-7_M86-1-5 810cm	810	2.4	0.0	77.5	0.5	27.8	0.2	174.2	1.2	1.30	0.01
	RO1172-8_M86-1-5 820cm	820	1.4	0.0	73.1	0.4	26.1	0.2	109.8	0.8	1.32	0.01
	RO1114-9_M86-1-5 8.3m	830	1.8	0.0	74.3	0.6	26.7	0.2	137.3	1.2	1.27	0.02
M86-1-06-1GC	**RO1190-1_M86-1-6 540cm**	540	1.1	0.0	85.1	0.5	30.9	0.2	69.3	0.5	1.17	0.01
	RO1195-2_M86-1-6 580cm	580	2.4	0.0	79.3	0.5	28.5	0.2	164.3	1.1	1.27	0.01
	RO1190-3_M86-1-6 590cm	590	2.5	0.0	72.6	0.4	26.0	0.2	194.4	1.4	1.31	0.01
	RO1195-4_M86-1-6 595cm	595	2.8	0.0	66.7	0.4	23.6	0.2	238.6	1.8	1.41	0.01
	RO1190-4_M86-1-6 600cm	600	1.7	0.0	70.0	0.4	24.6	0.2	134.7	1.0	1.45	0.01
	RO1190-5_M86-1-6 605cm	605	1.8	0.0	81.8	0.5	28.7	0.2	126.6	0.9	1.47	0.01
	RO1195-5_M86-1-6 610cm	610	2.2	0.0	65.8	0.4	22.9	0.1	193.0	1.4	1.55	0.01
	RO1190-7_M86-1-6 620cm	620	2.0	0.0	68.9	0.4	24.4	0.2	166.6	1.3	1.40	0.01
	RO1190-8_M86-1-6 630cm	630	3.4	0.0	63.6	0.4	22.2	0.1	300.3	2.2	1.51	0.01
	RO1190-9_M86-1-6 650cm	650	1.4	0.0	67.6	0.4	23.9	0.2	113.1	0.8	1.42	0.01
	RO1195-6_M86-1-6 660cm	660	2.2	0.0	65.0	0.4	22.7	0.2	192.0	1.4	1.54	0.01
P435/1-5GC	**RO1078-8_P435/1-5GC 720cm**	720	0.4	0.0	65.5	0.6	20.3	0.2	42.2	0.4	2.67	0.03
	RO1034-3_P435/1-5GC 8m	800	0.4	0.0	54.4	0.4	17.1	0.1	52.3	0.5	2.54	0.03
	RO1111-4_P435/1-5GC 880cm	880	0.6	0.0	53.3	0.4	17.2	0.2	64.7	0.7	2.25	0.03
	RO1087-5_P435/1-5GC 940cm	940	0.6	0.0	51.5	0.4	16.4	0.1	67.7	0.7	2.42	0.03
	RO968-3_P435/1-5 10m	1000	0.7	0.0	50.6	0.4	16.1	0.1	83.4	0.8	2.43	0.03
Surface samples	**EMB046/20-2 (map code 1)**	0.5-1	0.8	0.0	165.5	0.8	61.3	0.3	26.2	0.2	1.01	0.01
	318320-2 (map code 2)	0	3.5	0.0	61.4	0.3	21.1	0.1	330.4	1.7	1.67	0.01
	P435/10-2 MUC 1AW (map code 3)	0	0.9	0.0	117.1	1.0	37.9	0.3	46.8	0.4	2.24	0.03

Table 4.3: Radiocarbon samples analysed from the Skagerrak cores, showing raw ^{14}C ages and calibrated ages. A reservoir correction of ΔR = -150 years is used for all dates.

Sample	Depth (cm)	^{14}C age	Error	Material dated	1σ lower (cal BP)	1σ higher (cal BP)	2σ lower (cal BP)	2σ higher (cal BP)	Mid 1σ (cal BP)	Mid 2σ (cal BP)
M86-1-05-1GC	5.5	835	35	mix benthic forams	370	503	294	541	436.5	417.5
	145.5	2620	50	mix benthic forams	2211	2416	2116	2526	2313.5	2321
	300.75	3880	80	mix benthic forams	3724	3989	3613	4135	3856.5	3874
	450.75	6340	90	mix benthic forams	6634	6889	6493	7015	6761.5	6754
	690.75	9680	120	mix benthic forams	10415	10823	10268	11043	10619	10655.5
	760.75	10410	60	mix benthic forams	11524	11802	11382	11924	11663	11653
	834.75	11860	90	mix benthic forams	13218	13449	13109	13565	13333.5	13337
M86-1-07-1GC	625.5	9580	80	mix benthic forams	10334	10612	10221	10738	10473	10479.5
	669.5	10500	80	mix benthic forams	11636	11952	11463	12144	11794	11803.5
	710	12410	90	mix benthic forams	13807	14107	13683	14325	13957	14004
	735.5	11340	80	mix benthic forams	12719	12913	12652	13041	12816	12846.5
	810.5	12540	90	mix benthic forams	14006	14364	13828	14611	14185	14219.5
M86-1-06-1GC	590	10110	60	mollusc	11125	11318	11039	11479	11222	11259

Chapter 5: Conclusions and further work

This PhD study applies a multi-geochemical approach to look at tracking the glacial and oceanographic changes in response to changes in climate in two separate but comparatively similar palaeoceanographic locations of Baffin Bay and the Baltic Sea Basin. The results lead to an increased understanding of the dynamical response of ice sheets and sea to lake stages in these areas. Below, the final conclusions and key implications of each of the previous chapters are outlined as well as suggestions for future research.

5.1 Chapter 2: Ice sheet dynamics and glacial palaeoceanography of Baffin Bay for the last 40 kyrs: new insights from a multi-geochemical approach

Chapter 2 applied the use of several geochemical techniques including sedimentological characteristics, XRF, qXRD, REE, $^{187}Os/^{188}Os$ and radiocarbon analysis to further the understanding of the dynamic response of the ice sheets surrounding Baffin Bay in relation to changes in climate conditions and their synchronicity to each other.

The results of this research further constrain the timings of Baffin Bay detrital carbonate (BBDC) layers BBDC1 and BBDC0 found in sediment cores using the updated MARINE20 calibration curve to make a robust age-model chronology. The timing of these layers corresponds to the Bølling-Allerød and Older Dryas and the Younger Dryas, respectively. The geochemical signature of these layers (Ca, CaO, detrital carbonate, $^{187}Os/^{188}Os$ and REE patterns) indicate that the provenance of these sediments is not solely from the Palaeozoic carbonate outcrops covered by the IIS, and that ice sheet changes around the bay were not always synchronous. The data also suggest there is a radiogenic and felsic source synonymous with granites, granodiorites, gneisses and gabbros, typical of the geologies overlain by the GIS (west Greenland) at the time, although a Baffin Island source via the LIS cannot be fully ruled out. This study therefore suggests an extensive and dynamical response of both the IIS and GIS (and potentially LIS) to changes in climate, occurring more synchronously over BBDC1 in a warmer Bølling-Allerød climate, and asynchronously during BBDC0 over a cooler Younger Dryas climate.

5.2 Chapter 3: Postglacial palaeoceanography of the Baltic Sea Basin

Chapter 3 uses two new approaches to understand the late Pleistocene and Holocene history of Baltic Sea Basin recorded in basin sediment cores. These are the osmium isotope ratio ($^{187}Os/^{188}Os$) and BIT index (biomarker), coupled with XRF, diatom and sedimentology data. This approach was applied to be able to distinguish between the common sea to lake stages (Baltic Ice Lake, Yoldia Sea, Ancylus Lake, Littorina Sea) which has previously proven difficult in deeper basin sediment cores due to the lack of organic matter for dating and the absence of sand layers and other stratigraphic markers that allow differentiation in shallower settings. Several surface samples from the North Sea, Kattegat Bay, the Skagerrak Strait, the Danish Straits and within the Baltic Sea Basin were also analysed for their $^{187}Os/^{188}Os$ to determine the present-day composition of the area and how it changes in relation to salinity from marine to freshwater.

The surface sediment $^{187}Os/^{188}Os$ data show a positive correlation with salinity and prove that clear distinctions between the fresher-water Baltic Sea and an open marine setting exist, which can then be used to distinguish between past sea to lake stages. The data from core P435/1-5 GC show a clear transition into the freshwater Ancylus Lake stage and then from this into the brackish Littorina Sea stage up to the present day marked by a large magnitude change in $^{187}Os/^{188}Os$ and BIT index values, as well as the appearance of brackish diatoms. The transition from the Baltic Ice Lake into the Yoldia Sea however is not clearly depicted by these methods. The marine ingressions of the Yoldia Sea were small and short-lived, potentially not strong enough to influence the deeper basin waters or be within the residence times of the proxies used. This change therefore is only tentatively positioned in the core based on a probable change in conditions depicted by a set of contemporaneous changes in Re, $^{187}Os/^{188}Os$, BIT index, and K/Ti.

Although not wholly defining certain ephemeral events of the Baltic Basin (e.g., Yoldia Sea), combining present day surface data with past core records demonstrates that the $^{187}Os/^{188}Os$ record is capable of reconstructing drainage and inflow patterns of more restricted basins where exchanges between more marine and freshwater environments are more extensive and prolonged (e.g., Ancylus Lake stage). This is further discussed in Chapter 4.

5.3 Chapter 4: First evidence from the open Skagerrak of the absolute timing for the onset of Baltic Ice Lake drainage and evolution to the Baltic Sea since the LGM: Insights from radiocarbon ages, trace element and osmium geochemistry

Chapter 4 presents XRF, $^{187}Os/^{188}Os$ and biomarker data ($\%C_{37:4}$) for three cores in the central Skagerrak to show the first temporally constrained evidence for the final drainage of the Baltic Ice Lake in this area.

Several conclusions are drawn from the proxies presented. Firstly, $^{187}Os/^{188}Os$ and $\%C_{37:4}$ evidence agrees with the hypothesis that some amount of drainage from the Baltic Ice Lake was entering the Skagerrak before the main 'event', as early as 14 cal ka BP (age limit of this study). Secondly, the initial smaller drainage of the Baltic Ice Lake previously dated to have begun at 13 cal ka BP, before glacial readvance during the Younger Dryas, was not large enough to produce a visible detrital signature in the Skagerrak. Finally, and most importantly, combined, peaks in sand content, Ti/Ca, $\%C_{37:4}$, as well as lows in K/Ti, TIC alongside radiogenic $^{187}Os/^{188}Os$ values suggest a short-lived, high energy influx of freshwater into the Skagerrak, coincident in timing to the final catastrophic drainage of the Baltic Ice Lake. Hence, this data shows the first evidence of this drainage event recorded in the Skagerrak.

Additionally, this study also provides evidence adding to the debate of conservative versus non-conservative behaviour of osmium in estuarine environments. Osmium data from the central Skagerrak cores yields evidence for the conservative behaviour of osmium, increasing with increasing salinity.

5.4 Evaluation of proxies used

Throughout this thesis several different proxies have been used with the potential capabilities of differentiating between a marine and terrestrial source. The use of each has great benefits, especially when used in combination with other proxies, but there are still uncertainties to consider. The proxies used in this thesis include: $^{187}Os/^{188}Os$ ratios, biomarkers (BIT index and $\%C_{37:4}$) and XRF ratios.

The $^{187}Os/^{188}Os$ ratio can detect differences between older continental input, mantle/hydrothermal input, and open ocean input (Peucker-Ehrenbrink & Jahn, 2001; Peucker-Ehrenbrink & Ravizza, 2000). This has also been shown throughout the three study chapters in this thesis. The $^{187}Os/^{188}Os$ values show increased continental input

in Baffin Bay cores, the drainage of the Baltic Ice Lake into the Skagerrak, and are able to distinguish between some of the more freshwater vs brackish-marine water stages in the Baltic Sea basin. Whilst able to pick out large differences, the $^{187}Os/^{188}Os$ proxy seems less able to detect much weaker, short-lived influxes, for example with the marine incursion during the Yoldia Sea stage discussed in Chapter 3. It is also less able to distinguish between continuous influxes, for example, radiogenic $^{187}Os/^{188}Os$ is detected in the Skagerrak before the main Baltic Ice Lake drainage is thought to have occurred due to general outwash from the Baltic through other channels, so a continuously radiogenic record is shown over the whole time period, rather than something separate for when the drainage occurs.

The biomarker proxies of BIT index and $\%C_{37:4}$ were used in Chapters 3 and 4, respectively. The BIT index varies between 0 (marine environment) and 1 (terrestrial environment; Kim et al., 2006; Sinninghe Damsté et al., 2002). The BIT index has been useful in helping to identify some of the changes in the Baltic Sea stages recorded in the central Baltic Sea core, for example, higher values during the freshwater Ancylus Lake stage and values close to zero during the brackish Littorina Sea stage. However, the BIT index data still fluctuates considerably. This may be due to the fact that the terrestrial biomarkers associated with higher BIT values can also be produced (Warden et al., 2018 and references therein). Further, occurrences of the marine biomarker have also been found in river water (Kim et al., 2006). Therefore the BIT index, on its own, in the case of the central Baltic Sea (Chapter 3) does not provide a strong enough proxy to draw solid conclusions, however, when combined with other proxies it can aid in interpretations about the environment. The $\%C_{37:4}$ biomarker indicator is used to show the presence of lower surface salinities and hence the input of freshwater into the area (Bendle et al., 2005; Moros et al., 2016; Rosell-Melé, 1998; Rosell-Melé et al., 2002; Sicre et al., 2002), so is an indirect indicator of marine vs. terrestrial inputs. The analysis was undertaken on the deeper portion of a core from the Skagerrak (Chapter 4). In this case, it appears to be an effective proxy, showing an increase in values, and hence increased freshwater input, over the time considered to be the final drainage of the Baltic Ice Lake, and is also concurrent with other proxies used in that study, e.g., sand content and Ti/Ca. However, only one of the cores underwent $\%C_{37:4}$ biomarker analysis, and it was not for the whole length of the core. The other two cores from the Skagerrak should also be analysed for $\%C_{37:4}$ biomarkers to provide comparison, and the shallower portions of the cores should also be analysed

to confirm that the higher values recorded over the Baltic Ice Lake drainage are unique to that event, and the $\%C_{37:4}$ values remain lower for the rest of the core.

XRF ratios are also capable proxies between marine and terrestrial sources. The Ti/Ca ratio is an example of this, with higher values thought to represent more terrestrial inputs due to increased Ti, and lower values due to marine biogenic production of Ca (Rothwell & Croudace, 2015). However, in the Skagerrak cores (Chapter 4), the increase in Ti/Ca over the drainage of the Baltic Ice Lake is not due to increased Ti, but due to a decrease in Ca. This is because fine grained Baltic Ice Lake sediments have a high carbonate content (Bennike & Jensen, 2013; Gyllencreutz, 2005; Kögler & Larsen, 1979; Moros et al., 2002), and in a high energy environment, such as a sudden drainage event, these finer grained sediments cannot be deposited. This therefore shows that XRF ratios can be extremely useful, but care should be taken as there are a number of different factors that can affect how the ratio changes.

All of the proxies used in this PhD, on their own, have merit but also have uncertainties. However, when combined, the uncertainties become lower, and stronger conclusions can be made.

5.5 Future work

A multi-geochemical approach provides a strong method to help understand the glacial dynamics of northern hemisphere glaciated and marine influenced localities. However, there are still several limitations in terms of time constraints and interpretation of results.

For the study of JR175 in Baffin Bay and P435/1-5 GC in the central Baltic Sea, newer proxies were used, where no, or only small amounts of data have been previously collected in the studied areas, for example $^{187}Os/^{188}Os$, $\%C_{37:4}$, and BIT index analysis. This new data therefore provides new understandings of the glacial dynamics in the areas as described above, and to further these studies, similar analysis of cores at more localities within the study sites would be ideal to provide further data and comparison.

Numerous cores have been analysed in central Baffin Bay, however core JR175 is the first long core record of $^{187}Os/^{188}Os$ data in the centre. A $^{187}Os/^{188}Os$ record from a core in Disko Bugt and southern Davis Strait (Knutz et al., 2011; Rooney et al., 2016) is immensely helpful by providing some comparison. Taking this research forward,

the same set of multi-geochemical techniques applied to JR175 can be applied further to more cores from around Baffin Bay. For example, an east to west transect of cores ranging from the margin of west Greenland, through the centre of Baffin Bay to the margin of Baffin Island would provide a more in-depth picture of past glacial dynamics across the whole of Baffin Bay and could potentially help differentiate further between a west Greenland and Baffin Island provenance, which has long been proved difficult. This same east to west transect could then also be undertaken at a more northern positioning in Baffin Bay (closer to the IIS and Palaeozoic carbonate source), and from a more southern positioning closer to the Davis Strait, to assess if the influence of the detrital carbonate Ca-rich layers and the $^{187}Os/^{188}Os$ peaks change in strength over a north to east transect, again providing more information as to a provenance of the sediments.

A similar situation exists for the central Baltic Sea, only one core, P435/1-5 GC was analysed. Long core $^{187}Os/^{188}Os$ records from the Baltic Sea have not previously been analysed, and the BIT index is also a new application. Some Mn crusts/nodules and surface runoff samples have been previously measured to ascertain the present-day $^{187}Os/^{188}Os$ composition (Peucker-Ehrenbrink & Ravizza, 1996). Multiple cores for comparison and correlation across a sub-basin or multiple basins could provide further evidence that the changes seen are not just specific to one core and could help identify further changes relating to the transitions between the sea stages of the Baltic Ice Lake and the Yoldia Sea which proved difficult (see Chapter 3). This could also be taken further by analysing terrestrial core records, for example an east to west transect across south-central Sweden to further assess the connectivity between the Baltic Sea Basin and the Skagerrak, and then potentially through the Danish Straits.

The application of $^{187}Os/^{188}Os$ to more restricted basins such as the Baltic Sea Basin to determine periods of connection and isolation from an open marine source could be further applied to other basins and restricted seas. This has already been applied to the Mediterranean Sea (Kuroda et al., 2016), but could be applied further to for example, the Black Sea (Ravizza et al., 1991) and the Caspian Sea (Aghayeva et al., 2021; Washburn et al., 2019).

References

Aghayeva, V., Sachsenhofer, R. F., van Baak, C. G. C., Bechtel, A., Hoyle, T. M., Selby, D., Shiyanova, N., & Vincent, S. J. (2021). New Geochemical Insights Into Cenozoic Source Rocks in Azerbaijan: Implications for Petroleum Systems in the South Caspian Region. *Journal of Petroleum Geology*, *44*(3), 349–384. https://doi.org/10.1111/jpg.12797

Aksu, A. E., & Piper, D. J. W. (1987). Late Quaternary sedimentation in Baffin Bay. *Canadian Journal of Earth Sciences*, *24*(9), 1833–1846. https://doi.org/10.1139/e87-174

Aksu, A. E., & Piper, D. J. W. (1979). Baffin Bay in the past 100,000 yr. *Geology*, *7*(5), 245–248. https://doi.org/10.1130/0091-7613(1979)7<245:BBITPY>2.0.CO;2

Andrén, E., Andrén, T., & Kunzendorf, H. (2000). Holocene history of the Baltic Sea as a background for assessing records of human impact in the sediments of the Gotland Basin. *Holocene*, *10*(6), 687–702. https://doi.org/10.1191/09596830094944

Andrén, T., Björck, S., Andrén, E., Conley, D., Zillén, L., & Anjar, J. (2011). The Baltic Sea Basin. In J. Harff, S. Björck, & P. Hoth (Eds.), *The Baltic Sea Basin* (1st ed.). Springer Berlin Heidelberg. https://doi.org/10.1007/978-3-642-17220-5

Andrén, T., Jørgensen, B. B., Cotterill, C., Green, S., Andrén, E., Ash, J., Bauersachs, T., Cragg, B., Fanget, A.-S., Fehr, A., Granoszewski, W., Groeneveld, J., Hardisty, D., Herrero-Bervera, E., Hyttinen, O., Jensen, J. B., Johnson, S., Kenzler, M., Kotilainen, A., … Zhang, R. (2015). *Expedition 347 summary*. *347*. https://doi.org/10.2204/iodp.proc.347.101.2015

Andrén, T., Lindeberg, G., & Andrén, E. (2008). Evidence of the final drainage of the Baltic Ice Lake and the brackish phase of the Yoldia Sea in glacial varves from the Baltic Sea. *Boreas*, *31*(3), 226–238. https://doi.org/10.1111/j.1502-3885.2002.tb01069.x

Andrews, J. T. (1987). Late Quaternary Marine Sediment Accumulation in Fiord-Shelf-Deep-sea Transects, Baffin Island to Baffin Bay. *Quaternary Science Reviews*, *6*, 231–243.

Andrews, J. T., Bjork, A. A., Eberl, D. D., Jennings, A. E., & Verplanck, E. P. (2015). Significant differences in late Quaternary bedrock erosion and transport: East versus West Greenland ~70°N - evidence from the mineralogy of offshore glacial marine sediments. *Journal of Quaternary Science*, *30*(5), 452–463. https://doi.org/10.1002/jqs.2787

Andrews, J. T., & Eberl, D. D. (2011). Surface (sea floor) and near-surface (box cores) sediment mineralogy in Baffin Bay as a key to sediment provenance and ice sheet variations. *Canadian Journal of Earth Sciences*, *48*(9), 1307–1328. https://doi.org/10.1139/e11-021

Andrews, J. T., Gibb, O. T., Jennings, A. E., & Simon, Q. (2014). Variations in the provenance of sediment from ice sheets surrounding Baffin Bay during MIS 2 and 3 and export to the Labrador Shelf Sea: Site HU2008029-0008 Davis Strait. *Journal of Quaternary Science*, *29*(1), 3–13. https://doi.org/10.1002/jqs.2643

Andrews, J. T., Jennings, A. E., MacLean, B., Mudie, P. J., Praeg, D., & Vilks, G. (1991). The surficial geology of the Canadian eastern Arctic and Polar continental shelves. *Continental Shelf Research*, *11*(8–10), 791–819. https://doi.org/10.1016/0278-4343(91)90080-P

Andrews, J. T., Kirby, M. E., Aksu, A. E., Barber, D. C., & Meese, D. (1998). Late quaternary detrital carbonate (DC-) layers in Baffin Bay marine sediments (67°-74°N): Correlation with Heinrich events in the North Atlantic? *Quaternary Science Reviews*, *17*(12), 1125–1137. https://doi.org/10.1016/S0277-3791(97)00064-4

Andrews, J. T., Klein, A. J., Jenner, K. A., Jennings, A. E., & Campbell, C. (2018). The variability of Baffin Bay seafloor sediment mineralogy: The identification of discrete glacial sediment sources and application to Late Quaternary downcore analysis. *Canadian Journal of Earth Sciences*, *55*(6), 620–639. https://doi.org/10.1139/cjes-2017-0223

Andrews, J. T., Osterman, L. E., Jennings, A. E., Syvitski, J. P. M., Miller, G. H., & Weiner, N. (1996). Abrupt changes in marine conditions, Sunneshine Fiord, eastern Baffin Island, NWT during the last deglacial transition: Younger Dryas and H-0 events. *Geological Society Special Publication*, *111*(111), 11–27. https://doi.org/10.1144/GSL.SP.1996.111.01.03

Andrews, J. T., & Syvitski, J. P. M. (1994). Sediment Fluxes Along High-Latitude Continental Margins Northeast Canada and Eastern Greenland. In *Material Fluxes on the Surface of The Earth* (pp. 99–115). Ntional Academy Press, Washington, D.C.

Andrews, J. T., & Voelker, A. H. L. (2018). "Heinrich events" (& sediments): A history of terminology and recommendations for future usage. *Quaternary Science Reviews*, *187*, 31–40. https://doi.org/10.1016/j.quascirev.2018.03.017

Arz, H. W. (2011). *Short Cruise Report RV Meteor M86-1A*. https://fdir.brage.unit.no/fdir-xmlui/bitstream/handle/11250/2356609/110524.pdf?sequence=1&isAllowed=y

Baldini, L. M., McDermott, F., Baldini, J. U. L., Arias, P., Cueto, M., Fairchild, I. J., Hoffmann, D. L., Mattey, D. P., Müller, W., Nita, D. C., Ontañón, R., Garciá-Moncó, C., & Richards, D. A. (2015). Regional temperature, atmospheric circulation, and sea-ice variability within the Younger Dryas Event constrained using a speleothem from northern Iberia. *Earth and Planetary Science Letters*, *419*, 101–110. https://doi.org/10.1016/j.epsl.2015.03.015

Bamber, J., Van Den Broeke, M., Ettema, J., Lenaerts, J., & Rignot, E. (2012). Recent large increases in freshwater fluxes from Greenland into the North Atlantic. *Geophysical Research Letters*, *39*(19), 8–11. https://doi.org/10.1029/2012GL052552

Bendle, J., Rosell-Melé, A., & Ziveri, P. (2005). Variability of unusual distributions of alkenones in the surface waters of the Nordic seas. *Paleoceanography*, *20*(2), 1–15. https://doi.org/10.1029/2004PA001025

Bennike, O., & Jensen, J. B. (1995). Near-shore Baltic Ice Lake deposits in Fakse Bugt, southeast Denmark. *Boreas*, *24*(3), 185–195. https://doi.org/10.1111/j.1502-3885.1995.tb00772.x

Bennike, O., & Jensen, J. B. (2013). A Baltic Ice Lake lowstand of latest Allerød age in the Arkona basin, southern Baltic sea. *Geological Survey of Denmark and Greenland Bulletin*, *28*, 17–20. https://doi.org/10.34194/geusb.v28.4710

Bennike, O., Jensen, J. B., Nørgaard-Pedersen, N., Andresen, K. J., Seidenkrantz, M. S., Moros, M., & Wagner, B. (2021). When were the straits between the Baltic Sea and the Kattegat inundated by the sea during the Holocene? *Boreas*, *Munthe 1887*. https://doi.org/10.1111/bor.12525

Berglund, B. E., Sandgren, P., Barnekow, L., Hannon, G., Jiang, H., Skog, G., & Yu, S. Y. (2005). Early Holocene history of the Baltic Sea, as reflected in coastal sediments in Blekinge, southeastern Sweden. *Quaternary International*, *130*(1), 111–139. https://doi.org/10.1016/j.quaint.2004.04.036

Bergsten, H., & Nordberg, K. (1992). Late Weichselian marine stratigraphy of the southern Kattegat, Scandinavia: evidence for drainage of the Baltic Ice Lake between 12,700 and 10,300 years BP. *Boreas*, *21*(3), 223–252. https://doi.org/10.1111/j.1502-3885.1992.tb00030.x

Bhatia, M. R., & Crook, K. A. W. (1986). Trace element characteristics of graywackes and tectonic setting discrimination of sedimentary basins. *Contributions to Mineralogy and Petrology*, *92*(2), 181–193. https://doi.org/10.1007/BF00375292

Björck, S. (1995). A review of the history of the Baltic Sea, 13.0-8.0 ka BP. *Quaternary International*, *27*, 19–40. https://doi.org/10.1016/1040-6182(94)00057-C

Blaauw, M., & Christen, J. A. (2011). Flexible paleoclimate age-depth models using an autoregressive gamma process. *Bayesian Analysis*, *6*(3), 457–474. https://doi.org/10.1214/11-BA618

Blott, S. J., & Pye, K. (2001). Gradistat: A grain size distribution and statistics package for the analysis of unconsolidated sediments. *Earth Surface Processes and Landforms*, *26*(11), 1237–1248. https://doi.org/10.1002/esp.261

Bodén, P., Fairbanks, R. G., Wright, J. D., & Burckle, L. H. (1997). High-resolution stable isotope records from southwest Sweden: The drainage of the Baltic Ice Lake and Younger Dryas Ice Margin Oscillations. *Paleoceanography*, *12*(1), 39–49. https://doi.org/10.1029/96PA02879

Bøe, R., Rise, L., Thorsnes, H., de Haas, H., Sæther, H., & Kunzendorf, H. (1996). Sea-bed sediments and sediment accumulation rates in the Norwegian part of the Skagerrak. *Geological Survey of Norway Bulletin*, *430*, 75–84.

Briner, J. P., Håkansson, L., & Bennike, O. (2013). The deglaciation and neoglaciation of upernavik isstrøm, greenland. *Quaternary Research (United States)*, *80*(3), 459–467. https://doi.org/10.1016/j.yqres.2013.09.008

Briner, J. P., Miller, G. H., Davis, P. T., Bierman, P. R., & Caffee, M. (2003). Last glacial maximum ice sheet dynamics in Arctic Canada inferred from young erratics perched on ancient tors. *Quaternary Science Reviews*, *22*(5–7), 437–444. https://doi.org/10.1016/S0277-3791(03)00003-9

Briner, J. P., Miller, G. H., Davis, P. T., & Finkel, R. C. (2006). Cosmogenic radionuclides from fiord landscapes support differential erosion by overriding ice sheets. *Bulletin of the Geological Society of America*, *118*(3–4), 406–420. https://doi.org/10.1130/B25716.1

Brouard, E., & Lajeunesse, P. (2017). Maximum extent and decay of the Laurentide Ice Sheet in Western Baffin Bay during the Last glacial episode. *Scientific Reports*, *7*(1), 1–8. https://doi.org/10.1038/s41598-017-11010-9

Burton, K. W., Bourdon, B., Birck, J. L., Allègre, C. J., & Hein, J. R. (1999). Osmium isotope variations in the oceans recorded by Fe-Mn crusts. *Earth and Planetary Science Letters*, *171*(1), 185–197. https://doi.org/10.1016/S0012-821X(99)00139-9

Burton, K. W., Gannoun, A., Birck, J. L., Allègre, C. J., Schiano, P., Clocchiatti, R., & Alard, O. (2002). The compatibility of rhenium and osmium in natural olivine and their behaviour during mantle melting and basalt genesis. *Earth and Planetary Science Letters*, *198*(1–2), 63–76. https://doi.org/10.1016/S0012-821X(02)00518-6

Burton, K. W., Gannoun, A., & Parkinson, I. J. (2010). Climate driven glacial-interglacial variations in the osmium isotope composition of seawater recorded by planktic foraminifera. *Earth and Planetary Science Letters*, *295*(1–2), 58–68. https://doi.org/10.1016/j.epsl.2010.03.026

CDM. (2021). *When Were the Ice Ages and Why Are They Called That?* https://www.cdm.org/mammothdiscovery/wheniceages.html

Chauché, N., Hubbard, A., Gascard, J. C., Box, J. E., Bates, R., Koppes, M., Sole, A., Christoffersen, P., & Patton, H. (2014). Ice-ocean interaction and calving front morphology at two west Greenland tidewater outlet glaciers. *Cryosphere*, *8*(4), 1457–

1468. https://doi.org/10.5194/tc-8-1457-2014

Chen, C., Sedwick, P. N., & Sharma, M. (2009). Anthropogenic osmium in rain and snow reveals global-scale atmospheric contamination. *Proceedings of the National Academy of Sciences of the United States of America*, *106*(19), 7724–7728. https://doi.org/10.1073/pnas.0811803106

Clark, P. U., Alley, R. B., & Pollard, D. (1999). Northern hemisphere ice-sheet influences on global climate change. *Science*, *286*(5442), 1104–1111. https://doi.org/10.1126/science.286.5442.1104

Clark, P. U., Dyke, A. S., Shakun, J. D., Carlson, A. E., Clark, J., Wohlfarth, B., Mitrovica, J. X., Hostetler, S. W., & McCabe, A. M. (2009). The Last Glacial Maximum. *Science*, *325*(5941), 710–714. https://doi.org/10.1126/science.1172873

Cohen, A. S. (2004). The rhenium-osmium isotope system: Applications to geochronological and palaeoenvironmental problems. *Journal of the Geological Society*, *161*(4), 729–734. https://doi.org/10.1144/0016-764903-084

Cohen, A. S., Coe, A. L., Bartlett, J. M., & Hawkesworth, C. J. (1999). Precise Re-Os ages of organic-rich mudrocks and the Os isotope composition of Jurassic seawater. *Earth and Planetary Science Letters*, *167*(3–4), 159–173. https://doi.org/10.1016/S0012-821X(99)00026-6

Croudace, I. W., Rindby, A., & Rothwell, R. G. (2006). ITRAX: Description and evaluation of a new multi-function X-ray core scanner. *Geological Society Special Publication*, *267*, 51–63. https://doi.org/10.1144/GSL.SP.2006.267.01.04

De Jonge, C., Stadnitskaia, A., Cherkashov, G., & Sinninghe Damsté, J. S. (2016). Branched glycerol dialkyl glycerol tetraethers and crenarchaeol record post-glacial sea level rise and shift in source of terrigenous brGDGTs in the Kara Sea (Arctic Ocean). *Organic Geochemistry*, *92*, 42–54. https://doi.org/10.1016/j.orggeochem.2015.11.009

Demina, L. L., Novichkova, K. A., Lisitzin, A. P., & Kozina, N. V. (2019). Geochemical signatures of paleoclimate changes in the sediment cores from the gloria and snorri drifts (Northwest atlantic) over the holocene-mid pleistocene. *Geosciences (Switzerland)*, *9*(10). https://doi.org/10.3390/geosciences9100432

Dickens, A. W. (2013). *Late Quaternary palaeoceanographic evolution in the Skagerrak, north eastern North Sea* [Durham University]. http://etheses.dur.ac.uk/6934/

Dickin, A. P. (2018). *Radiogenic Isotope Geology* (3rd ed.). Cambridge University Press. https://doi.org/10.1017/9781316163009

Diekmann, B., Hofmann, J., Henrich, R., Fütterer, D. K., Röhl, U., & Wei, K. Y. (2008). Detrital sediment supply in the southern Okinawa Trough and its relation to sea-level and Kuroshio dynamics during the late Quaternary. *Marine Geology*, *255*(1–2), 83–95. https://doi.org/10.1016/j.margeo.2008.08.001

Du Vivier, A. D. C., Selby, D., Sageman, B. B., Jarvis, I., Gröcke, D. R., & Voigt, S. (2014). Marine 187Os/188Os isotope stratigraphy reveals the interaction of volcanism and ocean circulation during Oceanic Anoxic Event 2. *Earth and Planetary Science Letters*, *389*, 23–33. https://doi.org/10.1016/j.epsl.2013.12.024

Ducrotoy, J., & Elliott, M. (2008). The science and management of the North Sea and the Baltic Sea: Natural history, present threats and future challenges. *Marine Pollution Bulletin*, *57*(1–5), 8–21. https://doi.org/10.1016/j.marpolbul.2008.04.030

Dutton, J. W. R., Jefferies, D. F., Folkard, A. R., & Jones, P. G. W. (1973). Trace metals in the North Sea. *Marine Pollution Bulletin*, *4*(9), 135–138. https://doi.org/10.1016/0025-326X(73)90007-6

Dyke, A. S., Andrews, J. T., Clark, P. U., England, J., Miller, G. H., Shaw, J., & Veillette, J. J. (2002). The Laurentide and Innuitian ice sheets during the Last Glacial Maximum. *Quaternary Science Reviews*, *21*(1–3), 9–31. https://doi.org/10.1016/S0277-3791(01)00095-6

Eberl, D. D. (2003). User's guide to RockJock - A program for determining quantitative mineralogy from powder X-ray diffraction data. *U.S. Geological Survey Open File Report 2003-78*. https://doi.org/10.3133/ofr200378

Enderlin, E. M., Howat, I. M., Jeong, S., Noh, M.-J., van Angelen, J. H., & van den Broeke, M. R. (2014). An improved mass budget for the Greenland ice sheet. *Geophysical Research Letters*, *41*(3), 866–872. https://doi.org/10.1002/2013GL059010

England, J. (1999). Coalescent Greenland and Innuitian ice during the Last Glacial Maximum: Revising the Quaternary of the Canadian High Arctic. *Quaternary Science Reviews*, *18*(3), 421–456. https://doi.org/10.1016/S0277-3791(98)00070-5

England, J., Atkinson, N., Bednarski, J., Dyke, A. S., Hodgson, D. A., & Ó Cofaigh, C. (2006). The Innuitian Ice Sheet: configuration, dynamics and chronology. *Quaternary Science Reviews*, *25*(7–8), 689–703. https://doi.org/10.1016/j.quascirev.2005.08.007

Erbs-Hansen, D. R., Knudsen, K. L., Gary, A. C., Jansen, E., Gyllencreutz, R., Scao, V., & Lambeck, K. (2011). Late Younger Dryas and early Holocene palaeoenvironments in the Skagerrak, eastern North Atlantic: A multiproxy study. *Boreas*, *40*(4), 660–680. https://doi.org/10.1111/j.1502-3885.2011.00205.x

Esser, B. K., & Turekian, K. K. (1993). The osmium isotopic composition of the continental crust. *Geochimica et Cosmochimica Acta*, *57*(13), 3093–3104. https://doi.org/10.1016/0016-7037(93)90296-9

Etourneau, J., Schneider, R., Blanz, T., & Martinez, P. (2010). Intensification of the Walker and Hadley atmospheric circulations during the Pliocene-Pleistocene climate transition. *Earth and Planetary Science Letters*, *297*(1–2), 103–110. https://doi.org/10.1016/j.epsl.2010.06.010

Faure, G. (1986). *Principles of Isotope Geology*. Wiley: New York.

Feyling-Hanssen, R. W. (1964). Foraminifera in Late Quatenary deposits from Oslofjord area. *Norges Geologiske Undersøkelse*, *225*, 1–383.

Finlay, A. J., Selby, D., & Gröcke, D. R. (2010). Tracking the Hirnantian glaciation using Os isotopes. *Earth and Planetary Science Letters*, *293*(3–4), 339–348. https://doi.org/10.1016/j.epsl.2010.02.049

Furze, M. F. A., Pieńkowski, A. J., McNeely, M. A., Bennett, R., & Cage, A. G. (2018). Deglaciation and ice shelf development at the northeast margin of the Laurentide Ice Sheet during the Younger Dryas chronozone. *Boreas*, *47*(1), 271–296. https://doi.org/10.1111/bor.12265

Gannoun, A., & Burton, K. W. (2014). High precision osmium elemental and isotope measurements of North Atlantic seawater. *Journal of Analytical Atomic Spectrometry*, *29*(12), 2330–2342. https://doi.org/10.1039/c4ja00265b

Gottschalk, J., Szidat, S., Michel, E., Mazaud, A., Salazar, G., Battaglia, M., Lippold, J., & Jaccard, S. L. (2018). Radiocarbon measurements of small-size foraminiferal samples with the mini carbon dating system (MICADAS) at the University of bern: Implications for paleoclimate reconstructions. *Radiocarbon*, *60*(2), 469–491. https://doi.org/10.1017/RDC.2018.3

Grootes, P. M., & Stuiver, M. (1997). Time Resolution in Accumulated the. *Journal of Geophysical Research*, *102*(C12), 26,455-26,470.

Gyllencreutz, R. (2005). Late Glacial and Holocene paleoceanography in the Skagerrak from high-resolution grain size records. *Palaeogeography, Palaeoclimatology, Palaeoecology*, *222*(3–4), 344–369. https://doi.org/10.1016/j.palaeo.2005.03.025

Harrison, J. C., St-Onge, M. R., Petrov, O. V., Strelnikov, S. I., Lopatin, B. G., Wilson, F. H., Tella, S., Paul, D., Lynds, T., Shokalsky, S. P., Hults, C. K., Bergman, S., Jepsen, H. F., & Solli, A. (2011). Geological map of the Arctic. *Geological Survey of Canada*, *Map 2159A,*.

Heaton, T. J., Köhler, P., Butzin, M., Bard, E., Reimer, R. W., Austin, W. E. N., Bronk Ramsey, C., Grootes, P. M., Hughen, K. A., Kromer, B., Reimer, P. J., Adkins, J., Burke, A., Cook, M. S., Olsen, J., & Skinner, L. C. (2020). Marine20 - The Marine Radiocarbon Age Calibration Curve (0-55,000 cal BP). *Radiocarbon*, *62*(4), 779–820. https://doi.org/10.1017/RDC.2020.68

Heier-Nielsen, S., Heinemeier, J., Nielsen, H. L., & Rud, N. (1995). Recent Reservoir Ages for Danish Fjords and Marine Waters. *Radiocarbon*, *37*(3), 875–882. https://doi.org/10.1017/S0033822200014958

Hepp, D. A., Mörz, T., & Grützner, J. (2006). Pliocene glacial cyclicity in a deep-sea sediment drift (Antarctic Peninsula Pacific Margin). *Palaeogeography, Palaeoclimatology, Palaeoecology*, *231*(1–2), 181–198. https://doi.org/10.1016/j.palaeo.2005.07.030

Hiscott, R. N., Aksu, A. E., & Nielsen, O. B. (1989). Provenance and dispersal patterns, Pliocene-Pleistocene section at Site 645, Baffin Bay. *Proc., Scientific Results, ODP, Leg 105, Baffin Bay and Labrador Sea*, *105*, 31–52. https://doi.org/10.2973/odp.proc.sr.105.117.1989

Hopmans, E. C., Schouten, S., & Sinninghe Damsté, J. S. (2016). The effect of improved chromatography on GDGT-based palaeoproxies. *Organic Geochemistry*, *93*, 1–6. https://doi.org/10.1016/j.orggeochem.2015.12.006

Hudson, B., Overeem, I., McGrath, D., Syvitski, J. P. M., Mikkelsen, A., & Hasholt, B. (2014). MODIS observed increase in duration and spatial extent of sediment plumes in Greenland fjords. *Cryosphere*, *8*(4), 1161–1176. https://doi.org/10.5194/tc-8-1161-2014

Huguet, C., Hopmans, E. C., Febo-Ayala, W., Thompson, D. H., Sinninghe Damsté, J. S., & Schouten, S. (2006). An improved method to determine the absolute abundance of glycerol dibiphytanyl glycerol tetraether lipids. *Organic Geochemistry*, *37*(9), 1036–1041. https://doi.org/10.1016/j.orggeochem.2006.05.008

Hyttinen, O., Eskola, K. O., Kaakinen, A., & Salonen, V. P. (2014). First direct age determination for the Baltic Ice Lake/Yoldia Sea transition in Finland. *Gff*, *136*(2), 398–405. https://doi.org/10.1080/11035897.2013.813581

Jackson, R., Carlson, A. E., Hillaire-Marcel, C., Wacker, L., Vogt, C., & Kucera, M. (2017). Asynchronous instability of the North American-Arctic and Greenland ice sheets during the last deglaciation. *Quaternary Science Reviews*, *164*, 140–153. https://doi.org/10.1016/j.quascirev.2017.03.020

Jakobsson, M., Björck, S., Alm, G., Andrén, T., Lindeberg, G., & Svensson, N. O. (2007). Reconstructing the Younger Dryas ice dammed lake in the Baltic Basin: Bathymetry, area and volume. *Global and Planetary Change*, *57*(3–4), 355–370. https://doi.org/10.1016/j.gloplacha.2007.01.006

Jakobsson, M., Mayer, L., Coakley, B., Dowdeswell, J. A., Forbes, S., Fridman, B., Hodnesdal, H., Noormets, R., Pedersen, R., Rebesco, M., Schenke, H. W., Zarayskaya, Y., Accettella, D., Armstrong, A., Anderson, R. M., Bienhoff, P., Camerlenghi, A., Church, I., Edwards, M., … Weatherall, P. (2012). The International Bathymetric Chart of the Arctic Ocean (IBCAO) Version 3.0. *Geophysical Research Letters*, *39*(12), 1–6.

https://doi.org/10.1029/2012GL052219

Jennings, A. E., Andrews, J. T., Ó Cofaigh, C., Onge, G. S., Sheldon, C., Belt, S. T., Cabedo-Sanz, P., & Hillaire-Marcel, C. (2017). Ocean forcing of Ice Sheet retreat in central west Greenland from LGM to the early Holocene. *Earth and Planetary Science Letters*, *472*(August), 1–13. https://doi.org/10.1016/j.epsl.2017.05.007

Jennings, A. E., Andrews, J. T., Ó Cofaigh, C., St-Onge, G., Belt, S., Cabedo-Sanz, P., Pearce, C., Hillaire-Marcel, C., & Calvin Campbell, D. (2018a). Baffin Bay paleoenvironments in the LGM and HS1: Resolving the ice-shelf question. *Marine Geology*, *402*(September 2017), 5–16. https://doi.org/10.1016/j.margeo.2017.09.002

Jennings, A. E., Andrews, J. T., Ó Cofaigh, C., St-Onge, G., Belt, S. T., Cabedo-Sanz, P., Pearce, C., Hillaire-Marcel, C., & Calvin Campbell, D. (2018b). Baffin Bay paleoenvironments in the LGM and HS1: Resolving the ice-shelf question. *Marine Geology*, *402*(August 2017), 5–16. https://doi.org/10.1016/j.margeo.2017.09.002

Jennings, A. E., Sheldon, C., Cronin, T. M., Francus, P., Stoner, J., & Andrews, J. (2011). The holocene history of nares strait. *Oceanography*, *24*(3), 26–41. https://doi.org/10.5670/oceanog.2011.52

Jennings, A. E., Walton, M. E., Ó Cofaigh, C., Kilfeather, A., Andrews, J. T., Ortiz, J. D., De Vernal, A., & Dowdeswell, J. A. (2014). Paleoenvironments during Younger Dryas-Early Holocene retreat of the Greenland Ice Sheet from outer Disko Trough, central west Greenland. *Journal of Quaternary Science*, *29*(1), 27–40. https://doi.org/10.1002/jqs.2652

Jiang, H., Björck, S., & Knudsen, K. L. (1997). A palaeoclimatic and palaeoceanographic record of the last 11 000 14C years from the Skagerrak-Kattegat, northeastern Atlantic margin. *Holocene*, *7*(3), 301–310. https://doi.org/10.1177/095968369700700306

Johnsen, S. J., Clausen, H. B., Dansgaard, W., Gundestrup, N. S., Hammer, C. U., Andersen, U., Andersen, K. K., Hvidberg, C. S., Dahl-Jensen, D., Steffensen, J. P., Shoji, H., Sveinbjörnsdóttir, Á. E., White, J., Jouzel, J., & Fisher, D. (1997). The δ 18 O record along the Greenland Ice Core Project deep ice core and the problem of possible Eemian climatic instability. *Journal of Geophysical Research: Oceans*, *102*(C12), 26397–26410. https://doi.org/10.1029/97JC00167

Johnson, M. D., Ståhl, Y., Larsson, O., & Seger, S. (2010). New exposures of Baltic Ice Lake drainage sediments, Götene, Sweden. *Gff*, *132*(1), 1–12. https://doi.org/10.1080/11035891003597067

Kim, J., Schouten, S., Buscail, R., Ludwig, W., & Bonnin, J. (2006). *Validation study of terrestrial biomarker proxy (BIT index) in the Gulf of Lions (NW Mediterranean)*. *8*(2004).

Kirillova, V. (2017). *Radiogenic isotopes on marine sediments from the Baffin Bay: implications for the sediment supply during the last deglaciation*. Bremen University.

Knudsen, K. L., Conradsen, K., Heier-Nielsen, S., & Seidenkrantz, M. S. (1996). Palaeoenvironments in the Skagerrak-Kattegat basin in the eastern North Sea during the last deglaciation. *Boreas*, *25*(2), 65–78. https://doi.org/10.1111/j.1502-3885.1996.tb00836.x

Knutz, P. C., Sicre, M. A., Ebbesen, H., Christiansen, S., & Kuijpers, A. (2011). Multiple-stage deglacial retreat of the southern Greenland Ice Sheet linked with Irminger Current warm water transport. *Paleoceanography*, *26*(3), 1–18. https://doi.org/10.1029/2010PA002053

Knutz, P. C., Storey, M., & Kuijpers, A. (2013). Greenland iceberg emissions constrained by 40Ar/39Ar hornblende ages: Implications for ocean-climate variability during last

deglaciation. *Earth and Planetary Science Letters*, *375*, 441–449. https://doi.org/10.1016/j.epsl.2013.06.008

Kögler, F. C., & Larsen, B. (1979). The West Bornholm basin in the Baltic Sea: geological structure and Quaternary sediments. *Boreas*, *8*(1), 1–22. https://doi.org/10.1111/j.1502-3885.1979.tb00427.x

Kortekaas, M. (2007). Post-glacial history of sea-level and environmental change in the southern Baltic Sea. *Lundqua Thesis 57*, 1–34.

Krossa, V. R., Moros, M., Blanz, T., Jansen, E., & Schneider, R. (2015). Late Holocene Baltic Sea outflow changes reconstructed using C37:4 content from marine cores. *Boreas*, *44*(1), 81–93. https://doi.org/10.1111/bor.12093

Kuroda, J., Jiménez-Espejo, F. J., Nozaki, T., Gennari, R., Lugli, S., Manzi, V., Roveri, M., Flecker, R., Sierro, F. J., Yoshimura, T., Suzuki, K., & Ohkouchi, N. (2016). Miocene to Pleistocene osmium isotopic records of the Mediterranean sediments. *Paleoceanography*, *31*(1), 148–166. https://doi.org/10.1002/2015PA002853

Kylander, M. E., Ampel, L., Wohlfarth, B., & Veres, D. (2011). High-resolution X-ray fluorescence core scanning analysis of Les Echets (France) sedimentary sequence: New insights from chemical proxies. *Journal of Quaternary Science*, *26*(1), 109–117. https://doi.org/10.1002/jqs.1438

Lemke, W., Jensen, J. B., Bennike, O., Endler, R., Witkowski, A., & Kuijpers, A. (2001). Hydrographic thresholds in the western Baltic Sea: Late Quaternary geology and the Dana River concept. *Marine Geology*, *176*(1–4), 191–201. https://doi.org/10.1016/S0025-3227(01)00152-9

Levasseur, S. (1998). Direct Measurement of Femtomoles of Osmium and the 187Os/186Os Ratio in Seawater. *Science*, *282*(5387), 272–274. https://doi.org/10.1126/science.282.5387.272

Levasseur, S., Birck, J. L., & Allègre, C. J. (1999). The osmium riverine flux and the oceanic mass balance of osmium. *Earth and Planetary Science Letters*, *174*(1–2), 7–23. https://doi.org/10.1016/S0012-821X(99)00259-9

Levasseur, S., Rachold, V., Birck, J. L., & Allègre, C. J. (2000). Osmium behavior in estuaries: The Lena River example. *Earth and Planetary Science Letters*, *177*(3–4), 227–235. https://doi.org/10.1016/S0012-821X(00)00049-2

Li, G., Piper, D. J. W., & Calvin Campbell, D. (2011). The Quaternary Lancaster Sound trough-mouth fan, NW Baffin Bay. *Journal of Quaternary Science*, *26*(5), 511–522. https://doi.org/10.1002/jqs.1479

Liu, Z., Selby, D., Zhang, H., & Shen, S. (2020). Evidence for volcanism and weathering during the Permian-Triassic mass extinction from Meishan (South China) osmium isotope record. *Palaeogeography, Palaeoclimatology, Palaeoecology*, *553*(January), 109790. https://doi.org/10.1016/j.palaeo.2020.109790

Lloyd, J. M. (2006). Modern Distribution of Benthic Foraminifera From Disko Bugt, West Greenland. *The Journal of Foraminiferal Research*, *36*(4), 315–331. https://doi.org/10.2113/gsjfr.36.4.315

Longva, O., & Bakkejord, K. J. (1990). Iceberg deformation and erosion in soft sediments, southeast Norway. *Marine Geology*, *92*(1–2), 87–104. https://doi.org/10.1016/0025-3227(90)90028-I

Longva, O., & Thoresen, M. K. (1991). Iceberg scours, iceberg gravity craters and current erosion marks from a gigantic Preboreal flood in southeastern Norway. *Boreas*, *20*(1), 47–62. https://doi.org/10.1111/j.1502-3885.1991.tb00458.x

Luguet, A., Nowell, G. M., & Pearson, D. G. (2008). 184Os/188Os and 186Os/188Os measurements by Negative Thermal Ionisation Mass Spectrometry (N-TIMS): Effects of interfering element and mass fractionation corrections on data accuracy and precision. *Chemical Geology*, *248*(3–4), 342–362. https://doi.org/10.1016/j.chemgeo.2007.10.013

MacLean, B., Williams, G. L., & Srivastava, S. P. (1990). Geology of Baffin Bay and Davis Strait. *Geology of Canada No.2: Geology of the Continental Margin of Eastern Canada. Geological Survey of Canada*, 325–348.

Magnusson, B., & Westerlund, S. (1980). The determination of Cd, Cu, Fe, Ni, Pb and Zn in Baltic Sea water. *Marine Chemistry*, *8*(3), 231–244. https://doi.org/10.1016/0304-4203(80)90012-2

Margold, M., Stokes, C. R., & Clark, C. D. (2018). Reconciling records of ice streaming and ice margin retreat to produce a palaeogeographic reconstruction of the deglaciation of the Laurentide Ice Sheet. *Quaternary Science Reviews*, *189*, 1–30. https://doi.org/10.1016/j.quascirev.2018.03.013

Marshall, S. J., & Koutnik, M. R. (2006). Ice sheet action versus reaction: Distinguishing between Heinrich events and Dansgaard-Oeschger cycles in the North Atlantic. *Paleoceanography*, *21*(2), 1–13. https://doi.org/10.1029/2005PA001247

McCarty, D. K. (2002). Quantitative mineral analysis of clay-bearing mixtures: The “Reynolds Cup” contest. *International Union of Crystallography*, *27*, 12–16.

McDaniel, D. K., Walker, R. J., Hemming, S. R., Horan, M. F., Becker, H., & Grauch, R. I. (2004). Sources of osmium to the modern oceans: new evidence from the 190 Pt- 186 Os system 1 1Associate editor: E. M. Ripley. *Geochimica et Cosmochimica Acta*, *68*(6), 1243–1252. https://doi.org/10.1016/j.gca.2003.08.020

McLennan, S. M. (2001). Relationships between the trace element composition of sedimentary rocks and upper continental crust. *Geochemistry, Geophysics, Geosystems*, *2*(4), n/a-n/a. https://doi.org/10.1029/2000GC000109

Miller, G. H., Wolfe, A. P., Steig, E. J., Sauer, P. E., Kaplan, M. R., & Briner, J. P. (2002). The goldilocks dilemma: Big ice, little ice, or “just-right” ice in the eastern canadian arctic. *Quaternary Science Reviews*, *21*(1–3), 33–48. https://doi.org/10.1016/S0277-3791(01)00085-3

Missiaen, L., Wacker, L., Lougheed, B. C., Skinner, L., Hajdas, I., Nouet, J., Pichat, S., & Waelbroeck, C. (2020). Radiocarbon Dating of Small-sized Foraminifer Samples: Insights into Marine sediment Mixing. *Radiocarbon*, *62*(2), 313–333. https://doi.org/10.1017/RDC.2020.13

Moros, M., Lemke, W., Kuijpers, A., Endler, R., Jensen, J. B., Bennike, O., & Gingele, F. (2002). Regressions and transgressions of the Baltic basin reflected by a new high-resolution deglacial and postglacial lithostratigraphy for Arkona Basin sediments (western Baltic Sea). *Boreas*, *31*(2), 151–162. https://doi.org/10.1111/j.1502-3885.2002.tb01063.x

Moros, M., Lloyd, J. M., Perner, K., Krawczyk, D., Blanz, T., de Vernal, A., Ouellet-Bernier, M. M., Kuijpers, A., Jennings, A. E., Witkowski, A., Schneider, R., & Jansen, E. (2016). Surface and sub-surface multi-proxy reconstruction of middle to late Holocene palaeoceanographic changes in Disko Bugt, West Greenland. *Quaternary Science Reviews*, *132*, 146–160. https://doi.org/10.1016/j.quascirev.2015.11.017

Nordberg, K. (1991). Oceanography in the Kattegat and Skagerrak Over the Past 8000 Years. *Paleoceanography*, *6*(4), 461–484. https://doi.org/10.1029/91PA01132

Nørgaard-Pedersen, N., Spielhagen, R. F., Erlenkeuser, H., Grootes, P. M., Heinemeier, J., &

Knies, J. (2003). Arctic Ocean during the Last Glacial Maximum: Atlantic and polar domains of surface water mass distribution and ice cover. *Paleoceanography*, *18*(3), 1–19. https://doi.org/10.1029/2002pa000781

Nowell, G. M., Luguet, A., Pearson, D. G., & Horstwood, M. S. A. (2008). Precise and accurate 186Os/188Os and 187Os/188Os measurements by multi-collector plasma ionisation mass spectrometry (MC-ICP-MS) part I: Solution analyses. *Chemical Geology*, *248*(3–4), 363–393. https://doi.org/10.1016/j.chemgeo.2007.10.020

Ó Cofaigh, C., Dowdeswell, J. A., Jennings, A. E., Hogan, K. A., Kilfeather, A., Hiemstra, J. F., Noormets, R., Evans, J., McCarthy, D. J., Andrews, J. T., Lloyd, J. M., & Moros, M. (2013). An extensive and dynamic ice sheet on the west greenland shelf during the last glacial cycle. *Geology*, *41*(2), 219–222. https://doi.org/10.1130/G33759.1

Ó Cofaigh, C., Weilbach, K., Lloyd, J. M., Benetti, S., Callard, S. L., Purcell, C., Chiverrell, R. C., Dunlop, P., Saher, M., Livingstone, S. J., Van Landeghem, K. J. J., Moreton, S. G., Clark, C. D., & Fabel, D. (2019). Early deglaciation of the British-Irish Ice Sheet on the Atlantic shelf northwest of Ireland driven by glacioisostatic depression and high relative sea level. *Quaternary Science Reviews*, *208*, 76–96. https://doi.org/10.1016/j.quascirev.2018.12.022

Ownsworth, E., Selby, D., Ottley, C. J., Unsworth, E., Raab, A., Feldmann, J., Sproson, A. D., Kuroda, J., Faidutti, C., & Bücker, P. (2019). Tracing the natural and anthropogenic influence on the trace elemental chemistry of estuarine macroalgae and the implications for human consumption. *Science of the Total Environment*, *685*, 259–272. https://doi.org/10.1016/j.scitotenv.2019.05.263

Oxburgh, R. (1998). Variations in the osmium isotope composition of seawater over the past 200 000 years. *Earth and Planetary Science Letters*, *159*(3–4), 183–191. https://doi.org/10.1016/S0012-821X(98)00057-0

Oxburgh, R. (2001). Residence time of osmium in the oceans. *Geochemistry, Geophysics, Geosystems*, *2*(6). https://doi.org/10.1029/2000GC000104

Paquay, F. S., & Ravizza, G. (2012). Heterogeneous seawater 187Os/ 188Os during the Late Pleistocene glaciations. *Earth and Planetary Science Letters*, *349–350*, 126–138. https://doi.org/10.1016/j.epsl.2012.06.051

Pegram, W. J., Krishnaswami, S., Ravizza, G. E., & Turekian, K. K. (1992). The record of sea water 187Os186Os variation through the Cenozoic. *Earth and Planetary Science Letters*, *113*(4), 569–576. https://doi.org/10.1016/0012-821X(92)90132-F

Peters, K. E., Walters, C. C., & Moldowan, J. M. (2004). *The Biomarker Guide*. Cambridge University Press. https://doi.org/10.1017/CBO9780511524868

Pettijohn, F. J., Potter, P. E., & Siever, R. (1987). *Sand and Sandstone*. Springer New York. https://doi.org/10.1007/978-1-4612-1066-5

Peucker-Ehrenbrink, B., & Jahn. (2001). the Upper Continental Crust. *Geochemistry, Geophysics, Geosystems*, *2*, 1–22.

Peucker-Ehrenbrink, B., & Ravizza, G. (1996). Continental runoff of osmium into the Baltic Sea. *Geology*, *24*(4), 327–330. https://doi.org/10.1130/0091-7613(1996)024<0327:CROOIT>2.3.CO;2

Peucker-Ehrenbrink, B., & Ravizza, G. (2000). The marine osmium isotope record. *Terra Nova*, *12*(5), 205–219. https://doi.org/10.1046/j.1365-3121.2000.00295.x

Peucker-Ehrenbrink, B., & Ravizza, G. (2012). Osmium Isotope Stratigraphy. In *The Geologic Time Scale* (pp. 145–166). Elsevier. https://doi.org/10.1016/B978-0-444-59425-9.00008-1

Peucker-Ehrenbrink, B., & Ravizza, G. E. (2020). Osmium Isotope Stratigraphy. In *Geologic Time Scale 2020* (pp. 239–257). Elsevier. https://doi.org/10.1016/B978-0-12-824360-2.00008-5

Peucker-Ehrenbrink, Bernhard, & Blum, J. D. (1998). Re-Os isotope systematics and weathering of Precambrian crustal rocks: Implications for the marine osmium isotope record. *Geochimica et Cosmochimica Acta*, *62*(19–20), 3193–3203. https://doi.org/10.1016/S0016-7037(98)00227-0

Poirier, A., & Hillaire-Marcel, C. (2011). Improved Os-isotope stratigraphy of the Arctic Ocean. *Geophysical Research Letters*, *38*(14), 10–15. https://doi.org/10.1029/2011GL047953

Rasmussen, S. O., Andersen, K. K., Svensson, A. M., Steffensen, J. P., Vinther, B. M., Clausen, H. B., Siggaard-Andersen, M. L., Johnsen, S. J., Larsen, L. B., Dahl-Jensen, D., Bigler, M., Röthlisberger, R., Fischer, H., Goto-Azuma, K., Hansson, M. E., & Ruth, U. (2006). A new Greenland ice core chronology for the last glacial termination. *Journal of Geophysical Research Atmospheres*, *111*(6). https://doi.org/10.1029/2005JD006079

Rasmussen, S. O., Bigler, M., Blockley, S. P., Blunier, T., Buchardt, S. L., Clausen, H. B., Cvijanovic, I., Dahl-Jensen, D., Johnsen, S. J., Fischer, H., Gkinis, V., Guillevic, M., Hoek, W. Z., Lowe, J. J., Pedro, J. B., Popp, T., Seierstad, I. K., Steffensen, J. P., Svensson, A. M., … Winstrup, M. (2014). A stratigraphic framework for abrupt climatic changes during the Last Glacial period based on three synchronized Greenland ice-core records: Refining and extending the INTIMATE event stratigraphy. *Quaternary Science Reviews*, *106*, 14–28. https://doi.org/10.1016/j.quascirev.2014.09.007

Ravizza, G., & Peucker-Ehrenbrink, B. (2003). The marine 187Os/188Os record of the Eocene-Oligocene transition: The interplay of weathering and glaciation. *Earth and Planetary Science Letters*, *210*(1–2), 151–165. https://doi.org/10.1016/S0012-821X(03)00137-7

Ravizza, G., Turekian, K. K., & Hay, B. J. (1991). The geochemistry of rhenium and osmium in recent sediments from the Black Sea. *Geochimica et Cosmochimica Acta*, *55*(12), 3741–3752. https://doi.org/10.1016/0016-7037(91)90072-D

Ravizza, Greg, & Turekian, K. K. (1989). Application of the 187Re-187Os system to black shale geochronometry. *Geochimica et Cosmochimica Acta*, *53*(12), 3257–3262. https://doi.org/10.1016/0016-7037(89)90105-1

Reimer, P. J., Edouard Bard, B., Alex Bayliss, B., Warren Beck, B. J., Paul Blackwell, B. G., & Christopher Bronk Ramsey, B. (2013). Intcal13 and Marine13 Radiocarbon Age Calibration Curves 0–50,000 Years Cal Bp. *Radiocarbon*, *55*(4), 1869–1887. https://doi.org/10.1017/S0033822200048864

Rodhe, J., & Holt, N. (1996). Observations of the transport of suspended matter into the Skagerrak along the western and northern Coast of Jutland. *Journal of Sea Research*, *35*(1–3), 91–98. https://doi.org/10.1016/s1385-1101(96)90738-8

Rooney, A. D., Selby, D., Lloyd, J. M., Roberts, D. H., Lückge, A., Sageman, B. B., & Prouty, N. G. (2016). Tracking millennial-scale Holocene glacial advance and retreat using osmium isotopes: Insights from the Greenland ice sheet. *Quaternary Science Reviews*, *138*, 49–61. https://doi.org/10.1016/j.quascirev.2016.02.021

Rosell-Melé, A. (1998). Interhemispheric appraisal of the value of alkenone indices as temperature and salinity proxies in high-latitude locations. *Paleoceanography*, *13*(6), 694–703. https://doi.org/10.1029/98PA02355

Rosell-Melé, A., Jansen, E., & Weinelt, M. (2002). Appraisal of a molecular approach to infer variations in surface ocean freshwater inputs into the North Atlantic during the last glacial. *Global and Planetary Change*, *34*(3–4), 143–152.

https://doi.org/10.1016/S0921-8181(02)00111-X

Rosentau, A., Bennike, O., Uscinowicz, S., & Miotk-Szpiganowicz, G. (2017). The Baltic Sea Basin. In *Submerged Landscapes of the European Continental Shelf: Quaternary Paleoenvironments* (Issue July 2018). https://doi.org/10.1002/9781118927823.ch5

Rothwell, R. G., & Croudace, I. w. (2015). *Twenty Years of XRF Core Scanning Marine Sediments: What Do Geochemical Proxies Tell Us?* (pp. 25–102). https://doi.org/10.1007/978-94-017-9849-5_2

Scott, D. B., Medioli, F. S., & Schafer, C. T. (2001). *Monitoring in Coastal Environments Using Foraminifera and Thecamoebian Indicators*. Cambridge University Press. https://doi.org/10.1017/CBO9780511546020

Seierstad, I. K., Abbott, P. M., Bigler, M., Blunier, T., Bourne, A. J., Brook, E., Buchardt, S. L., Buizert, C., Clausen, H. B., Cook, E., Dahl-Jensen, D., Davies, S. M., Guillevic, M., Johnsen, S. J., Pedersen, D. S., Popp, T. J., Rasmussen, S. O., Severinghaus, J. P., Svensson, A., & Vinther, B. M. (2014). Consistently dated records from the Greenland GRIP, GISP2 and NGRIP ice cores for the past 104ka reveal regional millennial-scale δ18O gradients with possible Heinrich event imprint. *Quaternary Science Reviews*, *106*, 29–46. https://doi.org/10.1016/j.quascirev.2014.10.032

Selby, D., & Creaser, R. A. (2003). Re-Os geochronology of organic rich sediments: An evaluation of organic matter analysis methods. *Chemical Geology*, *200*(3–4), 225–240. https://doi.org/10.1016/S0009-2541(03)00199-2

Selby, D., Creaser, R. A., & Nesbitt, B. E. (1999). Major and trace element compositions and Sr-Nd-Pb systematics of crystalline rocks from the Dawson Range, Yukon, Canada. *Canadian Journal of Earth Sciences*, *36*(9), 1463–1481. https://doi.org/10.1139/e99-058

Selby, D., Cumming, V. M., Rooney, A. D., & Finlay, A. J. (2013). Encyclopedia of Scientific Dating Methods. *Encyclopedia of Scientific Dating Methods*, 1–7. https://doi.org/10.1007/978-94-007-6326-5

Shakun, J. D., & Carlson, A. E. (2010). A global perspective on Last Glacial Maximum to Holocene climate change. *Quaternary Science Reviews*, *29*(15–16), 1801–1816. https://doi.org/10.1016/j.quascirev.2010.03.016

Sharma, M., Papanastassiou, D. A., & Wasserburg, G. J. (1997). The concentration and isotopic composition of osmium in the oceans. *Geochimica et Cosmochimica Acta*, *61*(16), 3287–3299. https://doi.org/10.1016/S0016-7037(97)00210-X

Sharma, M., Wasserburg, G. J., Hofmann, A. W., & Butterfield, D. A. (2000). Osmium isotopes in hydrothermal fluids from the Juan de Fuca Ridge. *Earth and Planetary Science Letters*, *179*(1), 139–152. https://doi.org/10.1016/S0012-821X(00)00099-6

Sheldon, C., Jennings, A., Andrews, J. T., Ó Cofaigh, C., Hogan, K., Dowdeswell, J. A., & Seidenkrantz, M. S. (2016). Ice stream retreat following the LGM and onset of the west Greenland current in Uummannaq Trough, west Greenland. *Quaternary Science Reviews*, *147*, 27–46. https://doi.org/10.1016/j.quascirev.2016.01.019

Sicre, M.-A., Bard, E., Ezat, U., & Rostek, F. (2002). Alkenone distributions in the North Atlantic and Nordic sea surface waters. *Geochemistry, Geophysics, Geosystems*, *3*(2), 1 of 13–13 13. https://doi.org/10.1029/2001gc000159

Simon, Q., Hillaire-Marcel, C., St-Onge, G., & Andrews, J. T. (2014). North-eastern Laurentide, western Greenland and southern Innuitian ice stream dynamics during the last glacial cycle. *Journal of Quaternary Science*, *29*(1), 14–26. https://doi.org/10.1002/jqs.2648

Simon, Q., St-Onge, G., & Hillaire-Marcel, C. (2012). Late Quaternary chronostratigraphic framework of deep Baffin Bay glaciomarine sediments from high-resolution paleomagnetic data. *Geochemistry, Geophysics, Geosystems*, *13*(1), 1–24. https://doi.org/10.1029/2012GC004272

Sinninghe Damsté, J. S., Schouten, S., Hopmans, E. C., Van Duin, A. C. T., & Geenevasen, J. A. J. (2002). Crenarchaeol: The characteristic core glycerol dibiphytanyl glycerol tetraether membrane lipid of cosmopolitan pelagic crenarchaeota. *Journal of Lipid Research*, *43*(10), 1641–1651. https://doi.org/10.1194/jlr.M200148-JLR200

Sjöqvist, C., Godhe, A., Jonsson, P. R., Sundqvist, L., & Kremp, A. (2015). Local adaptation and oceanographic connectivity patterns explain genetic differentiation of a marine diatom across the North Sea-Baltic Sea salinity gradient. *Molecular Ecology*, *24*(11), 2871–2885. https://doi.org/10.1111/mec.13208

Solheim, A., & Grønlie, G. (1983). Quaternary sediments and bedrock geology in the outer Oslofjord and northernmost Skagerrak. *Norsk Geologisk Tidskrift*, *63*, 55–71.

Sproson, A. D., Selby, D., Gannoun, A., Burton, K. W., Dellinger, M., & Lloyd, J. M. (2018). Tracing the Impact of Coastal Water Geochemistry on the Re-Os Systematics of Macroalgae: Insights From the Basaltic Terrain of Iceland. *Journal of Geophysical Research: Biogeosciences*, *123*(9), 2791–2806. https://doi.org/10.1029/2018JG004492

Sproson, A. D., Selby, D., Suzuki, K., Oda, T., & Kuroda, J. (2020). Anthropogenic Osmium in Macroalgae from Tokyo Bay Reveals Widespread Contamination from Municipal Solid Waste. *Environmental Science and Technology*, *54*(15), 9356–9365. https://doi.org/10.1021/acs.est.0c01602

St-Onge, M. R., Van Gool, J. A. M., Garde, A. A., & Scott, D. J. (2009). Correlation of Archaean and Palaeoproterozoic units between northeastern Canada and western Greenland: Constraining the pre-collisional upper late accretionary history of the Trans-Hudson orogen. *Geological Society Special Publication*, *318*, 193–235. https://doi.org/10.1144/SP318.7

Stuiver, M., Reimer, P. J., Bard, E., Beck, J. W., Burr, G. S., Hughen, K. A., Kromer, B., McCormac, G., Van Der Plicht, J., & Spurk, M. (1998). INTCAL98 radiocarbon age calibration, 24,000-0 cal BP. *Radiocarbon*, *40*(3), 1041–1083. https://doi.org/10.1017/S0033822200019123

Stuiver, M., Reimer, P. J., & Reimer, R. W. (2021). *CALIB 8.2 [WWW program]*.

Stuiver, M, Reimer, P. J., & Reimer, R. W. (2020). *CALIB 7.1 [WWW program]*.

Stuiver, Minze, & Grootes, P. M. (2000). GISP2 Oxygen Isotope Ratios. *Quaternary Research*, *53*(3), 277–284. https://doi.org/10.1006/qres.2000.2127

Szidat, S., Salazar, G. A., Vogel, E., Battaglia, M., Wacker, L., Synal, H.-A., & Türler, A. (2014). 14 C Analysis and Sample Preparation at the New Bern Laboratory for the Analysis of Radiocarbon with AMS (LARA) . *Radiocarbon*, *56*(2), 561–566. https://doi.org/10.2458/56.17457

Tang, C. C. L., Ross, C. K., Yao, T., Petrie, B., DeTracey, B. M., & Dunlap, E. (2004). The circulation, water masses and sea-ice of Baffin Bay. *Progress in Oceanography*, *63*(4), 183–228. https://doi.org/10.1016/j.pocean.2004.09.005

Taylor, S. R., & McLennan, S. M. (1985). *The Continental Crust: Its Composition and Evolution*. Blackwell Scientific Publications.

Turekian, K. K., Sharma, M., & Gordon, G. W. (2007). The behavior of natural and anthropogenic osmium in the Hudson River-Long Island Sound estuarine system. *Geochimica et Cosmochimica Acta*, *71*(17), 4135–4140.

https://doi.org/10.1016/j.gca.2007.05.020

Tuuling, I., Bauert, H., Willman, S., & Budd, G. E. (2011). *The Baltic Sea: Geology and Geotourism Highlights*. NGO GEOGuide Baltoscandia.

van der Ploeg, R., Selby, D., Cramwinckel, M. J., Li, Y., Bohaty, S. M., Middelburg, J. J., & Sluijs, A. (2018). Middle Eocene greenhouse warming facilitated by diminished weathering feedback. *Nature Communications*, *9*(1), 2877. https://doi.org/10.1038/s41467-018-05104-9

Wang, H., Liu, W., Zhang, C. L., Liu, Z., & He, Y. (2013). Branched and isoprenoid tetraether (BIT) index traces water content along two marsh-soil transects surrounding Lake Qinghai: Implications for paleo-humidity variation. *Organic Geochemistry*, *59*, 75–81. https://doi.org/10.1016/j.orggeochem.2013.03.011

Warden, L., Moros, M., Weber, Y., & Sinninghe Damsté, J. S. (2018). Change in provenance of branched glycerol dialkyl glycerol tetraethers over the Holocene in the Baltic Sea and its impact on continental climate reconstruction. *Organic Geochemistry*, *121*, 138–154. https://doi.org/10.1016/j.orggeochem.2018.03.007

Washburn, A. M., Hudson, S. M., Selby, D., Abdullayev, N., & Shiyanova, N. (2019). Constraining the Timing and Depositional Conditions of the Maikop Formation Within the Kura Basin, Eastern Azerbaijan, Through the Application of Re-Os Geochronology and Chemostratigraphy. *Journal of Petroleum Geology*, *42*(3), 281–299. https://doi.org/10.1111/jpg.12734

Westman, P., Wastegård, S., & Schoning, K. (1999). Salinity change in the Baltic Sea during the last 8,500 years: evidence, causes and models. *Technical Report TR-99-38, Svensk Kärnbränslehantering AB, Stockholm*.

Wollenburg, J. E., Knies, J., & Mackensen, A. (2004). High-resolution paleoproductivity fluctuations during the past 24 kyr as indicated by benthic foraminifera in the marginal Arctic Ocean. *Palaeogeography, Palaeoclimatology, Palaeoecology*, *204*(3–4), 209–238. https://doi.org/10.1016/S0031-0182(03)00726-0

Supplementary Material

Additional Microsoft Excel files containing supplementary materials for Chapters 2, 3, and 4 are uploaded separately. References to supplementary material in this document are denoted by SM. For example, SM 2.1.